ADSORBED AND ABSORBED HYDROGEN ASSOCIATED WITH LEAD CATHODES IN AQUEOUS PERCHLORIC ACID

GOPALAKRISHNA M. RAO

ADSORBED AND ABSORBED HYDROGEN ASSOCIATED WITH LEAD CATHODES IN AQUEOUS PERCHLORIC ACID

A Thesis

by

Gopalakrishna M. Rao

Submitted in partial fulfillment of the requirements
for the degree of Doctor of Philosophy.

August, 1973

Memorial University
of Newfoundland

We certify that we have read, examined and approve the thesis submitted by Gopalakrishna M. Rao in partial fulfillment of the requirements for the Degree of Doctor of Philosophy in Chemistry at Memorial University of Newfoundland.

EJ Casey

E.J. Casey

Noel A. Hampson

N.A. Hampson

J.M.W. Scott

J.M.W. Scott

3 October 1973

ABSTRACT

Studies of overvoltage and capacity at lead cathodes in aqueous perchloric acid at room temperature have broadly confirmed earlier observations by Ives and Smith, that the overvoltage falls linearly as the logarithm of the cathodic charge (-Q) increases. Capacities were measured by open-circuit potential decay measurements and failed to indicate the presence at first of an adsorption pseudocapacity attributable to adsorbed hydrogen. However, growth of the measured capacities in the course of electrolysis is attributed to a growing pseudocapacity component and is analysed in terms of an increasing coverage of the cathode by adsorbed hydrogen atoms (θ_H). Indicated surface coverages range up to 2% of a monolayer for lead rods and up to 5% in one case with a lead foil.

The increase in capacity ($C_{expt.}$) at constant overvoltage was also linear with the logarithm of -Q. This parallelism between decreasing overvoltage and increasing pseudocapacity suggests a common origin which, following Ives and Smith, we propose to be the gradual accumulation of hydrogen atoms in the bulk of the metal with quasi-equilibrium existing with the adsorbed hydrogen.

Electrolytic permeation experiments indicate that the hydrogen and tritium atom concentrations just beneath the cathodic surface are 5×10^{-7} to 10^{-5} and 10^{-12} to 10^{-10} g. atom cm.$^{-3}$, respectively, at cathodic current densities (-i) of 11.3 to 46 mA. cm.$^{-2}$. Below 11.3 mA. cm.$^{-2}$ no permeation current was detectable nor was tritium

found to have passed through the lead membrane.

With the observed linear increase of $C_{expt.}$, taken to be proportional to the hydrogen surface coverage, with the logarithm of -Q and with the assumption that the bulk hydrogen concentration just beneath the cathodic surface (C_0) is directly proportional to -Q, since C_0 increases linearly with -i, an exponential relationship between C_0 and θ_H:

$$C_0 \propto \exp. (\theta_H)$$

is proposed.

A linear relationship has also been found between $C_{expt.}$ and the logarithm of -i, indicating that a linearly increasing hydrogen coverage results in a logarithmically increasing reaction rate at constant overvoltage. Changes at the surface alone cannot account for this catalysis. Ives and Smith suggested that catalysis arises from the increase of the bulk hydrogen content through donation of electrons to the metal by the dissolved hydrogen atoms. It is shown that the band structure of lead is favourable for electron donation to the conduction band, the density of donated electrons in the third Brillouin zone increasing at twice the rate at which the density of holes decreases in the second Brillouin zone. Catalysis apparently involves the increase in rate of the Volmer reaction of hydronium ion discharge rather than any increase of the Heyrovsky step.

The $S_{H,T} = 7.2 \pm 0.7$ and $S_{(H,T)_{DA}} = 0.9 \pm 0.5$, the hydrogen-tritium separation factors measured simultaneously on the cathode and diffusion sides of lead membranes are close to literature values. The anomalous nature of $S_{(H,T)_{DA}}$ is discussed.

To

My Mother

SARASWATHI

ACKNOWLEDGMENTS

I would first like to thank my supervisor, Dr. Frank R. Smith, for continuing encouragement, valuable suggestions and helpful criticism.

Thanks are also due to Dr. Ivan Cadersky for devising and constructing the prototype differentiating circuit.

The assistance of the personnel of the Electronics, Glassblowing and Machine Shop Sections of Technical Services, Memorial University, is highly appreciated.

I would like to thank the personnel of the School of Medicine, Memorial University, for assistance with and the use of their liquid scintillation facilities.

I am grateful to Mrs. Glenda E. Wallace for patiently typing this thesis. Thanks are also due to Mr. Lorne Boone for drawing Figures.

I would particularly thank my brother and sisters for their help and encouragement throughout my educational career.

Special thanks are due to Memorial University and the Defence Research Board of Canada for providing financial assistance.

CONTENTS

LIST OF SYMBOLS. vi

1. INTRODUCTION. 1
   - A. Hydrogen Overvoltage Measurements on Lead 2
   - B. Double-Layer Capacity Measurements on Lead. 8
   - C. Cathodic Disintegration of Lead 11
   - D. Interaction of Hydrogen with Lead 12
   - E. Objectives of the Present Work. 14

2. THEORETICAL BACKGROUND. 16
   - A. Hydrogen Overvoltage Theory 16
     - (1) Types of Overvoltage. 17
     - (11) The Electrical Double Layer 23
     - (111) Charge-Transfer Steps in h.e.r. 28
     - (1V) Double-Layer Effects on Charge Transfer . . . 37
     - (V) Temperature Dependence of Overvoltage 44
     - (V1) The Electrochemical Reaction Orders 46
     - (V11) The Isotopic Separation Factors 48
   - B. Theory of Hydrogen Adsorption and Adsorption Pseudocapacitance 49
     - (1) Enthalpies of Adsorption of Hydrogen. 50
     - (11) The Adsorption Pseudo-Capacitance 54
     - (111) Open-Circuit Decay Measurements 58
     - (1V) Adsorption Pseudo-Capacitance and Coverage. . 63
     - (V) Adsorption Pseudo-Capacitance and Isotherms . 65

C. Permeation of Hydrogen (or Tritium) Atoms Through Metals as a Diffusion Phenomenon 68

(1) Methods of Measuring Diffusion Coefficients of Hydrogen Isotopes. 72

(11) Proof of Diffusion-Controlled Permeation . . . 77

(111) Diffusivity and Solubility of Hydrogen Isotopes in Metals. 78

(1V) Hydrogen Absorption and the Hydrogen Evolution Reaction 81

D. Isotopic Separation in Hydrogen Evolution and Membrane Diffusion 85

(1) Separation Factors on the Cathodic Surface . . 85

(11) Separation Factors on the Diffusion Side of a Metal Membrane After Cathodisation and Membrane Diffusion 93

(a) Separation Factors for Hydrogen Isotope Evolution on the Diffusion Side. 94

(b) Separation Factors for Hydrogen Isotope Ionisation on the Diffusion Side 95

3. EXPERIMENTAL METHODS AND RESULTS 98

A. Experimental Method and Results of Hydrogen Overvoltage Measurements 101

(1) Materials. 101

(11) Purification of Solutions. 108

(a) Pre-electrolytic Purification. 108
(b) Adsorptive Purification. 112
(c) Analysis of Pre-electrolysed Perchloric Acid. 112
(111) Pre-treatment of the Lead Electrode. 119
(1V) Main Cells 129
(a) Cell for Rod Electrodes. 129
(b) Cell for Foil Electrodes 130
(V) Instrumentation and Procedure. 132
(V1) Results of Early Experiments 139
(a) Preliminary Experiments. 139
(b) Experiments with Electropolished Electrodes and Solution Pre-electrolysed at Too High Current Densities. 142
(c) Early Experiments with Scraped Electrodes and Solutions Pre-electrolysed at Low Current Densities. 148
(V11) Experiments with Electropolished Electrodes and Properly Pre-electrolysed Solutions. . . . 159
(a) Tafel Plots. 160
(b) Temperature Dependence of Overvoltage. . . 165
(c) Overvoltage as a Function of Total Cathodic Charge. 172
(d) Overshoot Hysteresis 181

(Vlll) Summarising Remarks on Overvoltage Measurements. 201

B. Experimental Method and Results of Adsorption Pseudo-Capacity. 204

(1) Instrumentation and Procedure 204

(11) Results of Early Experiments. 218

(a) Preliminary Experiments 218

(b) Experiments with Electropolished Electrodes and Solution Pre-electrolysed at Too High Current Densities 221

(111) Experiments with Electropolished Electrodes and Properly Pre-electrolysed Solutions . . . 224

(a) Results of Capacity Measurements. 224

(b) Relationships between Capacity, Overvoltage and Total Cathodic Charge 238

(c) Calculations of Hydrogen Coverage 253

(1V) Summarising Remarks on Capacity Measurements. 262

C. Electrolytic Hydrogen and Tritium Radiotracer Permeation Rates and Isotope Separation Factors on Cathode and Diffusion Sides of Lead Membrane. . . 264

(1) Materials 264

(11) Solution and Electrode Preparation. 267

(111) Cell. 269

(1V) Instrumentation and Procedure 272

(V) Results of Experiments with Electropolished Foils. 286

(Vl) Summarising Remarks on Separation Factor Measurements. 295

4. DISCUSSION 296

A. General. 296

B. Interaction of Atomic Hydrogen with Lead 303

C. Isotopic Separation in Hydrogen Evolution and Membrane Diffusion 318

D. Catalysis of Electrolytic Hydrogen Evolution at Lead by Absorbed Atomic Hydrogen 325

E. Concluding Remarks 350

REFERENCES. 352

LIST OF SYMBOLS

a	Tafel constant in equation (1.2)
a'	Quantity related to standard free energy of adsorption, $\Delta G^{o}_{H.ads.}$ in equation (2.46)
A	Quantity defined by the equation (2.25)
b	Tafel slope
b_1	Initial Tafel slope
b'	Slope of $-\eta$ versus $\log_{10}(-Q)$ plot
b"	Slope of $C_{expt.}$ versus $\log_{10}(-Q)$ plot
C	Double-layer capacity
C_1	Initial electrode capacity
$C_{expt.}$	Experimentally measured electrode capacitance
C_{ps}	Hydrogen adsorption pseudo-capacitance
$C_{min.}$	Minimum of differential capacity versus potential curve
C_f	Feed-back capacitor
C_i	Input capacitor
C_{H_2}	Concentration of dissolved H_2 in the solution
$C_{H_3O^+}$	Concentration of H_3O^+ ions in the bulk of the solution
$C^*_{H_3O^+}$	Concentration of H_3O^+ ions at the pre-electrode state

C_{ion}	Concentration of cations or anions in the solution
C_0	Concentration of absorbed H atoms just beneath the cathodic surface
$(C_0)_{Crit.H.}$	Critical hydrogen concentration within the bulk metal corresponding to the onset of hydrogen embrittlement
C_T	Total concentration of tritium atoms
dC_T/dt	Rate of disintegrations per second (D.P.S.)
C.P.M.	Counts per minute
Ci	Curie
D	Diffusion coefficient of hydrogen atom or isotope in the metal foil
D.P.M.	Disintegrations per minute
e	Charge on the electron
E	Electrode potential
E_e	Equilibrium electrode potential
$E_{ref.}$	Potential of the reference electrode
E_f	Energy corresponding to the Fermi level
E(M-H)	Binding energy of adsorbed hydrogen atoms
E_s	Reorganisation energy of the solvent (in the activation process) per electron transferred
$E_o^{\dagger}$	Activation energy for the $H_3O^+_{aq.}$ discharge step (2.1) in the absence of any electrical potential difference

$\Delta E^{\ddagger}$	Difference in activation energies between hydrogen and tritium isotopes (Fig. 4c)
f	Parameter accounting for heterogeneity or interaction between adsorbed atoms
F	Faraday
$\Delta\bar{G}^{\ddagger}_{-}$ and $\Delta\bar{G}^{\ddagger}_{+}$	Standard electrochemical free energies of activation for forward and backward reactions (2.1)
$\Delta G^{\ddagger}_{-}$ and $\Delta G^{\ddagger}_{+}$	Standard (chemical) free energies of activation for forward and backward reactions (2.1) at zero electrical potential difference
$\Delta G^{0}_{H_2 ads.}$	Standard free energy of dissociative hydrogen adsorption
$\Delta G^{\ddagger}$	Standard free energy of activation for H_3O^+ discharge step (2.1)
$\Delta G^{o}_{H.ads.}$	Standard free energy of adsorption of H atoms
$\overline{\Delta G}_{\theta}{}^{o}$	Standard free energy of adsorption at coverage θ_H
h	Planck's constant
(H)	Concentration of hydrogen atoms
$\Delta H^{\ddagger}_{\eta=0}$ and $\Delta H^{\ddagger}_{\eta}$	Enthalpy of activation at the equilibrium potential and at a given η
$\Delta H_{H.ads.}$	Enthalpy of adsorption of hydrogen atoms
$-i$	Cathodic current density
$-i_1$	Initial cathodic current density

$-i_t$	Cathodic current density at the time t after the current interruption
i_{v-} and i_{v+}	Partial current densities for the forward and backward steps of the Volmer reaction (2.1)
i_{h-} and i_{h+}	Partial current densities for the forward and backward steps of the Heyrovsky reaction (2.3)
i_- and i_+	Partial current densities for the forward and backward steps of a reaction
i_0	Apparent exchange current density
i_{10}	Initial apparent exchange current density
i'_0	Exchange current density associated with transport control
i''_0	Exchange current density for the recombination step (2.2)
i_{0Hg}	Exchange current density of h.e.r. on Hg
i^t_0	True exchange current density
$-I$	Cathodic current strength
J_∞	Steady-state permeation current for hydrogen atoms
J_t	Permeation current for hydrogen atoms at any time t
$(J_\infty)_T$	Steady-state permeation current for tritium atoms
k	Boltzmann's constant
k'	Total charge required to form a monolayer of adsorbed hydrogen atoms
k_r	Rate constant of H_3O^+ discharge step (2.1)

k''	Rate constant for the recombination step (2.2)
k_{v-} and k_{v+}	Rate constants for the forward and backward steps of the Volmer reaction (2.1)
k_{h-} and k_{h+}	Rate constants for the forward and backward steps of the Heyrovsky reaction (2.3)
K_1	Equilibrium constant for Volmer step (2.1)
L	Thickness of the metal membrane
n	Number of adsorption sites cm.$^{-2}$
N	Avogadro's number
pH	$-\log_{10}$ of hydrogen ion concentration
pHg	$-\log_{10}$ of mercurous ion concentration
$(P_H)_{eff.}$	Effective pressure of adsorbed hydrogen atoms
P	Pressure
(Pb^{++})	Concentration of Pb^{++} ions in the solution
q	Charge on the metal per unit area
q_1	Specifically-adsorbed charge on the metal per unit area
q_H	Charge equivalent to adsorbed hydrogen on the metal per unit area
Δq_H	Increase in charge equivalent to adsorbed hydrogen on the metal per unit area
$-Q$	Total charge passed during extended cathodic electrolysis
$-\Delta Q$	Additional charge passed during extended cathodic electrolysis
R	Gas constant
R_1	Reaction resistance for charging step (Fig. 3)

R_2	Reaction resistance for desorption step (Fig. 3)
R_f	Feed-back resistor
R_i	Input resistor
s'	Constant in equation (4.13)
s''	Constant in equation (4.14)
SCE	Saturated KCl calomel electrode
$S_{H,T}$ and $S_{H,D}$	Hydrogen-tritium and hydrogen-deuterium separation factors on the cathodic side of a foil
$S_{(H,T)_D}$ and $S_{(H,D)_D}$	The overall hydrogen-tritium and hydrogen-deuterium separation factors for cathodic discharge, diffusion through a foil and being evolved as gas on the diffusion side
$S_{(H,T)_{DA}}$	The overall hydrogen-tritium separation factor for cathodic discharge, diffusion through a foil and anodisation on the diffusion side
t	Time
t_0	Rise constant
$t_{0.5}$	Half-rise time
t_b	Breakthrough time
t_{lag}	Time lag
T	Absolute temperature
(T)	Concentration of tritium atoms
Z	Charge number of an ion

$Z_{H_3O^+}$	Electrochemical reaction order with respect to H_3O^+ ions
α	Cathodic transfer coefficient
$(1-\alpha)$	Anodic transfer coefficient
$\alpha(\varepsilon^*)$	Cathodic transfer coefficient as a function of ε^*
α_v	Transfer coefficient for the Volmer reaction (2.1)
α_h	Transfer coefficient for the Heyrovsky reaction (2.3)
α_1 and α_2	Angles of inclination of energy surfaces for $H_3O^+_{aq.}$ and $H_{ads.}$ (Fig. 2)
$\gamma^\ddagger$	Activity coefficient of the activated complex
$\delta+$ and $\delta-$	Representing +ve and -ve polarisation in a bond
ε	Dielectric constant in the diffuse layer
ε^*	Electron energy level making the main contribution to the total current
$\Delta\varepsilon_0$ and $\Delta\varepsilon_0^\ddagger$	Difference in zero-point energies between hydrogen and tritium in the initial state and the activated state (Fig. 4c)
$-\eta$	Cathodic hydrogen overvoltage
$-\eta_1$	Initial cathodic hydrogen overvoltage
$-\eta_t$	Cathodic hydrogen overvoltage corresponds to $-i_t$, at the time t after the current interruption
$-\eta_{corr.}$	Corrected cathodic hydrogen overvoltage using mercury as the reference state

η_m	Mass-transport or diffusion overvoltage
η_r	Reaction overvoltage
η_t	Charge-transfer overvoltage
η_Ω	I.R. Drop overvoltage
$\eta_{app.}$	The total apparent overvoltage $(\eta_t + \eta_r + \eta_m + \eta_\Omega)$
$\left(\frac{d\eta}{dt}\right)_{t=0}$	Initial rate of overvoltage decay with time $t=0$, the time of current interruption
$\left(\frac{d\eta}{dt}\right)_t$	Rate of variation of overvoltage with time at t, the time elapsed after the current interruption
$\Delta\eta$	Change in overvoltage with ϕ^* or with the time of cathodic polarisation; or overvoltage decay with time, after the current interruption
$\Delta\eta_1$ and $\Delta\eta_2$	Overvoltage decay with time for periods t_1 and t_2, after the current interruption
θ	Surface hydrogen atom or isotope coverage
θ_e	Surface hydrogen atom coverage at E_e
θ_H	Surface hydrogen atom coverage
$\Delta\theta_H$	Increase in surface hydrogen atom coverage
λ	Decay constant
μ	Chemical potential of the electrolyte
$\bar{\mu}_{H_3O^+}$	Electrochemical potential of H_3O^+ ions in solutions

$\bar{\mu}_{H.ads.}$	Electrochemical potential of adsorbed hydrogen atoms
τ	Dimensionless parameter in equation (2.57)
τ'	Constant in equation (2.40)
ϕ	Inner potential of electrode metal
ϕ_s	Inner potential of the bulk solution
ϕ_1	Potential in the inner Helmholtz plane
ϕ_2	Potential in the outer Helmholtz plane
ϕ^*	Potential at the pre-electrode state
ϕ^*_0	Constant in equation (2.12)
ϕ_e	Equilibrium (inner) potential of electrode metal
$\Delta\phi^*$	Change in ϕ^*

the topics:

A. Hydrogen overvoltage measurements on lead

B. Double-layer capacity measurements on lead

C. Cathodic disintegration of lead

D. Interaction of hydrogen with lead

and then, in a final section the objectives of the present work are stated.

A. Hydrogen Overvoltage Measurements on Lead

Tafel observed (1) that the overvoltage on lead electrodes rose during the first half-hour to a maximum value, whereas other metals took longer to reach their 'maximum' overvoltage.

Glasstone (2) investigated the properties of lead cathodes and anodes in sulphuric acid and sodium hydroxide solutions. Cathodic pretreatment of his electrodes at 150 mA. cm.$^{-2}$ before the measurements probably enabled Glasstone to minimise the dangers of contamination by the wax used to mask the electrode surface. The results at $i = -10$ and -100 mA. cm.$^{-2}$ were reasonable, with a b value of 0.11 V.

In contrast to this, Baars (3) and Erdey-Gruz and Wick (4) obtained Tafel slopes (b) of about 0.2 V. with lead in sulphuric acid. Erdey-Gruz and Wick suggested that the metal was covered by an oxide film which, because it was not reduced at high negative potentials, increased the hydrogen overvoltage.

Kabanov, Filippov, Vanyukova, Jofa and Prokofeva (5, 6) worked with chiselled spectroscopically pure lead in pre-electrolysed 0.01 N to 8 N sulphuric acid. They observed cathodic Tafel slopes of 0.12 V. over the current density range of 0.1 μA. to 1 mA. $cm.^{-2}$. Trouble was, however, encountered when the lead electrode was allowed to rest at potentials positive to -0.65 V. A bend in the overvoltage curve appeared between -0.60 and -0.70 V. (in 8 N H_2SO_4) and the cathodic Tafel slope could have any value between 0.12 and 0.22 V. At the same time, the double-layer capacity C,

$$C = (\partial q/\partial E)_{\mu,T,P.} \qquad (1.3)$$

defined as rate of change of charge q on the metal per unit area with electrode potential E at constant temperature T, pressure P and chemical potential of the electrolyte μ, was found to increase substantially at potentials positive to the electrocapillary maximum (-0.65 V.). Kabanov et al. carried out tests to ascertain the depolarising effects of oxygen by saturating the solution initially with 0.1, 1.0 and 10% oxygen in hydrogen. By subtracting the saturation current from the measured current in the mixed-potential region, corresponding to both the oxygen reduction and hydrogen evolution reactions, they confirmed that the rate of hydrogen evolution process was unaffected by the presence of oxygen in the solution. Jofa examined (7) the behaviour of lead in perchloric, hydrochloric and hydrobromic acids of varying concentrations. He concluded that anion adsorption at lead cathodes becomes important only in sufficiently concentrated solutions (e.g. H_2SO_4 > 8 N).

Vanyukova and Kabanov (8) studied the effects of a wide range of surface-active organic substances on hydrogen overvoltage at spongy lead electrodes, prepared by alternate anodisation and cathodisation, in 2 N and 8 N sulphuric acid. At the same 'true' current density but without surface active additives, the area having been estimated by double-layer capacity measurements, the overvoltages were 0.2 V. less negative than on the smooth lead electrodes of Kabanov and Jofa (5).

In 1941 Kolotyrkin and Frumkin (9) published a study of porous lead cathodes made from lead oxide-pasted accumulator plates and activated by alternate anodisation (to lead sulphate) and cathodisation to lead. Lead-lead oxide anodes were used in 8 N sulphuric acid and oxygen evolved from them was allowed to diffuse to the cathodes. Both the current and the hydrogen gas evolution rate were observed, but whereas Tafel curves based on the current deviated to less negative potentials at about 0.1 μA. cm.$^{-2}$, the volumetric measurements gave rise to linear Tafel plots down to 6×10^{-10} A. cm.$^{-2}$ (at the rest potential of -0.36 V.). Later, Kolotyrkin (10) examined the decay of overvoltage of spongy lead electrodes both when the cathodic current was switched off and when it was merely reduced. Electrodes subjected to prolonged cathodisation in a hydrogen atmosphere had Tafel curves based on the current and on the volume of hydrogen in good agreement, except close to the lead-lead sulphate potential. Two Tafel lines were, however, observed of 0.12 V. slope above 1 mA. cm.$^{-2}$ and 0.095 V. below, but without discontinuity. The results of Kolotyrkin and Bune (11), who used smooth lead electrodes in sulphuric acid solutions, broadly confirmed Kolotyrkin's observations, the separation of the upper and lower Tafel regions having increased from 160 mV. to 300 mV. The lower line was supposed to correspond to a lead surface at which sulphate ions are specifically adsorbed, whereas the upper line corresponds to measurements on a lead surface free from adsorbed anions. This conclusion was later confirmed by measurements of surface coverage of iodide ions by radiotracer methods (12, 13).

Lead and lead-plated copper were studied at high cathodic current densities (> 1 mA. cm.$^{-2}$) in N HCl using the commutator method by Hickling and Salt (14). Their crude technique of electrode preparation (wiping or scraping and washing with water or acid) resulted in a high b value of 0.3 V. and apparent approach to a constant overvoltage at cathodic current density > 100 mA. cm.$^{-2}$.

Experiments of Bockris et al. (15, 16, 17) using the direct method at -i up to 100 mA. cm.$^{-2}$ were said to confirm Hickling and Salt's finding of a constant maximum overvoltage. Bockris agreed with Hickling et al. that stringent deoxygenation was not necessary at cathodic currents of 1 mA. cm.$^{-2}$ and above, while Azzam (16, 17) did not find any differences above 1 mA. cm.$^{-2}$ attributable to the mode of surface preparation.

Ruetschi and Cahan (18) briefly studied the hydrogen overvoltage behaviour of knife-cut single crystal lead and lead alloys. In 10 N H_2SO_4, little or no dependence of overvoltage on orientation was found, the cathodic Tafel slope and exchange current apparently being in agreement with the results of Kabanov and Jofa (5). A fall of overvoltage with time was reported both above 10 mA. cm.$^{-2}$ and below 1 mA. cm.$^{-2}$.

In 1959, Gillibrand and Lomax (19) published hydrogen overvoltage measurements at porous electrodes prepared by conventional battery techniques. The overvoltages, reproducible to ±30 mV., lay close to a Tafel line of slope 0.12 V., while the growth of overvoltage curves had an initial slope $-\frac{d\eta}{dt}$ linear with $|i|$ and led to a calculated double layer capacity of 10^4 μF. cm.$^{-2}$, from which the real area was deduced to be 500 times the apparent. The overvoltage decay curves, on the other hand, were initially linear with $\log_{10}(t)$ with a slope close to $b = 0.12$ V.

Piontelli et al. (20,21,22,23) used perchloric acid and amidosulphuric acid (NH_2SO_3H) solutions in order to minimise the influence of anion adsorption or insoluble lead salts while studying single crystal electrodes of lead. The results were less satisfactory than might have been expected, two distinct Tafel slopes being found, one close to 0.12 V. in some cases and the other of greater magnitude. Tordesillas and Bicelli (20), who studied both polycrystalline and single faces of lead, claimed that overvoltage varied with orientation. However, Piontelli et al. (24) have shown orientation had no influence on the electrode potential from their study of lead single crystals in $Pb(NH_2SO_3)_2$ + 0.01 N NH_2SO_3H solution.

Essentially similar conclusions to Azzam were reached by Bockris and Srinivasan (25) who examined, among other metals, lead heated in hydrogen, chemically polished *or* electropolished. The best results were after 40 hours pre-electrolysis (Pt foil as pre-electrolysis cathode) of the solution, the measurements on chemically or anodically polished specimens being taken *without hydrogen passing through the cathode compartment*. Then, cathodic Tafel slopes of 0.125 ± 0.014 V. in

0.05 N H_2SO_4 and 0.129 ± 0.004 V. in 0.5 N HaOH were obtained. Initially, however, depolarisation at lower current densities and steep slopes of 6.9RT/F were observed, though polarographic analysis showed only $\approx 10^{-6}$ mole $1.^{-1}$ of Pb^{++} ions present.

Ives and Smith have carried out experiments with electropolished lead electrodes, both in perchloric acid and in sulphuric acid (26, 27), under the following conditions:

(i) Solutions were extensively pre-electrolysed and were subjected in the experimental cell to continuous adsorptive cleaning with activated carbon, to adsorptive and reductive cleaning at a large area of platinised platinum supplied with hydrogen and to a second stage of pre-electrolysis at an electropolished lead electrode (withdrawn whilst cathodic) precisely similar to the experimental electrode used for measurements.

(ii) Electropolished mirror-bright electrodes were employed.

(iii) Gases were carefully deoxygenated.

The observations of Ives and Smith (26, 27) cannot be correlated with specific anion adsorption, since most of them were made with perchloric acid.* The overvoltages, initially comparable with those of Bockris and Srinivasan (25) at -i of 10^{-4} A. $cm.^{-2}$, were observed to

---

* The capacity measurements of Kolotyrkin and Bune (31), with lead in acid solutions containing perchlorate, sulphate, or halide anions, show that the characteristically large increase in capacity of the anodic branch occurs at much less negative potentials in perchloric acid than in any other system. This is taken to indicate much weaker interaction of ClO_4^- with the metal than that of other anions.

decrease continuously at constant current during several weeks. Tafel plots initially exhibited bilinearity like those of Tordesillas and Bicelli (20), the slope at low current densities being 0.2 - 0.3 V., but after a few hours of cathodisation the plots became reasonably linear over a wide (1000 fold) current range. Together with the decrease of overvoltage, the slope of the main line was also observed to undergo a continuous decrease from 0.130 ± 0.010 V. initially, to 0.075 ± 0.010 V. after some days. The observations have been interpreted on the basis of an increasing surface coverage of the metal with hydrogen atoms in the course of cathodisation, in parallel with an assumed continuously increasing bulk concentration of atomic hydrogen. This idea was supported by the linear relations found between the overvoltage and the logarithm of total charge passed in cathodisation. Further evidence in support of this explanation is provided by the observation of reversible hysteresis phenomena in overvoltage measurements in which changes between currents were only made after a steady state had been established at one current. The long times required for the establishment of the steady states are consistent with bulk diffusion of hydrogen atoms to and from the surface. Bagotskaya and Oshe (28) also have observed similar effects at fairly high current densities with lead-(or mercury)coated iron cathodes, through which hydrogen atoms were diffused from the opposite face.

B. Double-Layer Capacity Measurements on Lead

Using an a.c. method, Borisova and Ershler et al.(29, 30) found that drop-like lead electrodes (in order to eliminate the frequency dispersion caused by irregular distribution of the current) had differential capacity versus potential curves like mercury with a flat minimum $C_{min.} = 25\mu F.\ cm.^{-2}$ in potassium chloride or sulphuric acid.

The capacity C determined for porous lead electrodes from potential decay curves by Kolotyrkin (10) was a function of the slowly established electrode steady state, increasing by 33% as the potential decreased from -0.6 to -0.8 V. However, on smooth lead electrodes, Kolotyrkin et al. found (12, 31) the value of $C = 18\text{-}20\mu F.\ cm.^{-2}$ at -1.0 V. Although specific adsorption of anions on mercury leads to a decrease in overvoltage and an increase in double-layer capacity, specific adsorption on lead (12, 31) is more complicated, leading either to a decrease or an increase in these quantities. In the case of lead, the decrease of double layer capacity was accounted for by assuming that the anions are more strongly bound than by coulombic forces alone. They are thus unable to respond to a.c. fluctuations during the differential capacity determination. It was suggested by Kolotyrkin that this *increases the distance between the effective planes of the double layer*, thus decreasing the capacity.

Ruetschi, Ockerman and Amlie (32) with porous lead and Brodd and Hackerman (33) with lead wire electrodes, measured double-layer capacities by the method of charging curves (33a). Ruetschi et al. found $11\mu F.cm.^{-2}$ for electrodes in 10 N H_2SO_4, while Brodd and Hackerman obtained a result of $52.5\mu F.\ cm.^{-2}$, in a 2 N sodium sulphate solution.

Palm and Past (34, 35) confirmed the absence of a 'pseudo-capacity' for the cases of lead in 1 N HCl, 1 N H_2SO_4 and 0.13 N $HClO_4$. The term 'pseudo-capacity' is used because it acts electrically as though it were a capacity. But, again, it is not a capacity, because the latter holds the charge which is added to it, whereas in a pseudo-capacity the charge leaks out across the double layer. In the present case, a 'pseudo-capacity' could arise from the discharge of hydrogen ions across the ionic double layer producing adsorbed hydrogen atom intermediates. The electrode capacity was 12.5 - 16 μF. cm.$^{-2}$ of apparent surface area (this value being reasonable for double layer alone) and was independent of both potential and time of cathodisation. Also, Palm and Past observed no accumulation of electrochemically active hydrogen on lead in alkaline solution (36, 37). However, they attributed the larger capacity of 18 μF. cm.$^{-2}$ in potassium hydroxide solution to the penetration of potassium into the cathode's crystal lattice.

Rybalka et al. (38, 39) recently studied the structure of the electrical double layer on a lead electrode, measuring the differential capaticance using an a.c. bridge method. In particular they studied the effects of anion and cation adsorption on lead. At sufficiently negative potentials ($\lesssim$ -1.0 V.) the structure of the double layer on lead, as in the case of mercury, was found to be independent of the nature of the ion. Rybalka et al.'s value of C was 18 μF. cm.$^{-2}$, in the absence of specific adsorption.

Carr et al. have also studied the differential capacitance of lead in aqueous H_2SO_4, H_3PO_4, HNO_3, KNO_3 (39a) and NaOH (39b) by the a.c. method. The observed capacity values at -1.1 V. lay between 14 - 22 μF. cm.$^{-2}$ at solute concentrations of 0.017 M (and a.c. frequency of 1000 Hz) and the capacities decreased with decrease of concentration. They also observed an initial instability in the measured capacity values in acid solutions, i.e. the capacity decreased with time (capacity of Pb in 0.0041 M sulphuric acid at -1.1 V. decreased from 18 to 14 μF. cm.$^{-2}$ in one hour). These changes were attributed to the specific adsorption of anions, in accordance with the earlier explanation of Kolotyrkin (12, 31).

C. Cathodic Disintegration of Lead

Two groups, those of van Muylder and Pourbaix (40) and of Salzberg and Gastwirt (41, 42) have obtained complementary evidence supporting the 'hydride' theory of 'cathodic disintegration'. Whereas Pourbaix et al. made only current and potential measurements, Salzberg measured the weight losses of lead cathodes resulting from the passage of known quantities of electricity. Ives and Smith (26) have also obtained evidence for 'cathodic disintegration' in 0.1 N $HClO_4$ at current densities $\lesssim$ 10 mA. cm.$^{-2}$ after sufficient time had elapsed for the supposed accumulation of discharged hydrogen atoms in the bulk of the metal.

The subject of ' cathodic disintegration' is still controversial. Kabanov et al. (43, 44) recently examined lead in alkaline solution and observed the cathodic incorporation of alkali metals into the metal. The initial incorporation rate was low, but increased when the electrode 'develops'. The incorporation rate is determined by the number of vacancies in the crystal lattice of the electrode metal near the surface.

Angerstein (45), whose experiments were limited to a maximum current density of 0.1 A. cm.$^{-2}$, failed to obtain 'cathodic disintegration' in 0.1 and 1 N solution of sulphuric acid free from metal cations. She also found that the potential of the beginning of disintegration varied with the cation (Na^+, K^+, Mg^{++}, Al^{+++}, NH_4^+ and Li^+), which she considered to be evidence in favour of 'the alkali metal alloy' hypothesis, i.e. cathodic incorporation of alkali metals. However, Bockris and Srinivasan (25) observed the presence of colloidal lead in alkaline solution at current densities of 10 mA. cm.$^{-2}$, presumably the result of cathodic disintegration.

D. Interaction of Hydrogen with Lead

Ives and Smith (26, 27) found that the cathodic hydrogen overvoltage at lead cathodes in acid solution decreased linearly with $\log_{10}(-Q)$, where -Q is the total charge passed during extended cathodic electrolysis. To account for this remarkable effect, they proposed that H atoms were being continuously adsorbed (or absorbed) by the lead and that in some way these catalysed the hydronium ion discharge step

$$H_3O^+_{aq.} + e^- + Pb \rightleftharpoons H_2O + Pb\text{-}H_{ads.} \quad (1.4)$$

This idea contradicts the assumption usually made in theories of hydrogen electrode kinetics that discharge of hydronium ions occurs only at empty sites, with the ion + atom reaction

$$H_3O^+_{aq.} + e^- + Pb\text{-}H_{ads.} \rightleftharpoons Pb + H_2 + H_2O \quad (1.5)$$

occurring on hydrogen-covered sites. Reasons advanced to account for this effect were (a) specific adsorption of hydronium ions, and (b) an increase in surface electron density arising from the presence in the lattice of 'metallic' hydrogen.

The argument of Ives and Smith (26, 27) for hydrogen entry into the lead lattice was based largely on grounds of plausibility, although some earlier (46) and some recent work (47, 48) was unfavourable to this hypothesis. Lead is not one of the metals listed by Barrer (49) as being able to dissolve hydrogen appreciably. This is almost certainly because the experimental method involved exposure to H_2, which would be incapable of dissolution without previous dissociation (50). Exposure to H atoms would not suffer from this drawback.

Roberts et al. (51, 118), however, have observed that evaporated and sintered films of lead take up atomic hydrogen at 0°C, reaching a composition of $PbH_{0.2}$ (or $PbH_{0.22}$ at -78°C). Phases richer in hydrogen desorbed H_2 with an activation energy for desorption of 16-20 k.cal.mole $^{-1}$, which they associated with a slow diffusion process (although recombination might have been rate limiting). Aside from early inconclusive work (52, 53), this was the first evidence for the existence of a lead hydride other than the transient PbH_4 (54). PbH_2 had been suggested as an intermediate in cathodic disintegration by Salzberg (41, 42), but not confirmed.

E. Objectives of the Present Work

The absence of evidence for a pseudo-capacity due to adsorbed hydrogen on Pb or diffusion of H atoms produced during electrolysis through Pb made it rather difficult to accept the ideas of Ives and Smith (26, 27). Systematic work in this field was needed in order to explain the observations of Ives and Smith (26, 27). It is the aim of the present work to study the electrolytic hydrogen evolution and the related adsorption and absorption of atomic hydrogen by lead in perchloric acid under the cleanest attainable experimental conditions. Special attention is paid to stringent deoxygenation, for it is thought that only under such conditions can the phenomena of hydrogen adsorption and absorption be studied. Adsorbed hydrogen is known to influence the rates of hydrogen reactions, whereas the effect of absorbed hydrogen in metals has only recently begun to be studied and is less well understood.

The present investigation was begun with the objects of
(a) confirming the work of Ives and Smith (26, 27), and
(b) making electrode capacity measurements on lead in aqueous perchloric

acid specifically to search for a hydrogen pseudo-capacity.

As the present work was in progress, Muju and Smith (55) found the over-all separation factor for cathodic discharge and diffusion through a lead foil polarised anodically on the opposite face to be anomalously less than unity. Exploration of this problem indicated the desirability of giving closer attention to the H-T separation factor on lead in perchloric acid. Both Bockris and Srinivasan (25), and Krishtalik and Tsionsky (56) found the H-T separation factor $S_{H,T} \simeq 7$ for cathodic gas evolution at lead in acid solution. The present work was then extended to measure simultaneously for the first time the H-T separation factors on the cathode and diffusion sides on lead membranes.

2. THEORETICAL BACKGROUND

A. Hydrogen Overvoltage Theory

Although the study of the hydrogen evolution reaction (h.e.r.) dates from the beginning of the century, all sorts of reaction steps have been proposed as part of the overall process; however, only two reaction paths involving three possible steps are regarded as likely. In acid medium, the discharge of H_3O^+ ions to H_2 molecules may occur through the following partial reactions:

Discharge (Volmer)	$H_3O^+_{aq.} + e^- + M \rightleftharpoons H_2O + M\text{-}H_{ads.}$	(2.1)
Combination (Tafel)	$M\text{-}H_{ads.} + M\text{-}H_{ads.} \rightleftharpoons 2M + H_2$	(2.2)
Ion + Atom (Heyrovsky)	$H_3O^+_{aq.} + M\text{-}H_{ads.} + e^- \rightleftharpoons H_2O + M + H_2$	(2.3)

Hydrogen evolution may occur by two routes which are (2.1) followed by (2.2):

$$2H^+_{aq.} + 2e^- + 2M \rightleftharpoons 2M\text{-}H_{ads.} \rightleftharpoons H_2 + 2M$$

or (2.1) followed by (2.3):

$$2H^+_{aq.} + 2e^- + M \rightleftharpoons M\text{-}H_{ads.} + H^+_{aq.} + e^- \rightleftharpoons M + H_2$$

In multistep consecutive reactions, the rate determining step (r.d.s.) controls the overall reaction rate. The condition for the existence of a single r.d.s. is that the activated state corresponding to the r.d.s. is higher in free energy* with respect to the initial state for the overall reaction than the activated state corresponding to any other step. However, if two steps have almost equal energies

---

* By 2.73 $k.cal.mole^{-1}$ for a hundred fold decrease in rate at 25°C

of activation, the two steps will exercise dual control over the rate of overall reaction and then the overall reaction is said to have a dual mechanism. Earlier, while considering the mechanism of multistep consecutive reactions, steps other than the r.d.s. were considered to be in quasi-equilibrium or of having negligible backward velocities in comparison with their forward velocities. Under the latter conditions, the overall reaction is said to be a coupled reaction. In a simple unbranched consecutive reaction, all steps must proceed at the same net velocity in the steady state, otherwise the surface coverage of the intermediate will change continuously before reaching a steady state.

(1) Types of Overvoltage

Overvoltage may arise from a number of causes, each of which may effect a retardation of the overall process. Depending on the origin, over-voltage can be divided into a number of additive (57) parts as follows:

Charge-Transfer Overvoltage, η_t, arises from a barrier to charge-transfer across the electrode-electrolyte interface, e.g. reactions (2.1) and (2.3). Much of the more detailed and advanced theoretical treatments of the h.e.r. have been concerned with the proton discharge step - not surprising, perhaps, since the balance of opinion (of the Frumkin School....and the Bockris School) over the past one or two decades has favoured it as the most probable rate-controlling step for discharge of hydrogen ions at high overvoltage metals {Zn, Cd, Pb, Hg, Tl, etc.} (86,88,88a). Charge-transfer overvoltage will be considered in detail in Section 2A (111).

Reaction Overvoltage, η_r, originates from a slow chemical reaction producing a reactant or removing a product of the charge-transfer step, which is indirectly retarded because of depletion or accumulation of reactants or products, respectively, e.g. reaction (2.2).

A b value of 0.029 V. at 25°C for the slow surface recombination step was originally advocated by Tafel (1). Many subsequent investigators (58,59,60) supported the view that the slow recombination of chemisorbed hydrogen atoms is the most likely rate-controlling step on catalytically active metals such as Pt, Au, etc. However, this view has been criticised by Knorr (65a), Ives (61) and Lewis (62). Ives finds it hard to concede the view that at Pt electrodes atom recombination is very fast, but is rate limiting, while at Hg it is very slow but is not rate limiting. Lewis, inspired by the work of Kandler, Knorr and Schwitzer (63) stressed the importance of mass-transport overvoltage, η_m, due to retarded diffusion of hydrogen molecules from the cathode (Pt and Pd in strongly acidic solution) surface. This will be discussed later.

Even if η_m is absent and the Tafel step is rate limiting, the equation relating overvoltage to current density must include a term arising from the possible contribution to the kinetics of the reverse step (2.2) at catalytically active metals (Pt, Au, etc.). The Hammett (64) and Knorr and Schwartz (65) treatment of retarded recombination takes this factor into account. The electrode potential, E, is related to the H atom surface coverage, θ, and hence to the rates of forward and backward reactions (2.2), the coverage, θ_e, at the equilibrium electrode potential, E_e, being determined solely by the atomisation-combination equilibrium with H_2, catalysed by the metal. The rates of atomisation and recombination are assumed independent of electrode potential. On the assumption that the surface recombination step is slow and rate-determining, (2.1) at equilibrium, (2.3) inoperative and mass transport hindrance negligible, they write

$$\eta_r = \frac{RT}{F} \ln\left(\frac{\theta}{\theta_e}\right) \qquad (2.4)$$

If the exchange current density of the supposed bimolecular recombination step,

$$i''_0 = 2Fk''\theta_e^2 \qquad (2.5)$$

where k" is the Tafel reaction rate constant, then at a cathodic current density -i, the hydrogen atom coverage may be greater because of the increased supply of hydrogen atoms and

$$(i''_0 - i) = 2Fk''\theta^2 \qquad (2.6)$$

On substitution of (2.5) and (2.6) in (2.4) we get

$$\eta_r = \frac{RT}{2F} \ln\left(1 - \frac{i}{i''_0}\right) \qquad (2.7)$$

A plot of η versus $\log_{10}\left(1 - \frac{i}{i''_0}\right)$ would give a straight line of slope 0.029 V. at 25°C. A plot of η versus $\log_{10}(-i)$ would be curved, but would yield a straight line with a slope of 0.029 V. at 25°C for $-i >> i''_0$, i.e. at high cathodic current densities {back reaction (2.2) is then negligible}.

Pure reaction overvoltage due to slow recombination (2.2) in h.e.r. is likely at Au and Pt cathodes of <u>low activity</u> because of the low H atom surface coverages (i.e. low exchange current density i_0'').

<u>Mass-Transport or Diffusion Overvoltage</u>, η_m, occurs when a slow <u>transport process</u> is responsible for depletion or accumulation of reactants or products, respectively, once again resulting in indirect retardation of charge transfer.

e.g. $H_3O^+_{aq.}$ (bulk solution) $\rightleftharpoons$ $H_3O^+_{aq.}$ (interface) and

H_2(surface) $\rightleftharpoons$ H_2(bulk).

Mass transport hindrance plays an important role in the h.e.r. at catalytically active metals such as Pt, Ir, Rh and Pd (62) where the rate of hydrogen ion discharge or hydrogen generation can be significantly greater than the rate at which H_2 is transported to or from the electrode.

The transport of H_3O^+ ions from the bulk solution to the electrode double layer is sometimes rate determining at pH $\geqslant$ 3 at quite small -i and at lower pH at sufficiently high -i. However, in the case of 0.1M and 1M acid solutions, calculated values of η_m (27,66) are less than 0.004 V. up to $-i = 50\text{mA.cm.}^{-2}$ (the maximum current density of the present work). Even though it does not seem possible to eliminate η_m entirely by extremely vigorous stirring of the catholyte, the contribution of η_m to the total apparent overvoltage can be made very small.

Control of evolution of hydrogen by transport through the solution implies that the surface of the electrodes are sufficiently catalytically active for the rate of combination of chemisorbed hydrogen atoms to proceed more rapidly than the transport step. Then, it is possible to write two equations (using Fick's first law of diffusion), one for hydrogen-saturated catholytes,

$$\eta_m = \frac{RT}{2F} \ln \left(\frac{i_0' - i}{i_0'}\right) \qquad (2.8)$$

and the other for inert gas-saturated catholytes,

$$\eta_m = \frac{RT}{2F} \ln \left(- \frac{i}{i_0'}\right) \qquad (2.9)$$

where i_0' is the exchange current density associated with transport control. The exchange current density i_0' depends on the diffusion coefficient of H_2 molecules in the solution, the thickness of the diffusion layer and the concentration of the hydrogen molecules at the surface of the reference electrode. Equation (2.8) is identical in form to η_r in (2.7). Provided that the hypothesis of diffusion control is correct, and the stirring conditions are the same in both hydrogen-saturated and inert gas (N_2, He, Ar)-saturated solutions (so that the thickness of the diffusion layer is the same), the plot of $\log_{10}(-i + i_0')$ versus η in hydrogen-saturated catholyte should be coincident with that of η versus $\log_{10}(-i)$ in an inert gas-saturated solution, and both should have a slope of $\frac{RT}{2F}$, i.e. 0.029 V. at 25°C. Kandler et al. (63) obtained at $-\eta$ up to

$\approx$ 15 mV., a good correlation in terms of equations (2.8) and (2.9) between the results in hydrogen-saturated and nitrogen-saturated catholytes at activated Pt and Pd cathodes.

<u>I.R. Drop Overvoltage</u>,* η_Ω, a term representing a potential drop between the reference electrode and the cathode, which is a function of the effective electrical resistance between these electrodes, and of the current flowing between the cathode and the anode during electrolysis. It follows that η_Ω will be reduced by placing the reference electrode (or generally the tip of a connection to it, designated a Luggin capillary) close to the cathode but this will not reduce the effect of a high resistance film on the surface of the cathode. Oscilloscopic techniques have been developed to measure the open-circuit electrode potential immediately subsequent to the interruption of electrolysis. This overvoltage will be exclusive of η_Ω.

Thus the total apparent overvoltage, $\eta_{app.}$, is the sum of individual overvoltages; i.e.,

$$\eta_{app.} = \eta_t + \eta_r + \eta_m + \eta_\Omega \qquad (2.10)$$

Charge-transfer overvoltage is frequently called 'activation overvoltage', however, this expression is ambiguous as noted by

---

* There have been criticisms of considering η_Ω as a true overvoltage term but it provides a convenient mode of description.

Vetter, because partial control of an electrode process by a chemical reaction also corresponds to an <u>activation</u> process associated with a significant activation energy.

(ii) <u>The Electrical Double Layer</u>

Electrochemical processes occurring at electrodes are affected by the structure of the region <u>in</u> and <u>near</u> the electrode-electrolyte <u>interphase</u> - generally known as 'the electrical double layer'. Because an electrode can exchange charged particles with the electrolyte, charges of opposite sign will normally be accumulated near the electrode-electrolyte interface, leading to the development of a potential difference across the electrode-electrolyte interface.

Using this simple idea, Helmholtz (67) gave the first model of the double layer. He proposed that the surface is a monomolecular layer of ions of opposite sign to the charge existing on the electrode and the electrical potential changes sharply from its value in the electrode to that at the centre of the ionic layer. The model advocated independently by Gouy (68) and by Chapman (69) was an extension of Helmholtz's model. The Gouy-Chapman theory leads to a Debye-Huckel ionic atmosphere type of distribution with the potential falling more gradually through the diffuse layer.

The Gouy-Chapman theory is not very suitable for the case of real ions and Stern (70) suggested that a satisfactory theory of the double layer must take into account both the finite size of the ions adsorbed and any specific chemisorption interaction they may suffer with the electrode surface. He considered that in the case of, e.g. a negatively charged surface, a layer of positive ions is held at the interface by chemisorptive or electrostatic attractions. The double-layer region from the surface to the centre of the first layer of positive ions may be referred to as the compact double layer; there is a sharp potential drop in the compact part of the double layer. Outside the compact layer, there is a diffuse layer over which the potential drops gradually to that in the bulk of the solution.

Subsequent to Stern's work there have been a number of further proposals which refine the model in various details. Strong specific adsorption (specific adsorption appears to have a chemical as distinct from electrostatic origin, dependent on the nature of the metal and ions involved) of, in particular, halide ions, led Grahame (71) to modify Stern's model. Grahame distinguished two different planes, one for specifically adsorbed ions and the other for hydrated ions, which are not specifically adsorbed (see Fig. 1a). In the case illustrated of positive polarisation of the metal, there is a change in potential from the electrode of potential ϕ, to the plane corresponding to the centres of a layer of specifically adsorbed ions (the inner Helmholtz plane). Then, there is a further drop to the plane corresponding to the centres of the layer of hydrated ions (outer Helmholtz plane or Gouy plane). Finally, there is a drop in potential to that of the bulk

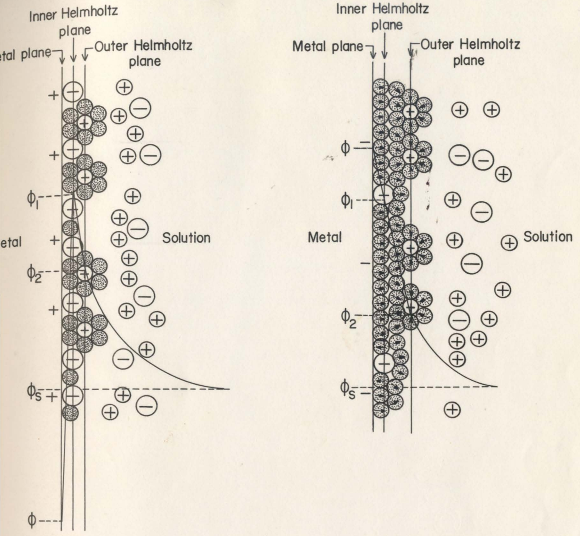

(a) (b)

Fig. I. Double – layer models : (a) according to Grahame, with positive polarisation of the metal, (b) according to Devanathan, Bockris and Muller with negative polarisation of the metal. + and – represent net positive and negative charges on the metal. ⊕ and ⊖ represent cation and anion, respectively. ● represents water molecule. ◉ represents oriented water dipole. ϕ , ϕ_1, ϕ_2 and ϕ_s are inner potential of electrode metal, potential in the inner Helmholtz plane, potential in the outer Helmholtz plane and inner potential of the bulk of solution, respectively.

of the solution ϕ_s, over the diffuse layer.

Grahame assumed that the specific adsorption is due to the formation of a covalent bond superimposed upon electrostatic interactions. He supported his assumption with the linear relationship between the differential capacity of Hg at the limit of positive potentials at which measurements can be made for various anions in the solution and the logarithm of the mercurous ion concentration* in aqueous solutions of salts corresponding to those anions. Comparison of the bond strengths (bond strength decreases in the anion series F^- to I^-) for mercury halides with the adsorbability (adsorbability increases in the anion series F^- to I^-) does not support this mechanism.**

Later, Levine, Bell and Calvert (72) suggested image energy resulting from image forces-interaction between the test (the adsorbed ion) and induced charges as the origin of specific adsorption in contrast with Grahame's view. Image energy can be calculated by considering that the electrode is replaced by an image charge (equal in magnitude and opposite in sign to the test charge) situated as far behind the plane corresponding to the metal

---

* The concentration of the mercurous ion, Hg_2^{++} was computed in a solution saturated with the appropriate mercurous salt. The results were converted to a negative logarithm scale like pH and called pHg.

** However, the hydration enthalpies increase in the order $F^- > Cl^- > Br^- > I^-$. This suggests that the adsorption must be the net effect of bond energy and solvation factors. The model of Bockris et al. (73), which takes account of solvation factors, will be discussed shortly.

surface as the test charge is in front of it.

Bockris, Devanathan and Muller (73) pointed out that image energy cannot be the sole origin of specific adsorption, because this would show a radius dependence of specific adsorption and such dependence is negligible. Also, specific adsorption is not restricted to anions, sufficiently large cations showing similar phenomena. Moreover, they advocated the degree and type of ionic hydration as the principal factor which determines specific adsorption.
Fig. 1b shows their model of a layer of adsorbed solvent molecules at the electrode surface held by charge-dipole forces. If the ions have sufficiently stable primary hydration shells (those which are associated during transport with a definite number of water molecules), they remain in the <u>outer layer</u>, and are not specifically adsorbed. Such adsorption may be called <u>equivalent</u> (equal charges on the electrode and in the solution part of the double layer). The plane drawn through the locus of centres of this layer of ions is referred to as the outer Helmholtz plane (Gouy plane), of potential ϕ_2. If the ions possess no primary hydration water, they can gain energy by replacing the surrounding water dielectric with the (infinite) dielectric constant of the metal and move out of the solution into contact with the metal: such an adsorption is termed <u>superequivalent</u> adsorption. The plane drawn through the locus of the centres of this layer of ions is referred to as the inner Helmholtz plane, of potential ϕ_1. In superequivalent adsorption, the charge on the metal is overcompensated so that the net

charges carried by inner and outer layers become opposite in sign. Outside the Gouy plane, there is a further drop of potential from ϕ_2 to the potential in the bulk of the solution. The ability for superequivalent adsorption increases in the anion series F^- to I^- and in the cation series (less markedly) Li^+ to Cs^+, respectively. The interpretation of Bockris et al. (73) was put in more quantitative terms by Andersen and Bockris (74).

Even though the theory of Bockris, Devanathan and Muller (73) gives a reasonable explanation of many of the previous anomalies, modification is desirable in particular cases; e.g. the role of the orientation of adsorbed dipoles of water and organic molecules at the electrode-electrolyte interface (75).

(111) Charge-Transfer Steps in the h.e.r.

The transfer of charge across the electrified interface consists essentially of the exchange of electrons between the electrode and particles on the solution side of the interface and such charge-transfer proceeds at rates slower than electronic transitions within the ions or molecules involved, probably because of slow solvent reorganisation. Reactions (2.1) and (2.3), previously considered in Section 2A, are important charge-transfer steps in the h.e.r. in acid solutions.

The foundations of the subject were laid in particular by Butler (76), Gurney (77), Frumkin (78), Volmer and Erdey-Gruz (79), Horiuti and Polanyi (80). According to Bockris and Matthews (81), tunnelling is possible only if the proton-water bond stretches until the electron can be accepted into a vacant state in the hydrated hydrogen ion.

Dogonadze, Kuznetsov and Levich (82, 83, 84) recently pointed out, however, that activation by the Horiuti et al. (80) model, i.e. by stretching of the covalent O-H bond, is extremely unlikely due to its large vibrational quanta so that the quantum nature of proton behaviour at ordinary temperature cannot be described by a quasi-classical approximation. In contrast to the case of heavy nuclei, both e^- and H^+ are thought to undergo quantum-mechanical jumps from the initial state (e^- in metal + H_3O^+ in solution) to the final state (adsorbed H atom + H_2O molecule) at constant energy only when a favourable solvent configuration, corresponding to the same energy value of initial and final states is attained. Solvent reorganisation, without preliminary stretching of O-H bond, is suggested as the source of the activation barrier.

However, Matthews (85) advocates that the rate-determining step and reaction path remain the same, but the mode of achieving electron tunnelling may vary with the potential, e.g. bond bending, bond stretching, stretching of different bonds or solvent libration etc. According to him, at any potential, the favoured mode will be that which tends to give the value of symmetry factor of 0.5 to satisfy the electron tunnelling condition (i.e. minimum activation energy which is related to symmetry factor) and microscopic reversibility of charge transfer reaction. Similar opinions can be found in recent text books (86, 87).

The electric field which results from the electrical double layer influences the h.e.r. rate due to (a) its influence on the concentration of H_3O^+ ions at the pre-electrode state and (b) its influence on the activation energy of the charge-transfer step. The pre-electrode state, of potential ϕ^*, is thought to be located at the outer Helmholtz plane (i.e. $\phi^* = \phi_2$) or, if the hydrogen ion is specifically adsorbed or if the reactant is a water molecule, at the inner Helmholtz plane (i.e. $\phi^* = \phi_1$).

Let us first discuss the effect (a). Assuming equilibrium between the concentration of H_3O^+ ions at the pre-electrode state $C^*_{H_3O^+}$ and the bulk concentration of H_3O^+ ions, $C_{H_3O^+}$, and applying the Boltzmann Distribution Law, $C^*_{H_3O^+}$ can be written as

$$C^*_{H_3O^+} = C_{H_3O^+} \exp. \left(- \frac{F\phi^*}{RT}\right) \qquad (2.11)$$

where $F\phi^*$ is the electrical work required to transport a unit charge from the bulk solution to the pre-electrode state. If the $\underline{H_3O^+ \text{ ions}}$ are the only <u>cations</u> present in the solution, the Gouy-Chapman (68, 69) treatment leads to the conclusion that ϕ^* will vary with $C_{H_3O^+}$ as,

$$\phi^* = \phi^*_0 + \frac{RT}{F} \ln C_{H_3O^+} \qquad (2.12)$$

where ϕ^*_0 is a constant. The comparison of (2.11) and (2.12) shows

$C^*_{H_3O^+}$ independent of $C_{H_3O^+}$. This is convincingly verified in h.e.r. at Hg in pure acid of $C_{H_3O^+}$ up to 0.1 N (88).

Effect (b) will be considered in the ensuing discussion of charge-transfer in terms of transition state theory (89) which, while it may not be strictly correct (see above discussion), has formed the basis for all but the most recent model of the h.e.r. and is more easily comprehended than the proton and electron quantum-mechanical mechanism (82,83,84). The magnitude of ϕ^* varies slowly with electrode potential under experimental conditions in which a large excess of supporting electrolyte is used or the rate measurements are made at least 0.5 V. cathodic to potential of zero charge (90). In such a case, we can assume that the potential that is applied in excess of the reversible potential, i.e. the overvoltage, operates only across the region between the electrode and the pre-electrode state, not across the diffuse layer, in aiding or opposing charge-transfer across the interface.

The effect of electrode potential on the charge-transfer process can be studied by considering a simple potential energy diagram of the type used by Horiuti et al. (80) as shown in Fig. 2. The solid curve at the left shows the potential energy of the final state ($M\text{-}H_{ads.}$ + H_2O molecule) and the dashed curve at the right shows the potential energy of the initial state (H_3O^+ in solution + e^- in the metal) respectively, plotted against the distance from the electrode surface in the absence of electrical potential difference. On applying the electrical potential ϕ, the whole initial state curve is shifted up by an amount $(\phi^* - \phi)F$ to the solid right hand line and the activation energy for H_3O^+ discharge is lowered by an

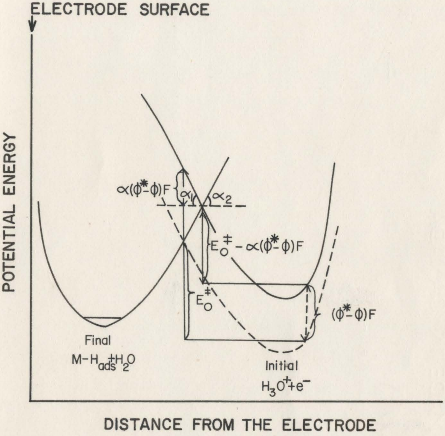

Fig. 2. Potential energy diagram for electrode reaction $H_3O^+_{aq.} + e^- + M = H_2O + M-H_{ads.}$ (2.1). The solid curve at the left and the dashed curve at the right represent the potential energy profiles of final and initial states, respectively, in the absence of electrical potential difference. The solid right hand curve represents the potential energy profile for initial state on applying the electrical potential

amount $\alpha(\phi^* - \phi)F$ respectively. Simultaneously, the activation energy for hydrogen ionisation increases by an amount $(1 - \alpha)(\phi^* - \phi)F$. Where $\alpha = \frac{\tan\alpha_1}{\tan\alpha_1 + \tan\alpha_2}$; α_1 and α_2 being angles of inclination of energy surfaces for $H_3O^+_{aq.}$ and $H_{ads.}$ (see Fig 2), respectively. α is a factor greater than zero but less than unity. Recent theories (81, 82, 83, 84) suggest the dependence of α, considered as a function of ε^*, the electron energy level making the main contribution to the total current on η

$$\alpha(\varepsilon^*) = 1/2 + (e\eta/2E_s) + \text{constant} \qquad (2.13)$$

where E_s is the reorganisation energy of the solvent (in the activation process) per electron transferred (82a). e is the charge on the electron. The constant term in equation (2.13) is very small.

With the concepts of absolute rate theory, the effect of electrochemical potential on activation energies; the <u>standard</u> <u>electrochemical</u> <u>free</u> <u>energy</u> <u>of</u> <u>activation</u> for forward $(\Delta\overline{G}^{\ddagger}_{-})$ and backward $(\Delta\overline{G}^{\ddagger}_{+})$ reaction can be discussed as follows:

Relative to a fixed final state curve ($H_{ads.}$ + H_2O molecule), shifting of the initial state (H_3O^+ in solution + e^- in metal) {see Fig. 2} favours the H_3O^+ ion discharge, the standard electrochemical free energy of activation of which becomes

$$\Delta\overline{G}^{\ddagger}_{-} = \Delta G^{\ddagger}_{-} - \alpha F\,(\phi^* - \phi) \qquad (2.14)$$

α being the cathodic transfer coefficient. Correspondingly, for ionisation of $H_{ads.}$ {backward step of (2.1)},

$$\Delta\bar{G}^{\ddagger}_{+} = \Delta G^{\ddagger}_{+} + (1 - \alpha)F(\phi^* - \phi) \qquad (2.15)$$

(1 - α) being the anodic transfer coefficient. Both $\Delta G^{\ddagger}_{-}$ and $\Delta G^{\ddagger}_{+}$ are standard (chemical) free energies of activation at zero electrical potential difference and depend on the chemical nature of the electrode and of the reaction.

Thus, the rates of the H_3O^+ discharge and ionisation of $H_{ads.}$ processes (2.1) can be expressed using modified activation energies and $C^*_{H_3O^+}$ at the pre-electrode state, in terms of partial current densities as,

$$i_{v-} = -k_{v-}F(1 - \theta)C^*_{H_3O^+} \exp.\left(\frac{\alpha_v F}{RT}(\phi^* - \phi)\right) \qquad (2.16)$$

and

$$i_{v+} = k_{v+}F\theta \exp.\left(-(1 - \alpha_v)\frac{F}{RT}(\phi^* - \phi)\right) \qquad (2.17)$$

where the rate constants k_{v-} and k_{v+} include $\frac{kT}{h}$ and the potential-independent parts of free activation energies, θ being the fractional coverage of $H_{ads.}$ atoms.

The corresponding partial current densities for the Heyrovsky reaction (2.3) are

$$i_{h^-} = -k_{h^-}FC^*_{H_3O^+}\,\theta \exp.\left(\frac{\alpha_h F}{RT}(\phi^* - \phi)\right) \qquad (2.18)$$

$$i_{h+} = k_{h+} F C_{H_2} (1 - \theta) \text{ exp. } \left(-(1 - \alpha_h) \frac{F}{RT} (\phi^* - \phi)\right) \qquad (2.19)$$

where k_{h-} and k_{h+} are appropriate rate constants including $\frac{kT}{h}$ and the potential-independent part of the free energy of activation, C_{H_2} is the concentration of the dissolved H_2 and α_h the transfer coefficient, not necessarily equal to α_v.

Parsons (91) showed that the exchange current density derived by equating $i_{v-} = i_{v+}$ and $i_{h-} = i_{h+}$ at the equilibrium potential, ϕ_e, is

$$i_0 = \left(\frac{kT}{h}\right) F C^{*\,1-\alpha}_{H_3O^+} \theta_e^{\alpha} (1 - \theta_e)^{1-\alpha} \text{ exp. } \left(-\{(1 - \alpha)\Delta G^{\ddagger}_{-} + \alpha \Delta G^{\ddagger}_{+}\} / RT\right) \qquad (2.20)$$

for both charge-transfer steps, where $\theta = \theta_e$ at ϕ_e. The i_0's have maximum values for both (2.1) and (2.3) when $\theta_e^{\alpha}(1 - \theta_e)^{1-\alpha}$ is a maximum (i.e. for $\theta_e = 0.5$, if $\alpha = 0.5$). For $\theta_e < 0.5$, step (2.1) will be faster than step (2.3) at any cathodic potential and conversely for $\theta_e > 0.5$. However, changes of θ with ϕ would, under these conditions, result in equal i_{v-} and i_{h-} at some potential, because θ would tend to 0.5 as $-\phi$ increases unless H desorption by some other route is possible. Parsons was able to show that i_0's should decrease both with decreasing and with increasing standard free energy of dissociative hydrogen adsorption $\Delta G^0_{H_2 ads.}$ ($2M + H_2(g) = 2M - H_{ads.}$) on the metal the maximum values of i_0 occurring at $\Delta G^0_{H_2 ads.} = 0$, for either of the two steps (2.1) and (2.3), and also for step (2.2), for which an expression similar to (2.20) was worked out.

Many workers (92,93) have attempted correlations of i_0 with various fundamental properties of the metal such as work function, atomic number, compressibility and heat of sublimation of the metal, etc. However, Kuhn, Mortimer, Bond and Lindley (94) recently concluded that such correlations as are found are probably due more to the general co-variation of <u>both</u> the electrocatalytic and the physical properties with periodic number than to any dependence of one on the other.

The net cathodic current density, $i = i_+ + i_-$, can be expressed in a simple form on the assumption that the variation of ϕ^* can be ignored (at least up to 1N pure acid solution) and $\theta \ll 1$ (for metals like Hg etc.) as

$$i = i_0 \left[\exp.\left(\frac{\{1 - \alpha\}\eta F}{RT}\right) - \exp. - \left(\frac{\alpha\eta F}{RT}\right) \right] \qquad (2.21)$$

For $|-\eta| \geq 0.1$ V., (2.21) becomes the Tafel equation,

$$-\eta = a - b \log_{10}(-i) \qquad (1.2)$$

where $b = \frac{2.303RT}{F}$. Plots $-\eta$ against $\log_{10}(-i)$ under the assumed conditions should be linear. The factor b = 0.116 V. at 25°C (if $\alpha = 0.5$) may be correlated with experimentally observed values of 0.12 V. Any deviation from the linear relationship of (1.2) may be explained by neglect of the ϕ-dependence of b and of the double-layer effects referred to above. Extrapolation of Tafel plots to η=0 in principle permits determination of i_0. This method, though not accurate, may be used for the determination of i_0 for many corrodible metals, for which experimental measurements are impossible close to ϕ_e.

(1V) Double-Layer Effects on Charge Transfer

The value of ϕ^* influences the rates of charge transfers because (a) the effective concentration of H_3O^+ ions (that at the pre-electrode state) is determined by ϕ^* and (b) the effective potential difference which enters into the activation energy is that between the electrode surface and the pre-electrode state, i.e. $\phi - \phi^*$. Although double-layer effects have been mentioned in Section A(111) of this chapter, the ϕ^* effect was ignored in the simple i-η relationship (2.21).

The current-potential relation (2.21) can, however, be rewritten with the ϕ^* term taken into account as

$$i = i_0^t \text{ exp.} \left(\frac{\{\alpha - 1\}\phi^* F}{RT}\right) \left[\text{exp.}\left(\frac{\{1 - \alpha\}\eta F}{RT}\right) - \text{exp.} -\left(\frac{\alpha\eta F}{RT}\right)\right] \tag{2.22}$$

where the true exchange current density i_0^t is equal to $i_- = i_+$ at the equilibrium potential, ϕ_e, i.e. in the absence of double-layer effects, setting $\phi^* = 0$. The measured exchange current density is related to i_0^t as

$$i_0 = i_0^t \exp.\left(\frac{\{\alpha - 1\}\phi^*F}{RT}\right) \qquad (2.23)$$

Since ϕ^* varies with the electrode potential and the concentration of ions in the solution, it is clear from (2.22) that kinetic parameters obtained from polarisation curves using relation (2.21) alone will be erroneous to varying extents. Therefore, in quoting accurate electrode kinetic data one must take into account ϕ^* effects.

The importance of the structure of the double layer for the quantitative interpretation of the H_3O^+ ion discharge on Hg was first pointed out by Frumkin (78). Developments in this field have been reviewed by Frumkin (88), Parsons (105), Delahay (106) and Andersen (90).

The equation (2.22) was first used by Frumkin (88) to account for the independence of hydrogen overvoltage on acid concentration up to 0.1 N (as discussed in Section A(111) of this chapter).

In many experiments, during the study of the behaviour of metals in pure acid solutions, it is not possible to add supporting electrolytes. In other cases in which such an electrolyte is added, the results often depend strongly on the ionic components of the supporting electrolytes. In order to rationalise these effects and to obtain accurate kinetic information from raw data, the terms containing ϕ^* must be understood.

Let us consider the case in which there is no specific adsorption of supporting electrolyte; e.g. in Cl^- media, using a Hg electrode at $\phi < -1$ V. The change in overvoltage $\Delta\eta$ resulting from the change in $\Delta\phi^*$ is at constant current

$$\Delta\eta = \left(1 - \frac{1}{\alpha}\right)\Delta\phi^* \qquad (2.24)$$

In the absence of specific adsorption of supporting electrolyte, $\Delta\phi^*$ can be calculated from diffuse double-layer theory by equating $\phi^* = \phi_2$ (i.e. the pre-electrode state at the outer Helmholtz plane). Then, ϕ_2 can be calculated using Gouy-Chapman theory from the charge on the metal (q) for a Z-Z electrolyte as

$$\phi_2 = \frac{2RT}{ZF}\sinh^{-1}\left(\frac{q}{2A}\right) \qquad (2.25)$$

and

$$A = \left(\frac{\varepsilon RTC_{ion}}{2\Pi}\right)^{\frac{1}{2}}$$

where ε is the dielectric constant in the diffuse layer and C_{ion} is the concentration of cations or anions (for a solution containing Z-Z electrolyte, $C_{cation} = C_{anion}$) in the solution.

Thus, calculated values of $\Delta\phi^*$ can be used to test equations (2.24) and thereby (2.22) with experimental results. The overvoltage increase upon addition of KCl to HCl solution has been quantitatively verified by Bagozky (107) and by Maznichenko, Damaskin and Jofa (108).

A quantitative comparison of theory and experimental results in the absence of specific adsorption usually proceeds by calculating the ϕ^*-containing term in equation (2.22) using independently obtained ϕ^* ($= \phi_2$). Then, if corrected $-i$ versus $-\eta$ results are independent of the supporting electrolyte, it is assumed that double-layer effects are suitably accounted for and accurate kinetic parameters may be obtained by using equation (2.22).

Equation (2.22) can be written for the cathodic h.e.r. at $|-\eta| \geq 0.1$ V. in the form

$$-i \exp.\left(\frac{F\phi_2}{RT}\right) = i_0^t \exp.\left(\frac{\{\phi_2 - \eta\}\alpha F}{RT}\right) \qquad (2.26)$$

Here, ϕ^* is assumed to be equal to ϕ_2. Then, the true value of α may be obtained from the slope of a plot of $\log_{10}\left((-i) \exp.\left[\frac{F\phi_2}{RT}\right]\right)$ versus $(\phi_2 - \eta)$.

Similarly, true values of exchange current density, reaction orders, activation energy, stoichiometric number (88, 105, 106) must be evaluated taking into account changes in the potential ϕ^*

with changes in overvoltage or electrolyte concentration.

The theory of double-layer effects can be extended simply to systems where specific adsorption of supporting electrolyte occurs, if it is assumed that the pre-electrode state layer may still be identified with the outer Helmholtz plane. Then, for a Z-Z electrolyte

$$\phi_2 = \frac{2RT}{ZF}\sinh^{-1}\left(\frac{q + q_1}{2A}\right) \qquad (2.27)$$

where A is previously defined in equation (2.25) and q_1 is the specifically-adsorbed charge. Specific adsorption of cations makes ϕ_2 more <u>positive</u> and <u>decreases</u> the rate of reduction of H_3O^+ ions at a given cathodic overvoltage. On the other hand, specific adsorption of anions makes ϕ_2 more <u>negative</u> and <u>increases</u> the rate of reduction of H_3O^+ ions at a given cathodic overvoltage.

Specific adsorption of anions from the supporting electrolyte causes pronounced distortion of Tafel plots for H_3O^+ ion discharge on Hg as found by Jofa et al. (109,110). The effects of anion specific adsorption on Hg become important at overvoltages <u>more positive</u> than -1.0 V. and in this region, polarisation curves at a given overvoltage show an increase in current for the h.e.r. on Hg in the sequence $Cl^- < Br^- < I^-$. Quantitative interpretation is still tentative and has been argued between Frumkin (88), Parsons (105, 111) and Krishtalik (112). In the presence of specifically adsorbed anions, Frumkin suggested that the charge centre of the activated complex for H_3O^+ discharge lies in a plane which is much nearer to the electrode than that in which the H_3O^+ ion centres are located. According to one approach used by him, it is the potential in the activated complex plane that figures as the ϕ^*-value in the equation (2.22)*. Therefore, the ϕ^* potential can assume greater negative values in presence of specific anion adsorption, significantly accelerating the H_3O^+ ion discharge. Parsons (111), however, suggested that the effect is not associated with ϕ^*, but is almost entirely due to a sharp decrease in the activity coefficient of the activated complex in the presence of halide ions. {Parsons wrote an expression for the rate constant of an electrochemical reaction using principles of absolute reaction rate theory (89):

$$k_r = (kT/h)(1/\gamma^{\ddagger}) \exp. (-\Delta G^{\ddagger}/kT) \qquad (2.27a)$$

where $\Delta G^{\ddagger}$ is the standard free energy of activation corresponding to some standard potential and $\gamma^{\ddagger}$ is the activity coefficient of the activated complex. The interaction between the activated complex and specifically adsorbed ions is expressed through the activity coefficient of the activated complex in equation (2.27a)}. This leads to a significant acceleration of H_3O^+ ion discharge.

---

[*] Here, Frumkin (88) identifies ϕ^*-plane with the <u>transition state</u> of the reaction rather than with the pre-electrode state of the ion in the double layer.

Recently, Krishtalik (112) criticised Parsons' view and supported Frumkin's earlier idea, but without the assumption of different potentials in the plane of location of discharging ions (ϕ_2) and activated complex (ϕ^*). {This view is in agreement with the quantum-mechanical theory of proton transfer of Dogonadze et al. (82,83), i.e. the activation process is due to solvent reorganisation with unchanged proton quantum state.} In order to explain his view, he advanced the idea that only the protons which are in <u>direct</u> contact with the electrode can discharge and this is only a small fraction of their total content in the double layer. Anion adsorption, he suggests, has a marked effect only on the concentration of <u>discharging ions</u> and hardly affects their total adsorption.

Another important factor that must be considered is the cation specific adsorption on Hg observed by Maznichenko et al. (108). They found that the overvoltage increase on addition of alkaline cations to pure HCl solution is larger than the $\Delta\eta$ value for Cs^+, i.e. $|\Delta\eta| > |\Delta\phi_2|$, but considerably smaller for Li^+, i.e. $|\Delta\eta| < |\Delta\phi_2|$.

Because double-layer theory is most thoroughly understood for the Hg electrode, quantitative treatments of coupled double-layer and kinetic phenomena apply mostly to mercury and to amalgams. The quantitative study of solid electrodes such as Pb is possible, if the charge on these metals is known as a function of potential such that ϕ^* can be calculated. Non-availability of ϕ^* data for Pb electrodes in perchloric acid limits us to the simple uncorrected Tafel equation (2.21). At this stage, we can stress the need for more fruitful studies of the double layer of solid electrodes.

(V) Temperature Dependence of Overvoltage

Temperature is another variable that controls the rate of the h.e.r. The influence of temperature on an electrode reaction can be studied either at constant current density or at constant potential. At constant current density the overvoltage usually decreases with rise of temperature. It is desirable to make measurements with the working electrode and the reference electrode at the same temperature. Otherwise some uncertainty is introduced into the results by thermo-electric potentials arising from the temperature difference between the working electrode and the reference electrode.

The enthalpy of activation at the equilibrium potential, $\Delta H^{\ddagger}_{\eta=0}$, is experimentally measured from the temperature dependence of the exchange current density, i_0. The result is only valid if i_0 is measured near the equilibrium potential.

For many corrodible metals such as lead, measurements close to the equilibrium potential are impossible. On such metals, the enthalpy of activation, $\Delta H^{\ddagger}_{\eta}$ at different constant overvoltages (205) are calculated using an expression

$$\log_{10}(-i) = -\frac{\Delta H^{\ddagger}_{\eta}}{2.303RT} + \text{constant} \qquad (2.28)$$

Therefore, the slope of the $\log_{10}(-i)$ versus $(1/T)$ plot at constant $-\eta$ should yield $\Delta H^{\ddagger}_{\eta}$. Then, the enthalpy of activation at the equilibrium potential, $\Delta H^{\ddagger}_{\eta=0}$, at $-\eta = 0$ may be calculated using the dependence

$$\Delta H^{\ddagger}_{\eta=0} = \Delta H^{\ddagger}_{\eta} + \alpha F(-\eta) \qquad (2.29)$$

where α is the cathodic transfer coefficient. The average transfer coefficient calculated from the Tafel slope as $(2.303RT/bF)$ is normally used.

The dependence of b on temperature is somewhat complicated for lead cathodes. For instance, Smith (27) has observed that the b value increased with increase of temperature on Pb in $HClO_4$. On the other hand, Lee's (206) results show a temperature-independent Tafel slope on Pb in KOH.

High values of $\Delta H^{\ddagger}_{\eta=0}$ (≥ 20 k.cal.g.ion^{-1}) are found with high overvoltage metals, e.g. $\Delta H^{\ddagger}_{\eta=0}$ values of 21.7 k.cal.g.ion^{-1} for Hg (112a) and 20 k.cal.g.ion^{-1} for Pb (22), respectively, in acid solution.

The enthalpy of activation calculated by the methods mentioned above may have a contribution from the temperature variation of the hydrogen coverage and of the double-layer effects which may be considerable. From a.c. impedance measurements on clean Pt, Breiter (112c) was able to show that the enthalpy of activation remained constant, ca. 5 k.cal.g.ion^{-1}, for $\theta < 0.7$ and then fell to about 2 k.cal.g.ion^{-1} at $\theta = 0.9$. To account for double-layer effects, detailed calculations, which follow directly from the theory of the diffuse layer {Section 2A (1V)}, by Parsons et al. (105,112d) led to the conclusion that the double-layer contribution to the enthalpy of activation can be very significant, even in 0.1 M solutions and in the absence of specific adsorption; when specific adsorption of tetra-alkylammonium cations occurred, the enthalpy of activation increased by tens of k.cal. for the V^{+++}/V^{++} redox reaction at Hg.

(V1) The Electrochemical Reaction Orders

The electrochemical reaction orders for a number of processes have been discussed by Vetter (57, 97), Conway and Salomon (98), and Enyo and Yokoyama (99). Since the electrochemical reaction order in electrochemistry is of the same importance as chemical reaction order in ordinary chemical kinetics, these values are helpful to understand the mechanism of h.e.r.

At constant electrode potential and at $\theta_H \approx 0$ the electrochemical reaction order for steps (2.1) and (2.3) of h.e.r. can be written as

$$z_{H_3O^+} = \left(\frac{d \ln(-i)}{d \ln C_{H_3O^+}}\right)_{\phi,\phi^*} \qquad (2.30)$$

i.e. the dependence of ln (rate) on ln $C_{H_3O^+}$. Thus, the electrochemical reaction order may be determined with respect to H_3O^+ ions in the bulk of the solution, but this usually requires the presence of an excess of supporting electrolyte to maintain ϕ^* constant while $C_{H_3O^+}$ is varied.

Only by evaluating the reaction order is a distinction possible between steps (2.1) and (2.3) involving H_3O^+ ions or steps (2.1) and (2.3) involving H_2O molecules at the electrodes, e.g. step (2.1) is probably r.d.s. for Hg, at pH < 8, $Z_{H_3O^+} = 1$ and at pH > 9, $Z_{H_3O^+} = 0$. Therefore, we can write for the step (2.1) the following equations

at pH < 8, $$H_3O^+_{aq.} + e^- + M \rightleftharpoons H_2O + M\text{-}H_{ads.} \qquad (2.1)$$

at pH > 9, $$H_2O + e^- + M \rightleftharpoons OH^- + M\text{-}H_{ads.} \qquad (2.31)$$

A second method, specifically suitable for fast reactions, is observation of the dependence of exchange current density on $C_{H_3O^+}$ ions. Then,

$$Z_{H_3O^+} - \alpha = \left(\frac{d \ln i_0}{d \ln C_{H_3O^+}} \right)_{\phi,\phi^*} \qquad (2.32)$$

and if α is known, we can determine the electrochemical reaction order from the concentration dependence of i_0. Again excess of supporting electrolyte must be present to minimise changes in ϕ^*.

For the h.e.r. on strongly adsorbing metals the situation is rather more complicated than at Hg because there is the possibility of large coverages with $H_{ads.}$ atoms and measured reaction orders may be misleading. If the step (2.3) is rate determining and the surface coverage of $H_{ads.}$ atoms is small,

$Z_{H_3O^+} = 2$. If the surface concentration of $H_{ads.}$ atoms approaches unity, however, $Z_{H_3O^+} = 1$, because of the saturation effect of $H_{ads.}$ atoms.

On the basis of kinetic considerations (having taken account of $H_{ads.}$ atoms), Conway and Salomon (98) have derived the values of electrochemical orders with respect to H_3O^+ ions for steps (2.1), (2.2) and (2.3), respectively, of the h.e.r. Many of them have the same dependence of current density upon H_3O^+ ions. Hence, reaction orders alone, like stoichiometric numbers alone, are not very useful in determining the reaction path of h.e.r.*

(V11) The Isotopic Separation Factors

Complementary information on the kinetics of the h.e.r. can be obtained through the study of isotope effects. The application of the isotopic separation factor to the h.e.r. was attempted as early as 1950 by Horiuti and Nakamura (100, 101) and later by Rome and Hiskey (102), Conway (103, 104), Bockris and Srinivasan (25), and Krishtalik and Tsionsky (56). If the isotopic

---

* Reaction order with respect to $H_{ads.}$ could also be evaluated if θ is measured.

effect is caused directly or indirectly by the mass differences of the isotopes (H:D:T = 1:2:3), the largest isotope effects are obtained with the hydrogen isotopes.

In aqueous solution containing T isotopes, the relative rates of H and T production can be characterised by the separation factor, $S_{H,T}$, defined by

$$S_{H,T} = \frac{\left(\dfrac{\frac{d(H)}{dt}}{\frac{d(T)}{dt}}\right)_2}{\left(\frac{(H)}{(T)}\right)_1} \qquad (2.33)$$

i.e. the ratio of the relative rates of generation of H- and T-containing species into phase 2 (e.g. gas or solution or metal) from phase 1 in which the total H and T concentrations are (H) and (T), respectively.

Isotopic separation factors will be further discussed in Section 2D(1).

B. Theory of Hydrogen Adsorption and Adsorption Pseudocapacitance

The study of hydrogen adsorption--a factor affecting the rate of the h.e.r.--is useful in evaluation of this process. During the h.e.r., adsorbed H atoms are produced and consumed. The surface concentration of H_{ads}. is thought to be potential dependent.

Information concerning the adsorption behaviour of hydrogen can be obtained from suitable kinetic studies involving measurements of the electrode capacity or surface coverage of the electrode by adsorbed hydrogen.

(1) Enthalpies of Adsorption of Hydrogen

It is generally supposed that the adsorbed hydrogen produced during H_3O^+ ion discharge in h.e.r. is chemisorbed on the metal. At the gas-solid interface, chemisorption of H atoms is usually associated with large exothermic enthalpies of adsorption in the range of 65-75 k.cal. $mole^{-1}$ at low coverage. In the presence of solvent molecules at electrodes, the magnitude of this energy might be expected to be diminished (113), but evidence exists to the contrary for Pt electrodes (113a). According to Breiter (113a) the magnitude of this energy depends on the nature of the ionic specific adsorption. Specific anion adsorption decreases the enthalpy of adsorption, while specific cation adsorption increases it.

Enthalpies of adsorption of hydrogen are known from gas phase H_2 adsorption studies on many transition metals generated as thin films in ultra-high vacua. Knowing $\Delta H_{H.ads.}$, the binding energies of adsorbed hydrogen atoms E(M-H) may be calculated from

$$E(M\text{-}H) = (51 + \tfrac{1}{2}\Delta H_{H.ads.})\ \text{k.cal. mole}^{-1} \qquad (2.34)$$

Thus, enthalpies for dissociative H_2 adsorption on clean metal surfaces (most of the values obtained on thin films generated in ultra-high vacuum) are expressible as binding energies E(M-H) of surface M-H bonds (116) as in Table 1.

Krishtalik (117) has estimated E(M-H) from h.e.r. data, mainly from i_0's obtained from the Tafel relationship, equation (2.20), and his results are listed in Table 1. The data in Table 1 are for negatively charged metal surfaces in sufficiently concentrated solution, so that the ϕ^* effects are relatively small, i.e. when the conditions correspond to those of calculation.

Agreement between the two sets of data is moderate, considering the experimental difficulties and simplifying assumptions of this approach. Doubtless, some discrepancies, e.g. Fe, Ni, Cu and Pb, are connected with the presence of oxide films on the electrode surface. Another difficulty is that $-\Delta H_{H.ads.}$ decreases markedly as θ increases with metals chemisorbing hydrogen strongly, e.g. on Fe, as θ increases from 0 to 1, $-\Delta H_{H.ads.}$ decreases by 19 k.cal. mole^{-1} (113).

Dissociative chemisorption can only occur on metals with E(M-H) $\gtrsim$ 51 k.cal. mole^{-1}. It cannot, therefore, be expected on metals such as Pb, Hg, Cd, Zn, Bi, Sn, In, Tl and Ga on which the enthalpy of chemisorption is positive, the entropy of adsorption probably being negative. Also, on these metals for which chemisorption is endothermic, desorption of H_2 often occurs at T $\gtrsim$ 195°K unless a bulk phase hydride is formed. This need not imply that H atoms are absent from these metals during the h.e.r., because in this case they are continuously supplied as atoms.

TABLE 1. BINDING ENERGIES OF HYDROGEN ADATOMS ON METALS $E(M\text{-}H)/k.cal.mole^{-1}$

Metal	Gas phase data (116, 117) {small θ}	Data from h.e.r. measurements (117)
Si	ca.80	
Ti	>75	80-85*
W	74-77.5	75*
Ta	74	>85*, >80*†
Cr	74.1	
Mo	71.5	73-76*
Fe	67.6-69.6	45-46**
Pd	65.5	
Pt	64.5	60***, 65-70*
Ni	64-72.5	45-49**
Co	64	46**
Ge	63	
Cu	56	43**
Al	56	
Ag	53	39.5**
Au	50	45-46**
Ga	<50	40**
Bi	<50	36**

TABLE 1 (Continued)

Metal	Gas phase data (116, 117) {small θ}	Data from h.e.r. measurements (117)
Zn	<50	33**
Sn	<50	33**
In	<50	30.5**
Cd	<50	28-29**
Hg	<50	29**
Tl	<50	26**
Pb	<50	26-27**

† Hydrogen saturated.

* Slow Heyrovsky desorption step (2.3) assumed.

** Slow Volmer discharge step (2.1) assumed.

*** Slow Tafel recombination step (2.2) assumed.

A reason why transition metals readily chemisorb gases whereas sp metals* do not, is that chemisorption probably requires specific interactions involving holes in the d band. Chemisorption directly from atomic hydrogen on sp metals does occur {e.g. on Pb, as found recently by Roberts and Young (118)} showing that holes in a d band are not necessarily required for atoms to be chemisorbed on metals. One has only to create conditions in which the metals are not required to break the H-H bond in the hydrogen molecule. A similar view may well be applicable to the electrolytic h.e.r. (119), where chemisorption results from an initial H_3O^+ ion discharge (2.1) in acid solution.

On the other hand, Trasatti (115) suggested that even though localised d orbitals may be present in the surface of metals, the possible promotion of electrons to or from the Fermi level makes the free energy of electrons always an important factor in the chemisorption process. Thus, the energy of electrons rather than their detailed configuration should be related to the behaviour of solid metals. In this respect, the density of electron states in the metal may be a relevant factor. The interpretation of electrochemical reactions on solid electrodes by application of solid state science is badly needed.

(11) The Adsorption Pseudo-Capacitance

Although the presence of $H_{ads.}$ atoms was realised earlier (120, 121), the existence of an adsorption pseudo-capacitance due to adsorbed H atoms was first predicted and demonstrated by Eucken and

---

* These are metals which have incompletely filled s and/or p orbitals but filled lower lying d orbitals.

Weblus (122). The term pseudo-capacitance was introduced by Grahame (123) to distinguish the capacitance arising from adsorption of intermediates (and from diffusion effects) from the strictly **non-faradaic capacitance** associated with the dependence of ionic and electronic charge in the double-layer on potential. Later, Bockris and Kita (124) extended the analysis and showed that an adsorption pseudo-capacity should be present, although not always measurable for any consecutive electrode process. Conway and Gileadi (125, 126) extended the analysis still further by use of Langmuir and Temkin adsorption isotherms.

The behaviour of the ionic distribution at an electrode-electrolyte interface as a function of electrode charge and potential was referred to (87) in terms of an ionic double-layer capacitance C (or more precisely in terms of a series combination of capacitances for the diffuse, inner and outer Helmholtz layers). C has a value of 17-20 μF.cm.$^{-2}$ on Hg at 25°C and varies slightly with potential and with the ionic solution concentrations.

Since adsorbed hydrogen atoms are produced from H_3O^+ ions by a charge-transfer process, the presence of these adsorbed intermediates on the surface is equivalent to the storage of electricity in the interface as in a condenser and the corresponding capacitance (pseudo-capacitance), C_{ps} behaves like an ordinary capacitance except that it may vary substantially (relative to the double-layer capacitance) with potential.

The electrochemical behaviour of the interface can be represented by an electrical analogue of the electrode-electrolyte system. Although many circuits have been suggested only two will be discussed here. The adsorption pseudo-capacitance, C_{ps}, must be charged up through the non-ohmic resistance,* R_1, corresponding to the reciprocal of the rate of H_3O^+ ion discharge step producing an $H_{ads.}$ atom. The series combination of C_{ps} and R_1 must be in parallel with C since they provide a leakage path across the double layer. Then, if recombination is the desorption step in the h.e.r., C_{ps} is also short-circuited by a non-ohmic resistance, R_2, {see Fig. 3a} which is the reciprocal of the rate of recombination. In the steady state, the current passes through R_1 and R_2 and is limited normally by R_2, if for the rate-controlling step, $R_2 >> R_1$. R_2 rapidly decreases with increasing negative potential and the charging process through R_1 becomes less and less efficient as a steady state is approached when, in the limit, the charging current is zero. The whole of the combination R_1, C_{ps} and R_2 is, as above, in parallel with C in the

---

* The resistances in this equivalent circuit are drawn (Fig. 3) in a special way to emphasize their non-ohmic character, which follows from the Tafel equation (1.2).

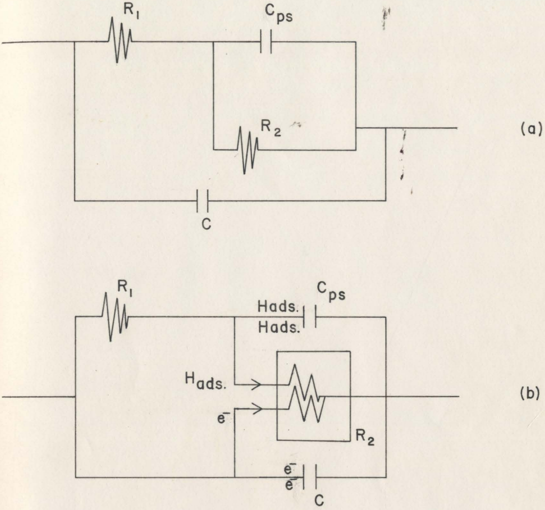

Fig. 3.

Equivalent circuit for adsorption pseudo - capacitance
(a) Volmer discharge with Tafel desorption step.
(b) Volmer discharge with Heyrovsky desorption step.
R – reaction resistance : R_1 for charging step and R_2 desorption step, respectively.

case of a non-ideally polarised* electrode. However, for Heyrovsky atom + ion desorption during the h.e.r., a special kind of representation as shown in Fig. 3(b) is necessary. The special representation of the reaction resistance has been introduced to indicate the separate origin of the electron from the metal and of H atoms from the adsorption pseudo-capacitance C_{ps}. Thus, the non-ohmic resistance, R_2, corresponding to the reciprocal rate of the Heyrovsky atom + ion desorption step is drawn with two parallel input channels, one for electrons and H_3O^+ ions and the other for the $H_{ads.}$ atoms removed as equivalent charge from C_{ps}.

(111) Open-Circuit Decay Measurements

The capacity-potential relationship has been determined by the following methods (a) geometrical differentiation of d.c. galvanostatic charging (127) or decay (128, 129) curves, (b) direct a.c. bridge capacitance studies (122, 130) and (c) by direct differentiation of charging or decay curves (131). The methods involving geometric differentiation rely on rather unsatisfactory manual differentiation procedures. Besides, one must account for the

---

* The characteristic of an ideal polarised electrode (139) is that there is no exchange of electric charge between the two phases. Consequently, the equilibrium set up at the electrode is electrostatic and mechanical, like that in a parallel plate condenser; but there is no chemical equilibrium between two phases, which have no component in common.

frequency dependence of capacity (down to low frequencies) in a.c. measurements and the rise-time dependence of the capacity in d.c. charging transients, in order to interpret the measured C_{ps} values from these methods. Direct differentiation of open-circuit decay curves is free from some of these disadvantages.

Conway, Gileadi and Angerstein-Kozlowska (132) advocated that any method based on the rate of decay of potential on open-circuit which will yield the equilibrium pseudo-capacitance, i.e. the value corresponding to extrapolation to zero a.c. frequency, is to be preferred. Therefore, a rapid open-circuit decay (direct differential galvanostatic method) is most suitable for studies of the potential-dependence of adsorption pseudo-capacities. This method is based on the assumption that the electrode reaction continues on open-circuit by a self-discharge* process which momentarily, at the commencement of the open-circuit transient, has the same rate as that corresponding to the steady-state current density at the instant of current interruption.

The electrode capacitance ($C_{expt.}$) can be calculated from the

---

* For example, h.e.r. involving (2.1) and (2.3) steps, the open-circuit discharge of the adsorption pseudo-capacitance occurring by continuing desorption of $H_{ads.}$ by step (2.3),with reverse step (2.1) providing the electrons for step (2.3).

initial rate of decay $\left(\frac{d\eta}{dt}\right)_{t=0}$ using the following equation

$$C_{expt.} = \frac{-i}{\left(\frac{d\eta}{dt}\right)_{t=0}} \qquad (2.35)$$

where -i is the cathodic current density at the time of current interruption, t=0 (t is the time elapsed after the current interruption). If $C_{expt.} >> C$, the double layer capacity, then $C_{expt.} \simeq C_{ps}$; otherwise $C_{ps} = (C_{expt.} - C)$ must be used to evaluate C_{ps} at the overvoltage corresponding to -i at t=0. By polarising at various current densities -i (and recording $-\eta$ at the instant of interruption of current density -i) followed by open-circuit decay, C_{ps} can be obtained as a function of overvoltage. This method is applicable to corrodible metals, if the current interruption period is kept as small as possible (say < 0.1 second).

The method described above can be extended to the whole of the decay curve (129a), if the current-potential relationship is well known experimentally in the range where the potential decay occurs. To evaluate $C_{expt.}$, one can make use of a relation (129a) similar to (2.35),

$$C_{expt.} = \frac{-i_t}{\left(\frac{d\eta}{dt}\right)_t} \qquad (2.36)$$

where $-i_t$ is the cathodic current density at η_t (the overvoltage at time t after the current interruption) and $\left(\frac{d\eta}{dt}\right)_t$ is the rate of variation of potential with time at t. The cathodic current density, $-i_t$, could be obtained from a $-\eta$ versus $\log_{10}(-i)$ relationship, i.e. rapid Tafel plot (duration of the measurement of the whole curve must be $\lesssim$ 1 minute) or

$$-i_t = i_0 \exp.\left(\frac{-\eta_t}{b}\right) \qquad (2.37)$$

if the Tafel parameters i_0 (the exchange current density) and b apply during open-circuit decay as during cathodic polarisation. This method is best suited for reactions where a transition region in the current-potential relation is observed.

Electrode capacities can be calculated from the fall of overvoltage on the potential decay curve. In deriving the equation for the overvoltage decrease $\Delta\eta$ from t=0 to a period of t after the interruption of the polarising current density, $-i$

$$\Delta\eta = b \log_{10}\left(1 + \frac{2.3(-i)t}{C_{expt.}\, b}\right) \qquad (2.38)$$

it was assumed (120, 120a) that the electrode capacity, $C_{expt.}$, and b remain constant for the whole range of potentials during open-circuit decay. On the other hand, Palm and Past (34) assumed that the $C_{expt.}$ and b remain constant for a small range of potentials during open-circuit decay and calculated $C_{expt.}$ using the formula (34, 133)

$$C_{expt.} = \frac{2.3(-i)}{b}(t_2-t_1)\left[10^{\Delta\eta_2/b} - 10^{\Delta\eta_1/b}\right]^{-1} \qquad (2.39)$$

where $\Delta\eta_1$ and $\Delta\eta_2$ are the values of the overvoltage decay from $t=0$ for periods t_1 and t_2 after the cessation of the polarising current density $-i$. The interval (t_2-t_1) must be small in order to obtain satisfactory $C_{expt.}$ values. They applied this method for the evaluation of C_{ps} of metals such as Pb, Hg etc. without much success, possibly because of their poor assumptions, such as the constancy of $C_{expt.}$ and b in the time interval between t_1 and t_2 or because of their poor experimental conditions.

A linear relationship is believed (120, 121, 134, 135) to exist between the overvoltage and $\log_{10} t$ at <u>sufficiently high values of t</u> ($t > 10\ \tau'$), the time after the cessation of polarisation at $-i$, i.e.

$$-\eta = a - b \log_{10}(t - \tau') \qquad (2.40)$$

where τ' is a function of $-i$ and $C_{expt.}$ and can be obtained experimentally from the observed $-\eta$ against $\log_{10} t$ behaviour by a trial and error method (134, 135). Combining equations (2.36 and (2.37), rearrangement and integration assuming $C_{expt.}$ remains constant for the small range of potentials over which τ' is evaluated, they obtained (120, 121, 134, 135) τ' as an integration constant

$$\tau' = \frac{C_{expt.}\ b}{(-i)} \qquad (2.41)$$

from which C_{ps} can be calculated as usual and corresponds to the overvoltage at $t=0$. Thus, by determining τ' for decay curves commenced at various overvoltages, the C_{ps} can be expressed as a function of overvoltage.

From an examination of the accuracy and underlying assumptions of the various methods described earlier, the rapid open-circuit decay method is the most satisfactory for the determination of C_{ps} and hence the coverage with adsorbed hydrogen atoms.

(1V) Adsorption Pseudo-Capacitance and Coverage

Each value of hydrogen coverage θ corresponds to a charge q required to reach that coverage from a coverage of zero, i.e.

$$q = k'\theta \qquad (2.42)$$

where k' is the value of q at $\theta = 1$, viz. the total charge required to form a monolayer of adsorbed hydrogen atoms. The variation of θ, and hence, q, with overvoltage gives rise to a pseudo-capacity,

$$C_{ps} = \frac{dq}{d\eta} = k'\frac{d\theta}{d\eta} \qquad (2.43)$$

Thus, knowledge of C_{ps} is helpful in evaluating θ values by integration of $\frac{1}{k'}\int C_{ps}d\eta$. In this method, only the change of coverage corresponding to a given change in potential can be obtained, unless the integration constant, i.e. the absolute value of the coverage at some reference potential, is known from an independent measurement.

The hydrogen coverage can also be determined directly by measuring precisely the charge required for deposition or removal of $H_{ads.}$ atoms over a certain potential range. This approach is used in the double charging experiments of Devanathan et al. (127) and a differential procedure described by Angerstein-Kozlowska et al. (131).

Another well known method of Breiter, Knorr, Volkl and Will (136, 137) involves the observation of the time-dependent charging current which results when a single or repetitive sweep is applied to an electrode by means of a potentiostat.

According to Bockris and Reddy (86), the dependence of hydrogen coverage on overvoltage can be used in the evaluation of the r.d.s. in the h.e.r. The quantity ($d\eta/d \log_{10} \theta$) has the following values for the four most probable reaction mechanisms all for the case where $\theta << 1$: discharge rate-determining, followed by Tafel desorption:- (4x2.303RT/F); discharge followed by rate-determining Tafel desorption or Heyrovsky desorption:-(2.303RT/F); and discharge rate-determining followed by Heyrovsky desorption:- 0: respectively. In the case of the h.e.r. on Fe in 10^{-4} M NaOH + 0.1 M Na_2SO_4 at 25°C, Kim and Wilde (138) observed* that the variation of θ with overvoltage was in close agreement with the theory:($d\eta/ d \log_{10} \theta$) was -0.29 V. decade^{-1}, measured experimentally and -0.24 V. decade^{-1}, i.e. (-4x2.303RT/F), theoretically. Hence, for Fe in alkaline solution the rate-determining step seems to be water discharge followed by Tafel desorption.

---

* However, these values are not those quoted by Kim and Wilde, their values being inconsistent with their Fig. 7 (138) and as well with their theoretical value quoted. They quoted the inverse slopes for both cases.

(V) Adsorption Pseudo-Capacitance and Isotherms

The combined effect of the properties of *both* phases determines the dependence of the concentration of *intermediates* on the external variables (P, T and ϕ) which define the type of adsorption isotherm applicable to the system and the standard free energy of adsorption. Therefore, it is necessary to discuss some important adsorption isotherms at this stage.

In order to apply an isotherm, it is necessary to assume equilibrium between hydrogen in the adsorbed state and H_3O^+ ions in the solution at an ideal polarised electrode and the corresponding electrochemical potentials are equal (i.e. $\bar{\mu}_{H_3O^+} = \bar{\mu}_{H.ads.}$, where $\bar{\mu}_{H.ads.}$ and $\bar{\mu}_{H_3O^+}$ are electrochemical potentials in the adsorbed state and in solution, respectively).

Conway et al. (87, 126, 128, 129, 140) applied the Langmuir isotherm* for low θ (i.e. $\theta < 0.2$) and high θ (i.e. $\theta > 0.8$), to the case of reaction (2.1) at quasi-equilibrium, followed by a slow Heyrovsky step (2.3) in the h.e.r. They obtained a relation

---

* The Langmuir isotherm can be written as $\frac{\theta}{1-\theta} = a' \left(p_H\right)_{eff.}$, where a' is related to the standard free energy of adsorption, $\Delta G^o_{H.ads.}$, by $a' = \exp.\left(-\frac{\Delta G^o_{H.ads.}}{RT}\right)$ and the effective pressure of $H_{ads.}$ atoms $\left(p_H\right)_{eff.}$ is related to ϕ by $\left(p_H\right)_{eff.} = \exp.\left(-\frac{\phi F}{RT}\right)$

$$C_{ps} = \frac{k'F}{RT}\,\theta(1 - \theta) \qquad (2.44)$$

which obviously has a maximum value of $\frac{k'F}{4RT}$ (i.e. $\frac{k'F}{4RT} \simeq 1600$ μF. cm.$^{-2}$ for a density of adsorption sites $\simeq 10^{15}$ cm.$^{-2}$) at $\theta = 0.5$ and must be symmetrical with respect to θ as θ rises from zero to unity. In terms of potential ϕ

$$C_{ps} = \frac{k'F}{RT}\left[\frac{K_1 \exp.\left(-\frac{\phi F}{RT}\right)}{\left(1 + K_1 \exp.\left[-\frac{\phi F}{RT}\right]\right)^2}\right] \qquad (2.45)$$

which is symmetrical with respect to the electrode potential at which $\theta = 0.5$; K_1 is the equilibrium constant for (2.1) {Volmer discharge step}. At low coverages ($\theta \simeq 0$), when ϕ is small or positive, $C_{ps} > 0$ and varies as exp. $\left(-\frac{\phi F}{RT}\right)$, whereas at large θ, at high **negative** potential values, C_{ps} varies as exp. $\left(\frac{\phi F}{RT}\right)$, respectively, in accordance with (2.45). Both cases have been verified experimentally by Conway and MacDonald (141) during open-circuit decay studies at Au for the case of low θ and NiO electrodes (142) in the case of high θ (with $O_{ads.}$).

For the Temkin case, in which the standard free energy of adsorption is a function of coverage (in the range of $0.2 < \theta < 0.8$) and of potential, the corresponding isotherm can be written as,

$$\frac{\theta}{1-\theta}\exp.(f\theta) = a'\,(p_H)_{eff.} \qquad (2.46)$$

where f is a parameter accounting for heterogeneity or interaction between adsorbed atoms, fRT being the rate of change of the apparent standard free energy of adsorption with coverage,

$$fRT = \frac{d\,\overline{\Delta G_\theta}^{\circ}}{d\theta} \qquad (2.47)$$

where $\overline{\Delta G_\theta}^{\circ}$ is the standard free energy of adsorption at coverage θ. Then, conditions being the same as in (2.44),

$$C_{ps} = \frac{k'F}{RT}\left[\frac{\theta(1-\theta)}{1 + f\theta(1-\theta)}\right] \qquad (2.48)$$

According to Conway and Gileadi (87, 126), equation (2.48) cannot be explicitly solved for C_{ps} as a function of potential, but can be solved indirectly with the assumed value of K_1. Small values of f decrease the maximum C_{ps} appreciably and cause C_{ps} to have an appreciable dependence on potential over a **wider range of potentials** than in the Langmuir case (f=0). At high values of f, C_{ps} tends to become independent of ϕ, as discussed by Temkin (143) for hydrogen adsorption at Pt.

There are many other isotherms proposed such as Henry's Law $\{ \left(p_H\right)_{eff.} a' = \theta$, at $\theta < 0.1 \}$, Virial isotherm (modified form of Henry's Law) and Frumkin isotherm (modified form of Langmuir isotherm) etc. Particle-particle interaction has been accounted for in both cases. Recently, Breger and Gileadi (144) proposed the possible combination of Langmuir and Frumkin isotherms for the adsorption of hydrogen on some noble metals.

C. Permeation of Hydrogen (or Tritium) Atoms Through Metals as a Diffusion Phenomenon

Permeation studies of hydrogen isotopes through metals are usually carried out in one of two ways: either by exposing the metal to gaseous molecular hydrogen (or H atoms) usually at high temperature and pressure; or by the cathodic evolution of hydrogen on the metal surface. In contrast to gas phase studies, Devanathan and Stachurski (145),**Zuchner** and Boes (145a); and Muju and Smith (55) have devised convenient and sensitive electrochemical and radiochemical methods for permeation experiments. It is usually desired to prove that the rate of permeation of hydrogen isotopes is controlled by diffusion in the metal membrane. Such diffusion control is present if the rate of permeation is inversely proportional to the thickness of the membrane and the diffusion coefficient is independent of the thickness of the membrane. From measurements of permeation currents, it is possible to determine solubilities and diffusion coefficients of hydrogen isotopes in metals. Determinations of permeation and of diffusion coefficients have been made by electrochemical and radiochemical methods at room temperature and in some cases at temperatures up to 80°C, at different potentials (or cathodic currents), for various thicknesses of metal membranes for Pd, Pt, Ni, Pb, Fe, steel, Fe-Cr, Fe-Ni and Pd-Ag alloys, among others.

The electrode is usually in the form of a membrane or a bielectrode of thickness L which separates two regions of solution as shown in Fig. 4a. The discharged H (D or T) atoms at one side (conveniently termed the cathodic side) of the membrane electrode acting as a cathode in the left-hand compartment enters the metal and diffuses through the metal with a diffusion coefficient, D, to the other side of the membrane. The other side of the membrane (conveniently termed the diffusion side), acting as an anode, is maintained sufficiently anodic so that H (D or T) atoms reaching it are quantitatively ionised. The permeation current produced in this manner yields the quantity of hydrogen isotope which diffuses through the membrane. With some metals, the current of anodic dissolution is comparable with hydrogen ionisation but may be diminished by Pd coating the diffusion side of the foil.

Let the concentration of hydrogen isotope at $x = 0$ be maintained (by cathodic polarisation) at C_0 throughout, while at $x = L$ it is maintained at $C = 0$. Initially, the concentration of the adsorbed hydrogen isotope θ on both cathodic and anodic sides is assumed to be zero.

Then, using Fick's first law, the steady-state permeation current may be written as

$$J_\infty = \frac{D}{L} C_0 \qquad (2.49)$$

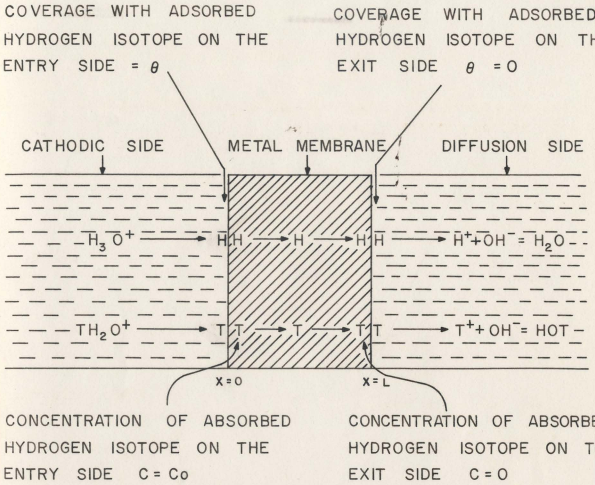

Fig. 4a. Metal diffusion membrane with hydrogen isotope cathodisation on entry side and hydrogen isotope ionisation on exit side.

where D = the diffusion coefficient of hydrogen isotope, L = thickness of the metal membrane, and C_0 = concentration of absorbed hydrogen isotope.

If a steady state does not exist, i.e. if the concentration at some point in the membrane is changing with time, then Fick's second law applies

$$\frac{\partial C}{\partial t} = D \frac{\partial^2 C}{\partial x^2} \quad ; \qquad 0 < x < L \qquad (2.50)$$

where C = concentration of hydrogen isotope, t = time after switching on of the cathodic polarisation. By the application of the operation of Laplace transformation to equation (2.50) with the boundary conditions:

$$C = C_0 \; ; \quad x = 0 \; ; \qquad t = 0 \, .$$

$$C = 0 \; ; \quad x = L \; ; \qquad t \lessgtr 0 \, .$$

$$C = 0 \; ; \quad 0 < x < L \; ; \quad t < 0 \, .$$

McBreen, Nanis and Beck (146) solved equation (2.50) to obtain the hydrogen isotope concentration C at x at any time t:

$$\frac{C_{(x,t)}}{C_0} = \sum_{n=0}^{\infty} (-1)^n \operatorname{erfc.} \frac{x + 2nL}{2\sqrt{Dt}} - \sum_{n=0}^{\infty} (-1)^n \operatorname{erfc.} \frac{2L(n+1) - x}{2\sqrt{Dt}} \qquad (2.51)$$

The measured permeation current at time t, at x = L is

$$J_t = -D\left(\frac{\partial C_t}{\partial x}\right)_{x = L} \tag{2.52}$$

(1) Methods of Measuring Diffusion Coefficients of Hydrogen Isotopes

Time-Lag Method: By integrating the rising part of the permeation current versus time curve, the quantity of hydrogen isotope which has permeated through the metal membrane can be obtained at various times. An extrapolation to C = 0 of the plot of this quantity versus time gives the time lag, t_{lag}. The time lag is related to the diffusion constant by

$$t_{lag} = \frac{L^2}{6D} \tag{2.53}$$

Devanathan et al. (145) have shown that t_{lag} may be equated to the time at which the rate of permeation is 0.63 times the steady-state value J_∞ (Fig. 4b). The corrected t_{lag} for the relaxation time* gave D for H in Pd in agreement with D calculated by other methods (145).

---

* This time of relaxation may be regarded as being due to the finite rate constant for transfer of hydrogen atoms from the surface into the metal phase.

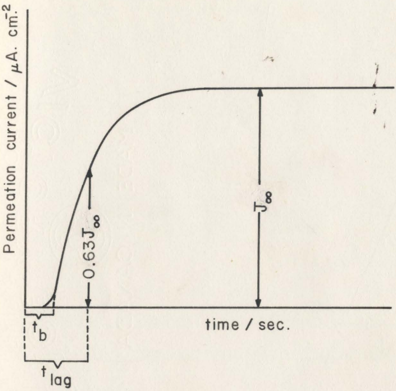

Fig. 4b. Hydrogen permeation transient.

Rise-Time Method: According to Devanathan et al. (145), the equation of the rising transient is given by

$$\ln\left(\frac{J_t - J_\infty}{J_\infty}\right) = \ln(1 - e^{-3t/t_0} + e^{-8t/t_0}) + \ln 2 - \frac{t}{t_0} \quad (2.54)$$

where the rise constant t_0 is related to the diffusion constant by the equation,

$$t_0 = \frac{L^2}{\Pi^2 D} \quad (2.55)$$

The first term of the right hand side (r.h.s.) of the equation (2.54) converges to zero at large t. Hence, a plot of $\ln\left(\frac{J_t - J_\infty}{J_\infty}\right)$ versus t must be a straight line with an intercept of ln2 and a gradient of $\frac{1}{t_0}$. Thus, from the gradient, D can be calculated using equation (2.55). Cadersky, Muju and Smith (147) used this type of calculation to evaluate D for H in Pb.

Also, using equations (2.49), (2.51) and (2.52) McBreen et al. (146) have shown (for $\tau < 0.3$),

$$\frac{J_t}{J_\infty} = \frac{2}{\Pi^{\frac{1}{2}}\tau^{\frac{1}{2}}} \sum_{n=0}^{\infty} (-1)^n e^{-(2n + 1)^2/4\tau} \quad (2.56)$$

and

$$\tau = \frac{Dt}{L^2} \quad (2.57)$$

is a dimensionless parameter. The first term (n = 0) approximation of (2.56) gives

$$\frac{J_t}{J_\infty} = \frac{2}{\Pi^{\frac{1}{2}}\tau^{\frac{1}{2}}}\, e^{-1/4\tau} \qquad (2.58)$$

This approximation is valid up to $J_t = 0.965J_\infty$. It is possible to calculate D by finding the time to attain any fraction of the steady-state permeation rate. For a particular case (most commonly used) of $\frac{J_t}{J_\infty} = 0.5$, the parameter τ has a value of 0.138 and the corresponding time $t_{0.5}$, denoted as the half-rise time, is given by

$$t_{0.5} = \frac{0.138L^2}{D} \qquad (2.59)$$

The D values calculated by Cadersky et al. (147) using equations (2.55) and (2.59) for the diffusion of H atoms through Pb are in excellent agreement at -i = 10 and 20 mA. cm.$^{-2}$, but not at -i = 50 mA. cm.$^{-2}$.

<u>Breakthrough Time t_b:</u> The breakthrough time, t_b, as represented in Fig. 4b can be written as the difference between the time lag, t_{lag}, and the rise-time constant t_0. Then, from equations (2.53) and (2.55)

$$t_{lag} = t_b + t_0 \qquad (2.60)$$

therefore,

$$t_b = \frac{L^2}{D}\left(\frac{1}{6} - \frac{1}{\Pi^2}\right)$$

$$= \frac{L^2}{15.3D} \qquad (2.61)$$

Decay-Time Constant: The decrease in permeation current for the decay transient (145), from the time of interruption of cathodic current (i.e. $t = 0$) is given by

$$J_{x=0,t} = J_{x=0,t=0} \exp.\left(-\frac{t}{t_0}\right) \qquad (2.62)$$

where $J_{x=0,t=0}$ is the permeation current at the time $t = 0$ and and $t_0 = \frac{L^2}{\Pi^2 D}$. Hence, a plot of $\log_{10}\left(\frac{J_t}{J_{t=0}}\right)$ versus time must be a straight line with slope $\frac{\Pi^2 D}{L^2}$. Devanathan et al. (145) corrected the decay time constant for the relaxation time to obtain the transients on a time scale which refers to concentrations in the membrane rising at $t = 0$ to C_0 at $x = 0$.

McBreen et al. (146) solved Fick's second law (2.50) for the decay of permeation current (for $\tau < 0.3$) from the steady state when charging is stopped. If a virtually impenetrable surface is formed, i.e. if none of the already present dissolved hydrogen leaves via the entry side, the condition of zero flux at the entry side may be stated as

$$\frac{\partial C}{\partial x} = 0,\ x = 0;\ t > 0$$

where t = time, defined from the instant of current interruption. For $t < 0$, steady-state permeation exists, with a linear concentration gradient so that the initial condition for the decay problem is

$$C = C_0 \left(1 - \frac{x}{L}\right); \; 0 < x < L; \; t < 0$$

and the corresponding boundary conditions after interruption are:

$$C = 0; \; x = 0; \; t > 0$$

and $C = 0; \; x = L; \; t \lesseqgtr 0$

Using these initial and boundary conditions, they derived a relation

$$\frac{J_t}{J_\infty} = 1 - 2 \sum_{n=0}^{\infty} \frac{1}{\Pi^{\frac{1}{2}}\tau^{\frac{1}{2}}} e^{-(2n + 1)^2/4\tau} \qquad (2.63)$$

The first term (n = 0) approximation of (2.63){see equations (2.56) and (2.58)} gives

$$\frac{J_t}{J_\infty} = 1 - \frac{2}{\Pi^{\frac{1}{2}}\tau^{\frac{1}{2}}} e^{-1/4\tau} \qquad (2.64)$$

D can be determined as mentioned earlier.

(11) Proof of Diffusion-Controlled Permeation

The activation energy for the diffusion of hydrogen through a metal like Fe (150) may arise from the creation of sites (distorted octahedral holes) within the metal into which they can jump. However, Beck et al. (150) have pointed out that in steel there is a strong interaction between dissolved hydrogen and the alloy and, as a result, its breaking rather than the formation of interstitial sites, becomes rate-determining in diffusion. The literature shows that recently determined activation energies for hydrogen diffusion through Pt (148), Ni (149), Pd (149), Ta (145a) and Armco Fe (150) are 9.6, 7.9, 4.2, 4.0, and 1.33 k.cal.g. atom^{-1}, respectively.

Evidence for diffusion-controlled permeation of hydrogen isotopes through metal membranes can come from the following tests of experimental results. The steady-state permeation rate, J_∞, plotted as a function of $\frac{1}{L}$ must yield a straight line passing through the origin. This relationship is obeyed for metals such as Pt (148), Pd (144, 145), Pb (55), Fe (150). The slope of this straight line equals DC_0, allowing determination of C_0 if D is known from an independent method.

A second test of the assumption of diffusion-controlled permeation is to plot $t_{0.5}$ versus L^2 as in equation (2.59). The slope of this linear plot should be $\frac{0.138}{D}$. This relationship has been experimentally verified for metals such as Pd (144, 145), Fe (150) and Pt (148).

(111) Diffusivity and Solubility of Hydrogen Isotopes in Metals

The diffusion constant of hydrogen in metals is dependent on bulk metal properties and usually on bulk H concentration but may be considered independent of cathodic potential (144), cathodic current (144a, 144b, 148), composition of the solution {in particular the presence of traces of added surface poisons (148)} except where these cause changes in, e.g. bulk H concentration, as found for Pb (147) and Fe (151) {D in Pb and Fe increases with -i}. The bulk H concentration depends on the solubility. The solubility of H apparently decreases with an increase in enthalpy of absorption and decreases as the number of d-vacancies decreases in transition metals (149). θ is a function of the state of the surface and C_0 may show similar dependence. Diffusion constants increase with rise of temperature. The diffusion constant might be expected to decrease in the order H,D,T, but actual behaviour is more complicated, e.g. diffusivity of H isotopes in Pd and Pd-Ag alloys (145a, 176, 177a) decreases in the order D,H,T.

A diminished D with very thin Fe foils has been attributed to effects at the cathode surface caused either by impurities, structural changes or blocking by gas bubbles liberated during electrolysis or by rate-control by the adsorbed → absorbed transition rather than by lattice diffusion. However, to account for the deviation from simple diffusion behaviour, Darken and Smith (152) have proposed a concept of hydrogen trapping* in steel.

---

* The physical identity of traps may be interface boundaries, internal free surfaces, lattice imperfections (such as dislocations or vacancies) or foreign atoms.

Later, McNabb and Foster (153) analysed mathematically diffusion accompanied by trapping and untrapping. The diffusivity that includes trapping is expected to be lower than the true diffusivity. Recently, Oriani (154) considered the theory of hydrogen diffusion with trapping on the assumption that an equilibrium exists between the lattice hydrogen and the trapped hydrogen. He applied this concept to obtain trap densities in steel from hydrogen charging or permeation measurements.

While explaining the anomalous behaviour of hydrogen permeation through Fe and Fe-Ni alloys at high overvoltages* (i.e. at high cathodic current densities), Bockris and Subramanyan (155) interpreted the commencement of hydrogen damage in the metals in terms of the nucleation of traps when the H fugacity reaches sufficient values to cause spreading of micro-cracks formed by dislocation pile-ups. They derived a mathematical relationship for the hydrogen permeability with the consideration that the traps are 'switched on' when the concentration of H in the metal exceeds the critical hydrogen concentration, $(C_0)_{\text{Crit.H.}}$, corresponding

---

* Overvoltages above the critical overvoltage at which permanent damage like cracks are produced by hydrogen in metals.

to the onset of hydrogen embrittlement. According to them, the flux at $t << \infty$ is reduced by the traps, i.e. the permeability decreases from the normal permeability and gives rise to the prominent hump seen in the permeation build-up transients with iron and steel. At $t = \infty$ (i.e. at the steady state) the permeability is given by equation (2.49) which is the same as in the absence of traps.

Bockris et al. (156) have suggested that $(C_0)_{Crit.H.}$ for Ni should be larger than for Fe by a factor e^6 and for Pd the factor becomes e^9. These are so high as to be of no consequence. The $(C_0)_{Crit.H.}$ corresponding to a decrease in permeation has been observed in the case of Fe and Pt but not for Ni and Pd (149). The $(C_0)_{Crit.H.}$ increases with temperature in the case of Fe but decreases slightly in the case of Pt. The $(C_0)_{Crit.H.}$ also varies with the external stress; tensile stress lowers it while compressive stress raises it (156).

(1V) Hydrogen Absorption and the Hydrogen Evolution Reaction

Hydrogen absorption by metals during the h.e.r. can be regarded as a side effect of the overall hydrogen evolution process in which protons are discharged (in acid medium) and liberated as hydrogen gas. According to Bockris, McBreen and Nanis (157), the adsorbed hydrogen state is the same precursor for hydrogen entry into

Fe and for hydrogen gas evolution. This may well be true for metals in general. Thus absorbed H may influence the rate of h.e.r.

Since hydrogen evolution can be affected by the condition of the bulk metal phase via the interface, a correlation between θ and C_0 is essential. Many workers (138, 157, 160) assumed the relationship $\theta \propto C_0$ at low coverages. However, Breger and Gileadi showed by simultaneous measurements of C_0 and θ on Pd (144) that at low $\theta \lesssim 0.15$, $C_0 \propto \exp. (\theta)$; while at $\theta \simeq 0.5$, $C_0 \propto \theta$.

The dependence on overvoltage of J_∞ is of interest because $J_\infty \propto C_0$ {see equation (2.49)}. Bockris et al. (157) showed the overvoltage dependence of J_∞, using the assumption $\theta \propto C_0$, as

$$\frac{d\eta}{d\ \ln(J_\infty)} = \frac{d\eta}{d\ \ln\ \theta}$$

This quantity was used to evaluate the r.d.s. of h.e.r. {see Section 2B (lV)}. Also, Bockris and Thacker (157a) predicted qualitatively h.e.r. mechanisms depending on the variation of permeation current with the applied cathodic current. Application of these theories to various metals other than Fe (144c, 157) are yet to come.

The variation of $-\eta$ with time of electrolysis during the h.e.r. was observed for many metals such as Pt (148, 148a), Pb (26, 27), Fe (172) and Pd (148b). Both increases in $-\eta$ (on Pd, Pt, Fe) and decreases in $-\eta$ (on Pb) with time were interpreted in terms of a change in the properties of the electrode due to hydrogen absorption. Earlier plausible explanations were later confirmed by independent permeation experiments for Pd (144, 145) and Pb (55, 147); and simultaneous overvoltage and permeation measurements on Pt* (148) and Fe (172), respectively.

The influence of absorbed H on h.e.r. kinetics may also be studied using simultaneous e.m.f. and resistivity measurements on Pd (158). The hydrogen contents of Pd are deducible from e.m.f. measurements up to $PdH_{0.02}$ ($E - E_e > 50$ mV.) and above $PdH_{0.58}$ ($E - E_e < 50$ mV.) or preferably from the resistivity over the range Pd to $PdH_{0.75}$, at which it is 1.8 times that of pure Pd. It seems possible that an increase of θ accompanies the change from $\alpha\ PdH_{0.025\ max.}$ to $\beta\ PdH_{0.58\ min.}$, but the increase in h.e.r. i_0 from

---

* Bockris et al. (148) pointed out that the steady value of $-\eta$ on the cathodic side of Pt was reached after a relatively short time (a few minutes) during permeation experiments in contrast to the long time (a few hours) variation of $-\eta$ observed in their hydrogen evolution studies on Pt (148a). No explanation was suggested.

1.8 to 6 mA. cm.$^{-2}$ observed at this transition was attributed to the lattice constant increase of 0.131Å. Effects of geometric factors are anticipated in catalysis but other possible explanations of the increase in activity are: a change of electronic band structure or an increase of θ.

Dissolved H in metals is probably ionised to interstitial H^+ and e^-, the latter entering the electron gas of the metal. This is particularly true for transition metals with high electron state densities near the Fermi energy. This "screened proton" model (177b) of H in metals explains many features of H solubility in metals and alloys in terms of their electronic band structures. This view of hydrogen in metals will probably have applicability to the understanding of the h.e.r. at metals dissolving significant amounts of H.

Alternatively, according to Krishtalik (159) the decrease in the energy of H adsorption on the metal after H absorption in comparison with the pure metal might explain the variation of $-\eta$ with time. Supporting evidence for this can be seen from the permeation experiments by the Bockris school with Pt and Fe, using solutions containing poisons. In a H permeation study with As_2O_3-poisoned Pt (148), $-\eta$ for h.e.r. increased with t in a parallel manner to J_t, i.e. presumably parallel with C_0. Also, poisons such as

CN^-, I^- etc. in solution are found to increase the hydrogen permeation through Fe (157). Bockris et al. (148, 157) attributed this effect to the preferential adsorption of poisons on more active sites, decreasing the mean M-H bond strength repressing H atom recombination and probably favouring H absorption relative to adsorption.

D. Isotopic Separation in Hydrogen Evolution and Membrane Diffusion

(1) Separation Factors on the Cathodic Surface

A brief account of isotopic separation factors has been given in Section 2A (Vll). The H-T separation factor on the cathodic side of a metal membrane is defined as

$$S_{H,T} = \frac{\left[\frac{(H)}{(T)}\right]_g}{\left[\frac{(H)}{(T)}\right]_s} \qquad (2.65)$$

where $\left[\frac{(H)}{(T)}\right]_g$ and $\left[\frac{(H)}{(T)}\right]_s$ are the ratios of atomic concentrations of H and T in the gas phase and the solution on the cathodisation side, respectively. From acid solutions dilute in T with respect to H, the gaseous species produced in the electrolysis are principally H_2 and HT, and the dischargeable species in solution are mainly H_3O^+ and TH_2O^+.

The experimental $S_{H,T}$ represents a quantity characterising the process as a whole and not any one step of it. Comprehensive calculations for steps (2.1), (2.2), (2.3) and slow molecular hydrogen diffusion were made for $S_{H,T}$ by Conway (103, 104), Bockris and Srinivasan (25, 161) and Krishtalik and Tsionsky (56, 162).

Haynes (167) showed that $S_{H,T}$ on Hg in 0.5 N H_2SO_4 at 0.01 A. $cm.^{-2}$ and $-\eta = 1.150$ V. was constant at a value of 5.9 ± 0.2 when the concentration of T was varied from 0.2 $\mu Ci.ml.^{-1}$ to 20 $\mu Ci.ml.^{-1}$*. Also he proved experimentally that the observed $S_{H,T}$ (at least for the metals Hg, Cd, Sn, Pt, Fe, W, Ag and Ni under their experimental conditions) is unaffected by the isotopic exchange reaction,

$$HT(g) + H_2O(l) \rightleftharpoons H_2(g) + HTO(l) \qquad (2.66)$$

whether catalysed by H_2O, 1 N HCl or anodically activated Pt electrode.

Separation of H from T (or D) is thought to be largely due to activation energy differences in the r.d.s. Support for this idea

---

* However, Bucur and Lewis (174) found H-D separation on Pd in aqueous solution decreased with increase of hydrogen content of solution.

comes (163) from the correlation $\frac{\ln S_{H,T}}{\ln S_{H,D}} = 1.4 \pm 0.1$ which is obeyed by experimental H-T and H-D separation factors determined simultaneously.

The difference of activation energies ($\Delta E^{\ddagger}$) is determined essentially by the difference of the changes in zero-point energies from the initial state ($\Delta\varepsilon_0$) to the activated state ($\Delta\varepsilon_0^{\ddagger}$) {see Fig. 4c}. In a number of studies (164, 164a, 164b, 165), an estimate was made of the properties of the activated state originally suggested by Horiuti and Polanyi (80), i.e. the state in which hydrogen is bonded both to oxygen and to the metal and these bonds were stretched from their equilibrium lengths. Using Dogonadze, Kuznetsov and Levich's quantum mechanical theory (82, 83, 84) of the h.e.r. (i.e. activation by reorganisation of solvent without preliminary stretching of the O-H or M-H bonds), Krishtalik (162) was able to show that the activation energy of the solvent reorganisation depends on the relative arrangement of the corresponding electron-proton terms, i.e. on the difference of the initial and final state energies, which incorporates also the differences of the corresponding zero-point energies. Hence, zero-point energies enter into the expression for the activation energy, just like the remaining components of the energy difference of the initial and final states.

Bockris, Gileadi and Haynes (166, 167) concluded that for high overvoltage metals such as Hg, Pb, Cd, etc., that the proton discharge

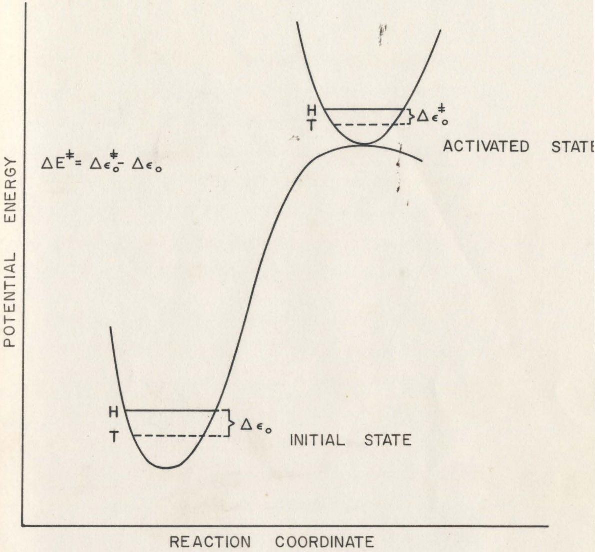

Fig. 4c. Potential energy as a function of the reaction coordinate. Initial state; H_3O^+, TH_2O^+ in solution and e^- in metal. Activated state; $M \cdots H \cdots OH_2$ and $M \cdots T \cdots OH_2$ for H and T, respectiv Zero-point energy levels are indicated by solid line for H and dashed line for T, respectively. $\Delta E^{\ddagger}$ is the difference in activation energies between H and T isotopes. $\Delta\epsilon_o$ and $\Delta\epsilon_o^{\ddagger}$ are the differences in zero-point energies between H and T isotopes for the initial and activated states, respectively.

step (2.1) is r.d., since $S_{H,T}$ varies with potential. Also, for low and medium overvoltage metals such as Ni and Ag in which $S_{H,T}$ is independent of potential over a certain range, but then changes to another value at a certain potential and remains constant as the potential is changed further, they deduced that there is a change in the mechanism of reaction, a change in r.d.s. or both {according to them the probable r.d.s. for transition metals such as Ni and Ag is the atom + ion step (2.3)}.

Conway and Salomon (168) investigated the kinetics of proton and deuteron discharge at Hg down to -125°C in alcoholic solutions and found that (a) the Tafel slopes were the same for H- and D-transfer; (b) the pre-exponential factor ratio was 1.20 to 1.25, but not less than unity and, (c) the apparent heat of activation at the reversible potential was independent of temperature. According to them, these results are contrary to appreciable proton tunnelling. However, Bockris and Matthews (169) examined the same experimental data (168) for higher cathodic potentials ($-\eta = 1.0$ V.) and concluded that tunnelling may then be appreciable. This effect could arise because the barrier height would then be substantially less than that at the reversible potential.

In order to explain the potential dependence of the separation factor and the influence of temperature on the separation factor at constant potential, many of the earlier workers (56, 162, 166, 167, 170, 171) included a tunnelling correction for hydrogen isotopes in their separation factor calculation. In explaining proton and deuteron transfer probabilities (pre-exponential factors) many of them (103, 104, 161, 165, 169) used the original Horiuti-Polanyi (80) model, in which the proton transfer probability is determined by the shape and height of the same potential barrier as determined the activation energy (barrier formed by the potential energy curves of the O-H and M-H bonds). According to this model, increase of overvoltage diminishing the activation energy for discharge involves a decrease of the height and possibly a change in the shape of the potential barrier through which the proton must tunnel. Thus, tunnelling is facilitated and, hence, the isotope spearation factor decreases. Then, if proton tunnelling is significant, the separation factor should not depend on the metal, but only on the barrier parameters. For a valid comparison of the separation factor for the high overvoltage metals where proton tunnelling is thought to be significant, the comparison should be made at the same barrier height. Haynes (167) compared the $S_{H,T}$ for metals such as Hg, Cd, Sn at the same barrier height with the corrected overvoltage $-\eta_{corr.}$ instead of $-\eta$, using Hg as the reference state

$$-\eta_{corr.} = -\eta + (2RT/F)\ln(i_0/i_{0Hg}) \qquad (2.67)$$

where i_{0Hg} is the apparent exchange current density of h.e.r. on Hg.

The plots of $-\eta_{corr.}$ versus $S_{H,T}$ for Hg, Cd, Sn lie quite close to each other, providing support for a significant contribution of proton tunnelling to the discharge process (2.1) at high overvoltage metals.

In the Dogonadze, Kuznetsov and Levich (82, 83, 84) model the activation energy is determined by the solvent reorganisation process and bears no immediate relation to the proton tunnelling probability, which depends on the nature of the overlapping of the wave functions in the initial state (e^- in the metal + H_3O^+ in solution) and the final state ($H_{ads.}$ + H_2O molecule). Within the framework of this theory, Krishtalik and Tsionsky (56) proposed that the more localised is the proton in one of the states, i.e. the stronger are the M-H bonds, the lower the probability of its sub-barrier jump. This is completely at variance with the Horiuti-Polanyi (80) model. Accordingly, in this case the difference in the tunnelling ability of the light and heavy isotopes is more appreciable, i.e. the larger the separation factor should be. In other words, the separation factor of the hydrogen isotopes increases with increasing binding energy. Krishtalik and Tsionsky (56) supported this view with the comparison of $S_{H,T}$ of different metals such as Hg, Pb, Ga at the same electrode surface charge. The $S_{H,T}$ increases in the series: Pb < Hg < Ga, i.e. as predicted by them in the direction of increasing M-H binding energy. Comparison at constant electrode surface charge means that comparison is made at the same field acting directly on the discharging ion. Further, they showed that for a Hg cathode the potential-dependence of $S_{H,T}$, which is different for different solutions (56) {solutions with ions such as Cl^-, Br^-, I^- and $(C_4H_9)_4N^+$ etc.}, is the same if $S_{H,T}$ is expressed as a function of the potential jump in the inner part of the double layer (after deducting ϕ^* potential from the measured overvoltage), i.e. as a function of the field acting directly on the ions*. Accordingly, the decrease of $S_{H,T}$ as $-\eta$ increases has been explained by the fact that the increase of electric field strength causes the H_3O^+ ion to approach the electrode closer and hence enhance the overlapping of the wave functions of the initial state (e^- in metal + H_3O^+ in solution) and final state ($H_{ads.}$ + H_2O molecule), thus facilitating the proton jump. This explains why a much greater effect of the electric field on the separation factor during the discharge of the charged H_3O^+ ions is found than in the discharge of uncharged water molecules, i.e. in solutions of high pH.

Another factor to be considered, especially with hydrogen-absorbing cathodes is the time-dependence of the separation factor.

---

* However, Haynes (167) showed that $S_{H,T}$ at constant overvoltage has the <u>same</u> <u>numerical</u> <u>value</u> in the presence of the anions Cl^-, SO_4^{--}, ClO_4^- and the cation $(C_3H_7)_4N^+$, in disagreement with the Russian work.

The electrolytic $S_{H,D}$ on Fe in 1 M H_2SO_4 -10% D_2O decreased with time (172) before reaching a plateau value in the range 7.35 ± 0.5. On the other hand, $S_{H,D}$ on 25% Ag-Pd alloy in 0.7 M K_2CO_3 in 90% D_2O rose from 3.7 to 6.7 as the period of electrolysis increased from 0.6 to 6 hours (173). These effects were interpreted in terms of progressive changes in the M-H and M-D bond strengths due to changes in the sorbed H and D content in the metal electrode.

Although many theories have been developed as discussed above, many of them fail to explain the observed experimental results under ultrapure conditions. It must be admitted that theory is not yet in the position optimistically predicted (86, 87, 101, 104, 161) of being able to identify h.e.r. mechanism from $S_{H,D}$ or $S_{H,T}$ measurements.

(11) Separation Factors on the Diffusion Side of a Metal Membrane After Cathodisation and Membrane Diffusion

In Section 2D (1), the effect of dissolved hydrogen isotopes on $S_{H,D}$ has already been mentioned, i.e. $S_{H,D}$ may vary with time. The dissolved hydrogen may diffuse through a membrane to the diffusion side where these hydrogen isotopes are removed by either (a) gas evolution or (b) ionisation. In these cases, therefore, there is additional separation of hydrogen isotopes by diffusion through the metal membrane and by the desorption process at the diffusion side of the metal membrane.

(a) Separation Factors for Hydrogen Isotope Evolution on the Diffusion Side

The overall separation factor for H and T originating in the catholyte, entering the metal membrane, diffusing through the metal membrane and being evolved as gas on the diffusion side is defined as

$$S_{(H,T)_D} = \frac{\left[\frac{(H)}{(T)}\right]_g}{\left[\frac{(H)}{(T)}\right]_s} \qquad (2.68)$$

where $\left[\frac{(H)}{(T)}\right]_g$ and $\left[\frac{(H)}{(T)}\right]_s$ are the ratios of atomic concentrations of H and T in the gas phase on the diffusion side and the solution in the cathodisation side, respectively.

The recent simultaneous measurements of H-D separation factors on both the cathode and diffusion sides of 25% Ag-Pd (173) and Fe (172) indicated that $S_{(H,D)_D} > S_{H,D}$. The higher value for $S_{(H,D)_D}$ was accounted for by the additional separation of H from D by diffusion through the membrane. These authors calculated diffusion separation factors $\left[= \frac{S_{(H,D)_D}}{S_{H,D}}\right]$ which range from 1.35 to 1.6 over the -i range 19.1 to 255 mA. cm.$^{-2}$ for Fe (172) and 1.2 to 1.1 at 20 mA. cm.$^{-2}$ for 25%Ag-Pd (173), respectively. These are close to the value of Brodowsky, Gibmeier and Wicke (175)* of 1.6 ± 0.1 independent

---

* They introduced H and D from H_2 and D_2 in the gas phase at one side of Pd metal and anodised H and D on the other side.

of temperature in pure Pd. Brodowsky et al. explained the observed H-D diffusion separation factor in terms of the product of the equilibrium (solubility) ratio of 2.4 and the diffusivity ratio of 0.7. The higher diffusivity for D than for H in Pd is associated with a higher energy of activation for the lighter isotope (176). However, the hydrogen flow through Pd is greater than the deuterium flow because Pd dissolves H preferentially and the higher concentration gradient thus built up outweighs the higher mobility of the individual D atoms.

Like $S_{H,D}$, $S_{(H,D)_D}$ on 25% Ag-Pd alloy (173) increased with time, while $S_{(H,D)_D}$ on Fe (172) decreased with time, as might be expected.

(b) Separation Factors for Hydrogen Isotope Ionisation on the Diffusion Side

The overall separation factor for H and T originating in the catholyte, entering the metal membrane, diffusing through the metal membrane and being ionised into the diffusion side electrolyte is defined as

$$S_{(H,T)_{DA}} = \frac{\dfrac{J_\infty}{(J_\infty)_T}}{\left[\dfrac{(H)}{(T)}\right]_s} \qquad (2.69)$$

where J_∞ and $(J_\infty)_T$ are the measured atom fluxes (expressed in the same units) of H and T on the diffusion side and $\left[\frac{(H)}{(T)}\right]_s$ is the ratio of atomic concentrations of H and T in the solution of the cathodisation side.

Muju and Smith (55) recently obtained the anomalous result $S_{(H,T)_{DA}} = 0.3 \pm 0.15$ on Pb from their permeation experiments of this type. This separation includes cathodic discharge from H_3O^+, TH_2O^+, diffusion of H and T atoms through Pb and anodisation to H_2O and HOT, respectively. Gibmeier et al. (175, 177) were able to show from their measurements* that the H-D separation factor for the anodic process in Pd under these conditions is equal to unity since their observed anodic H-D separation factor (1.7 independent of temperature) is due entirely to the rate-limiting diffusion of H and D in Pd. These results suggested that there would be no additional separation during anodisation to H_2O and HOT. Therefore, the additional separation might be caused solely by the diffusion of H and T. This is extremely improbable because H diffuses faster than T in Pd (177a) although D diffuses faster than H (145a, 176) {the activation energy for diffusion decreases in the order

---

* Their experimental technique has been mentioned earlier in Section D (11a) of this chapter.

T > H > D for Pd and Pd-Ag alloys at room temperature}. It is thought that the anomaly observed by Muju and Smith (55) originates from the low observed H atom permeation currents probably because H atoms can leave the foil other than by anodisation, e.g. by aerial oxidation. Such an error is not anticipated in the radiochemical counting method for T.

Only a few experimental studies of this nature have appeared in the literature until now. Measurements do not yet seem sufficiently comprehensive to make any theoretical predictions. It is hoped that further work may resolve some of the uncertainties, such as $S_{(H,T)_{DA}}$ on Pb being less than unity.

3. EXPERIMENTAL METHODS AND RESULTS

This chapter describes the techniques used and results obtained in the three separate parts of the work with lead electrodes in perchloric acid solution. These parts are: (A) measurements of hydrogen overvoltage as a function of time, (B) measurements of hydrogen pseudo-capacity and overvoltage as a function of time, and (C) measurements of hydrogen-tritium separation factors.

The work described in Section A is largely a repetition under different experimental conditions of the work of Ives and Smith (26, 27) with electropolished lead in 0.1 M $HClO_4$. In the present work, both 0.1 M and 1 M $HClO_4$ were used; some electrodes were prepared by mechanical scraping, some by chemical polishing and the remainder by electropolishing. Furthermore, the experimental cell was improved in various ways and the gas purification train was considerably superior to that used in the earlier work.

It was desired to confirm the unusual findings of Ives and Smith with regard to the time-dependence of overvoltage, which suggested a several orders of magnitude increase in catalytic activity of lead electrodes during cathodic treatment. Such behaviour had not been observed in the course of a great many investigations with scraped and porous lead electrodes by Russian workers. The present results indicate that the effects observed by Ives and Smith also may be found when scraped lead is used, the earlier results being broadly confirmed. However, it was found that conducting pre-electrolysis at too high a current density resulted in degradation of electrode behaviour in such pre-electrolysed solutions.

Since electrochemical and radiochemical permeation experiments as a method of studying absorbed H atoms were started by Cadersky et al. (147, 55) in this laboratory, we undertook the task of trying to detect H atoms adsorbed at a Pb surface with the aid of capacities measured by the rapid open-circuit decay method while simultaneously measuring the overvoltage. These measurements are reported in Section B. Although initial capacities were small (14 - 25 μF. $cm.^{-2}$, increasing with $-\eta$ and consistent with an initial $\theta_H \approx 0$), capacities of Pb have been found to increase with the period of cathodisation, while $-\eta$ was observed to decrease during the same period. The increase in capacity is attributed to the growth of an adsorption pseudo-capacity component, arising from a growing hydrogen surface coverage (θ_H) of the electrode. Both increases in capacity and decreases in overvoltage were found to depend linearly on the logarithm of -Q, as observed by Ives and Smith (26, 27) for the decrease of overvoltage.

In addition to electrochemical permeation of H atoms through Pb foils as evidence for the presence of dissolved H atoms, Muju and Smith (55) demonstrated permeation of electrochemically generated

H and T atoms through Pb foils in radiochemical and electrochemical experiments. Their over-all separation factor $S_{(H,T)_{DA}}$ for cathodic discharge, diffusion through a Pb foil and anodisation on the opposite face, was less then unity. This quantity was very small in comparison with the $S_{H,T} \approx 7$ observed by Bockris and Srinivasan (25), and by Krishtalik and Tsionsky (56) for cathodic gas evolution at Pb in acid solution. Therefore, it was decided to measure $S_{H,T}$ and $S_{(H,T)_{DA}}$ simultaneously on Pb foils at various cathodic currents. The results reported in Section C show once again that $S_{H,T} \approx 7$ and $S_{(H,T)_{DA}} < 1$ at all applied cathodic currents. In addition, the H and T fluxes through the foil were found to increase with the magnitude of the applied cathodic current.

A. Experimental Method and Results of Hydrogen Overvoltage Measurements

In this section, the experimental techniques and results obtained in hydrogen overvoltage measurements on lead cathodes in aqueous $HClO_4$ are described.

(1) Materials

Lead: Lead rods (3 mm. diameter) were made by Johnson-Matthey and Co. either from Specpure (99.995%) or from Associated Lead high-purity lead ingots (99.9998%). Also, Fisher lead foils (L27, ca. 99% pure) of thickness = 0.02 cm. and Goodfellow Metals (99.9%) foils of thickness = 0.025 cm. were used.

Perchloric acid: 70% double vacuum distilled $HClO_4$ (Cl^-, 0.0001%; silicate and phosphate, 0.0005%; nitrogen compounds, 0.001%; SO_4^{--}, 0.001%; Fe, 0.00001%) from G. F. Smith and Co. was diluted to 1 M or 0.1 M for the experimental solution or to 50 - 60% for chemical and electropolishing solutions.

Triple-distilled water: Deionised water was first distilled over alkaline $KMnO_4$ solution. This water was further distilled three times; initial and final fractions were rejected during each distillation.

Charcoal: Sugar charcoal (Fisher Scientific Co.,1% SO_4^{--}, 1% ash) was activated by electrically heating to a dull redness in a silica test tube in air. Initially, charcoal activated in this manner was purified by repeated washing with constant boiling HCl (prepared in this laboratory) in an all-glass Soxhlet extractor for several weeks. Repeated washing with boiling 3 x distilled water in a Soxhlet extractor for 8 - 10 months eliminated adsorbed Cl^- ions (no turbidity of the washings with silver nitrate). Trace analysis of sugar charcoal using atomic absorption spectro-photometry (UNICAM SP90) indicated the presence of negligible amounts of impurities (< 1 p.p.m.) such as Fe^{+++} and Ca^{++}. This enabled the former step, i.e. washing with constant boiling HCl in later charcoal purification, to be omitted. Before use, the charcoal was reactivated by electrically heating it to dull redness in a silica test tube with nitrogen streaming over its surface.

Platinum: Johnson-Matthey platinum (apparatus grade, i.e. grade 4) was used for reference and counter electrodes and for pinch-seals and other electrical connections. All Pt foils and cylindrical electrodes were cleaned with boiling HNO_3, washed with 3 x distilled water (sometimes dipped momentarily in aqua regia, washed with deionised water, cleaned with boiling concentrated HNO_3 and washed with 3 x distilled water) and steamed with steam from 3 x distilled water. Then, they were platinised (204) in 2% chloroplatinic acid solution at 8 - 10 mA. cm.$^{-2}$ for 8 - 10 minutes for anodes, and at 15 - 20 mA. cm.$^{-2}$ for 15 - 20 minutes for reference hydrogen electrodes. These electrodes were washed with 3 x distilled water, concentrated HNO_3, 3 x distilled water, steamed with steam from 3 x distilled water and stored in the experimental solution before use. Fresh electrodes were prepared for each experiment.

Glassware: Pyrex was used throughout. All glassware was cleaned first with sodium hydroxide, washed with deionised water, then cleaned with fuming nitric acid and washed with deionised water and finally with 3 x distilled water. After final cleaning with steam from 3 x distilled water, most of the apparatus was dried in a stainless steel oven reserved for clean glassware and then assembled.

Washers: Teflon washers, used in a few experiments (F5, F6)*, were found unsuitable because the solution crept out through the Pb-Teflon interface. Therefore, Parafilm washers were used in all the other experiments employing Pb foils in between flat glass flanges.

Tubing: Tygon tubing was used in early experiments (F1, F2) for gas lines but not in later ones. Heat-shrinkable Teflon tube was used to connect between the water reservoir of the electropolishing unit and the electrode holder (see Fig. 9**). Initially the electrode

---

* Electrodes are identified by capital letters (R for rods, F for foils), by numerals (indicating the experiments carried out with fresh solutions and new electrodes), by small letters (indicating new electrodes only, but reused solution) and by primes (each prime denoting that the same electrode was used again after a further pre-treatment).

** p. 125

(R1 to R3) was mounted with the aid of a tight Teflon tube at the end of the ground glass plunger but later, heat-shrinkable Teflon tubing was substituted (see Figs. 6, 9 and 10*). All Teflon tubing was cleaned as mentioned earlier for glassware.

Gases: Hydrogen from two sources were used. Block diagrams of the gas purification system and its connection to cell (a) for rods and to cell (b) for foils are shown in Figs. 5a and 5b, respectively.

Elhygen ultra-pure H_2 (< 10 p.p.b. impurities), electrolytically generated and diffused through a Pd - Ag alloy cathode, was passed through copper and Pyrex tubing, a liquid N_2-cooled trap and a 3 x distilled water-filled presaturator to the cathode compartment. The pre-electrolysis cell was similarly supplied from a separate Elhygen generator, except in earlier experiments (R1 to R3) where Matheson pre-purified hydrogen, purified further as described below but without use of BTS catalyst, was used.

Reference, charcoal-cleaning and anode compartments of cells utilising Pb rods were supplied with Matheson pre-purified H_2 (H_2, 99.95% minimum purity; O_2 < 20 p.p.m.; N_2 < 100 p.p.m.; moisture < 10 p.p.m.; hydrocarbons 1 - 10 p.p.m.) purified further by an Engelhard Deoxo cartridge (1 p.p.m. O_2) and passed through copper and Pyrex tubing, divided into separate streams (if necessary) by greased (Dow Corning silicone high vacuum grease) taps followed in all cases by a liquid N_2-cooled trap and one presaturator, filled

---

* pp. 110, 125 and 126

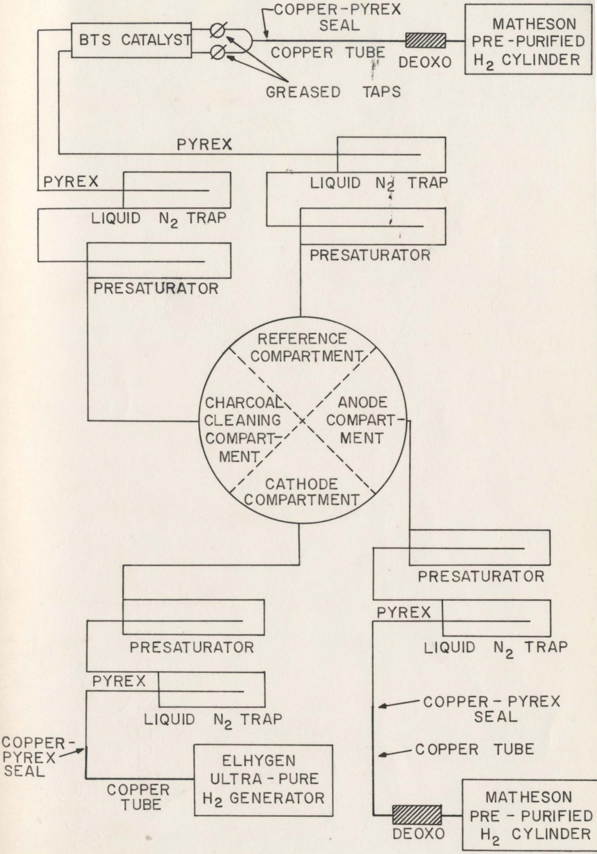
BTS CATALYST
COPPER-PYREX SEAL
COPPER TUBE
DEOXO
MATHESON PRE-PURIFIED H_2 CYLINDER
GREASED TAPS
PYREX
PYREX
LIQUID N_2 TRAP
LIQUID N_2 TRAP
PRESATURATOR
PRESATURATOR
REFERENCE COMPARTMENT
CHARCOAL CLEANING COMPARTMENT
ANODE COMPARTMENT
CATHODE COMPARTMENT
PRESATURATOR
PRESATURATOR
PYREX
PYREX
LIQUID N_2 TRAP
LIQUID N_2 TRAP
COPPER-PYREX SEAL
COPPER-PYREX SEAL
COPPER TUBE
COPPER TUBE
ELHYGEN ULTRA-PURE H_2 GENERATOR
DEOXO
MATHESON PRE-PURIFIED H_2 CYLINDER

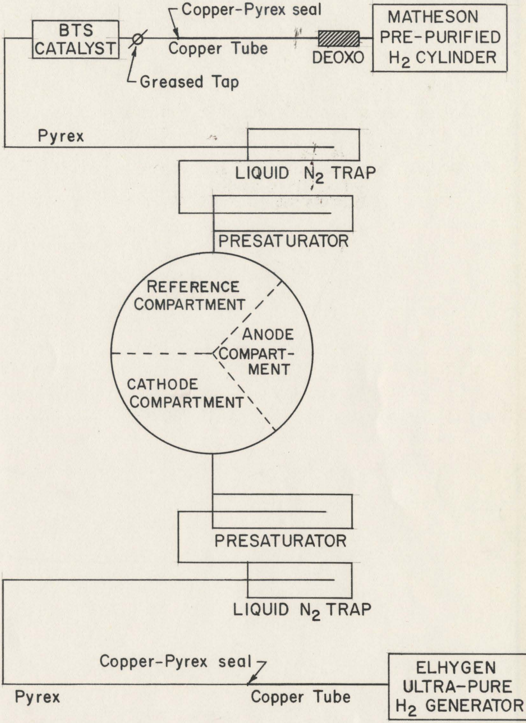

Fig. 5b.

GAS PURIFICATION SYSTEM AND CELL (b) FOR FOILS.

with 3 x distilled water. In later experiments (R4 to R5, F6 to F14) prereduced BTS catalyst (178, 179) from Badische Anilin-und Soda-Fabrik (contains 30% copper in a very finely dispersed form, stabilised on a carrier, activated by various reagents, and removes O_2 to less than 0.1 p.p.m.) placed in a glass tube and maintained at 140°C with the vapours of boiling n-amyl alcohol was placed before the liquid N_2-cooled trap. In experiments with foils, the reference compartment was usually supplied with pre-purified H_2, further purified by Deoxo and by BTS catalyst, as described above. No gas was supplied to the anode compartment in these experiments.

Hyrdogen supplied to the electropolishing and washing apparatus passed through a similar gas train but without BTS catalyst or a presaturator.

Matheson pre-purified N_2 (N_2, 99.997% minimum purity; O_2, 0.0008%; moisture, 0.0005%; CO_2, 0.0001%; Ar, 0.001%; hydrocarbons, 0.05 p.p.m.), used in some experiments, was further purified by the same purification train as for pre-purified hydrogen except that the liquid N_2-cooled trap was replaced by a solid CO_2-and-ethanol-cooled trap.

(11) Purification of Solutions

It was decided to use 0.1 M and 1 M $HClO_4$ in this work for the following reasons:

(i) The perchlorate ion does not form a sparingly soluble lead salt; indeed, lead perchlorate is exceptionally soluble in water.

(ii) Although specific adsorption of perchlorate ions at a Hg interface was reported by Grahame (179b) and although a negative displacement of the electrocapillary maximum occurs, this is not to be regarded as specific interaction of a potential-determining type but rather as a result of squeezing out of large structure-breaking ions from the water.

(iii) The relatively high purity of available $HClO_4$.

Different workers prefer different methods for minimising the contamination of electrodes during measurements. One such method is anodic activation, which is suitable for noble metals. This method consists in the use of an anodic pulse immediately before taking a rapid sequence of measurements (130). It is, however, quite inapplicable to metals such as lead which readily dissolve anodically (or even when unpolarised).

(a) Pre-electrolytic Purification

For metals like lead, the extensively used pre-electrolytic purification is useful. The pre-electrolytic purification method is to deposit the impurities on a cathode (the same material as the working cathode is most desirable) under a hydrogen atmosphere for a sufficiently long time until impurities have been essentially eliminated.

Pre-electrolysis of $HClO_4$ was not carried out in the preliminary experiments (F1 to F8). Pre-electrolysis in pure hydrogen-saturated solution was conducted in the reservoir cell (3 liters), shown in diagrammatic form in Fig. 6. Both anode and cathode were attached to glass plungers moving in ground glass sleeves so that one or both could be removed from the solution. As lead cathode in earlier experiments, R1 to R3, ca. 30 cm.^{2} Pb foil, beaten from Pb rods (Johnson-Matthey and Co.) and in F9, ca. 70 cm.^{2} Pb foil (Fisher Scientific Co.) were used. For the remaining experiments, 4 - 5 cm.^{2} area Pb rods as shown in Fig. 6 were preferred {to avoid the contamination of Pb while beating and also to avoid the possible bimetallic (Pb/Pt joint) contact with the solution} and a large platinised Pt anode (25 cm.^{2} area) supplied with ultra-pure hydrogen, treated as mentioned in Section 3A(1), were used; the reactions in hydrogen atmosphere being hydrogen ion discharge and molecular hydrogen ionisation, respectively. All cup-cones, sockets and gas-solution control taps were water sealed. Pt-Pyrex pinch seals (179a) were used for electrode connections. Broad Pt filaments (3 mm.) were successfully made into pinch contacts for the electrodes for which high current-carrying capacity was required. Contact to Pb

Fig. 6.

PRE-ELECTROLYSIS CELL

1. Reservoir Cell (3 liters)
2. Plungers
3. Lead Cathode
4. Platinum Anode
5. Gas-Solution Control Taps;
   Water Sealed
6. Heat Shrinkable Teflon

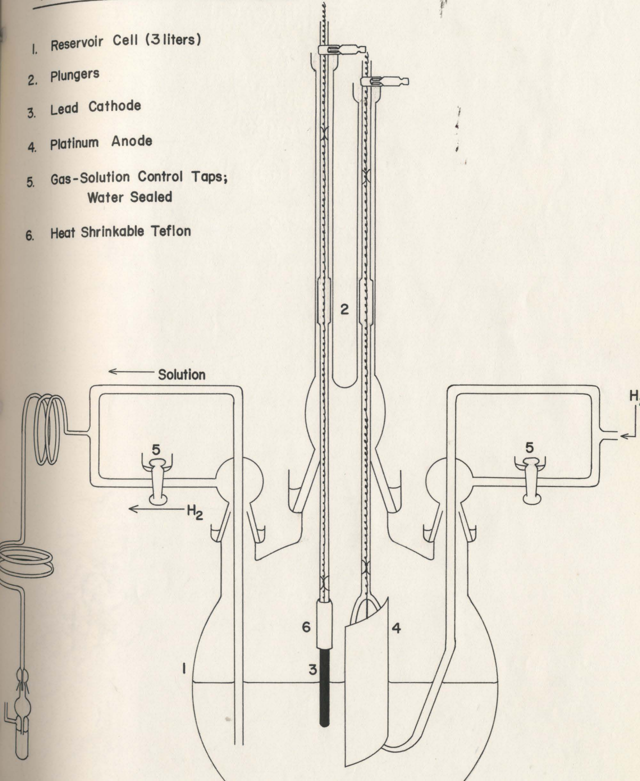

was made with a fine Pt wire inserted into a freshly-cut slot, closed-up tight and protected from the solution by heat-shrinkable Teflon tubing, fitting tightly over the lead and the glass tubing enclosing the wire. Contact to the Pt anode was with a fine Pt wire, sealed to Pt foil supported with glass hooks and the glass tubing enclosing the wire. Perchloric acid (0.1 M and 1 M) was deaerated by bubbling hydrogen for a minimum of 24 hours and pre-electrolysis was carried out at $-i = 0.5 - 2$ mA. cm.$^{-2}$ for up to a month. The current was maintained by a 1 - 30 V. d.c. regulated power supply (Heathkit model IP - 28). Although higher cathodic currents were attempted ($-i$ up to 6 mA. cm.$^{-2}$) for pre-electrolysis (F11 - F14, R4a), they were found unsuitable {see Section 3A(11c)}. Further, pre-electrolysed solutions were subjected to a second pre-electrolysis (R3c, R4 and R5) in the experimental cell and to continuous adsorptive cleaning with activated carbon in a special compartment of the cell (a) {Fig. 10*}. The pre-electrolysis cell was attached to the main cell by means of a flexible glass spiral and Quickfit B7 joint (cup-cone and socket), when the solution was to be passed from it into the cell. The first portion of the solution, used for washing out the tubing between the pre-electrolysis cell and the main cell, was discarded.

---

* see p. 126

(b) Adsorptive Purification

Although pre-electrolysis is thought to result in the removal from the solution of surface-active non-electrolytes, such substances are unlikely to be strongly adsorbed at a strongly polarised electrode, as normally used in pre-electrolysis. It is, therefore, useful to supplement this method by the addition of some unpolarised adsorbing medium. For more than a decade, activated charcoal has been used to remove such impurities in electrochemical studies (180, 180a). Cleaning solutions with activated charcoal has enabled the differential capacities of tranquil pool and dropping mercury electrodes to be brought into coincidence (181). Whereas the adsorption of uncharged molecules occurs on all charcoals, the adsorption of electrolytes depends both on the charcoal composition and on its pre-treatment. Thus, according to Bikerman (182), an ash-free carbon heated in air carried a negative surface charge in water, whereas heating in the absence of air at 900 - 1000°C caused the surface charge to be positive on subsequent immersion. The latter type of charcoal was used in much of the present work in experiments R3b', R3c, R4 and R5.

(c) Analysis of Pre-electrolysed Perchloric Acid

Anodic stripping analysis is a very powerful tool for trace analysis of elements at concentrations as low as 10^{-9} - 10^{-10} M. It consists of two separate and distinct operations: electrolysis to form a concentrated deposit on the working electrode, and subsequent dissolution (stripping) of this deposit. The method of deposition and stripping need not be the same; in practical stripping analysis the two electrochemical techniques are combined in an appropriate manner so as to utilise the best qualities of each in performing its required function (183, 184, 185). In the present work, the apparatus shown in Fig. 7 was used. The electrolysis was carried out in a 150 ml. beaker fitted with a 4-holed rubber cap. The hanging Hg drop electrode (Metrohm Electrode, Micro feeding device E - 410, Brinkmann Instruments) was through one of the holes. The electrode was prepared as by Smith and Delahay (186), using triple-distilled Hg (McArthur Chemical Co. Ltd., Canada). Glass tubes through the other two holes were used for N_2 {L grade from Canadian Liquid Air (N_2, 99.99%; O_2, 20 p.p.m. maximum; moisture < 10 p.p.m.; Ar, 80 p.p.m.)} inlet and outlet, respectively. The external saturated calomel reference electrode (Coleman Instruments Inc.,U.S.A.)was in a beaker containing 1 M $NaNO_3$ and was connected via a bridge containing 1 M $HClO_4$ to the cell. A glass-enclosed magnet was also used for stirring. To eliminate possible contamination, the tips of the bridge, gas inlet, beaker and magnetic stirrer were washed carefully, rinsed with 3 x distilled water and finally rinsed with the test solution. The hanging Hg drop was renewed for each run. The stirring rate, Hg drop size etc., were maintained the same for all runs. Experiments were carried out in an air bath

STRIPPING ANALYSIS CELL

1. Beaker Containing Test Solution
2. Beaker Containing IM Sodium Nitrate
3. Bridge Containing IM Perchloric Acid
4. Metrohm Electrode
5. Saturated Calomel Electrode
6. Hanging Mercury Drop
7. Magnet In Glass
8. Wires For Electrical Contact

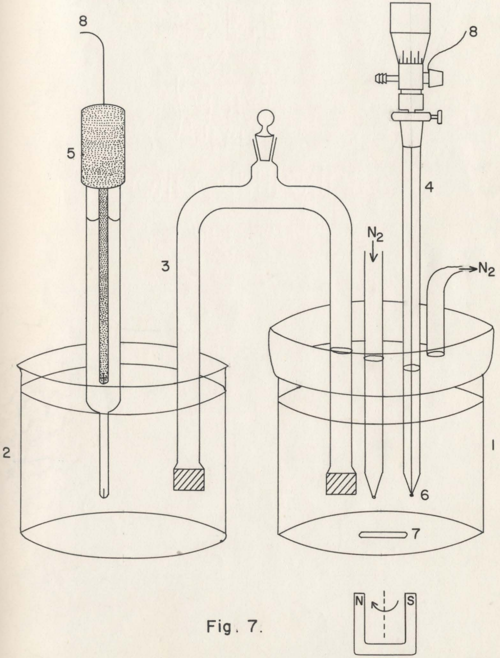

Fig. 7.

maintained at 25 ± 1°C. For the analysis, various low concentrations of Pb^{++} {$Pb(ClO_4)_2 \cdot 3H_2O$, reagent grade G.F. Smith Chemical Co.} dissolved in 1 M $HClO_4$ were prepared. Each solution was analysed by placing about 80 ml. in the cell. The solution was deaerated by bubbling N_2 through it. Concentrating electrolysis of the Hg drop was performed for a pre-determined time (from 5 minutes to 1 hour - depending on the concentration of Pb^{++} ions) with vigorous stirring (bubbling N_2 gas through solution and magnetic stirring) of the solution, at a potential of -0.900 V. versus a saturated KCl calomel electrode, using a Beckman Electroscan 30 as a potentiostat.
5 - 15 seconds after the stirring was stopped (the period necessary for the solution to come to rest), the potential was changed linearly at 20 mV. $sec.^{-1}$ in the anodic direction. The oxidation of Pb at the Hg drop was recorded, the characteristic peak of the anodic stripping current being obtained. The results of the analysis (average of four different runs in each case) are given in Table 2.

The concentration of Pb^{++} ions in 1 M $HClO_4$, prepared without pre-electrolytic purification, as calculated from the calibration curve (Fig. 8) was 7.1×10^{-10} M.

Table 3 shows that high currents are not suitable for pre-electrolysis of 1 M $HClO_4$ at Pb cathodes since the concentrations of Pb^{++} after such pre-electrolysis are found to be in the order of 10^{-6} M. In satisfactory experiments (fall of overvoltage with -Q and regular hysteresis) pre-electrolysis was carried out at low current densities only, i.e. 1 - 2 mA. $cm.^{-2}$.

TABLE 2. STRIPPING ANALYSIS OF Pb^{++} IN AQUEOUS PERCHLORIC ACID
(lead-free double vacuum distilled $HClO_4$ from G.F. Smith and Co.):
CALIBRATION DATA

Solution composition	Time of electrolysis /minutes	Anodic stripping current /μA.	Anodic stripping current computed for 15 minutes of electrolysis /μA.
1 M $HClO_4$ (untreated)	60	0.0098	0.00245
1.18×10^{-8} M Pb^{++} in 1 M $HClO_4$	15	0.024	0.024
1.18×10^{-7} M Pb^{++} in 1 M $HClO_4$	15	0.264	0.264
1.18×10^{-6} M Pb^{++} in 1 M $HClO_4$	15	2.3	2.3
1.18×10^{-5} M Pb^{++} in 1 M $HClO_4$	15	16	16
1.18×10^{-4} M Pb^{++} in 1 M $HClO_4$	5	37.7	103

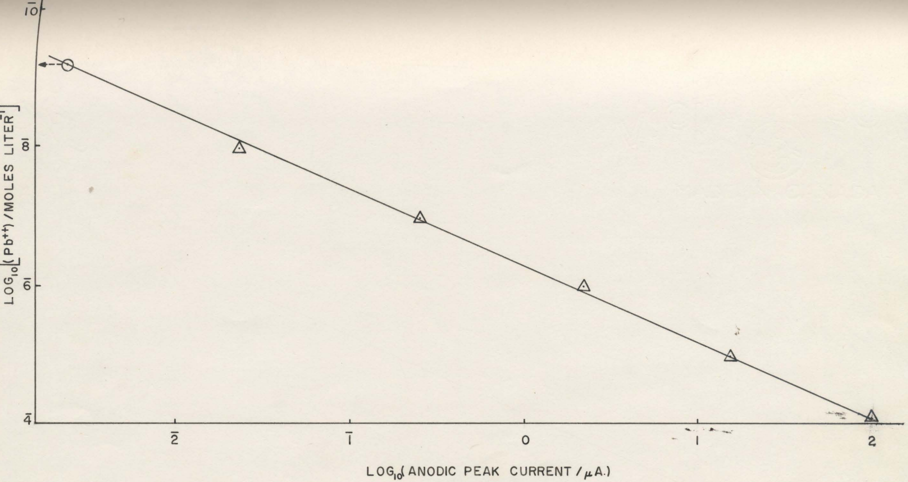

Fig. 8. CALIBRATION CURVE FOR Pb^{++} STRIPPING ANALYSIS IN THE CONCENTRATION RANGE $10^{-4} - 10^{-8}$M. SUPPORTING ELECTROLYTE 1M $HClO_4$ ACID. ELECTROLYSIS TIME 15 min. (OR COMPUTED VALUES FOR 15 min.) AT − 0.900 V. VS SCE VOLTAGE SWEEP RATE 20 mV./sec. ⊙ CONCENTRATION OF Pb^{++} IN 1M $HClO_4$ = 7.1 X 10^{10}M.

TABLE 3. ANALYSIS FOR Pb^{++} BY ANODIC STRIPPING OF 1 M $HClO_4$ SOLUTION PRE-ELECTROLYSED AT HIGH CURRENT DENSITY

Solution composition	Time of electrolysis /minutes	Anodic stripping current /μA.	Anodic stripping current computed for 15 minutes of electrolysis /μA.	Concentration of Pb^{++} deduced from anodic peak
1 ml. of 9.3×10^{-6} M of Pb^{++} + 99 ml. of pre-electrolysed 1 M $HClO_4$, for a month at 4 mA. $cm.^{-2}$ *	5	2.68	8.04	5.4×10^{-6} M
Pre-electrolysed 1 M $HClO_4$, for 2 months at 4 mA. $cm.^{-2}$	5	3.65	10.95	7.2×10^{-6} M
Pre-electrolysed 1 M $HClO_4$, for 2 months and a day at 4 mA. $cm.^{-2}$	15	7.6	7.6	5.0×10^{-6} M

* Addition did not significantly change the concentration of Pb^{++} in the solution.

(111) Pre-treatment of the Lead Electrode

The requirement of an unstrained, uncontaminated and oxide-free lead surface can be met by only a few methods of surface preparation. In this case of electrodes prepared outside the experimental cell, besides meeting the above requirements, the method would also have to permit rapid transfer of the electrode to the cell in order to minimise tarnishing.

Ordinary mechanical methods of cutting or abrading lead renders a rough surface smooth and lustrous, but causes surface damage to a depth of tens of microns (187) and probably enhances surface oxidation. Contamination is also likely from the metal (or glass) tools and polishing powder used. The surface colour of the mechanically polished surface varies with the technique of the polisher, especially when the operation is conducted by hand. Furthermore, although lead, being a soft metal, is self-annealing and recovers quickly from strain at room temperature (188) it may not be free from oxide films or other impurities.

Annealing or melting in hydrogen might seem attractive at first sight. The former has been employed by Bockris and Conway (189) in much of their h.e.r. work. Apart from oxide reduction, however, no essential cleaning action takes place, except that, in melting, the initial surface contamination may be distributed throughout the bulk of the metal. The possibility of contamination from the enclosing vessel forced Bockris et al. (189) to use arsenic-free glass bulbs, in which they heat-treated and sealed up their electrodes in hydrogen, later breaking the bulb beneath the solution in the cell.

The preliminary experiments (R1, R2a, R2b, R3a, R3b and R3b') indicated the unsatisfactory nature of scraping as a method of surface preparation for lead. So, it was decided to use chemical polishing or preferably electropolishing as had Ives and Smith (26, 27). Chemical polishing and electrolytic (anodic) polishing are the most efficient methods of surface cleaning, with the possible exception of ion-bombardment in vacuo, which will not be considered because of its unsuitability for the present work. Aqueous perchloric acid as a polishing agent was selected because it was important to minimise the possible sources of contamination of the cell solution with surface-active organic substances and other foreign anions and cations, to minimise the possible explosion of perchloric acid + organic mixtures (often used for electropolishing) and because lead perchlorate is highly soluble.

Although chemical polishing has been used for preparing clean surfaces of lead, the early work of Jacquet (190) established electropolishing as a controllable means of removing plastically deformed and cold-worked regions from a metal surface. Electropolishing is especially useful for soft metals. The function of an ideal polishing process can be distinguished as (a) smoothing by elimination of large scale irregularities (above 10^{-4} cm. size) and (b) brightening by removal of small scale irregularities (down to 10^{-6} cm.in size). These two features of electropolishing are thought to operate by different mechanisms. Smoothing results when the metal dissolution rate is controlled by the diffusion, either of metal ions to the bulk solution or of acceptor anions or molecules to the electrode. Although Edwards (191) supposed that the random arrival of solvating acceptors at an electrode could account for the absence of crystallographic etching, this does not seem to be the generally accepted mechanism of brightening. Hoar and Mowat (192) suggested that polishing only takes place when a thin compact oxide film (uniformly attacked by the electrolyte) is present on the anode. The random arrival of cation vacancies at the metal-film interface was supposed to account for the supression of etching. Several workers (193, 194, 195, 196, 197) were able to obtain evidence for the presence of oxide films on many metals (Al, Au, Fe, Ni, Zn, Pb, Sn, W, Cu, Mo, Cd, Ag, Ti, U and In) while these were being polished but not while they were undergoing etching. The evidence in favour of this theory comes from:

(i) Non-wetting of the anode by mercury which suggested the presence of oxide, even in perchloric acid baths.

(ii) Periodic oscillations of current-voltage prior to the establishment of polishing conditions: the existence of a non-metallic layer was suggested.

(iii) The impossibly high cell resistance, which increases with increase of anodic current density in the transition region (the region in which a solid film is being formed). However, in the post-transition region, the cell resistance decreases with the increase of anodic current density.

(iv) The detection of films by a.c. impedance and ellipsometry. All of the evidence confirms the existence of thin-films 6 - 60 Å thick.

In contrast, Darmois and Epelboin (198, 199), who have done much work with perchlorate-containing solutions assumed, in agreement with the views of Wagner (200) and Edwards (191), that water molecules are the acceptors in such solutions. They also proposed that a layer of adsorbed perchlorate ions adjacent to the anode provides a high field for random dissolution. In spite of the high anode potentials often found, the Joule heating was insufficient to melt solid Ga undergoing electropolishing at just below its melting point. This was regarded as good evidence that no (resistive) oxide film was present in this case. The work of Casey and Bergeron (201) is specially relevant in that these workers found that Pb and other metals having slightly basic oxides could not be polished in alkaline solutions (in contrast to Al and Zn which could), even when ammonium acetate, which dissolves PbO, was also present. This evidence, together with that of Epelboin, Brouillet and Froment (202), that lead enters perchlorate solutions as the divalent ion and that neither gassing nor pitting attack of the electrode occurs under electropolishing conditions, strongly suggests that the electropolishing of Pb in solutions of perchloric acid does not require the presence of a thin oxide film. Furthermore, the results of Nikiforova and Jofa (203), that passivation of Pb in concentrated perchloric acid does not occur at anodic current densities < 0.1 A. cm.$^{-2}$ confirms that it is difficult for oxides to form in this system. This evidence denies the presence of an oxide film. Therefore, if an oxide were present after electropolishing, its thickness is unlikely to be great, certainly less than 60 Å, as mentioned earlier.

In the present work, both Pb rods and foils were initially treated as follows:

(i) Degreased in refluxing benzene for 4 - 8 hours.

(ii) Washed with ethyl alcohol, followed by 3 x distilled water.

(iii) Dipped in 4 M NaOH for 1 minute, washed with 3 x distilled water.

(iv) Dipped in 1 M $HClO_4$, washed with 3 x distilled water and then subjected to chemical polishing and electropolishing.

After the initial cleaning as above but before electropolishing, electrodes were chemically polished for 2 minutes in 50% $HClO_4$ in contact with a large Pt foil (≃ 20 cm.^{2}), washed with 3 x distilled water and then steamed (steam from 3 x distilled water) until grease-free (for ≥ 1 hour). The oxide film that developed during this treatment had no effect on subsequent behaviour.

Lead rods were then electropolished at 1 A. in 50% $HClO_4$ for 5 minutes under a H_2 atmosphere in a separate cell (Fig. 9). The polishing cell for rods consisted of a large cylindrical Pt cathode (area 35 cm.^{2}), surrounding the central Pb anode. A water-sealed outflow tap was used to remove the washings. The water reservoir was connected to the side arm of the plunger as shown in Fig. 9. The Pb electrode assembly, electrode connections and Pt-Pyrex pinch seals were similar to those described in Section 3A(11a). All cup-cones, sockets and gas-solution control taps were water sealed. The polishing solution was deaerated by bubbling hydrogen. A water reservoir containing 3 x distilled water was saturated with hydrogen (pre-purified cylinder H_2 passed via a purification train) for at least 24 hours. After polishing, the mirror-bright electrode was thoroughly washed for a few minutes with H_2- saturated 3 x distilled water and transferred wet, protected by a rapid stream of hydrogen gas, directly to the cell (a) {Fig. 10}. It became automatically cathodic on meeting the solution.

Lead foils, after initial cleaning, chemical polishing and washing, were mounted in the cell (b) {Fig. 11} and electropolished in situ in pre-electrolysed 1 M $HClO_4$ at 95 mA. for 5 minutes. After polishing, the electrode was thoroughly washed, also with pre-electrolysed 1 M $HClO_4$. Finally, the electrode was made cathodic and the cell filled with pre-electrolysed solution under a hydrogen atmosphere.

1. LEAD ANODE.
2. PLATINUM CATHODE.
3. PLUNGER TUBE WITH SIDEARM.
4. WATER RESERVOIR (5 liters)
5. HEAT SHRINKABLE TEFLON.
6. GAS – SOLUTION CONTROL TAPS; WATER SEALED.
7. OUTFLOW TAP.
8. FINE PLATINUM WIRE FOR ELECTRICAL CONTACT.

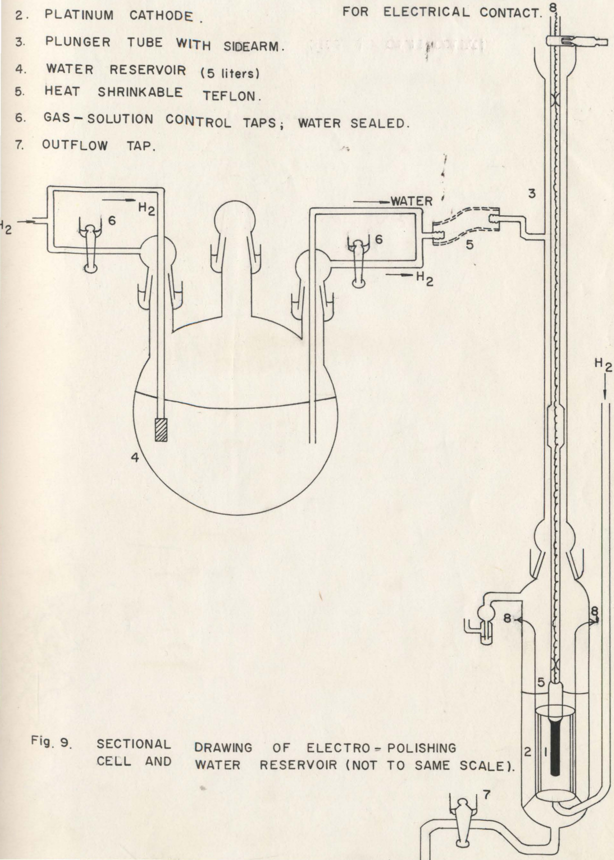

Fig. 9. SECTIONAL DRAWING OF ELECTRO-POLISHING CELL AND WATER RESERVOIR (NOT TO SAME SCALE).

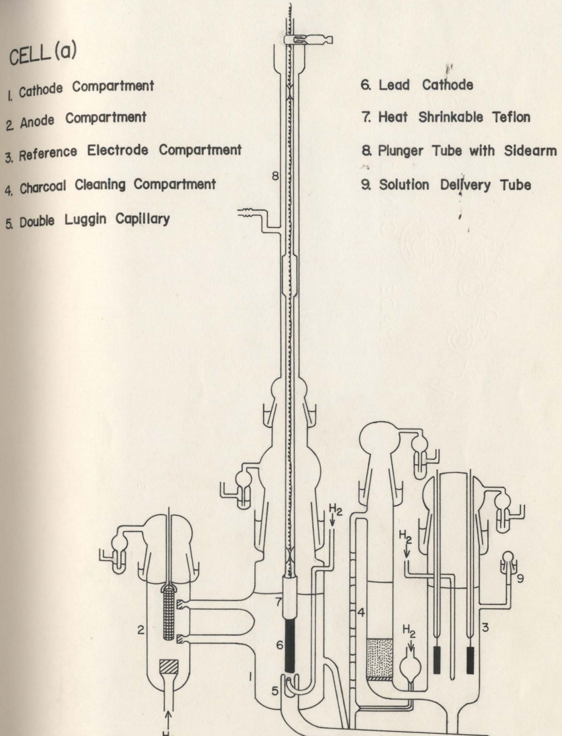
CELL (a)
1. Cathode Compartment
2. Anode Compartment
3. Reference Electrode Compartment
4. Charcoal Cleaning Compartment
5. Double Luggin Capillary
6. Lead Cathode
7. Heat Shrinkable Teflon
8. Plunger Tube with Sidearm
9. Solution Delivery Tube
8
H2
H2
H2
9
7
4
2
H2
3
6
1
5
H2

Fig. 10.

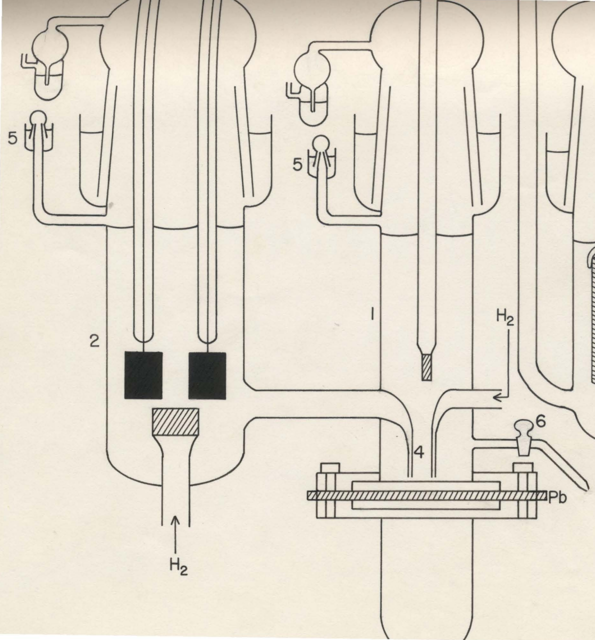

Fig. II.

CELL (b)

1. Cathode Compartment
2. Reference Electrode Compartment
3. Anode Compartment
4. Luggin Capillary
5. Solution Delivery Tube
6. Outflow Microtap

The electropolishing power supply was a Heathkit model EUW - 17 in both cases.

(1V) Main Cells

Two types of cells were used, one type for rods and another for foils.

(a) Cell for Rod Electrodes

The Pyrex cell is illustrated in Fig. 10. It consisted of four compartments (cathode, anode, carbon-cleaning and reference electrode) each fitted with presaturators and all glass gas-supply lines. The cathode compartment was supplied with ultra-pure hydrogen from an Elhygen generator. In the cathode compartment, the Pb rod was mounted with the aid of a heat-shrinkable Teflon tube at the end of a precision-ground glass plunger, down which a fine Pt wire passed for electrical contact. The plunger slid within a similarly ground tube, equipped with a protective hood through which gas could be passed; the essential features of this device are shown in Fig. 10. Leakage of air down the cathode plunger was retarded by maintaining a positive pressure of hydrogen in the cell, as far as possible. The anode compartment, containing a large lightly platinised cylindrical Pt gauze (area 110 $cm.^2$), and the cathode compartment were separated by two sintered Pyrex discs. In the first few experiments (R1 to R3) the cathode and anode were not separated; instead a lightly platinised Pt cylindrical anode (area 35 $cm.^2$) surrounding the centrally placed lead rod cathode (as in the present cathode compartment) was used. The charcoal-cleaning compartment, in which activated carbon was supported by a fine sintered filter disc was supplied with a continuous flow of solution by a hydrogen gas-lift. Charcoal-cleaning was not used in the first few experiments (R1, R2a, R2b, R3a and R3b). A Luggin capillary, situated beneath the lead cathode, communicated with the reference electrode compartment via a long spiral tube (forming the return path of the solution circulation system). The reference electrode compartment contained two platinised Pt hydrogen electrodes (204).

(b) Cell for Foil Electrodes

The Pyrex cell is illustrated in Fig. 11. It consisted of three compartments (cathode, reference and anode) the first two being fitted with presaturators and all glass gas-supply lines. The cathode compartment was supplied with ultra-pure H_2 from an Elhygen generator. The Pb foil (cathode) was mounted in the cell with one or two layers of 0.01 - 0.02 cm. thick Parafilm gaskets between the flat flanges which, with aluminium alloy clamps secured, produced seals which could hold 10^{-5} torr. after heating with a hot air blower (172). A large lightly platinised cylindrical Pt gauze (204) anode (area 110 cm.^{2}) and the Pb cathode were separated by a doubly-bent length of tubing, terminating in a fine frit. The reference electrode compartment contained two platinised Pt hydrogen electrodes (204). The tip of the Luggin capillary from the reference electrode compartment was situated very close to the cathode surface. A solution-wetted outflow microtap (Springhams, 1 mm. bore) was used to facilitate the removal of solution and washings after in situ electropolishing of the lead. Leakage of air through the tap was diminished by maintaining a positive pressure of hydrogen in the cell, as far as possible. No charcoal-cleaning compartment was employed in this cell because of the difficulty of preventing its contamination and because it was desired to separate anode and cathode, the former being a source of anodically evolving O_2 during the cathodisation of the lead.

All cup-cones and sockets in both cells (a) and (b) were water sealed. Electrode connections and Pt-Pyrex pinch seals were similar to those described under pre-electrolysis {Section 3A(11a)}.

(V) Instrumentation and Procedure

The polarising circuit consisting of a galvanostat and a microswitch are shown diagrammatically in Fig. 12. The galvanostat consisted of a battery (45 or 90 V.) and variable precision resistors (to permit variation of the current from 1 μA. to 100 mA.) soldered to different positions of a make-before-break switch, in series with the battery, so that different currents were switched on without breaking the circuit.

The microswitch used was similar to that of Hammerli, Mislan and Olmstead (170). It operates over a current range up to 800 mA. and potential range up to 60 V. and is switched by a single pulse. The theoretical frequency of the switch is 250 MHz, which corresponds to a break of 4 nanoseconds. The practical response was about 200 nanoseconds. Operation of the circuit depends on the fact that one state of the bi-stable or flip-flop circuit, consisting of the two 220 pF. capacitors, the diodes D_9, D_{10} and micrologic element E_3 (type MC 914G), turns on the transistors, Q_1 and Q_2 (type 2N2219) and the other state of the bistable circuit turns them off. When the transistors are conducting, the current source is short-circuited to ground, but diodes D_1 - D_8, since they will then be back-biased, prevent the cell from also being short-circuited. When the transistors are not conducting, current readily flows through the cell because diodes D_1 - D_8 are then forward-biased. Micrologic elements E_1 and E_2

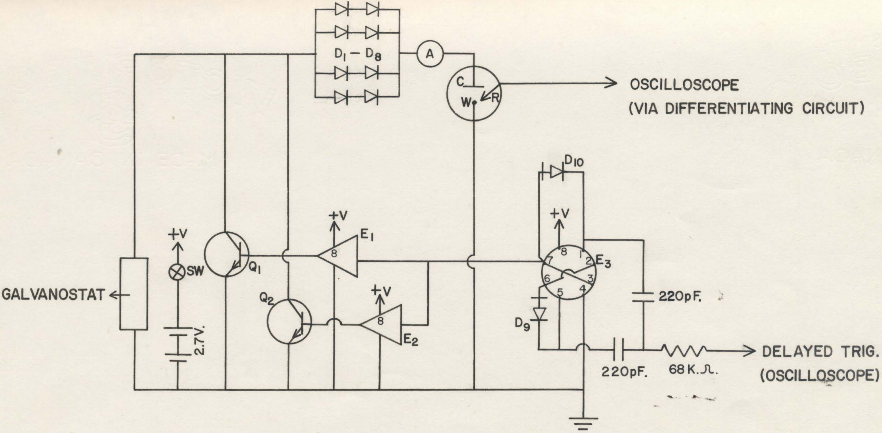

Schematic of transistor switch: W=cathode, C=counter electrode, R=reference electrode, D$_1$······D$_{10}$-diodes, E$_1$,E$_2$,E$_3$ -micrologic elements, Q$_1$ and Q$_2$-transistors, SW-power switch, A-current meter.

Fig. 12.

(type MC 900G) serve as buffer elements and ensure enough current is supplied to Q_1 and Q_2. The micrologic elements are powered by two mercury batteries in series, i.e. by 2.7 V. The 68 k.Ω. resistance serves to isolate the bistable from the delay trigger output (of the Tektronix 547 oscilloscope). The +V signal was connected to pin 8 of E_1, E_2 and E_3. The bistable was triggered by the delay trigger that supplies a sharp positive-going spike of about 10 V. at the end of the delay period, as set by the delay time switch and the delay multiplier control of the oscilloscope, to interrupt the current to the cell. The next pulse turned the transistors off and the current to the cell was restored.

In order to correct for I.R. drop overvoltage, the overvoltage signal from the Analog Devices 147A operational amplifier output {Fig. 38*, this will be discussed in Section 3B(1)} was fed to channel 1 of the 1A1 dual trace plug-in unit on the Tektronix 547 oscilloscope. Using a single sweep technique, the trace on the oscilloscope screen before, during and after the current interruption was photographed with Polaroid Land roll film type 47 in a Tektronix oscilloscope camera C-12. A typical oscillograph of the I.R. drop between the cathode and the Luggin capillary is shown in Fig. 13. The observed discontinuity in the ordinate at $t = 0$, the time of current interruption, corresponds to the I.R. drop overvoltage.

---

* see p. 205

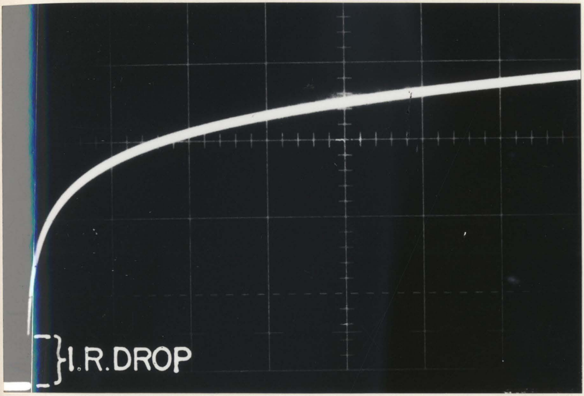

Fig. 13. OSCILLOGRAPH OF I.R. DROP FOR $-i = 50$ mA. cm.$^{-2}$, ORDINATE / 0.1V. cm.$^{-1}$, ABSCISSA / 1 MSEC. cm.$^{-1}$, I.R. DROP OVERVOLTAGE CALCULATED = 65 mV.

In this way, the I.R. drops at different currents were determined. A typical plot of I.R. drop versus cathodic current is given in Fig. 14. I.R. drop overvoltage determined in this way was used to correct measured overvoltages.

Lead electrodes were cathodised galvanostatically (initially at 30 μA. to 1 mA.) and the overvoltage variation with time was recorded. Overvoltages were measured with one of the following combinations of instruments:

(i) Experiments R1 to R3 and F1 to F5: a Fluke 891 Voltmeter and a Heath EUW 24 recorder (10 or 100 mV. full-scale sensitivity).

(ii) Experiments F6 - F12: a high impedance (10^{14} Ω) buffer amplifier (M.U.N. made), based on an Analog Devices 311K operational amplifier with a Fairchild Model 7050 digital multimeter.

(iii) Experiments F13, F14, R4 and R5: the above buffer amplifier, a Keithley 370 recorder (recorded expanded in scale, using a potentiometer to offset part of the voltage).

Currents were measured with Simpson meters (models 373 and 374) in experiments R1 to R2, F12 to F14, R4 to R5 or with a Philips electronic multimeter, type 2400-02, in experiments R3, F1 to F11. Tafel plots {equation (1.2)} were studied by the rapid-run method, the current being kept constant for predetermined periods (0.1 - 5 minutes) uniform within each run, between current changes. Most experiments were carried out essentially at one, or in some

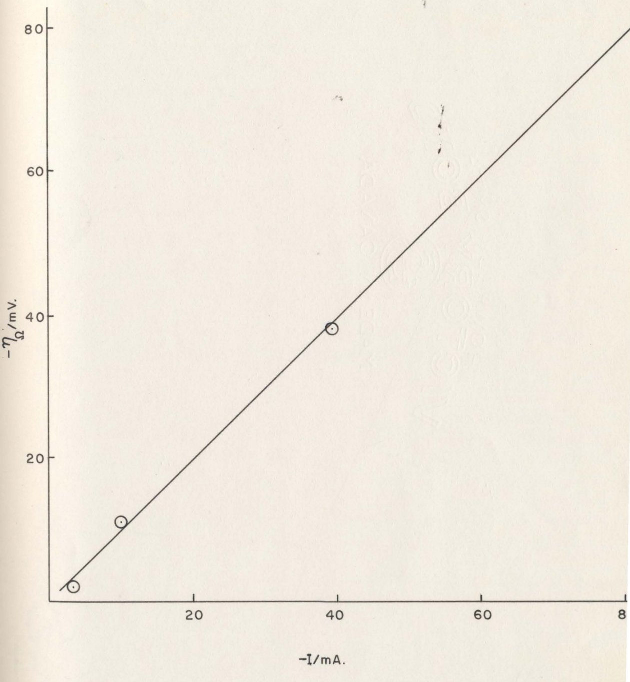

Fig. 14. TYPICAL PLOT OF I. R. DROP OVERVOLTAGE VERSUS CATHODIC CURRENT FOR ELECTRODE R4b.

cases, two currents except for short excursions (say 30 - 60 minutes) to higher or lower currents and Tafel runs.

All experiments except R2 and R3, were carried out in air at room temperature (thermostated to 25 ± 2°C). However, the cell (a) was mounted in water in a Tamson model TE9 thermostatic bath, Neslab Instruments Inc., (temperature regulation ± 0.01°C) for experiments R2 and R3, to study the influence of temperature on overvoltage. Most of the experiments except R1 to R3 and F1 to F5, were conducted within an earthed metallic cage to diminish the effects of a.c. pick-up.

(VI) Results of Early Experiments

(a) Preliminary Experiments

Some preliminary experiments were made with unpurified $HClO_4$ for the purpose of testing the new cell (b) designed for work with Pb foil. The first few experiments (F1, F2, F3) were very crude (99% Fisher Pb, gases supplied through Tygon tubing, unpurified $HClO_4$) and were not satisfactory because of the poor conditions. Steep Tafel slopes $\geqslant$ 450 mV. and large kicks of overvoltage (ca. 200 mV.) were observed in these experiments with low purity Pb, which developed a black surface film, probably of impurities, during chemical polishing.

Later experiments (F4 to F8) were made with hydrogen supplied through copper and Pyrex tubing, but without BTS catalyst in some cases (F4, F5). Electrodes of 99.9% pure Goodfellow Pb, 0.025 cm. thick, were electropolished in situ and used in unpurified 1 M $HClO_4$. Parafilm washers were used except for F5 and F6 in which Teflon was substituted. This was not satisfactory because of leakage, as already mentioned in Section 3A(1). In all these experiments in less pure solutions, $-\eta$ increased rather than decreased with $-Q$, both at 20 and 525 μA. cm.$^{-2}$. As indicated in Table 4, experiments were begun at 20 μA. cm.$^{-2}$ and the increase of $-\eta$ was greatest at this current density. Fig. 15 illustrates the increase of $-\eta$ at every current density studied, coupled with a decrease of Tafel slope

TABLE 4. HYDROGEN OVERVOLTAGES FOR LEAD IN AQUEOUS PERCHLORIC ACID IN SOME PRELIMINARY EXPERIMENTS {see also Tables 22 and 23 in Section 3B (11a)}

Experiment number	Current density to which quoted $-\eta$'s correspond /mA. cm.$^{-2}$	Maximum current density passed for ≥ 30 minutes /mA. cm.$^{-2}$	Initial $-\eta$/mV.	Final		Conditions of electrode and solution
				$-\eta$/mV.	$-Q$/coulombs	
F7	0.02	0.02	269	567	5	Electropolished (95 mA. for 5 minutes) foils in unpre-electrolysed 1 M $HClO_4$
F7	0.525	0.525	996	1090	137	
F8	0.02	0.525	445	804	368	
F8	0.525	0.525	805	1073	368	

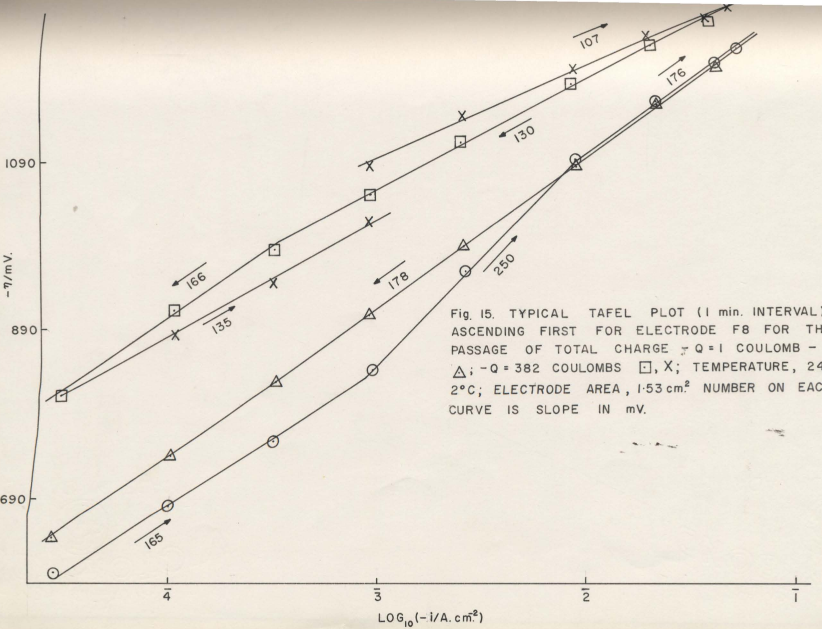

Fig. 15. TYPICAL TAFEL PLOT (1 min. INTERVAL) ASCENDING FIRST FOR ELECTRODE F8 FOR THE PASSAGE OF TOTAL CHARGE $-Q = 1$ COULOMB − ⊙, △; $-Q = 382$ COULOMBS ⊡, X; TEMPERATURE, 24 ± 2°C; ELECTRODE AREA, 1·53 cm^2 NUMBER ON EACH CURVE IS SLOPE IN mV.

from the range 160 to 250 mV. to the range 105 to 165 mV. Some capacity measurements on these electrodes are reported in Section 3B (11a).

(b) Experiments with Electropolished Electrodes and Solution Pre-electrolysed at Too High Current Densities

Pre-electrolysis at too high a current density led to the presence of analytically detectable Pb^{++} ions as confirmed by stripping analysis {Section 3A (11c)}. Electrodes studied in solutions purified in this manner might be expected to behave differently from those studied in purer solutions. Four lead foils (F11 to F14 inclusive) and one lead rod (R4a) were studied under these conditions. Electrodes F11 and R4a were studied in 1 M $HClO_4$ that had been pre-electrolysed for thirty days at ca. 4 mA. $cm.^{-2}$ while the solutions for F12 and F13 had been pre-electrolysed for lesser periods (6 to 16 days, respectively) at the same current density. Table 5 gives some results of work with these electrodes. It will be noted that the overvoltage increased with the extent of cathodisation in F12, F13 and F11 but decreased for R4a, an experiment in which solution cleaning over activated charcoal was carried out. Fig. 16 shows that the decrease of $-\eta$ with $-Q$ for electrode R4a was linear, with two branches of slopes 20 and 118 mV., respectively. This is the kind of behaviour observed by Ives and Smith (26, 27) and in satisfactory experiments of the present investigation. The behaviour

TABLE 5. HYDROGEN OVERVOLTAGES FOR LEAD IN AQUEOUS PERCHLORIC ACID PRE-ELECTROLYSED AT TOO HIGH CURRENT DENSITIES

Experiment number	Current density to which quoted $-\eta$'s correspond /mA. cm.$^{-2}$	Maximum current density passed for ⩾ 30 minutes /mA. cm.$^{-2}$	Initial $-\eta$ or maximum (if $-\eta$ decreased initially /mV.	$-\eta$ at $-Q$=100 coulombs /mV.	Final		Conditions of electrode and solution
					$-\eta$/mV.	$-Q$/coulombs	
F12	0.535	0.535	642	813	903	321	Electropolished foil (95 mA. for 5 minutes) and 1 M $HClO_4$ pre-electrolysed at 4 mA. cm.$^{-2}$ for 6 days
F13	0.535	29.0	523	592	649	315	Electropolished foil (95 mA. for 5 minutes) and 1 M $HClO_4$ pre-electrolysed at 4 mA. cm.$^{-2}$ for 16 days
F11	0.535	0.535	435	501	524	336	Electropolished foil (95 mA. for 5 minutes) and 1 M $HClO_4$ pre-electrolysed at 4 mA. cm.$^{-2}$ for 30 days

TABLE 5. (Continued)

Experiment number	Current density to which quoted $-\eta$'s correspond /mA. cm.$^{-2}$	Maximum current density passed for $\geq$ 30 minutes /mA. cm.$^{-2}$	Initial $-\eta$ or maximum (if $-\eta$ decreased initially /mV.	$-\eta$ at $-Q=100$ coulombs /mV.	Final		Conditions of electrode and solution
					$-\eta$/mV.	$-Q$/coulombs	
R4a	0.665	0.665	976	904*	845	378	Electropolished rod (1 A. for 5 minutes) and 1 M $HClO_4$ pre-electrolysed at 4 mA. cm.$^{-2}$ for 30 days. Adsorptive cleaning of solution with activated carbon

* interpolated value

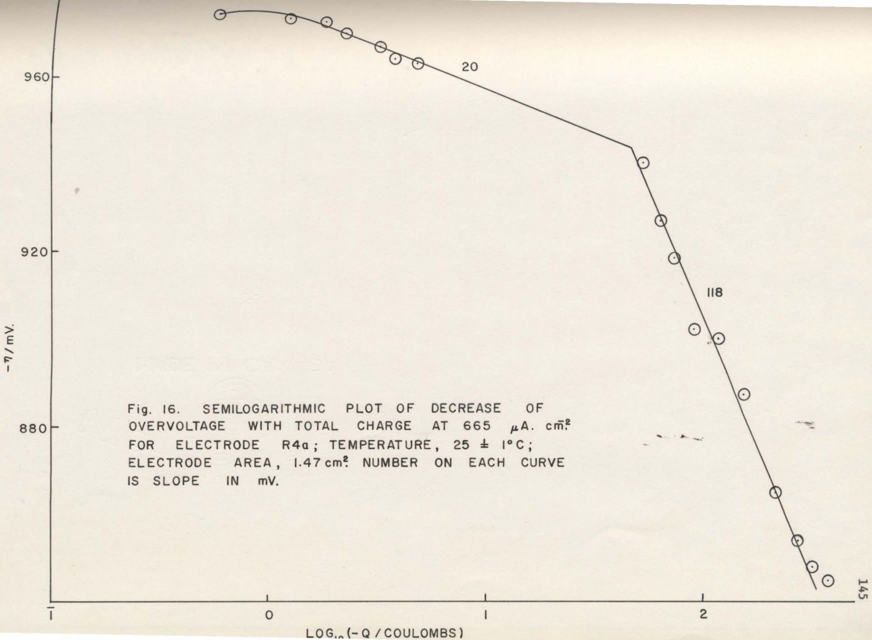

Fig. 16. SEMILOGARITHMIC PLOT OF DECREASE OF OVERVOLTAGE WITH TOTAL CHARGE AT 665 μA. cm^{-2} FOR ELECTRODE R4a; TEMPERATURE, 25 ± 1°C; ELECTRODE AREA, 1.47 cm^2. NUMBER ON EACH CURVE IS SLOPE IN mV.

of R4a was essentially normal, presumably because circulation of solution over charcoal removed Pb^{++} ions introduced in the preceding high current pre-electrolysis. Thus, its Tafel behaviour (Fig. 17) was fairly normal above 10^{-4} A., with Tafel slopes of 140 - 170 mV.

Table 5 also shows that the initial overvoltage was lower the larger the period of previous high current pre-electrolysis. Further, the overvoltages after passage of some 300 coulombs cathodically were still in the same order, i.e. F12 > F13 > F11. The Tafel plots for F11 to F14 were curved and had large amounts of hysteresis, as shown for F11 in Fig. 17, in contrast with R4a.

Overshoot hysteresis, defined by Ives and Smith* (26, 27), was not observed in experiments F11, F13, F14, but was observed rarely in F12 and in R4a. This is another indication of the unsatisfactory state of the system in these experiments with solution pre-electrolysed at too high current densities.

Nevertheless, other electrodes (R4a', R4a" and R4b) were studied in the solution from R4a, because its behaviour was

---

* When an electrode initially in a steady-state ($\Delta\eta/\Delta t << 1$ mV. min.$^{-1}$) was subjected to step changes of current, the immediate potential jump was followed by roughly exponential change of potential in the reverse direction, described as "overshoot hysteresis".

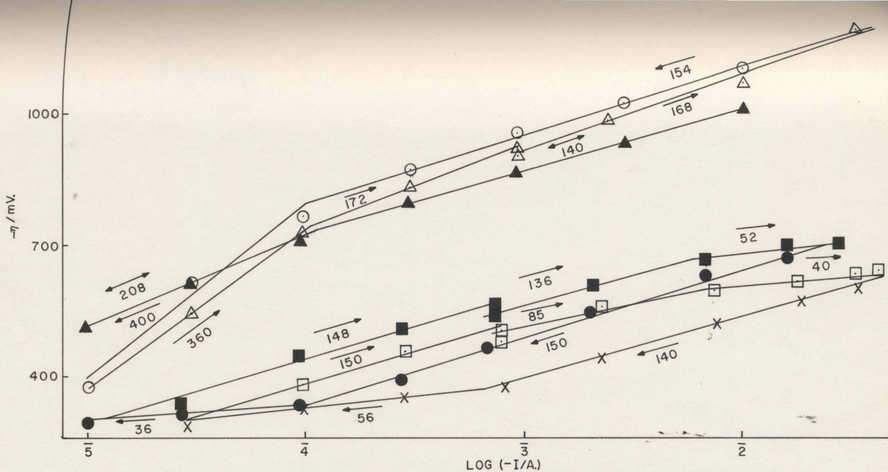

Fig. 17. TYPICAL TAFEL PLOTS (0.1 min. INTERVAL, ASCENDING FIRST) FOR ELECTRODE F11 (AREA, 1.52 cm^2) FOR THE PASSAGE OF TOTAL CHARGE -Q = 59 COULOMBS -⊡, X ; -Q = 260 COULOMBS-■,●; AND FOR ELECTRODE R4a (AREA, 1.47 cm^2) FOR THE PASSAGE OF TOTAL CHARGE -Q = 50 COULOMBS -△,⊙; -Q = 300 COULOMBS -▲. TEMPERATURE, 26 ± 1° C. NUMBER ON EACH CURVE IS SLOPE IN mV.

satisfactory apparently owing to the presence of charcoal. Furthermore, some electrodes (R2a, R3a and R5a) were used for a second in situ pre-electrolysis, in some cases (R3c and R5) in conjunction with adsorption on charcoal. Care was, however, taken that such pre-electrolysis was not carried out at current densities > 2 mA. cm.$^{-2}$ in order to avoid contamination.

(c) Early Experiments with Scraped Electrodes and Solutions Pre-electrolysed at Low Current Densities

Many Russian workers used scraped electrodes in their h.e.r. studies on Pb. However, they failed to observe any time dependence of $-\eta$. The work on scraped Pb was needed to clarify whether the effects observed by Ives and Smith (time dependence of $-\eta$) on polished electrodes were due to special features of the polishing treatment.

In experiments R1, R2 and R3, the Pb rods were dipped into 1 M $HClO_4$ {see Section 3A (111)}, washed with 3 x distilled water and then dried. They were then scraped with a sharp stainless steel razor blade, Pb fragments removed with tissue paper, pickled briefly in 4 M $HClO_4$, washed with 3 x distilled water and transferred quickly into cell (a) {Fig. 10} which, however, had a platinised Pt anode symmetrically surrounding the lead cathode, the compartment to the left (in Fig. 10) being absent. Electrodes were instantly cathodised at a constant current of 315 - 330 μA. cm.$^{-2}$ (R1a was polarised at 1.5 μA. cm.$^{-2}$ for the first 4 hours and than at 160 μA. cm.$^{-2}$) in pre-electrolysed (at $-i \leqslant 2$ mA. cm.$^{-2}$ for 10 - 30 days) 0.1 M $HClO_4$. No activated charcoal was present in the cell nor was BTS catalyst used in the gas purification train {otherwise as described in Section 3A (1)}. All electrodes were studied at 25 ± 0.01°C, except Rla at 24 ± 1°C.

Tafel plots for electrodes Rla, R2a and R2b, initially were curved or multilinear with $b \simeq 200$ mV. at $-I \gtrsim 10^{-4}$ A., $b \gtrsim 600$ mV. at $-I \simeq 10^{-5}$ A. and almost a horizontal line at $-I \lesssim 10^{-5}$ A. (see Fig. 18) with a large hysteresis. After prolonged polarisation at $-i \geqslant 160$ μA. cm.$^{-2}$, the very steep slope at $-I \simeq 10^{-5}$ A. disappeared, but high Tafel slopes ($b \gtrsim 190$ mV.) still persisted. Throughout, overvoltages for increasing current runs were lower than those for decreasing current runs.

Variation of overvoltage, $-\eta$, with the logarithm of the total charge passed cathodically, $\log_{10}(-Q)$, is shown in Fig. 19. Disregarding the deviations at low $-Q$ {$-\eta$ increased in R2b and fell sharply in Rla (this may have been due to trouble with the potential-measuring instrument during initial measurements)}, $-\eta$ for Rla and R2b decreased slowly initially and then rapidly at higher $-Q$ values in a similar manner to Ives and Smith's observations with electro-polished Pb electrodes (26, 27). R2a showed an initial increase

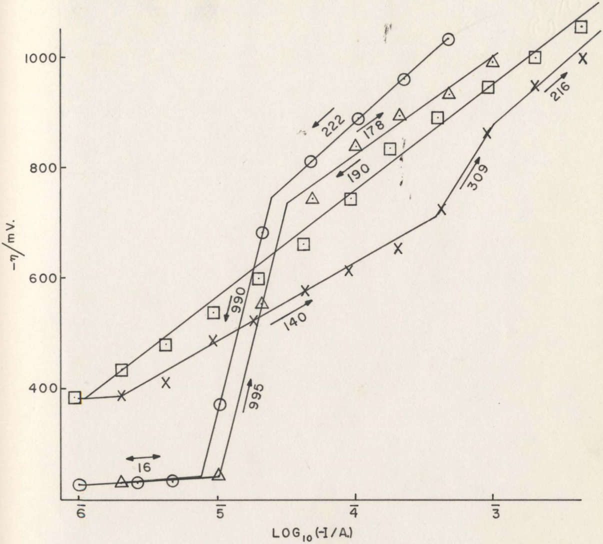

Fig. 18. TAFEL PLOTS (100 sec. INTERVAL) DESCENDING FIRST FOR A SCRAPED Pb ELECTRODE RIa FOR THE PASSAGE OF TOTAL CHARGE −Q = 12 COULOMBS −○, △; −Q = 469 COULOMBS −⊡, X; TEMPERATURE, 24 ± 1°C; ELECTRODE AREA, 3 cm^2. NUMBER ON EACH CURVE IS SLOPE IN mV.

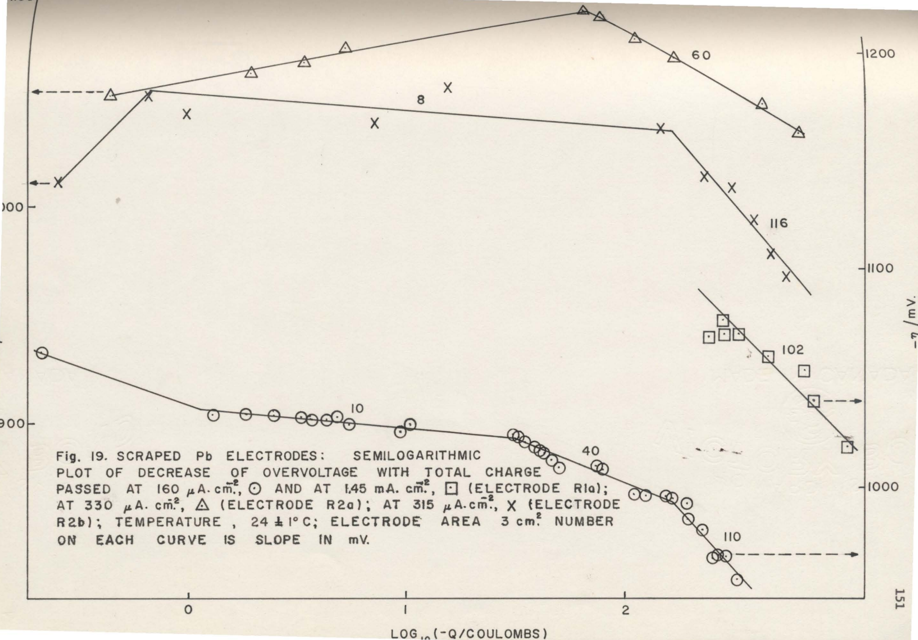

Fig. 19. SCRAPED Pb ELECTRODES: SEMILOGARITHMIC PLOT OF DECREASE OF OVERVOLTAGE WITH TOTAL CHARGE PASSED AT 160 μA$\cdot$cm^{-2}, ⊙ AND AT 1.45 mA. cm^{-2}, ⊡ (ELECTRODE R1a); AT 330 μA. cm^{-2}, △ (ELECTRODE R2a); AT 315 μA$\cdot$cm^{-2}, X (ELECTRODE R2b); TEMPERATURE, 24 ± 1°C; ELECTRODE AREA 3 cm^2. NUMBER ON EACH CURVE IS SLOPE IN mV.

of $-\eta$* up to $-Q = 70$ coulombs and then decreased with $-Q$. Slopes of these plots ranged from 10 to 115 mV., steep slopes (> 100 mV.) being observed for $-Q \geqslant -150$ coulombs for two electrodes (R1a and R2b).

In an attempt to see whether the $-\eta$ versus $\log_{10}(-Q)$ relation depends on the current density at which $-\eta$ was measured, Fig. 19 shows that the slopes at 160 μA. cm.$^{-2}$ and 1.45 mA. cm.$^{-2}$ in the case of R1a are nearly the same, being 110 and 102 mV., respectively.

The results indicate that Ives and Smith's (26, 27) linear $-\eta$ versus $\log_{10}(-Q)$ relation can be extended to scraped electrodes, even in the absence of activated charcoal. The delay in appearance of the higher $-\eta$ versus $\log_{10}(-Q)$ slopes (at $-Q \gtrsim 70$ coulombs) for scraped Pb electrodes in contrast to polished ones, which showed higher slopes from the beginning of cathodisation (or shortly afterwards) as observed by Ives and Smith (26, 27) and in this present work, may be due to gradual removal of an oxide film initially present on the scraped electrode surface. The presence of oxide film is suggested by the observed high $-\eta$'s for scraped electrodes (Table 6) in comparison with the lower values for ths polished electrodes of Ives and Smith (26, 27) and the polished electrodes used in this

---

* It became necessary to do glass-blowing on the gas lines immediately after the beginning of this experiment. This might have resulted in letting air into the system which remained during the early part of this experiment.

TABLE 6. HYDROGEN OVERVOLTAGES FOR SCRAPED Pb RODS IN AQUEOUS $HClO_4$ WITHOUT CHARCOAL CLEANING

Experiment number	Current density to which quoted $-\eta$'s correspond /mA. cm.$^{-2}$	Maximum current density passed for ≥ 30 minutes /mA. cm.$^{-2}$	Initial $-\eta$ or maximum (if $-\eta$ decreased initially) /mV.	$-\eta$ at $-Q$=100 coulombs /mV.	Final		Conditions of electrode and solution
					$-\eta$/mV.	$-Q$/coulombs	
R1a	0.160	1.45	1063	1003*	958	336	Scraped rod and 0.1 M $HClO_4$, pre-electrolysed at 0.5 mA. cm.$^{-2}$ for 30 days
	1.45	1.45	-	1126*	1019	1128	
R2a	0.330	0.330	1092	1082*	1033	649	Scraped rod and 0.1 M $HClO_4$, pre-electrolysed at 2 mA. cm.$^{-2}$ for 10 days
R2b	0.315	0.315	1051	1035*	967	566	Freshly scraped rod and solution from R2a

* interpolated values

present work.

Overshoot hysteresis*, as observed by Ives and Smith (26, 27), was repeatedly seen in these experiments. Figs. 20 and 21 show some examples of such plots for electrode R1a. From Fig. 20 it can be seen that the extent of overshoot increases with the magnitude of the current ratio and that the overshoot hysteresis was relatively reproducible. The curves in Figs. 20 and 21 suggest that there may be an exponential relation between overvoltage and time; the plots $-\eta$ versus $\log_{10} t$ (Figs. 22 and 23) confirm this to be the case.

Three other scraped electrodes (R3a, R3b and R3b') used in the same solution gave high Tafel slopes ($\geq$ 150 mV.), $-\eta$ increased with time of cathodisation and large kicks of $-\eta$ up to 200 mV. were observed, especially for R3a. These electrodes must have been affected by the presence in the system of some depolarising impurity, such as O_2. Moreover, addition of activated charcoal during experiment R3b' did not improve the electrode behaviour. This indicates that for a system of inadequate purity, carbon cleaning will not improve its behaviour.

---

* for definition see footnote on p. 146

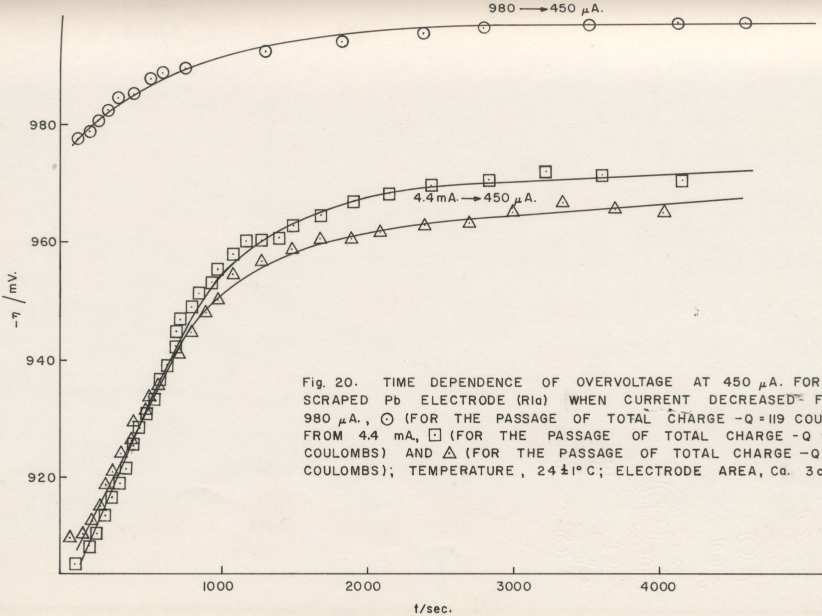

Fig. 20. TIME DEPENDENCE OF OVERVOLTAGE AT 450 μA. FOR A SCRAPED Pb ELECTRODE (RIa) WHEN CURRENT DECREASED FROM 980 μA., ⊙ (FOR THE PASSAGE OF TOTAL CHARGE $-Q = 119$ COULOMBS); FROM 4.4 mA., ⊡ (FOR THE PASSAGE OF TOTAL CHARGE $-Q = 292$ COULOMBS) AND △ (FOR THE PASSAGE OF TOTAL CHARGE $-Q = 317$ COULOMBS); TEMPERATURE, 24 ± 1° C; ELECTRODE AREA, Ca. 3 cm^2.

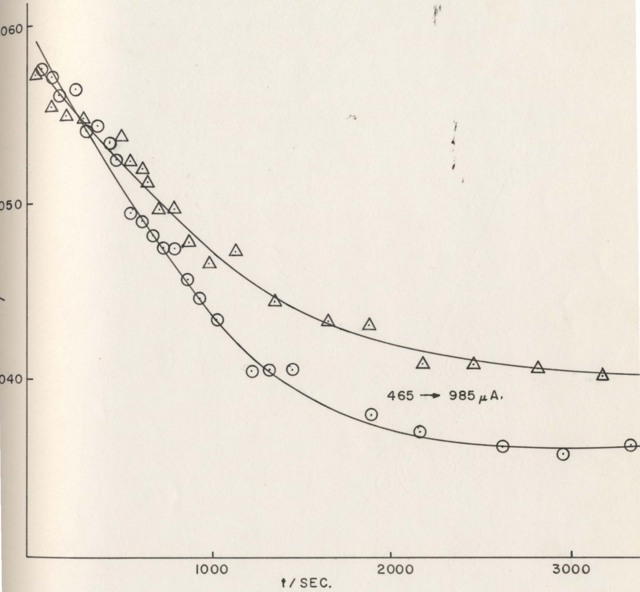

Fig. 21. TIME DEPENDENCE OF OVERVOLTAGE AT 985 μA. FOR A SCRAPED Pb ELECTRODE (R1a) AFTER INCREASING THE CURRENT FROM 465 μA. AT -Q = 116 COULOMBS, ⊙ ; AT -Q = 162 COULOMBS, △ ; TEMPERATURE, 24 ± 1°C; ELECTRODE AREA, Ca. 3 cm^2.

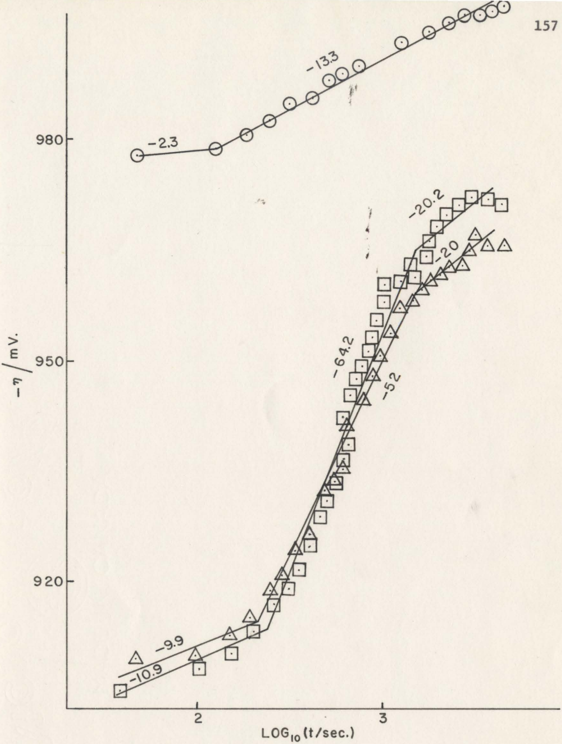

Fig. 22. DATA FROM Fig. 20 PLOTTED SEMI-LOGARITHMICALLY: OVERVOLTAGE VERSUS LOG$_{10}$ t AT 450 μA. FOR A SCRAPED Pb ELECTRODE (RIa) WHEN CURRENT DECREASED FROM 980 μA., ⊙ (FOR THE PASSAGE OF TOTAL CHARGE $-Q = 119$ COULOMBS); FROM 4.4 mA., ⊡ (FOR THE PASSAGE OF TOTAL CHARGE $-Q = 292$ COULOMBS) AND ◬ (FOR THE PASSAGE OF TOTAL CHARGE $-Q = 317$ COULOMBS); TEMPERATURE, 24±1°C; ELECTRODE AREA Ca. 3 cm^2. NUMBER ON EACH CURVE IS SLOPE IN mV.

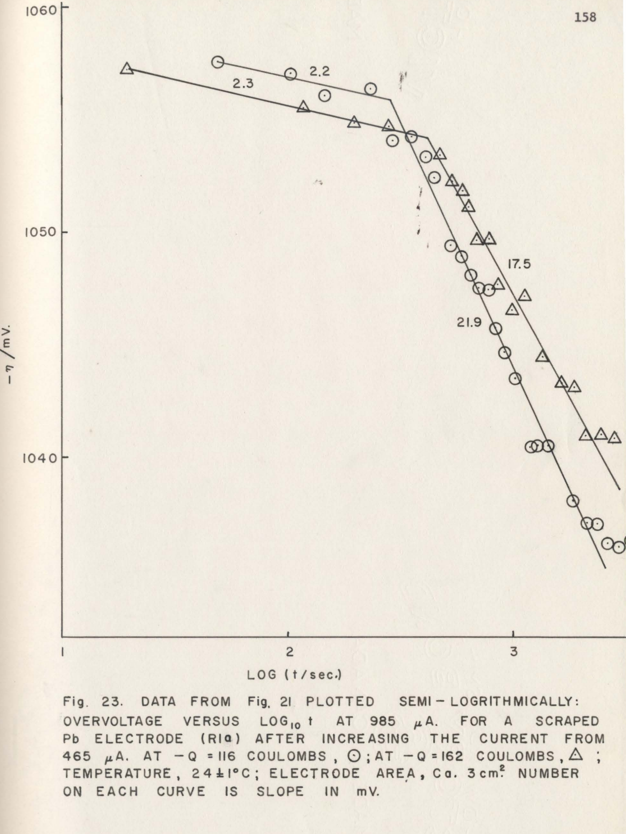

Fig. 23. DATA FROM Fig. 21 PLOTTED SEMI-LOGRITHMICALLY: OVERVOLTAGE VERSUS LOG_{10} t AT 985 μA. FOR A SCRAPED Pb ELECTRODE (R1a) AFTER INCREASING THE CURRENT FROM 465 μA. AT $-Q = 116$ COULOMBS, ⊙; AT $-Q = 162$ COULOMBS, △; TEMPERATURE, 24±1°C; ELECTRODE AREA, Ca. 3 cm^2 NUMBER ON EACH CURVE IS SLOPE IN mV.

(V11) Experiments with Electropolished Electrodes and "Properly Pre-electrolysed" Solutions

The work detailed in this Section was needed to confirm the findings of Ives and Smith (26, 27) {i.e. the overshoot hysteresis, the decrease of $-\eta$ linearly with the logarithm of total cathodic charge ($-Q$) and the simultaneous decrease of Tafel slopes} under superior experimental conditions.

Ten experiments are described in this Section. Eight were with rods, electropolished at 1 A. for 5 minutes in 50% $HClO_4$ (R3c, R4a', R4a", R4b, R5a, R5b, R5c and R5d) and two (F9, F10) with foils, electropolished at 95 mA. for 5 minutes in pre-electrolysed 1 M $HClO_4$. In all of these except R3c in pre-electrolysed 0.1 M $HClO_4$, 1 M $HClO_4$, pre-electrolysed for 5 - 20 days at $-i \leq 2$ mA. cm.$^{-2}$ was used in cell (a) or cell (b), as appropriate. The foils were electropolished <u>in situ</u>, while rods were polished in a separate cell and transferred under a hydrogen atmosphere (except R3c, quickly transferred through the air) into cell (a). Charcoal-cleaned pre-electrolysed solutions were only used for rods. Moreover, R3b', R4a' and R5a were used as a second adsorptive and pre-electrolytic stage of purification for later electrodes. The possibly oxygen-evolving anode was separated from the cathode in all experiments except R3c. BTS catalyst was used in the gas purification train for cylinder H_2 (see Figs. 5a and 5b), but was omitted in experiment R3c.

Certain electrodes (R4a', R5a and F9) were not well-behaved. Electrodes R4a' and R5a were electropolished but not bright. Initial $-\eta$'s were rather low, Tafel slopes were high (ca. 160 mV.) and $-\eta$ continued increasing with prolonged cathodisation during 24 - 36 hours, at the end of which period the experiments were terminated. Electrode F9, studied in pre-electrolysed (with impure Fisher Pb, at 2 mA. cm.$^{-2}$ for 5 days) 1 M $HClO_4$ was anomalous. No systematic fall of $-\eta$ with $-Q$ was observed at any current density (0.019, 0.535, 4.80 and 19.6 mA. cm.$^{-2}$) studied. Tafel slopes of 130 - 150 mV. were, however, observed. No improvement was found after 9 - 10 days of cathodisation. The pre-electrolysed solution may have been contaminated by impurities in the Fisher lead.

The results with the remaining electrodes (R3c, R4a", R4b, R5b, R5c, R5d and F10) will be considered under four different headings: (a) Tafel plots, (b) temperature-dependence of $-\eta$, (c) $-\eta$ as a function of $-Q$ and (d) overshoot hysteresis.

(a) Tafel Plots

Rapid Tafel runs were carried out with intervals between changes of current of 0.1 to 5 minutes. The Tafel plots changed in character during long-term experiments (days to weeks) on a given electrode. Typical examples are shown in Figs. 24 and 25 for electrodes R3c and R5c, respectively. The following common features

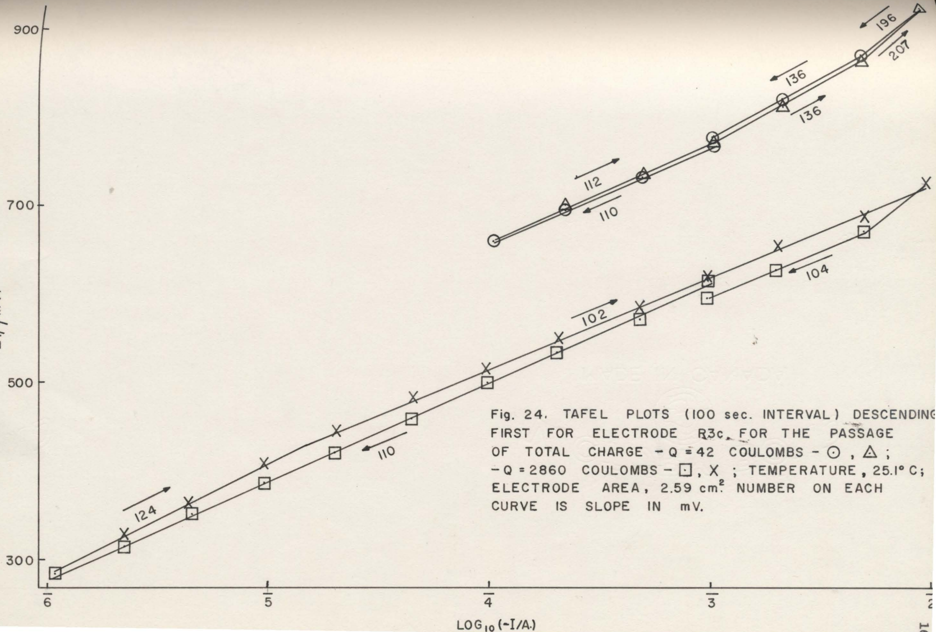

Fig. 24. TAFEL PLOTS (100 sec. INTERVAL) DESCENDING FIRST FOR ELECTRODE R3c, FOR THE PASSAGE OF TOTAL CHARGE $-Q = 42$ COULOMBS − ⊙ , △ ; $-Q = 2860$ COULOMBS − ⊡, X ; TEMPERATURE, 25.1° C; ELECTRODE AREA, 2.59 cm^2 NUMBER ON EACH CURVE IS SLOPE IN mV.

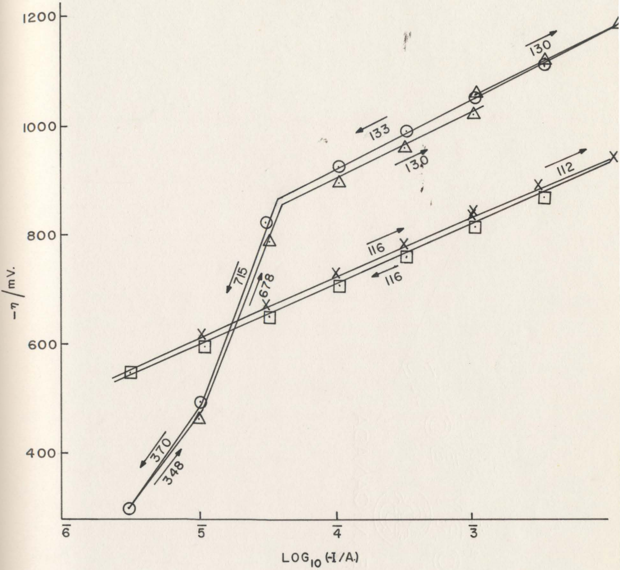

Fig. 25. TAFEL PLOTS (0.1 min. INTERVAL, ASCENDING FIRST FROM 920 μA.) FOR ELECTRODE R5c FOR THE PASSAGE OF OF TOTAL CHARGE − Q = 15 COULOMBS. ⊙ , △ ; − Q = 1100 COULOMBS − ⊡ , X ; TEMPERATURE, 25±1°C; ELECTRODE AREA, 1.2 cm^2. NUMBER ON EACH CURVE IS SLOPE IN mV.

as found earlier by Ives and Smith (26, 27) have been observed:

(i) Measurements on freshly prepared electrodes gave bilinear or curved plots with steeper slope at low currents, especially $-I \leqslant 30$ μA. {Fig. 25} (except R4a" - in which a linear Tafel slope of ≃ 100 mV. was observed from the beginning of the experiment). Initial Tafel runs (50 - 100 second intervals) for R3c were multilinear with slopes b ≃ 110 mV. at currents < 10^{-3} A., and b ≃ 135 mV. above 10^{-3} A. (Fig. 24). However, when the cathodic current density was increased from the initial 385 μA. cm.$^{-2}$ to 3.85 mA. cm.$^{-2}$ and kept at this value for the next 50 hours (i.e. $-Q = 520$ to 2290 coulombs), the observed Tafel plot at $-I \geqslant 10$ μA. after this treatment was similar to that shown in Fig. 25 for R5c at low - Q (15 coulombs), but was almost horizontal (b < 10 mV.) at currents $\lesssim 10$ μA. Steep slopes $\gtrsim 300$ mV. at low currents vanished on prolonged polarisation (Fig. 25) {slope < 10 mV. for R3c also vanished on prolonged cathodisation at 385 μA. cm.$^{-2}$ (Fig. 24)} and are attributed to depolarisation effects.

(ii) Continued cathodisation led to plots approaching linearity (Figs. 24 and 25).

(iii) Excluding those affected by low current depolarisation, Tafel slopes decreased on prolonged cathodisation from 120 - 140 mV. to ca. 90 mV. Thus, in one case (Fig. 26), the slope fell from 127 to 94 mV. as $-Q$ increased from 25 to 196 coulombs. Although such a

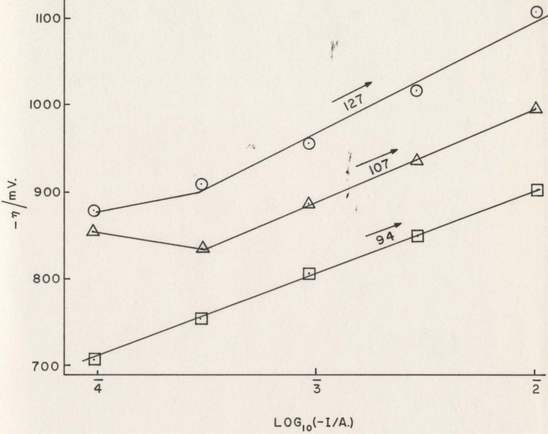

Fig. 26. TAFEL PLOTS (5 min. INTERVAL) FOR ELECTRODE R4a" FOR THE PASSAGE OF $-Q = 25$ COULOMBS, ⊙; $-Q = 105$ COULOMBS, △; $-Q = 196$ COULOMBS, ⊡; TEMPERATURE, 25±1° C; ELECTRODE AREA, 1.44 cm^2. NUMBER ON EACH CURVE IS SLOPE IN mV.

rapid decrease in b was less common, the trend was observed for the first few days of cathodisation of all electrodes. Sometimes, on further cathodisation, these slopes increased to 110 mV. or so, but the most commonly observed slope was 110 ± 10 mV.

(iv) Hysteresis was observed. In the first few runs on a freshly prepared electrode, the overvoltages for the descending branch were greater than those for the ascending branch (Fig. 25), with a hysteresis of 20 - 30 mV. These relative positions were not, however, observed in all cases (e.g. for R3c in Fig. 24). On continued cathodisation, the "normal" hysteresis of about 10 - 20 mV. was observed, i.e. overvoltage for the descending branch were lower than those for the ascending branch (see Figs. 24 and 25).

(b) Temperature Dependence of Overvoltage

In one experiment R3c, the temperature variation of overvoltage was studied. The time variation of $-\eta$ required that we carry out Tafel runs at different temperatures (25 - 45°C) on the same day.

Since the descending branch was more linear over the current range than was the ascending branch, typical Tafel plots for the descending branch at 25 - 45°C were selected at different periods of polarisation. One such plot at $-Q = 2600$ coulombs is shown in Fig. 27, which shows that the overvoltage decreased with increase

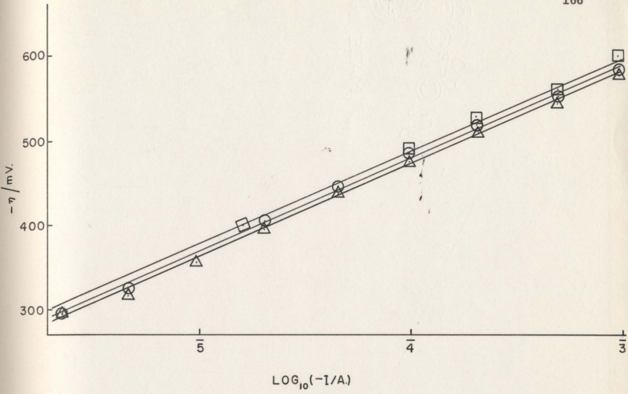

Fig. 27. TYPICAL TAFEL PLOTS (DESCENDING BRANCH, b ≈ 110 mV. AND 100 sec. INTERVAL) FOR ELECTRODE R3c FOR THE PASSAGE OF TOTAL CHARGE − Q ≈ 2600 COULOMBS; TEMPERATURES; ⊡, 25.1°C; ⊙, 35.1°C; △, 45.1°C; ELECTRODE AREA, 2.59 cm^2.

of temperature and that the Tafel slope was in this case independent of temperature*, being $b \simeq 110$ mV.

Arrhenius plots $\{\log_{10}(-I)$ versus $\frac{1}{T}\}$ 25 - 45°C, shown in Fig. 28 enable the experimental enthalpy of activation, $\Delta H^{\ddagger}_{\eta}$ at different constant overvoltages to be calculated using the equation (2.28)

$$\log_{10}(-i) = -\frac{\Delta H^{\ddagger}_{\eta}}{2.303RT} + \text{constant} \tag{2.28}$$

and enthalpy of activation at the equilibrium potential, $\Delta H^{\ddagger}_{\eta=0}$, at $-\eta = 0$ was calculated using the dependence

$$\Delta H^{\ddagger}_{\eta=0} = \Delta H^{\ddagger}_{\eta} + \alpha F(-\eta) \tag{2.29}$$

α in equation (2.29) being obtained from the Tafel slope as $\frac{2.303RT}{bF}$. The calculated α's, using $b = 110$ mV., independent of temperature, at 25, 35 and 45°C were 0.54, 0.56 and 0.57, respectively. The average value, $\alpha_{av.} = 0.56$ was used in the present calculation. Table 7 gives the enthalpies of activation at $-Q \geq 2600$ coulombs at $-\eta = 400$ mV., 500 mV., 600 mV. and zero, respectively. Although the average $\Delta H^{\ddagger}_{\eta=0} \simeq 9.3 \pm 1.3$ k. cal. g. ion^{-1} is close to the value of Lee (206) for lead in alkaline solution ($\Delta H^{\ddagger}_{\eta=0} = 8.8$ k. cal. g. ion^{-1}), this value is far less than the

---

* However, Ives and Smith (26, 27) have observed that the Tafel slope increased with increase of temperature on Pb in 0.1 M $HClO_4$.

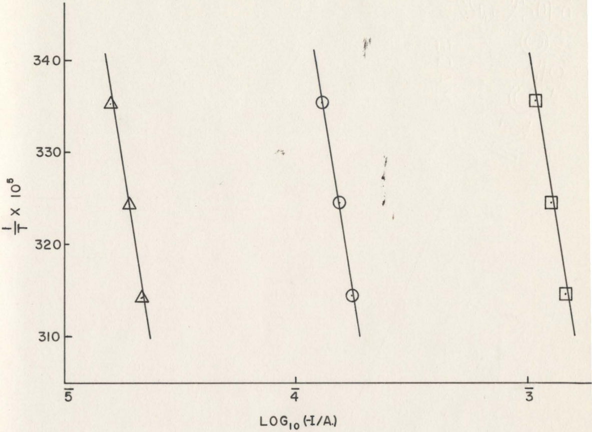

Fig. 28. TYPICAL ARRHENIUS PLOTS OF LOG$_{10}$(-I) VERSUS FOR ELECTRODE R3c FOR THE PASSAGE OF TOTAL CHARGE $-Q \approx 2600$ COULOMBS; OVERVOLTAGES: △, 0.4V; ⊙, 0.5V; ⊡, 0.6V; ELECTRODE AREA, 2.59 cm^2.

TABLE 7. ACTIVATION ENTHALPIES ($\Delta H^{\ddagger}_{\eta}$ AND $\Delta H^{\ddagger}_{\eta=0}$) AT CONSTANT OVERVOLTAGE FOR HYDROGEN EVOLUTION REACTION AT LEAD ROD R3c IN 0.1 M $HClO_4$

$-Q$/coulombs	$-\eta$/mV.	Activation enthalpies	
		$\Delta H^{\ddagger}_{\eta}$/k.cal.g.ion^{-1}	$\Delta H^{\ddagger}_{\eta=0}$ */k.cal.g.ion^{-1}
2608	400	2.80	7.93
	500	2.81	9.22
	600	2.87	10.56
2675	400	3.48	8.61
	500	3.28	9.69
	600	2.12	9.81
		Average $\Delta H^{\ddagger}_{\eta=0}$	$= 9.3 + 1.3$

* α taken to be 0.56.

$\Delta H^{\ddagger}_{\eta=0} \simeq 20$ k. cal. g. ion^{-1} for lead in $HClO_4$, observed by Piontelli and Bicelli (22). The value of $\Delta H^{\ddagger}_{\eta=0} \simeq 20$ k. cal. g. ion^{-1} for lead in acid solution is reasonable, if one equates $\Delta H^{\ddagger}_{\eta=0}$ for Pb to that of Hg $\{\Delta H^{\ddagger}_{\eta=0} = 21.7$ k. cal. g. ion^{-1} for Hg (112a) in HCl$\}$ since both are high overvoltage metals and the discharge step (2.1) is considered to be rate determining. Then, the observed low $\Delta H^{\ddagger}_{\eta=0}$ at $-Q \geqslant 2600$ coulombs in this work may be explained by a decrease of $\Delta H^{\ddagger}_{\eta=0}$ with $-Q$. Since no data are available at $-Q < 2600$ coulombs from this work, enthalpies of activation at $-Q \simeq 600 - 700$ coulombs at 550 mV., 650 mV. and $-\eta = 0$ were calculated as mentioned earlier from Smith's data (27) and are listed in Table 8. Although a temperature dependence of Tafel slope and high α values were observed in Smith's work (27), the calculated $\Delta H^{\ddagger}_{\eta=0}$ values at $-Q \simeq 600 - 700$ coulombs are higher than the $\Delta H^{\ddagger}_{\eta=0}$ at $-Q \geqslant 2600$ coulombs obtained in this work. Moreover, $\Delta H^{\ddagger}_{\eta=0}$ at $-Q \simeq 600 - 700$ coulombs are less than 21.7 k. cal. g. ion^{-1}. This decrease in enthalpy of activation with $-Q$ might be the explanation of the enhancement of the rate of h.e.r. as $-Q$ increases.

TABLE 8. ACTIVATION ENTHALPIES ($\Delta H^{\ddagger}_{\eta}$ AND $\Delta H^{\ddagger}_{\eta=0}$) AT CONSTANT OVERVOLTAGE FOR HYDROGEN EVOLUTION REACTION AT LEAD ROD XIIb*** IN 0.1 M $HClO_4$ FROM SMITH'S DATA (27)

-Q/coulombs	$-\eta$/mV.	Activation enthalpies**	
		$\Delta H^{\ddagger}_{\eta}$/k.cal.g.ion^{-1}	$\Delta H^{\ddagger}_{\eta=0}$ */k.cal.g.ion^{-1}
600-700	550	7.94 ± 0.1	17.52 ± 0.1
	650	2.37 ± 0.2	13.71 ± 0.2
		Average $\Delta H^{\ddagger}_{\eta=0}$ = 15.6 ± 2	

* α taken to be 0.76.

** Average of three runs taken on successive days.

*** Numbering of the electrodes are as in reference (27). Electrodes were identified by Roman numerals (the same piece of Pb having the same number throughout), by small letters (indicating the number of times an electrode had been polished and transferred to the cell).

(c) Overvoltage as a Function of Total Cathodic Charge

In all satisfactory experiments (R3c, R4a", R4b, R5b, R5c, R5d and F10) overvoltages at constant current densities initially rose slightly and then fell continuously with -Q (Figs. 29, 30 and 31), as anticipated from the earlier work of Ives and Smith (26, 27). The initial rise could be associated with a failure to eliminate traces of O_2 or Pb^{++} ions (Pb^{++} ions may have entered along with the introduction of freshly polished electrodes or they may have been present in the solution used from the previous experiment in which high currents had been applied). It is apparent from the observed decrease in $-\eta$ with -Q in experiment F10, where no charcoal was involved, that charcoal cleaning is not essential to show this phenomenon in a system that is sufficiently clean. This also disproves that the formation of a Pb-C matrix (206a)* is a relevant factor accounting for the decrease in $-\eta$ with -Q.

It is evident from Figs. 29, 30 and 31 that slopes of $-\eta$ versus $\log_{10}(-Q)$ ranging from 40 - 90 mV. were obtained for $-Q \lesssim 100$ coulombs while slopes ranging from 150 to 685 mV. were obtained for $-Q \gtrsim 100$ coulombs. Moreover, the slopes for $-\eta$ versus $\log_{10}(-Q)$ at 385 μA. cm.$^{-2}$ and at 3.85 mA. cm.$^{-2}$ for R3c (Fig. 29)

---

* Jenkins and Weedon (206a) recently reported the formation of a carbonaceous matrix on Pb during their h.e.r. study on Pb in charcoal-cleaned solution.

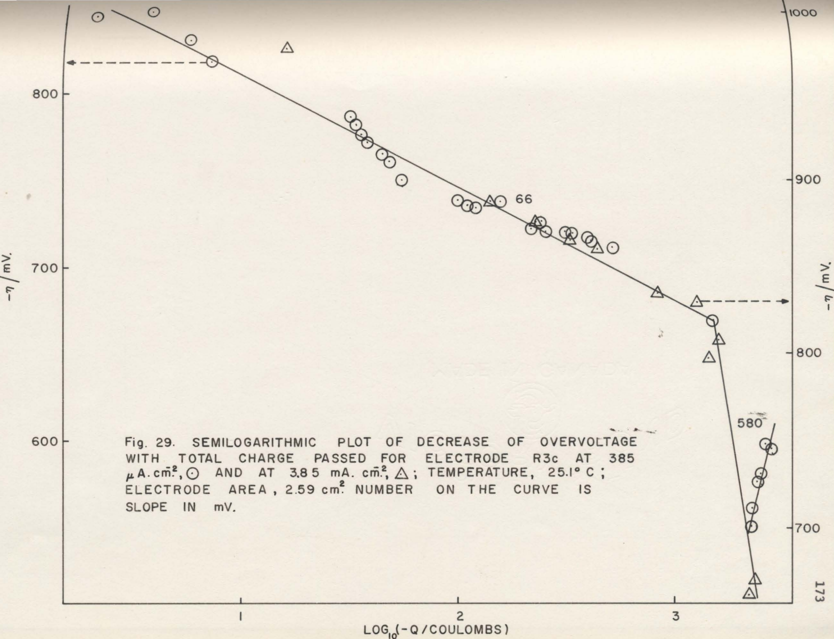

Fig. 29. SEMILOGARITHMIC PLOT OF DECREASE OF OVERVOLTAGE WITH TOTAL CHARGE PASSED FOR ELECTRODE R3c AT 385 $\mu A.cm^{-2}$, ⊙ AND AT 3.85 $mA.cm^{-2}$, △; TEMPERATURE, 25.1° C; ELECTRODE AREA, 2.59 cm^2. NUMBER ON THE CURVE IS SLOPE IN mV.

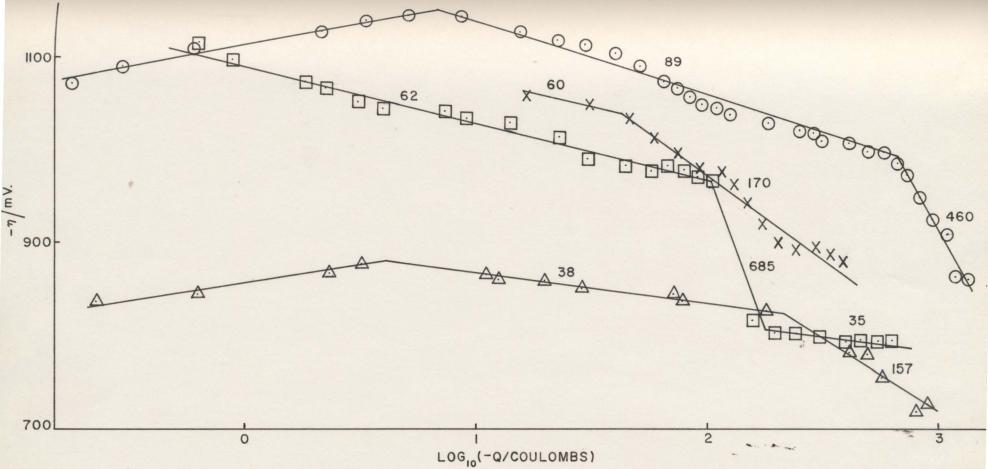

Fig. 30. SEMILOGARITHMIC PLOT OF DECREASE OF OVERVOLTAGE WITH TOTAL CHARGE PASSED AT 505 μA. cm^{-2} (ELECTRODE F10, △; AREA, 1.52 cm^{2}), AT 570 μA. cm^{-2} (ELECTRODE R5d, X; AREA, 1.75 cm^{2}), AT 650 μA. cm^{-2} (ELECTRODE R5b, ⊙; AREA, 1.54 cm^{2}), AT 655 μA. cm^{-2} (ELECTRODE R4a", ⊡; AREA, 1.44 cm^{2}); TEMPERATURE, 25±1°C. NUMBER ON EACH CURVE IS SLOPE IN mV.

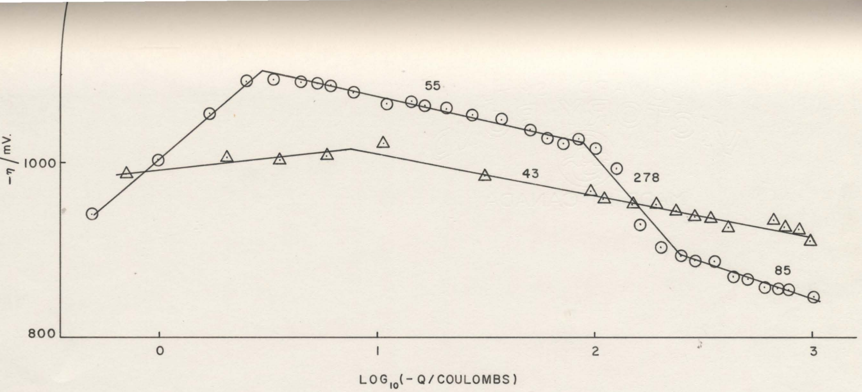

Fig. 31. SEMILOGARITHMIC PLOT OF DECREASE OF OVERVOLTAGE WITH TOTAL CHARGE PASSED AT 775 μA. cm^{-2}. (ELECTRODE R5c, ⊙ ; AREA, 1.2 cm^{2}.), AT 790 μA. cm^{-2} (ELECTRODE R4b, △ ; AREA, 1.29 cm^{2}.), TEMPERATURE, 25±2°C. NUMBER ON EACH CURVE IS SLOPE IN mV.

were the same (66 mV. up to $-Q = 1520$ coulombs and then increasing to 580 mV. for $-Q = 1520$ to 2400 coulombs). This confirms that linear relationships exist between $-\eta$ versus $\log_{10}(-Q)$, as previously found by Ives and Smith (26, 27) for Pb in $HClO_4$.

In experiment R3c, the change from a small to a steep slope (from 66 to 580 mV., see Fig. 29) occurred during cathodisation at 3.85 mA. $cm.^{-2}$ after the polarisation at an initial constant current, $-i = 385$ μA. $cm.^{-2}$, up to $-Q = 522$ coulombs. Later a cathodic current of 385 μA. $cm.^{-2}$ was switched back at $-Q = 2293$ coulombs. Further cathodisation at 385 μA. $cm.^{-2}$ increased $-\eta$ as shown in Fig. 29. This is consistent with the progressive removal of Pb^{++} ions from the solution, presumably formed during the cathodic disintegration of Pb at the higher current density. No other reason could be found for the change in slope to very high values for other electrodes except cathodic disintegration, but this suggestion cannot be regarded as proven.

Some of the observed and interpolated overvoltages for different electrodes (initial and at different $-Q$ values) are listed in Tables 9, 10 and 11. These Tables illustrate the difficulty of achieving uniformity of behaviour from one electrode to another. This might be partly due to the difficulty in reproducing a polished surface of the same activity or to errors in the measured geometric surface area. However, results obtained for different electrodes studied in the same solution (in particular, $-\eta$'s at $-Q = 100$ coulombs

TABLE 9. OVERVOLTAGES FOR LEAD IN AQUEOUS PERCHLORIC ACID

Experiment number	Current density to which quoted $-\eta$'s correspond /mA. cm.$^{-2}$	Maximum current density passed for $\geqslant$ 30 minutes /mA. cm.$^{-2}$	Initial $-\eta$ or maximum (if $-\eta$ decreased initially) /mV.	$-\eta$ at $-Q$=100 coulombs /mV.	Final		Conditions of electrode and solution
					$-\eta$/mV.	$-Q$/coulombs	
R3c	0.385	3.85	853	738	612	2885	Electropolished rod (2 A. for 7 minutes) and solution from R3b used. Adsorptive cleaning of solution with activated carbon
	3.85	3.85	976	896*	670	2287	
F10	0.505	0.505	878	834*	725	904	Electropolished foil (95 mA. for 5 minutes) and 1 M $HClO_4$, pre-electrolysed at 1.5 mA. cm.$^{-2}$ for 4-5 days

* interpolated value

TABLE 10. OVERVOLTAGES FOR LEAD IN AQUEOUS PERCHLORIC ACID

Experiment number	Current density to which quoted $-\eta$'s correspond /mA. cm.$^{-2}$	Maximum current density passed for ≥ 30 minutes /mA. cm.$^{-2}$	Initial $-\eta$ or maximum (if $-\eta$ decreased initially) /mV.	$-\eta$ at $-Q$=100 coulombs /mV.	Final		Conditions of electrode and solution
					$-\eta$/mV.	$-Q$/coulombs	
R4a"	0.655	0.655	1114	967	792	616	Electropolished rod (1 A. for 5 minutes) and solution from R4a' used. Adsorptive cleaning of solution with activated carbon
R4b	0.790	0.790	1021	964	910	988	Electropolished rod (1 A. for 5 minutes) and solution from R4a" used. Adsorptive cleaning of solution with activated carbon

TABLE 11. OVERVOLTAGES FOR LEAD IN AQUEOUS PERCHLORIC ACID

Experiment number	Current density to which quoted $-\eta$'s correspond /mA. cm.$^{-2}$	Maximum current density passed for $\geq$ 30 minutes /mA. cm.$^{-2}$	Initial $-\eta$ or maximum (if $-\eta$ decreased initially) /mV.	$-\eta$ at $-Q$=100 coulombs /mV.	Final		Conditions of electrode and solution
					$-\eta$/mV.	$-Q$/coulombs	
R5d	0.570	0.570	1056	970*	879	384	Electropolished rod (1 A. for 5 minutes) and solution from R5c used. Adsorptive cleaning of solution with activated carbon
R5b	0.650	0.650	1147	1048	848	1340	Electropolished rod (1 A. for 5 minutes) and solution from R5a used. Adsorptive cleaning of solution with activated carbon

* interpolated value

TABLE 11. (Continued)

Experiment number	Current density to which quoted $-\eta$'s correspond /mA. cm.$^{-2}$	Maximum current density passed for $\geqslant$ 30 minutes /mA. cm.$^{-2}$	Initial $-\eta$ or maximum (if $-\eta$ decreased initially) /mV.	$-\eta$ at $-Q$=100 coulombs /mV.	Final		Conditions of electrode and solution
					$-\eta$/mV.	$-Q$/coulombs	
R5c	0.775	0.775	1095	1068	858	1039	Electropolished rod (1 A. for 5 minutes) and solution from R5b used. Adsorptive cleaning of solution with activated carbon

and final $-\eta$ values) were very good, e.g. experiments R4 (Table 10) and R5 (Table 11).

The observed overvoltages for electrode XIIb, the best electrode studied by Ives and Smith (26, 27) at 600 μA. cm.$^{-2}$ at $-Q = 0$ and $-Q = 100$ coulombs were 0.960 and 0.790 mV., respectively. These $-\eta$ values are comparable with the quoted values for R3c and F10 in Table 9, but are lower than those of the other electrodes (Tables 10 and 11).

In general, the trend in overvoltage decreasing by 150 - 300 mV. at the end of long periods of cathodic polarisation was common for all electrodes. This suggests a several orders of magnitude increase in catalytic activity of lead electrodes during cathodic h.e.r. As proposed by Ives and Smith (26, 27), continued accumulation of adsorbed H atoms on the surface or absorbed H atoms in the bulk metal may explain the increase in catalytic activity of Pb during such cathodic treatment.

(d) Overshoot Hysteresis

Long-term current changes ($\gtrsim$ 30 minutes) were begun from steady-state overvoltages in the experiments R3c and in the later part of R4a". For each step-change, the immediate potential jump was followed by an exponential change of potential in the reverse direction. This phenomenon is termed overshoot hysteresis. Overshoot hysteresis, as observed by Ives and Smith (26, 27), was common throughout these experiments, except during the initial stages of cathodisation. Typical examples for increasing currents at constant temperature, decreasing current at constant temperature and decreasing current at different temperatures (25 - 45°C) are shown in Figs. 32, 33 and 34, respectively. Fig. 32 shows that the extent of overshoot increases with the magnitude of the current step and decreases as -Q increases. Temperature dependence of overshoot hysteresis has been observed in the range of 25 - 45°C for decreasing currents in the experiment R3c. These measurements were carried out after Tafel runs (100 seconds interval). Fig. 34 shows that the extent of overshoot decreases with the increase of temperature. Full development of these overshoot effects seems to depend on the maintenance of adequate deoxygenation and cleanliness.

Figs. 35, 36 and 37 confirm that exponential relations ($-\eta$ linear with $\log_{10} t$) exist for the data of Figs. 32, 33 and 34. This is the case for all examples of overshoot hysteresis in the present work and in that of Smith (27). Unfortunately, the slopes of such plots, listed in Tables 12 to 18, are not constant but vary with time in a somewhat unpredictable manner. It is difficult to generalise on the basis of the present results, but taking them together with those of Smith, not previously evaluated in this way, certain trends appear to be present. Cases of increasing currents and decreasing currents will be dealt with separately.

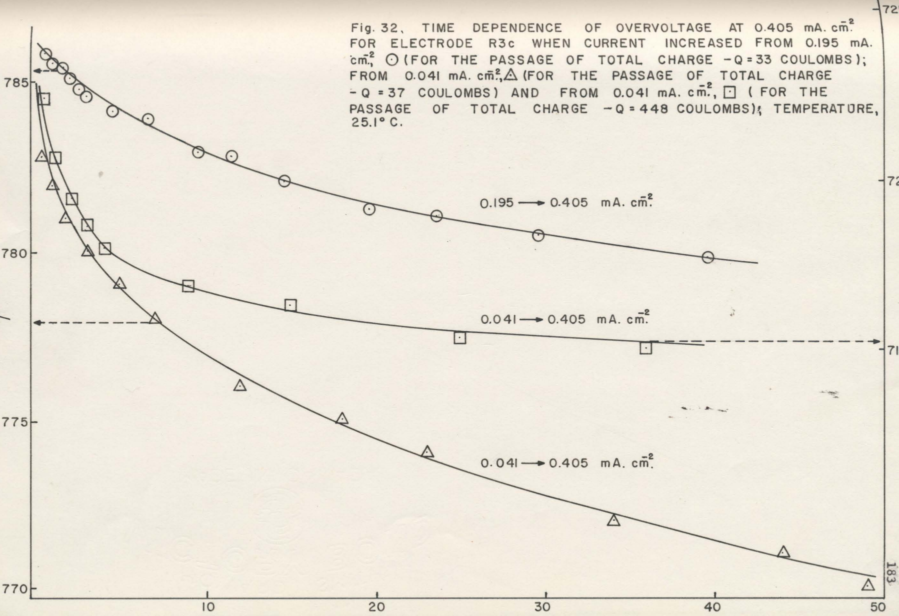

Fig. 32. TIME DEPENDENCE OF OVERVOLTAGE AT 0.405 mA. cm^{-2}. FOR ELECTRODE R3c WHEN CURRENT INCREASED FROM 0.195 mA. cm^{-2}, ⊙ (FOR THE PASSAGE OF TOTAL CHARGE $-Q = 33$ COULOMBS); FROM 0.041 mA. cm^{-2}, △ (FOR THE PASSAGE OF TOTAL CHARGE $-Q = 37$ COULOMBS) AND FROM 0.041 mA. cm^{-2}, ⊡ (FOR THE PASSAGE OF TOTAL CHARGE $-Q = 448$ COULOMBS); TEMPERATURE, 25.1° C.

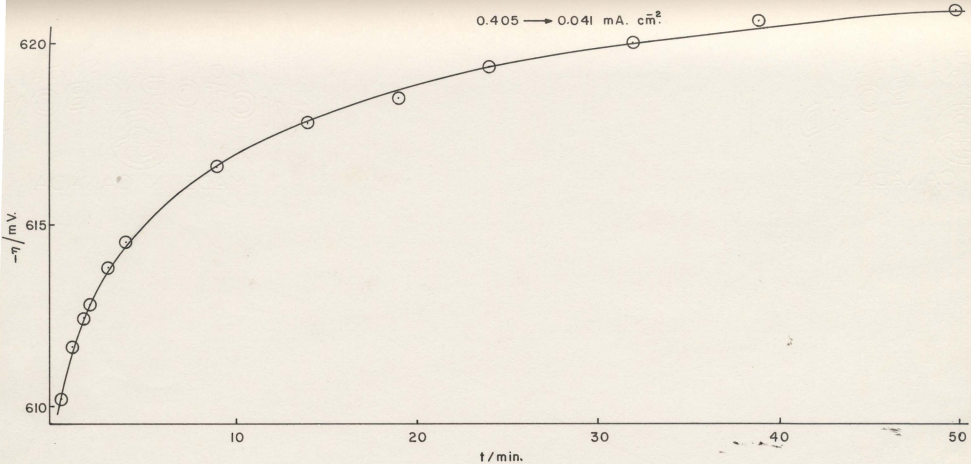

Fig. 33. TIME DEPENDENCE OF OVERVOLTAGE AT 0.041 mA. cm^{-2} AFTER DECREASING CURRENT FROM 0.405 mA. cm^{-2} FOR ELECTRODE R3c FOR THE PASSAGE OF TOTAL CHARGE −Q = 214 COULOMBS; TEMPERATURE, 25.1° C.

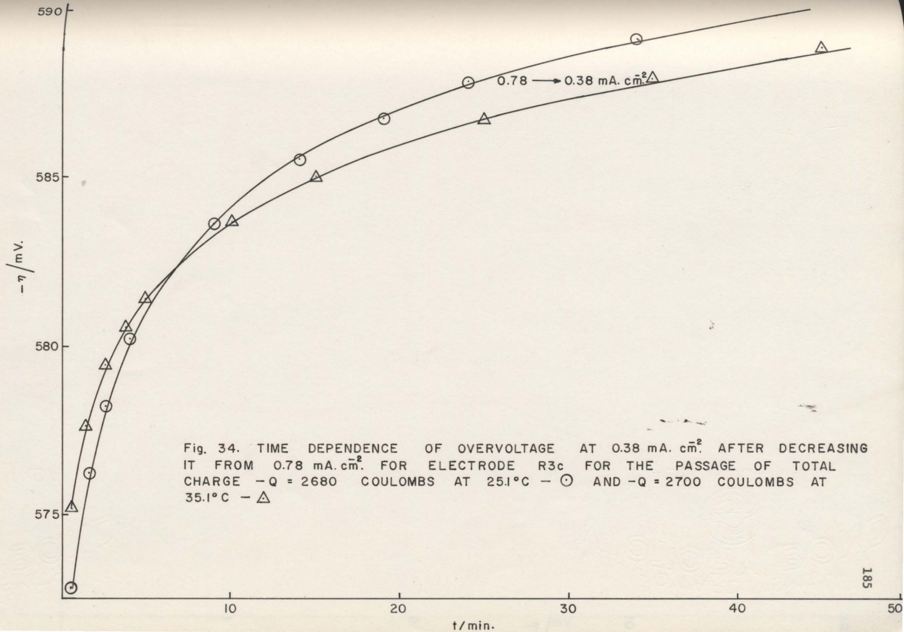

Fig. 34. TIME DEPENDENCE OF OVERVOLTAGE AT 0.38 mA. cm^{-2} AFTER DECREASING IT FROM 0.78 mA. cm^{-2}. FOR ELECTRODE R3c FOR THE PASSAGE OF TOTAL CHARGE $-Q$ = 2680 COULOMBS AT 25.1°C — ⊙ AND $-Q$ = 2700 COULOMBS AT 35.1°C — △

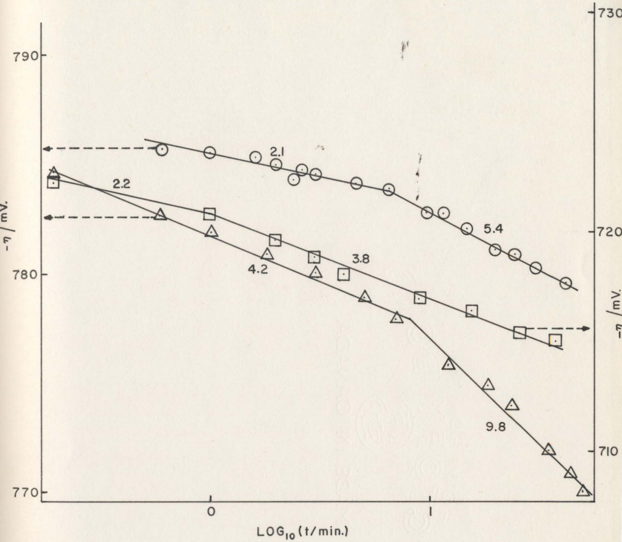

Fig. 35. DATA FROM Fig. 32 PLOTTED SEMI-LOGARITHMICALLY: OVERVOLTAGE VERSUS LOG$_{10}$t AT 0.405 mA.cm^{-2} FOR ELECTRODE R3c WHEN CURRENT INCREASED FROM 0.195 mA. cm^{-2}, ⊙ (FOR THE PASSAGE OF TOTAL CHARGE -Q = 33 COULOMBS) AND FROM 0.041 mA. cm^{-2}, △ (FOR THE PASSAGE OF TOTAL CHARGE -Q = 37 COULOMBS) AND FROM 0.041 mA.cm^{-2}, ⊡ (FOR THE PASSAGE OF TOTAL CHARGE -Q = 448 COULOMBS); TEMPERATURE, 25.1°C., NUMBER ON EACH CURVE IS SLOPE IN mV.

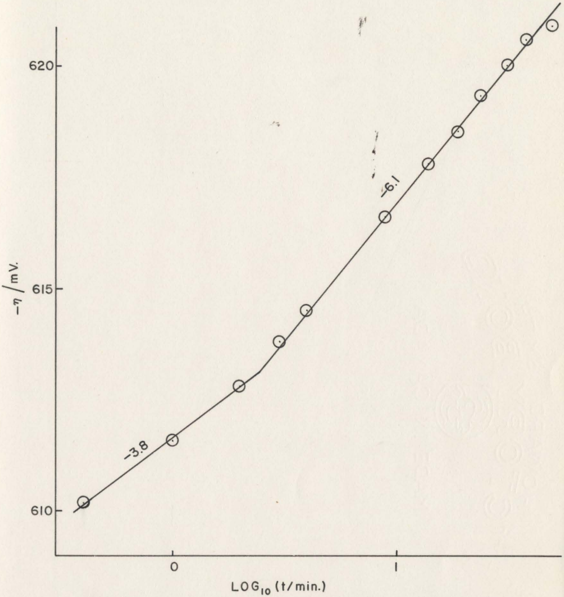

Fig. 36. DATA FROM Fig. 33 PLOTTED SEMI-LOGARITHMICALLY OVERVOLTAGE VERSUS LOG$_{10}$t AT 0.041 mA. cm^{-2}. AFTER DECREASING CURRENT FROM 0.405 mA. cm^{-2} FOR ELECTRODE R3c FOR THE PASSAGE OF TOTAL CHARGE $-Q = 214$ COULOMBS; TEMPERATURE, 25.1°C; NUMBER ON EACH CURVE IS SLOPE IN mV.

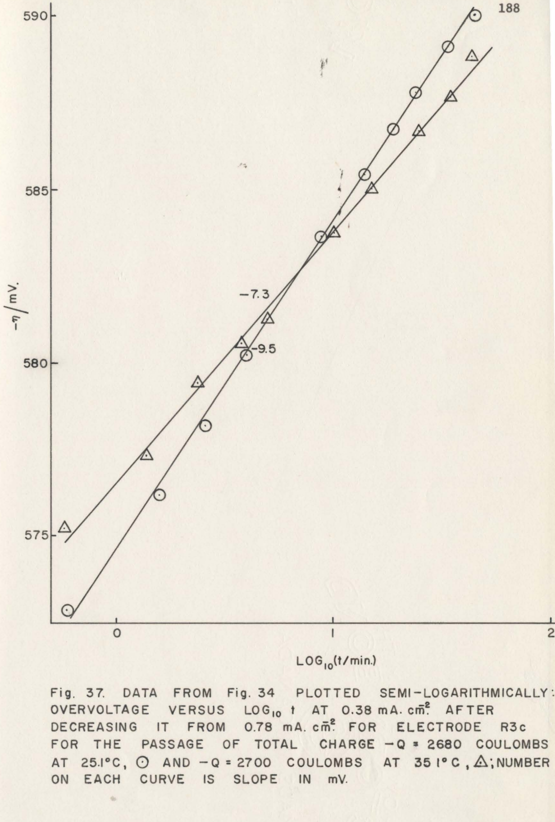

Fig. 37. DATA FROM Fig. 34 PLOTTED SEMI-LOGARITHMICALLY: OVERVOLTAGE VERSUS LOG_{10} t AT 0.38 mA. cm^{-2}. AFTER DECREASING IT FROM 0.78 mA. cm^{-2} FOR ELECTRODE R3c FOR THE PASSAGE OF TOTAL CHARGE −Q = 2680 COULOMBS AT 25.1°C, ⊙ AND −Q = 2700 COULOMBS AT 35.1°C, △; NUMBER ON EACH CURVE IS SLOPE IN mV.

TABLE 12. SLOPES OF $-\eta$ VERSUS $\mathrm{LOG}_{10}\,t$ PLOTS IN OVERSHOOT HYSTERESIS (INCREASING CURRENTS)

Experiment number	Temperature /°C	-Q/ coulombs	Current change/ mA. $\mathrm{cm.}^{-2}$		Slope/ mV. decade^{-1}	Time range corresponding to the slope/ minutes
			from	to		
R3c	25.1	33	0.195	0.405	2.1	0.5-6
					5.4	6-40
		37	0.041	0.405	4.2	0.2-8
					9.8	8-49
		151	0.041	0.405	6.3	0.4-1
					4.4	1-22
		218	0.041	0.405	6.1	0.4-24
					1.6	24-70
		343	0.041	0.405	4.5	0.4-25
					2.5	25-90
		448	0.041	0.405	2.2	0.2-1
					3.8	1-36
		522	0.40	3.85	1.3	1-5
					14.3	5-50

TABLE 13. SLOPES OF $-\eta$ VERSUS $\log_{10} t$ PLOTS IN OVERSHOOT HYSTERESIS (INCREASING CURRENTS)

Experiment number	Temperature /°C	-Q/ coulombs	Current change/ mA. cm.$^{-2}$		Slope/ mV. decade^{-1}	Time range corresponding to the slope/ minutes
			from	to		
R4a"	25 ± 1	637	0.655	7.10	6.1	1-7
					8	7-38
		692	0.655	7.10	3	1-34
					6.5	34-116
		2204	0.655	23.0	3	1-20
					5	20-50

TABLE 14. SLOPES OF $-\eta$ VERSUS $\log_{10} t$ PLOTS IN OVERSHOOT HYSTERESIS (DECREASING CURRENTS)

Experiment number	Temperature /°C	-Q/ coulombs	Current change/ mA. cm.$^{-2}$		Slope/ mV. decade^{-1}	Time range corresponding to the slope/ minutes
			from	to		
R3c	25.1	37	0.405	0.041	-2.1	0.2-2
					-8	2-18
		151	0.405	0.041	-3.7	0.4-3.5
					-5.4	3.5-18
		214	0.405	0.041	-3.8	0.4-2.5
					-6.1	2.5-50
		343	0.405	0.041	-4.7	0.6-6
					-6.7	6-34
		448	0.405	0.041	-3.8	0.4-3
					-6.2	3-24
		442	3.85	0.390	-2.9	0.4-2
					-6.2	2-20
		1521	3.65	0.365	-15.6	0.6-1
					-10	1-11
		2270	3.55	0.360	-6.6	0.4-34
		2293	3.55	0.360	-6.6	0.6-14

TABLE 15. SLOPES OF $-\eta$ VERSUS LOG$_{10}$ t PLOTS IN OVERSHOOT HYSTERESIS (DECREASING CURRENTS)

Experiment number	Temperature /°C	$-Q$/ coulombs	Current change/ mA. cm.$^{-2}$		Slope/ mV. decade^{-1}	Time range corresponding to the slope/ minutes
			from	to		
R4a"	25 ± 1	662	7.10	0.655	-3.1	1-26
					-5.1	26-86
		2199	7.10	0.655	-2	1-10
					-3.5	10-38
		2847	23.0	0.655	-8.5	1-82

TABLE 16. TEMPERATURE DEPENDENCE OF $-\eta$ VERSUS $\log_{10} t$ SLOPES IN OVERSHOOT HYSTERESIS (DECREASING CURRENTS AFTER 100 SECONDS INTERVAL TAFEL RUNS COMPLETED)

Experiment number	Temperature /°C	$-Q$/ coulombs	Current change/ mA. cm.$^{-2}$		Slope/ mV. decade^{-1}	Time range corresponding to the slope/ minutes
			from	to		
R3c	35.1	2608	0.78	0.38	-5	0.8-12
					-6.4	12-71
	45.1	2619	0.78	0.38	-3.9	0.8-5
					-5.2	5-54
	25.1	2651	0.78	0.38	-7.6	0.6-1.5
					-9.9	1.5-50
	25.1	2680	0.78	0.38	-9.5	0.6-45
	35.1	2700	0.78	0.38	-7.5	0.6-44
	45.1	2722	0.78	0.38	-4.8	0.4-5
					-6.9	5-30

TABLE 17. SLOPES FOR $-\eta$ VERSUS LOG$_{10}$ t PLOTS IN OVERSHOOT HYSTERESIS (INCREASING CURRENTS) FROM SMITH'S DATA (27)

Experiment number	Day	Time		Temperature /^{o}C	Current change/ mA.		Slope/ mV. decade^{-1}	Time range corresponding to the slope/ minutes
		hours	minutes		from	to		
VIIIa	Oct. 6, 1959	15	55	21	0.25	0.80	8	0.75-66
	Oct. 9, 1959	14	15	21	0.25	0.80	5	1-4.5
							6.9	4.5-180
IXa	Nov. 24, 1959	12	23	25	0.25	0.80	4.3	0.4-0.7
							1.8	0.7-13
							5.5	13-92
	Nov. 24, 1959	15	21	25	0.25	2.50	2.1	0.75-5
							8	5-16
							17.8	16-88
XIIb	Mar. 18, 1960	23	15	50	0.08	1.50	2.6	0.5-3
							5.4	3-10

TABLE 17. (Continued)

Experiment number	Day	Time		Temperature /°C	Current change/ mA.		Slope/ mV. decade^{-1}	Time range corresponding to the slope/ minutes
		hours	minutes		from	to		
XIIb	Mar. 20, 1960	12	31	21.25	0.15	0.34	4	0.5-1
							2.3	1-4.5
	Mar. 22, 1960	20	20	21.25	0.35	0.80	3.5	0.4-7
							1.6	7-88

TABLE 18. SLOPES FOR $-\eta$ VERSUS $\text{LOG}_{10}\, t$ PLOTS IN OVERSHOOT HYSTERESIS (DECREASING CURRENTS) FROM SMITH'S DATA (27)

Experiment number	Day	Time		Temperature /°C	Current change/ mA.		Slope/ mV. decade^{-1}	Time range corresponding to the slope/ minutes
		hours	minutes		from	to		
IXa	Nov. 24, 1959	13	54	25	0.80	0.25	-3.5	2-4
							-2	4-31
		16	52	25	2.50	0.25	-4.1	2-88
	Nov. 25, 1959	14	01	25	2.50	0.25	-1.1	1-6
							-4.3	6-53
							-8.8	53-198
	Nov. 26, 1959	15	06	25	2.50	0.25	-1.5	0.66-6
							-5.1	6-54
							-7.6	54-214

TABLE 18. (Continued)

Experiment number	Day	Time		Temperature /$^{\circ}$C	Current change/ mA.		Slope/ mV. decade^{-1}	Time range corresponding to the slope/ minutes
		hours	minutes		from	to		
XIIb	Mar. 13, 1960	20	55	21.5	1.50	0.15	-12	0.75-1
							-6.1	1-7
							-4.5	7-85
	Mar. 17, 1960	20	15	23.3	0.35	0.15	-5.6	0.5-8
							-2.7	8-55
	Mar. 18, 1960	14	00	20.25	0.15	0.08	-5	0.5-70
		17	28	35	0.15	0.08	-1.4	0.5-5
	Mar. 21, 1960	22	24	21.25	0.80	0.35	-8.7	1-3
							-4.5	3-10

For increasing currents at constant temperature:

(i) The slopes tend to decrease as -Q increases, for changes between the same current densities, e.g. Table 12 for experiment R3c shows a decrease from 4.2 and 9.8 mV. at -Q = 37 coulombs to 2.2 and 3.8 mV. at -Q = 448 coulombs for a tenfold current increase from 41 to 405 μA. cm.$^{-2}$. Smith's experiment VIIIa shows a similar trend (Table 17), while the evidence of experiment R4a" (Table 13) does not negate this claim.

(ii) The larger the current ratio (at constant Q), the larger the slope (at least, of the main $-\eta$ versus $\log_{10} t$ line), e.g. Table 12 shows as examples, the changes from 41 and 195 to 405 μA. cm.$^{-2}$ at -Q = 35 ± 2 coulombs, the slopes being, respectively, 4.2 and 9.8 mV., and 2.1 and 5.4 mV. Smith's data (experiment IXa, Table 17) contains another example, the changes from 0.25 to 0.80 and 2.50 mA., respectively, with slopes of 1.8 and 5.5 mV. in the first and 2.1, 8.0 and 17.8 mV. in the second case.

(iii) The slope appears to be higher the higher the final current density, comparing the cases of changes from 41 to 405 μA. cm.$^{-2}$ and from 0.4 to 3.85 mA. cm.$^{-2}$, with main slopes of 3.8 and 14.3 mV., respectively, in Table 12. Although comparison of results for different experiments (R3c and R4a" in Tables 12 and 13) is unhelpful, Smith's data provides some support for this increase of slope as the final current density increases, i.e. the slopes in the

0.25 and 2.50 mA. change in experiment IXa (Table 17).

For decreasing currents at constant temperature:

(i) The slopes remained nearly constant as -Q increased, e.g. as -Q increased from 37 to 448 coulombs, for a change from 405 to 41 μA. cm.$^{-2}$, the observed slopes lay between -2.1 and -4.7 mV. at low t values and -5.4 and -8.0 mV. at larger t, with no definite trend (Table 14, experiment R3c). The results of Smith in experiments IXa (Table 18), changing from 2.5 to 0.25 mA., confirm the lack of trend, the main slopes being -4.1, -4.3 and -5.1 mV. (these differences cannot be regarded as significant). In experiment R4a" (Table 15) the change from 7.10 to 0.655 mA. at -Q = 622 and 2199 coulombs, had slopes of -3.1 and -5.1 mV., and -2 and -3.5 mV., respectively, which may be suggestive of a trend.

(ii) The slopes apparently do not depend on the absolute magnitude of the initial and final current densities, e.g. in Table 14, changes from 405 to 41 μA. cm.$^{-2}$ and from 3.55 to 0.36 mA. cm.$^{-2}$ had essentially the same main slopes of -6.6 mV., regardless of -Q. Smith's results (Table 18, experiments IXa and XIIb) lend some support to this, but it must be stressed that slopes on different electrodes with the same changes of current density are not identical, just as found in the overall $-\eta$ versus $\log_{10}(-Q)$ relations {Section 3A (Vllc)}.

For decreasing currents, the effect of temperature has been reported in Tables 16 and 18. In the first case, at constant Q, rise of temperature decreased the magnitude of the main negative slopes from 9.7 ± 0.2 mV. at 25.1°C to 5 and 6.4 or 7.5 mV. at 35.1°C and to 3.9 and 5.2 or 4.8 and 6.9 mV. at 45.1°C, in two sets of data obtained after Tafel runs in experiment R3c (Table 16). Smith's results for a similar current ratio, but lower current densities in experiment XIIb, agree with this trend, his slopes being -5 mV. at 20.25°C and -1.4 mV. at 35°C (Table 18).

The above conclusions must be regarded as somewhat tentative in view of the limited quantity of data available on this type of behaviour. It is evident, however, that the true nature of overshoot hysteresis will only be ascertained by the gathering and resolution of such data, so that a clear pattern of behaviour can be established. This is not likely to be possible until really reproducible overvoltage-charge relations are obtained on different electrodes, for it seems likely that the two phenomena are closely related, as Ives and Smith (26, 27) suggested.

(V111) Summarising Remarks on Overvoltage Measurements

1. In most of the experiments with scraped and electropolished electrodes in $HClO_4$, pre-electrolysed at $-i \lesssim 2$ mA. cm.$^{-2}$, the overvoltage at constant current density rose initially and then began to fall. For scraped electrodes, this fall was very slow at first {slope of $-\eta$ versus $\log_{10}(-Q) < 10$ mV.} and then, the overvoltage fell with a steeper slope of about 100 mV. per decade of charge. However, electropolished electrodes showed at first a fall of 40 - 90 mV. per decade of charge and then fell with steeper slopes ranging from 150 - 685 mV. per decade of charge, i.e. a total decrease in overvoltage by 150 - 300 mV. at the end of long periods of cathodisation was observed on such electrodes. In contrast, $-\eta$ for electropolished lead in $HClO_4$, pre-electrolysed at $-i = 4 - 6$ mA. cm.$^{-2}$, increased continuously except in experiment R4a (charcoal-cleaning was used in this experiment).

2. Except for a few, electropolished electrodes showed well-behaved Tafel lines from the beginning, measurements on freshly prepared electrodes in $HClO_4$, pre-electrolysed at $-i \lesssim 2$ mA. cm.$^{-2}$, gave bilinear or curved Tafel plots with steeper slopes at lower currents because of depolarisation, presumably by Pb^{++} or O_2. Continued cathodisation led to plots approaching rectilinearity. Then the commonly observed slope was 110 ± 10 mV. Normal or overshoot hysteresis was observed, more prominently on continued

cathodisation. Although Tafel slopes decreased in a few cases to 90 mV. during the initial cethodisation, the decrease of b from 130 - 140 mV. only to 110 mV. was frequent. The Tafel slope was found to be apparently independent of temperature. After prolonged cathodisation, calculated values of $\Delta H^{\dagger}_{\eta=0}$ decrease with the increase of -Q.

Improved Tafel behaviour was observed both for scraped electrodes in $HClO_4$, pre-electrolysed at $-i \leq 2$ mA. cm.$^{-2}$, and for electropolished electrodes in $HClO_4$, pre-electrolysed at $-i = 4 - 6$ mA. cm.$^{-2}$, as the electrodes aged, but the behaviour never was comparable to that of electropolished electrodes in properly pre-electrolysed (i.e. at low current densities) solutions.

3. Overshoot hysteresis was universal for electropolished electrodes in $HClO_4$, pre-electrolysed at $-i \leq 2$ mA. cm.$^{-2}$, but was observed less frequently for scraped electrodes under similar experimental conditions. Overshoot hysteresis was only rarely seen for electropolished electrodes in $HClO_4$, pre-electrolysed at $-i = 4 - 6$ mA. cm.$^{-2}$. The extent of overshoot increases with the magnitude of the current-step, decreases as -Q increases at constant temperature and decreases as the temperature increases at approximately the same Q value. For each step-change, the immediate potential jump was followed by an exponential change of potential in the reverse direction. The computed slopes for plots of $-\eta$ versus $\log_{10} t$

decreased as -Q increased; but increased with the magnitude of the final current in the step-change and with an increase in the current ratio (between final and initial) at approximately the same Q value, for increasing currents only. However, the slope for decreasing currents in a step-change at constant temperature was found to be independent of Q. For decreasing currents at approximately the same Q, rise of temperature decreased the absolute magnitude of the slope.

B. Experimental Method and Results of Adsorption Pseudo-Capacity

In this section, the experimental techniques and results obtained in capacity measurements on lead cathodes in aqueous perchloric acids are described.

Cells, materials, gas purification, methods of preparation of solutions and electrodes and other experimental conditions, unless stated otherwise, were identical with those described in Section 3A.

(1) Instrumentation and Procedure

Since overvoltage and capacity measurements were carried out simultaneously, the polarising circuit (Fig. 12) and instruments were the same as described in Section 3A (V) in the capacity measurements. Capacity measurements were made by observing the rapid open-circuit decay on an oscilloscope, a standard technique (131), which we have improved (207). The voltage decay and its derivative were measured with a microswitch {as described in Section 3A (V) using the circuit of Fig. 12*} in combination with a differentiating circuit (Fig. 38). The differentiating circuit consisted of an operational amplifier (Analog Devices 147A) used in a non-inverting circuit to provide both high input impedence (10^{12} Ω) and fast response (10 MHz) at the input stage of the oscilloscope. To improve the stability of the non-inverting amplifier and to eliminate the high frequency noise, a capacity of 330 pF. was inserted between the + terminal of the 147A amplifier

---

* see p. 133

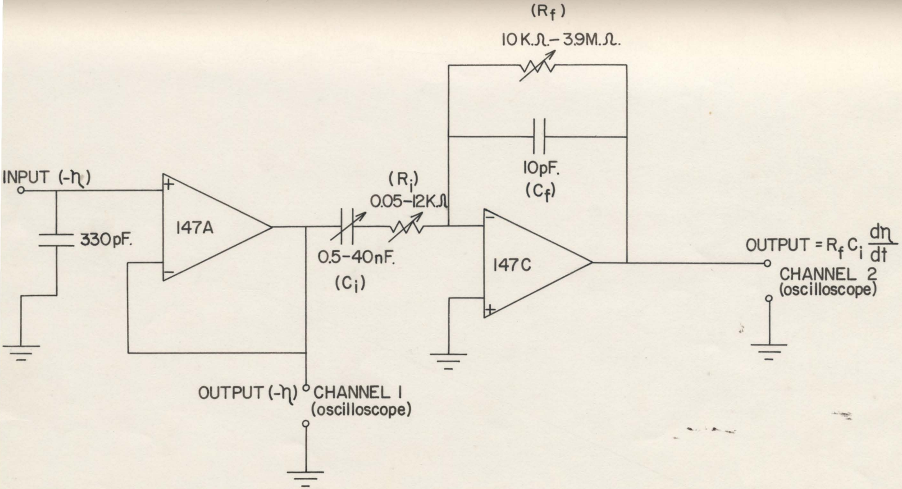

Fig. 38. DIFFERENTIATING CIRCUIT.

and ground. The differentiating unit of the circuit consisted of an operational amplifier (Analog Devices 147C), having similar characteristics to the 147A, but superior in certain respects, e.g. input offset voltage of $\pm$ 2 µV./°C of 147C compared with $\pm$ 15 µV./°C of 147A, in an inverting circuit. A known variable input capacitor C_i (0.5 - 40 nF.) was in series with an ohmic feed-back link, R_f (10 k.Ω. - 3.9 M.Ω.), which was itself between the input and output of the amplifier 147C. A small noise-suppression capacitor C_f (10 pF.) in parallel with the feed-back resistor R_f increased the stability of the circuit and the transient response. The variable resistors* (0.05 - 12 k.Ω.) in series with C_i at the input stage of 147C was used to isolate the capacity load at high frequency and to improve the stability of the circuit.

The input signal ($-\eta$) through the 147A (output = $-\eta$) was fed to channel 1 of a Tektronix 1A1 dual trace plug-in unit in a Tektronix 547 oscilloscope, and its derivative, obtained from the differentiating unit, of output = $R_f C_i (d\eta/dt)$, was fed simultaneously to channel 2. Both signals were photographed simultaneously with Polaroid Land roll film type 47 in a Tektronix oscilloscope camera C-12. The magnitude of $C_i R_f$ was kept as small as possible to achieve the best performance of the differentiator. The accuracy of the method

---

* Generally, R_i = 1 k.Ω. or 4.9 k.Ω. (i.e. $R_f \gg R_i$) was used to minimise the effect of this resistor on the output voltage.

was examined by using a variable linear saw-tooth input signal, the slope of which could be measured from oscillographic photographs, as mentioned above. A typical record is shown in Fig. 39. The trace inclined to the abscissa is the saw-tooth signal, whereas the trace parallel to the abscissa is its differentiated signal. The differential signal was switched in during the course of a single saw-tooth transient and the magnitude of the differential coefficient is proportioned to the height of the discontinuity exhibited by the channel 2 trace. Such calibration data are shown in Table 19 for a range of voltage sweep rates from 5.9×10^{-1} to 5.8×10^{4} V. sec.$^{-1}$. From Fig. 39, $\frac{dV}{dt} = 114$ V. sec.$^{-1}$ from the saw-tooth input voltage sweep rate, while the differential curve gives $\frac{dV}{dt} = 117$ V. sec.$^{-1}$, calculated from the height of the discontinuity exhibited by the channel 2 trace, i.e. 35 mV. and the values of $R_f = 10$ k.Ω. and $C_i = 30$ nF. The calculated error was 2.6%. It is evident from Table 19 that agreement within 3% was obtained between the known voltage sweep rate and the differentiated signal for all the sweep rates examined. No systematic error with decreasing time base was indicated up to the minimum value of 10 μsec. cm.$^{-1}$, as shown by the linear relationship Fig. 40. The least squares value of the slope of Fig. 40 is 1.000 ± 0.004, the corresponding intercept is -0.002 ± 0.011, i.e. zero, within experimental error.

In addition, the differentiator was calibrated by using the

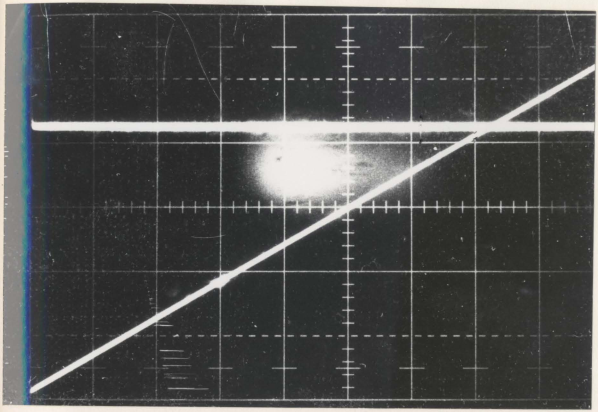

Fig. 39. SAW-TOOTH SIGNAL (RISING CURVE, CHANNEL 1) AND DIFFERENT SAW-TOOTH SIGNAL (HORIZONTAL CURVE, CHANNEL 2, $R_f = 10$ k.Ω., $C_i = 30$ nF.). VOLTAGE ON ORDINATE: CHANNEL 1 - 1V. cm^{-1}, CHANNEL 2 - 0.02 TIME BASE ON ABSCISSA: 5 MSEC. cm^{-1}.. THE BOTTOM AND TOP LINES OF THE GRID ARE THE BASE LINES FOR THE SAW-TOOT SIGNAL AND THE DIFFERENTIATED SIGNAL, RESPECTIVELY.

TABLE 19. CALIBRATION DATA FOR THE DIFFERENTIAL GALVANOSTATIC METHOD

Time base/ msec. cm.$^{-1}$	Saw-tooth signal		Differential curve				
	Vertical sensitivity/ V. cm.$^{-1}$	$\frac{dV}{dt}\Big/$ V. sec.$^{-1}$	R_f/k.Ω.	C_i/nF.	Vertical sensitivity/ V. cm.$^{-1}$	Output signal/mV. $= R_f C_i \left(\frac{dV}{dt}\right)$	$\frac{dV}{dt}\Big/$ V. sec.$^{-1}$ from R_f and C_i values
1×10^3	1	5.9×10^{-1}	3.9×10^3	30	0.02	69	5.9×10^{-1}
1×10^2	1	5.9	1×10^3	30	0.05	175	5.8
1×10^1	1	5.9×10^1	2×10^2	30	0.1	340	5.7×10^1
5	1	1.1×10^2	1×10^1	30	0.02	35	1.2×10^2
1	1	5.9×10^2	5×10^1	10	0.05	285	5.7×10^2
1×10^{-1}	1	5.9×10^3	3×10^1	1	0.05	180	6.0×10^3
5×10^{-2}	1	1.2×10^4	1×10^1	1	0.02	115	1.5×10^4
2×10^{-2}	1	2.9×10^4	1×10^1	1	0.1	300	3.0×10^4
1×10^{-2}	1	5.8×10^4	1×10^1	0.5	0.05	285	5.7×10^4

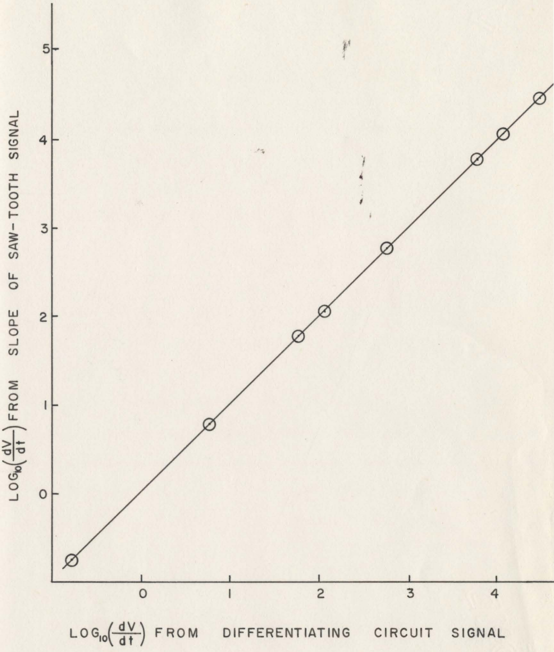

Fig. 40. LINEAR RELATION BETWEEN CALIBRATION $\left(\frac{dV}{dt}\right)$ AND
CALCULATED FROM C_i AND R_f FROM THE DIFFERENTIATED
VOLTAGE SIGNAL (LOG SCALES)

initial slope, (i.e. slope at t = 0 after the interruption of the polarising current) obtained from the geometrical differentiation of the overvoltage decay curve (channel 1) and the corresponding slope calculated from the output voltage of the differentiated signal and values of R_f and C_i (channel 2), i.e. under real experimental conditions. Such calibration data are shown in Table 20 for $(d\eta/dt)_{t=0}$ from 2.5 to 1.7×10^3 V. sec.$^{-1}$, both from geometrical differentiation of the overvoltage decay curves and its differentiated signal. A typical record of overvoltage decay (channel 1 - lower curve) and its differentiated signal (channel 2 - upper curve) are shown in Fig. 41. From Fig. 41 $(d\eta/dt)_{t=0}$ = 170 V. sec.$^{-1}$ from the initial slope of the overvoltage decay curve, while the corresponding slope from the differential curve gives 175 V. sec.$^{-1}$, calculated from the output voltage = 175 mV. and the values of R_f = 100 k.Ω. and C_i = 10 nF. The calculated error was 2.9%. Although errors of 10 - 15% could be seen for $(d\eta/dt)_{t=0} < 10$ V. sec.$^{-1}$, the probable error was about 5%. The observed error was never greater than 5% in most of our experimental results reported in this Section. Besides this, no systematic error in slopes obtained from both methods with the time base was indicated up to the minimum value of 100 μsec. cm.$^{-1}$ as shown by the linear relationship in Fig. 42. The least squares value of the slope of Fig. 42 is 1.016 ± 0.02. Corresponding intercept is 0.045 ± 0.026, i.e. zero, within experimental error.

ABLE 20. CALIBRATION DATA FOR THE DIFFERENTIAL GALVANOSTATIC METHOD

Time base/ msec. cm.$^{-1}$	Decay Curve		Differential curve				
	Vertical sensitivity /V. cm.$^{-1}$	$\left(\frac{d\eta}{dt}\right)_{t=0} \Big/$ V. sec.$^{-1}$ from geometrical differentiation	R_f/k.Ω.	C_i/nF.	Vertical sensitivity /V. cm.$^{-1}$	Output signal/mV. $= R_f C_i \left(\frac{d\eta}{dt}\right)_{t=0}$	$\left(\frac{d\eta}{dt}\right)_{t=0} \Big/$ V. sec.$^{-1}$ from R_f and C_i values
50	0.1	2.5	1×10^3	20	0.02	59	3.0
2	0.02	3.6	1×10^3	2	0.01	7	3.5
10	0.1	8.2	5×10^2	20	0.02	100	10
5	0.1	3.2×10^1	2×10^2	20	0.05	110	2.8×10^1
2	0.1	4.1×10^1	1×10^2	20	0.05	85	4.3×10^1
2	0.1	5.0×10^1	1×10^2	20	0.05	110	5.4×10^1
2	0.1	6.0×10^1	1×10^2	20	0.05	135	6.8×10^1
1	0.1	1.7×10^2	1×10^2	10	0.05	175	1.8×10^2
0.5	0.1	2.6×10^2	5×10^1	10	0.05	130	2.6×10^2
0.5	0.1	3.2×10^2	5×10^1	10	0.05	160	3.2×10^2
0.5	0.2	4.3×10^2	5×10^1	10	0.05	215	4.3×10^2
0.1	0.1	7.9×10^2	3×10^1	3.3	0.05	810	8.2×10^2
0.2	0.2	1.1×10^3	5×10^1	4	0.05	205	1.0×10^3
0.1	0.2	1.6×10^3	3×10^1	3	0.05	155	1.7×10^3

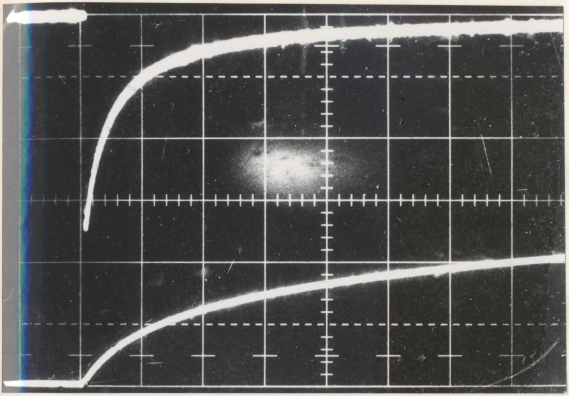

Fig. 41. OVERVOLTAGE DECAY SIGNAL (LOWER CURVE, CHANNEL 1) AND ITS DIFFERENTIATED SIGNAL (UPPER CURVE, CHANNEL 2 ; R_f = 100 k. Ω., C_i = 10 nF.). VOLTAGE ON ORDINATE: CHANNEL 1 – 0.1 V. cm^{-1}., CHANNEL 2 – 0.05 V. cm^{-1}.. TIME BASE ON ABSCISSA: 1 MSEC. cm^{-1}. BOTTOM AND TOP LINES OF THE GRID ARE THE BASE LINES FOR OVERVOLTAGE DECAY AND ITS DIFFERENTIATED SIGNAL, RESPECTIVELY.

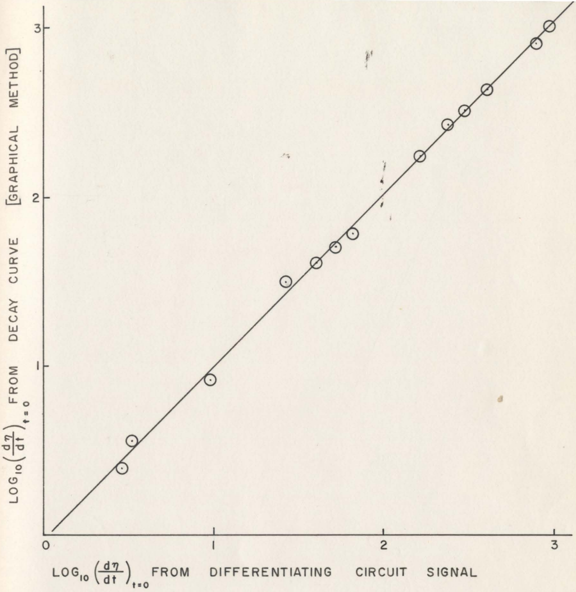

Fig. 42. LINEAR VARIATION BETWEEN CALIBRATION $\left(\frac{d\eta}{dt}\right)_{t=0}$ CALCULATE FROM THE GEOMETRICAL DIFFERENTIATION OF THE VOLTAGE DECAY CURVE AND $\left(\frac{d\eta}{dt}\right)_{t=0}$ CALCULATED FROM C_i AND R_f FROM THE DIFFERENTIATED VOLTAGE SIGNAL (LOG SCALES).

Knowing $\left(\frac{d\eta}{dt}\right)_{t=0}$, $C_{\text{expt.}}$ was calculated using the equation

$$C_{\text{expt.}} = \frac{-i}{\left(\frac{d\eta}{dt}\right)_{t=0}} \qquad (2.35)$$

where -i is the cathodic current density at the time of current interruption, t = 0 (t is the time elapsed after the current interruption).

As mentioned in Section 3A (V), Pb electrodes were cathodised galvanostatically (initially at 30 μA. to 1 mA.) and the overvoltage variation with time was recorded. In experiments considered satisfactory, capacity measurements were begun only after observing both a linear Tafel line over the range of currents used in the capacity measurements <u>and</u> the decrease of overvoltage with the total cathodic charge passed. Then, the overvoltage decay and its derivative were measured as described earlier. Also, $-\eta$ corresponding to the cathodic current density, -i at the time of current interruption, t = 0 was recorded. Thus, the calculated $C_{\text{expt.}}$ using equation (2.35) and the measured $\left(\frac{d\eta}{dt}\right)_{t=0}$ and -i correspond to $-\eta$ recorded at t = 0. Later, the steady-state current density was changed to other values in a step-wise manner, either increasing or decreasing, and kept constant at this new current density for a pre-determined time (5 - 10 minutes). At the end of the pre-determined time (say 5 - 10 minutes), the open-circuit decays were followed at each polarisation current. The overvoltages at the instant of current interruption, at each current, were also recorded. Thereby, we calculated $C_{expt.}$ at different $-\eta$. This sequence of measurements was repeated for 10 to 15 days.

Some of the capacity values of Pb in 1 M $HClO_4$ at nearly constant η and Q for the different time-base settings of the oscilloscope are listed in Table 21. Table 21 evidently shows that the $C_{expt.}$ at constant η and Q are independent of the time-base setting of the oscilloscope within the experimental error.

TABLE 21. DEPENDENCE OF ELECTRODE CAPACITY ($C_{expt.}$) ON TIME-BASE SETTING OF THE OSCILLOSCOPE FOR SOME EXPERIMENTS WITH Pb FOILS

Experiment number	Total cathodic charge passed $-Q$ /coulombs	Time base /msec. cm.$^{-1}$	$-\eta$/mV.	$C_{expt.}$ / μF. cm.$^{-2}$	Average $C_{expt.}$/ μF. cm.$^{-2}$
F9	754	5	862	16.8	16.6 ± 0.2
		0.5	858	16.7	
		0.1	856	16.4	
F10	0.025	20	844	9.3	9.8 ± 0.5
		5	846	10.3	
		2	846	10.3	
		1	848	9.9	
		0.1	847	9.7	
	491	5	981	105	107 ± 3
		0.5	980	106	
		0.1	983	110	

(11) Results of Early Experiments

(a) Preliminary Experiments

No satisfactory measurements were made with Pb foils F1 to F6, mentioned in Section 3A (V1a), either because of the use of low purity Pb, a leaking cell or troubles with electronic circuitry. A few capacity measurements made with in situ electropolished electrodes F7 and F8 are tabulated in Tables 22 and 23. These results, obtained with 1 M $HClO_4$, not pre-electrolysed or otherwise purified, are atypical because the capacities at low current densities < 1.5 mA. cm.$^{-2}$ were very low, in some cases less than 1 μF. cm.$^{-2}$. The capacities at higher current density are quite large, ranging up to ca. 100 μF. cm.$^{-2}$ at 32 mA. cm.$^{-2}$.

As can be seen in Table 22, as -Q increased from 3 to 5 coulombs, at current density < 500 μA. cm.$^{-2}$, both $-\eta$ and $C_{expt.}$ decreased while at higher current density, $-\eta$ increased and $C_{expt.}$ remained constant or increased at the highest current densities. Further cathodisation at 525 μA. cm.$^{-2}$ (to -Q = 119 coulombs) caused no change in $C_{expt.}$ from 2.3 μF. cm.$^{-2}$ but $-\eta$ increased further to 1083 mV. (c.f. Table 22).

Table 23 shows a similar variation of $C_{expt.}$ with current density for electrode F8. Continued cathodisation at 525 μA. cm.$^{-2}$, increasing -Q from 5 to 64 coulombs led to increases both of $-\eta$

TABLE 22. ELECTRODE CAPACITY OF AN ELECTRODE F7 IN AQUEOUS PERCHLORIC ACID

Total cathodic charge passed $-Q$/ coulombs	Cathodic current density $-i$/mA. cm.$^{-2}$																	
	0.02		0.065		0.190		0.525		1.50		5.05		12.0		23.0		29.5	
	$-\eta$/ mV.	$C_{expt.}$ /μF. cm.$^{-2}$	$-\eta$/ mV.	$C_{expt.}$ /μF. cm.$^{-2}$	$-\eta$/ mV.	$C_{expt.}$ /μF. cm.$^{-2}$	$-\eta$/ mV.	$C_{expt.}$ /μF. cm.$^{-2}$	$-\eta$/ mV.	$C_{expt.}$ /μF. cm.$^{-2}$	$-\eta$/ mV.	$C_{expt.}$ /μF. cm.$^{-2}$	$-\eta$/ mV.	$C_{expt.}$ /μF. cm.$^{-2}$	$-\eta$/ mV.	$C_{expt.}$ /μF. cm.$^{-2}$	$-\eta$/ mV.	C_{expt} /μF. cm.$^{-2}$
3	619	0.9	765	0.5	890	2.1	1017	2.3	1082	4.4	1139	13.3	1176	24.4	1190	40	1191	51.1
5	491	0.6	708	0.7	826	1	1056	2.2	1116	4.4	1164	14.1	1197	27.6	1218	45	1211	62.8

TABLE 23. ELECTRODE CAPACITY OF AN ELECTRODE F8 IN AQUEOUS PERCHLORIC ACID

Total cathodic charge passed $-Q$/ coulombs	Cathodic current density $-i$/mA. cm.$^{-2}$																	
	0.02		0.065		0.190		0.525		1.50		5.05		12.5		24.5		32.0	
	$-\eta$/ mV.	$C_{\text{expt.}}$ /µF. cm.$^{-2}$	$-\eta$/ mV.	$C_{\text{expt.}}$ /µF. cm.$^{-2}$	$-\eta$/ mV.	$C_{\text{expt.}}$ /µF. cm.$^{-2}$	$-\eta$/ mV.	$C_{\text{expt.}}$ /µF. cm.$^{-2}$	$-\eta$/ mV.	$C_{\text{expt.}}$ /µF. cm.$^{-2}$	$-\eta$/ mV.	$C_{\text{expt.}}$ /µF. cm.$^{-2}$	$-\eta$/ mV.	$C_{\text{expt.}}$ /µF. cm.$^{-2}$	$-\eta$/ mV.	$C_{\text{expt.}}$ /µF. cm.$^{-2}$	$-\eta$/ mV.	C_{exp} /µF. cm.
3	606	0.9	685	1.6	758	4.3	888	3.8	1033	9.3	1124	19.5	1180	38.2	1203	73	1203	99.

and of $C_{expt.}$, to 1066 mV. and 8.1 µF. cm.$^{-2}$, respectively. During further cathodisation up to -Q of 335 coulombs, both -η and $C_{expt.}$ remained essentially constant.

(b) Experiments with Electropolished Electrodes and Solution Pre-electrolysed at Too High Current Densities

Because electrodes F11 to F14 did not give satisfactory overvoltage results, as reported in Section 3A (V1b), in particular that -η increased rather than decreased with -Q, few capacity measurements were made with them. A systematic study was, nevertheless, done for electrode F12 as indicated in Table 24. Cathodisation was continued at 535 µA. cm.$^{-2}$ but C and -η measurements extended from 185 µA. cm.$^{-2}$ to 21.5 mA. cm.$^{-2}$. $C_{expt.}$ increased with -Q at current density < 4.8 mA. cm.$^{-2}$ but decreased at 4.8 mA. cm.$^{-2}$ and higher current densities, very high values (up to 220 µF. cm.$^{-2}$) being observed initially at the highest current densities. Evidently, this high value is associated with significant concentrations of Pb^{++} in the solution and the decrease of $C_{expt.}$ with the decrease of (Pb^{++}) during cathodisation.

Some capacity measurements with electrode R4a, in which charcoal-cleaning of solution apparently diminished concentrations of Pb^{++} arising from the previous high current density pre-electrolysis, are as follows: $C_{expt.}$ = 12.1 µF. cm.$^{-2}$ at

TABLE 24. ELECTRODE CAPACITY OF AN ELECTRODE F12 IN AQUEOUS PERCHLORIC ACID

Total cathodic charge passed $-Q$/ coulombs	Cathodic current density $-i$/mA. cm.$^{-2}$											
	0.185		0.535		1.45		4.8		12.0		21.5	
	$-\eta$/ mV.	$C_{expt.}$ /μF. cm.$^{-2}$	$-\eta$/ mV.	$C_{expt.}$ /μF. cm.$^{-2}$	$-\eta$/ mV.	$C_{expt.}$ /μF. cm.$^{-2}$	$-\eta$/ mV.	$C_{expt.}$ /μF. cm.$^{-2}$	$-\eta$/ mV.	$C_{expt.}$ /μF. cm.$^{-2}$	$-\eta$/ mV.	$C_{expt.}$ /μF. cm.$^{-2}$
10	712	9.5	797	9.7	876	11.9	980	25.6	1040	117	1078	219.3
123	742	17.8	819	18.5	892	19.6	1002	26	1078	38.2	1114	52
192	727	16.6	821	16.4	906	16.8	1011	21.5	1072	28.1	1106	35.7

$-\eta$ = 848 mV. (and $-i$ = 665 μA. cm.$^{-2}$); $C_{expt.}$ = 14 μF. cm.$^{-2}$ at $-\eta$ = 1022 mV. (and $-i$ = 7 mA. cm.$^{-2}$); both at $-Q$ = 324 coulombs.

(111) Experiments with Electropolished Electrodes and "Properly Pre-electrolysed" Solutions

(a) Results of Capacity Measurements

Capacity measurements were carried out in eight experiments thought satisfactory, six with electropolished rods, in solutions cleaned continuously over activated charcoal, and two with electropolished foils without this treatment. In all cases the $HClO_4$ was pre-electrolysed at $-i \lesssim 2$ mA. cm.$^{-2}$ for 5 to 20 days. Overvoltage measurements on these electrodes have been described in Section 3A (V11).

The most interesting capacity measurements were obtained with electrodes F10, R4a", R4b, R5b, R5c and R5d. These electrodes were electropolished and cathodised at a constant current density of from 500 to 800 μA. cm.$^{-2}$ in 1 M $HClO_4$. Lower currents were avoided to overcome the low current hysteresis described by Ives and Smith (26, 27). Electrode F10 differed from the rest as it was electropolished and washed in situ in the cell (b), Fig. 11, but the solution was not subjected to charcoal-cleaning. The other electrodes were electropolished in an external apparatus and transferred to the cell (a), Fig. 10, under a rapid stream of hydrogen.

Electrode capacities, $C_{expt.}$, measured at different current densities and after different periods of polarisation in these experiments are listed in Tables 25 to 30. The current densities are

TABLE 25. ELECTRODE CAPACITY OF AN ELECTRODE F10 CATHODISED AT $-i = 505$ μA. cm.$^{-2}$ IN 1 M PERCHLORIC ACID

Total cathodic charge passed $-Q$/ coulombs	Cathodic current density $-i$/mA. cm.$^{-2}$															
	0.019		0.062		0.180		0.505		1.40		4.85		12.0		22	
	$-\eta$/ mV.	$C_{expt.}$ /μF. cm.$^{-2}$	$-\eta$/ mV.	$C_{expt.}$ /μF. cm.$^{-2}$	$-\eta$/ mV.	$C_{expt.}$ /μF. cm.$^{-2}$	$-\eta$/ mV.	$C_{expt.}$ /μF. cm.$^{-2}$	$-\eta$/ mV.	$C_{expt.}$ /μF. cm.$^{-2}$	$-\eta$/ mV.	$C_{expt.}$ /μF. cm.$^{-2}$	$-\eta$/ mV.	$C_{expt.}$ /μF. cm.$^{-2}$	$-\eta$/ mV.	$C_{expt.}$ /μF. cm.$^{-2}$
75	641	13.5	708	12.6	776	11.4	842	11.7	898	12	961	16	1001	23.7	1051	31.6
173	638	12.9	705	12.7	774	12.2	834	13.2	906	14.4	968	19.8	1017	32	1052	39.4
246	638	14	707	14.5	772	14.9	836	15.3	906	17	981	26.3	1027	38.2	1056	49.2
324	627	16.8	701	16.6	767	15.5	799	16.4	858	18.7	933	27.5	988	48.3	1016	65.1
421	601	18.1	664	17.3	721	17.7	776	19.9	835	23.1	911	38	962	59.2	975	86.8
491	603	22.5	667	19.2	724	19.7	781	20	845	25.7	916	43.3	956	70.1	980	106

TABLE 26. ELECTRODE CAPACITY OF AN ELECTRODE R4a" CATHODISED AT $-i$ = 655 μA. cm.$^{-2}$ IN 1 M PERCHLORIC ACID

Total cathodic charge passed $-Q$/ coulombs	Cathodic current density $-i$/mA. cm.$^{-2}$							
	0.067		0.210		0.655		2.05	
	$-\eta$/ mV.	$C_{expt.}$ /μF. cm.$^{-2}$	$-\eta$/ mV.	$C_{expt.}$ /μF. cm.$^{-2}$	$-\eta$/ mV.	$C_{expt.}$ /μF. cm.$^{-2}$	$-\eta$/ mV.	$C_{expt.}$ /μF. cm.$^{-2}$
25	879	19.2	908	20.2	958	18.7	1020	18.9
105	853	23.2	833	22.1	886	22.1	937	21.7
194	707	33.7	758	26.2	805	26.8	852	24.9
262	704	24.9	754	25.6	805	23.7	853	24
420	674	21.1	727	21.7	779	21.6	833	19.6
495	685	19.8	736	19.5	788	20.4	841	18.9

TABLE 27. ELECTRODE CAPACITY OF AN ELECTRODE R4b CATHODISED AT $-i$ = 790 µA. cm.$^{-2}$ IN 1 M PERCHLORIC ACID

Total cathodic charge passed $-Q$/ coulombs	Cathodic current density $-i$/mA. cm.$^{-2}$													
	0.083		0.255		0.790		2.45		8.70		30.5		64.0	
	$-\eta$/ mV.	$C_{expt.}$ /µF. cm.$^{-2}$	$-\eta$/ mV.	$C_{expt.}$ /µF. cm.$^{-2}$	$-\eta$/ mV.	$C_{expt.}$ /µF. cm.$^{-2}$	$-\eta$/ mV.	$C_{expt.}$ /µF. cm.$^{-2}$	$-\eta$/ mV.	$C_{expt.}$ /µF. cm.$^{-2}$	$-\eta$/ mV.	$C_{expt.}$ /µF. cm.$^{-2}$	$-\eta$/ mV.	$C_{expt.}$ /µF. cm.$^{-2}$
32	860	21.3	929	18.8	987	19.7	1051	20.8	1120	21.2	–	–	–	–
93	850	18.8	909	18.5	966	18.8	1031	20.4	1103	21	–	–	–	–
194	827	18.5	893	18.3	957	19.1	1017	21	1081	25.4	–	–	–	–
276	816	20.5	883	21.0	941	21.2	1002	22.6	1069	25.9	–	–	–	–
633	806	23.3	873	23	936	23.5	997	24.7	1065	27.1	1123	31.6	1151	34.8
727	793	23.3	861	22.9	926	24.3	989	24.7	1056	27.5	1117	31.9	1145	35.2
820	789	23	856	22.7	921	24.3	985	24.6	1053	28	1116	32	1144	35.3

TABLE 28. ELECTRODE CAPACITY OF AN ELECTRODE R5b CATHODISED AT $-i = 650\ \mu A.\ cm.^{-2}$ IN 1 M PERCHLORIC ACID

Total cathodic charge passed $-Q$/ coulombs	Cathodic current density $-i$/mA. $cm.^{-2}$									
	0.650		1.95		6.90		24.0		49.5	
	$-\eta$/ mV.	$C_{expt.}$ /μF. $cm.^{-2}$	$-\eta$/ mV.	$C_{expt.}$ /μF. $cm.^{-2}$	$-\eta$/ mV.	$C_{expt.}$ /μF. $cm.^{-2}$	$-\eta$/ mV.	$C_{expt.}$ /μF. $cm.^{-2}$	$-\eta$/ mV.	$C_{expt.}$ /μF. $cm.^{-2}$
145	1044	19.9	1112	21.8	1168	23.3	-	-	-	-
260	1028	21.2	1083	22.6	1142	24.7	-	-	-	-
325	1015	22.7	1070	23	1128	26.9	-	-	-	-
420	1011	24.5	1066	25.4	1126	28.4	-	-	-	-
510	1003	26.3	1060	25.7	1120	26.6	-	-	-	-
602	991	26.2	1050	27.1	1113	28.1	1185	32.7	1210	32.1
702	986	27.4	1047	27.5	1110	30.1	1183	33.5	1221	36.2
765	976	27.4	1038	27.9	1112	30.8	1181	34	1208	32.5
838	951	27.8	1014	28.4	1083	30.8	1168	35	1212	36.5
1118	910	27.7	973	26	1039	29	1129	32.5	1190	35.4

TABLE 29. ELECTRODE CAPACITY OF AN ELECTRODE R5c CATHODISED AT $-i$ = 775 μA. cm.$^{-2}$ IN 1 M PERCHLORIC ACID

Total cathodic charge passed $-Q$/ coulombs	Cathodic current density $-i$/mA. cm.$^{-2}$					
	0.775		2.40		8.45	
	$-\eta$/ mV.	$C_{expt.}$ /μF. cm.$^{-2}$	$-\eta$/ mV.	$C_{expt.}$ /μF. cm.$^{-2}$	$-\eta$/ mV.	$C_{expt.}$ /μF. cm.$^{-2}$
92	1036	20.4	1079	23.7	1140	26.7
149	959	22.8	1007	26.3	1066	28.1
254	899	22.8	946	24	998	24.9
322	892	21.6	937	23.3	988	25.3

TABLE 30. ELECTRODE CAPACITY OF AN ELECTRODE R5d CATHODISED AT $-i = 570$ µA. cm.$^{-2}$ IN 1 M PERCHLORIC ACID

Total cathodic charge passed $-Q$/ coulombs	Cathodic current density $-i$/mA. cm.$^{-2}$							
	0.570		2.85		5.70		30.5	
	$-\eta$/ mV.	$C_{expt.}$ /µF. cm.$^{-2}$	$-\eta$/ mV.	$C_{expt.}$ /µF. cm.$^{-2}$	$-\eta$/ mV.	$C_{expt.}$ /µF. cm.$^{-2}$	$-\eta$/ mV.	$C_{expt.}$ /µF. cm.$^{-2}$
95	976	13.6	1051	14.8	1084	17.9	1175	23.3
267	893	12.7	955	14.8	985	15.5	1073	23.4

average values, accurate to ± 3%. The following common features have been observed:

(i) $C_{\text{expt.}}$ at constant current density frequently increased with −Q in some cases remaining unchanged or decreasing with −Q. In such cases,

(ii) $C_{\text{expt.}}$ invariably increased with −Q when values at constant η are compared (see Figs. 43 to 47).

(iii) At a given −Q, $C_{\text{expt.}}$ increased with −i (and with $-\eta$) above a minimum value which was either the lowest current density of the measurements (Tables 28 to 30) or was a current density close to 0.2 mA. cm.$^{-2}$ (Tables 25 and 27). Results reported in Table 26 do not conform to this trend.

It is to be noted that the increase of $C_{\text{expt.}}$ was generally accompanied by a decrease of $-\eta$, e.g. in F10 at −i = 22 mA. cm.$^{-2}$, $C_{\text{expt.}}$ rose from 31.6 to 106 μF. cm.$^{-2}$ while $-\eta$ decreased from 1051 to 980 mV., during the passage of an additional 415 coulombs at 505 μA. cm.$^{-2}$ (Table 25).

Even in experiment R4a" (Table 26), an increase of capacity occurred at various current densities as $-\eta$ decreased, but later $C_{\text{expt.}}$ decreased also. This change of behaviour after −Q = 194 coulombs coincides with a steep fall of $-\eta$ (slope 685 mV. in Fig. 30). A similar case is that of electrode R5b (Table 28) for which $C_{\text{expt.}}$

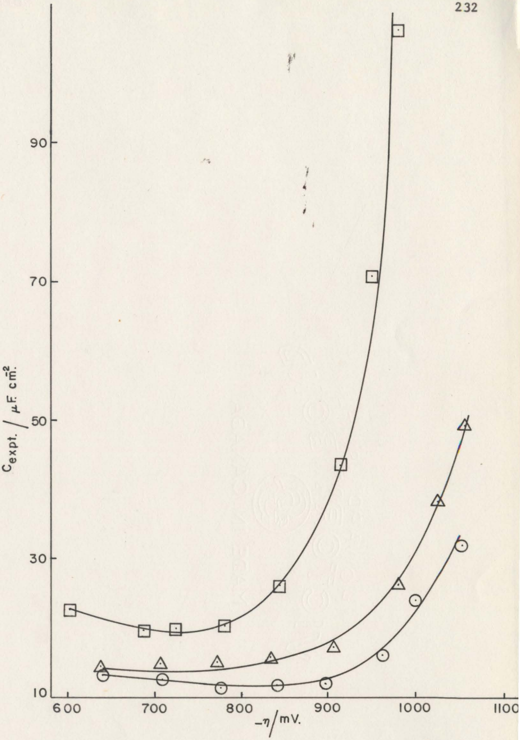

Fig. 43. VARIATION OF ELECTRODE CAPACITY FOR ELECTRODE F10 WITH PERIOD OF POLARISATION AT $-i$ = 505 $\mu A.cm^{-2}$ (CAPACITIES ARE SHOWN AS A FUNCTIO OF OVERVOLTAGE); ⊙ , AT $-Q$ = 75 COULOMBS; △ , AT $-Q$ = 246 COULOMBS; ⊡ , AT $-Q$ = 491 COULOMBS.

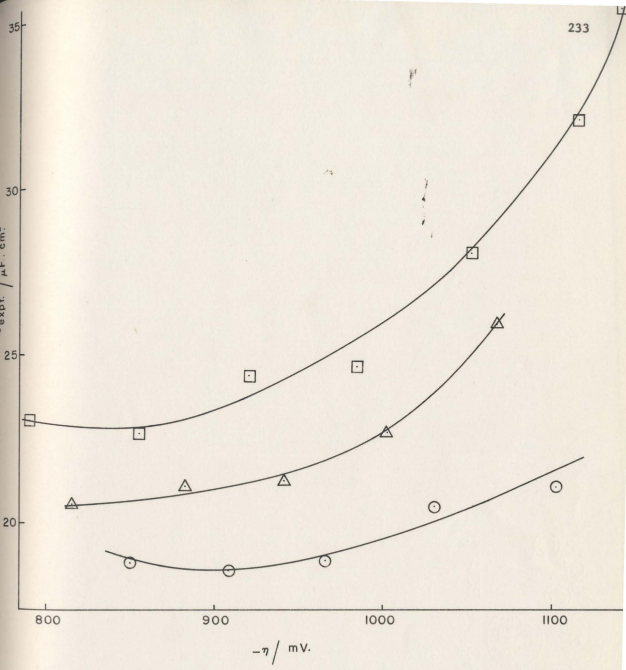

Fig. 44. VARIATION OF ELECTRODE CAPACITY FOR ELECTRODE R4b WITH PERIOD OF POLARISATION AT $-i = 790$ μA. cm^{-2} (CAPACITIES ARE SHOWN AS A FUNCTION OF OVERVOLTAGE); ⊙, AT $-Q = 93$ COULOMBS; △, AT $-Q = 276$ COULOMBS; ⊡, AT $-Q = 820$ COULOMBS.

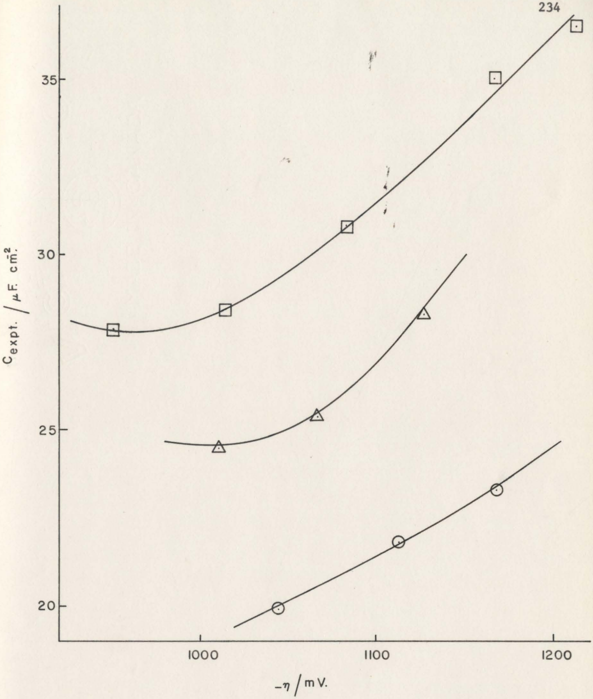

Fig. 45. VARIATION OF ELECTRODE CAPACITY FOR ELECTRODE R5b WITH PERIOD OF POLARISATION AT $-i = 650\ \mu A.\ cm^{-2}$ (CAPACITIES ARE SHOWN AS A FUNCTION OF OVERVOLTAG ⊙, AT $-Q = 145$ COULOMBS; △, $-Q = 420$ COULOMBS; ⊡, AT $-Q = 838$ COULOMBS.

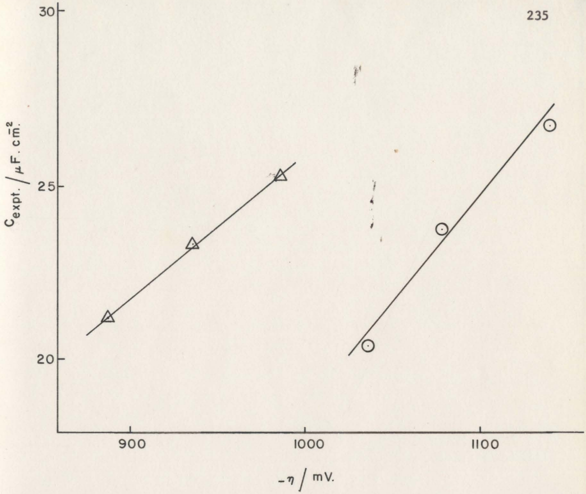

Fig. 46. VARIATION OF ELECTRODE CAPACITY FOR ELECTROD
R5c AT CONSTANT $-i = 775\ \mu A. cm^{-2}$ (CAPACITIES ARE SHOWN
AS A FUNCTION OF OVERVOLTAGE); ⊙, AT $-Q = 92$ COULOMBS
△, AT $-Q = 322$ COULOMBS.

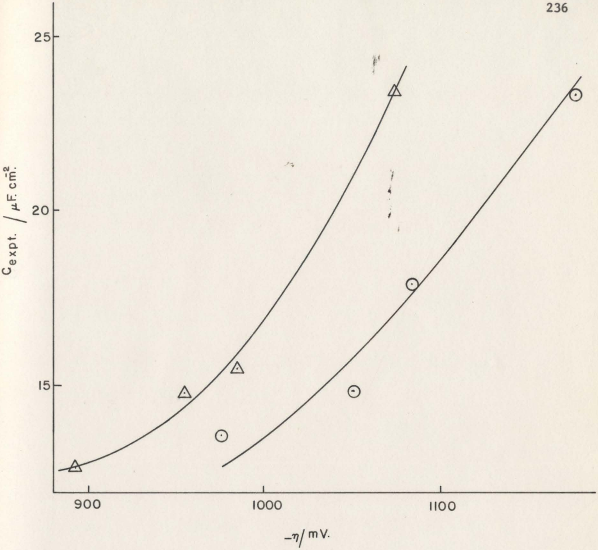

Fig. 47. VARIATION OF ELECTRODE CAPACITY FOR ELECTRODE R5d WITH PERIOD OF POLARISATION $-i = 570\ \mu A.\ cm^{-2}$ (CAPACITIES ARE SHOWN AS A FUNCTION OF OVERVOLTAGE); ⊙, AT $-Q = 95$ COULOMBS; △, AT $-Q = 267$ COULOMBS.

decreased slightly every current density beyond $-Q = 838$ coulombs. This point also corresponds to a steep slope of 460 mV. in Fig. 30, i.e. a steeper fall of $-\eta$ with $\log_{10}(-Q)$.

In yet another case, R5c (Table 29), in which $C_{expt.}$ increased at first and then remained the same or decreased, the change of behaviour at ca. 200 coulombs corresponds to two changes of slope of $-\eta$ versus $\log_{10}(-Q)$, namely from 55 to 278 mV. at 90 coulombs and back to 85 mV. at 250 coulombs (Fig. 31).

In R5d (Table 30) $C_{expt.}$ decreased at most current densities, but increased at constant η, as Fig. 47 shows.

In an early experiment with a rod electrode, R3c quickly transferred through the air after electropolishing, and cathodised in 0.1 M $HClO_4$ first at 385 μA. cm.$^{-2}$ up to $-Q = 522$ coulombs, then at 3.85 mA. cm.$^{-2}$ up to 2293 coulombs and finally at 385 μA. cm.$^{-2}$ again (c.f. Fig. 29). During this last period, at $-Q = 3000$ coulombs, some capacities were measured, as follows:

$C_{expt.} = 20$ μF. cm.$^{-2}$ at $-\eta = 500$ mV.; $C_{expt.} = 21$ μF. cm.$^{-2}$ at $-\eta = 566$ mV.; $C_{expt.} = 29$ μF. cm.$^{-2}$ at $-\eta = 633$ mV. and $C_{expt.} = 34$ μF. cm.$^{-2}$ at $-\eta = 716$ mV.

One other foil electrode (F9) was used for capacity measurements, but the pre-electrolysis had been conducted at low purity lead. The capacities ranged from 6.3 to 11.6 μF. cm.$^{-2}$ at

19 μA. cm.$^{-2}$ to 19.6 mA. cm.$^{-2}$, respectively and are of marginal interest only.

(b) Relationships between Capacity, Overvoltage and Total Cathodic Charge

Figs. 43 to 47 are plots of the essential features of Tables 25 and 27 to 30, i.e. the relationship between $C_{expt.}$ and η at particular values of Q. Data of Table 26 were not plotted because this experiment appears atypical in that the capacity increases were larger at low -i but later on decreased with -Q, as mentioned earlier.

In all cases plotted, the capacity increased monotonically with -Q, in some cases by large amounts, e.g. in Fig. 43 for F10 at $-\eta$ = 800 mV., $C_{expt.}$ increased by 3.3 μF. cm.$^{-2}$ for $-\Delta Q$ (additional cathodic charge) of 171 coulombs and by a further 7 μF. cm.$^{-2}$ for a further $-\Delta Q$ of 255 coulombs. In this one case of a foil electrode, the capacities at $-\eta > 900$ mV. rose to very large values, ca. 100 μF. cm.$^{-2}$, probably indicative of a pseudo-capacity caused by adsorbed hydrogen. In experiment R5b (Fig. 45) with a rod electrode $C_{expt.}$ at $-\eta$ = 1100 mV. increased by 5.5 μF. cm.$^{-2}$ for the passage of an additional 275 coulombs and by a further 4.6 μF. cm.$^{-2}$ for a further 418 coulombs.

From the graphs of $C_{expt.}$ versus η on a given electrode at various times, it was possible to demonstrate that $C_{expt.}$ and -Q are related in a similar manner to the relationship between $-\eta$ and $\log_{10}(-Q)$, namely, that at a given overvoltage, $C_{expt.}$ increased linearly with $\log_{10}(-Q)$ with sections of different slopes (b") both at one overvoltage, e.g. b" = 6.3 and 85 μF. cm.$^{-2}$ (decade)$^{-1}$ for electrode F10 at $-\eta$ = 920 mV., (Fig. 48) and at different overvoltage, e.g. 16.5, 20.6, 40.5 and 85 μF. cm.$^{-2}$ (decade)$^{-1}$ at $-\eta$ = 700, 800, 860 and 920 mV., respectively, also on F10 (Fig. 48).

A number of plots of $C_{expt.}$ versus $\log_{10}(-Q)$ at several potentials in most cases, are given in Figs. 48 to 53, with plots of parts of the $-\eta$ versus $\log_{10}(-Q)$ relations for the same electrode for comparison with the former plots. Since capacity measurements were normally not begun until it had been established that electrode behaviour was satisfactory, i.e. that $-\eta$ was decreasing with $-Q$, comparison over a wider range of Q is not practicable. The entire $-\eta$ versus $\log_{10}(-Q)$ plots are to be found in Figs. 30 and 31.

Several features must be commented upon:

(i) The slopes, b", of $C_{expt.}$ versus $\log_{10}(-Q)$ plots range from 1.9 to 85 μF. cm.$^{-2}$ per decade of $-Q$, with negative values in one or two instances.

(ii) The slopes, b", are either indistinguishable within experimental error as η is changed (Fig. 51), ranging from 11.6 to 13.1 μF. cm.$^{-2}$ (decade)$^{-1}$, or there is a trend to higher slopes as $-\eta$ is increased,

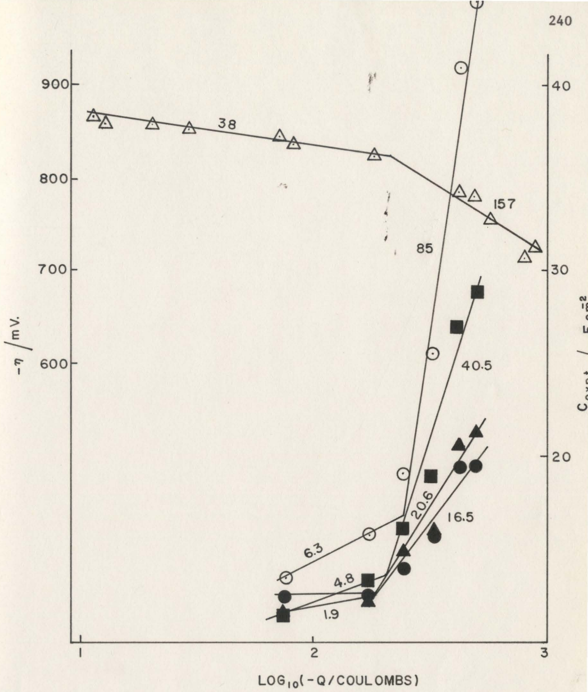

Fig. 48. LINEAR RELATIONSHIPS BETWEEN HYDROGEN OVERVOLTAGE AT CONSTANT $-i$ (= 505 μA.cm^{-2}) AND LOG$_{10}$ (−Q), △, AND BETWEEN ELECTRODE CAPACITIES AT CONSTANT $-\eta$'s (●, 700 mV.; ▲, 800 mV.; ■, 860 mV.; ⊙, 920 mV.) AND LOG$_{10}$(−Q) FOR ELECTRODE F10. NUMBERS ON EACH CURVE ARE RESPECTIVE SLOPES IN mV. AND μF. cm^{-2}.

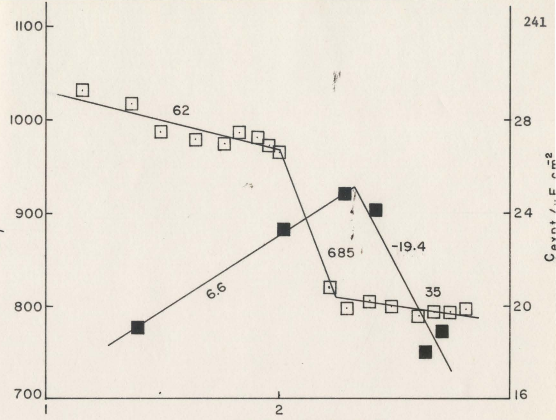

Fig. 49. LINEAR RELATIONSHIPS BETWEEN HYDROGEN OVERVOLTAGE AT CONSTANT $-i$ (= 665 μA. cm^{-2}.) AND LOG_{1} $(-Q)$, ⊡, AND BETWEEN ELECTRODE CAPACITY AT CONSTANT $-\eta$ (=850 mV.) AND $LOG_{10}(-Q)$, ■, FOR ELECTRO R4a." NUMBERS ON EACH CURVE ARE RESPECTIVE SLOPE IN mV. AND μF. cm^{-2}.

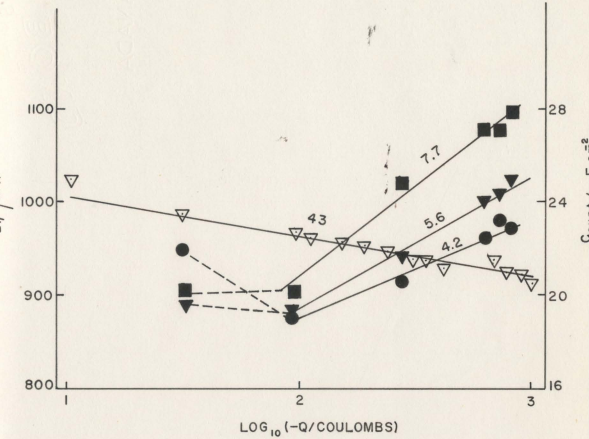

Fig. 50. LINEAR RELATIONSHIPS BETWEEN HYDROGEN OVERVOLTAGE AT CONSTANT $-i$ (= 790 μA. cm^{-2}) AND LOG$_{10}$ (−Q), ▽, AND BETWEEN ELECTRODE CAPACITIES AT CONSTANT $-\eta$'s (●, 850 mV.; ▼, 950 mV.; ■, 1050 mV.) AND LOG$_{10}$ (−Q), FOR ELECTRODE R4b. NUMBERS ON EACH CURVE ARE RESPECTIVE SLOPES IN mV. AND μF. cm

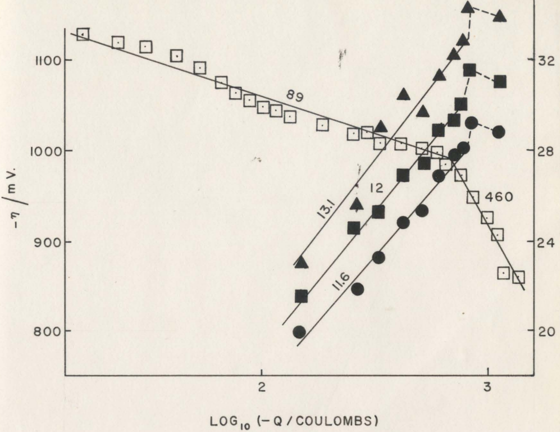

Fig. 51. LINEAR RELATIONSHIPS BETWEEN HYDROGEN OVERVOLTAGE AT CONSTANT $-i$ (= 650 μA. cm^{-2}) AND LOG$_{10}$ (−Q), ⊡, AND BETWEEN ELECTRODE CAPACITIES AT CONSTANT $-\eta$'s (●, 1040 mV.; ■, 1100 mV.; ▲, 1160 mV.) AND LOG$_{10}$ (−Q) FOR ELECTRODE R5b. NUMBERS ON EACH CURVE ARE RESPECTIVE SLOPES IN mV. AND μF. cm^{-2}.

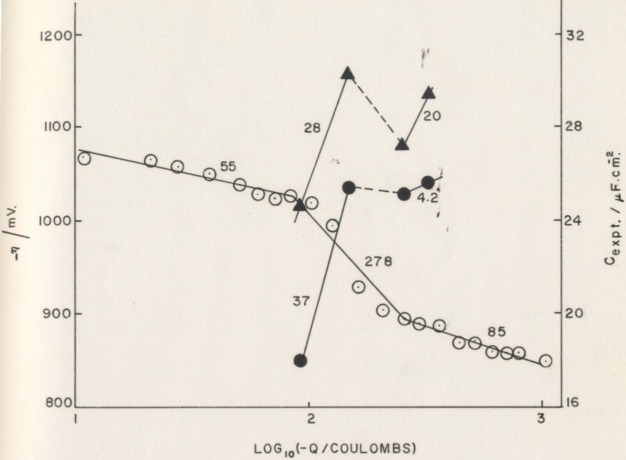

Fig. 52. LINEAR RELATIONSHIPS BETWEEN HYDROGEN OVERVOLTAGE AT CONSTANT $-i$ (= 775 μA. c$\bar{m}^2$) AND LOG$_{10}$ (-Q), ⊙ , AND BETWEEN ELECTRODE CAPACITIES AT CONSTANT $-\eta$'s (●, 1000 mV.; ▲ , 1100 mV.) AND LOG$_{10}$ (-Q), FOR ELECTRODE R5c. NUMBERS ON EACH CURVE ARE RESPECTIVE SLOPES IN mV. AND μF. c$\bar{m}^2$.

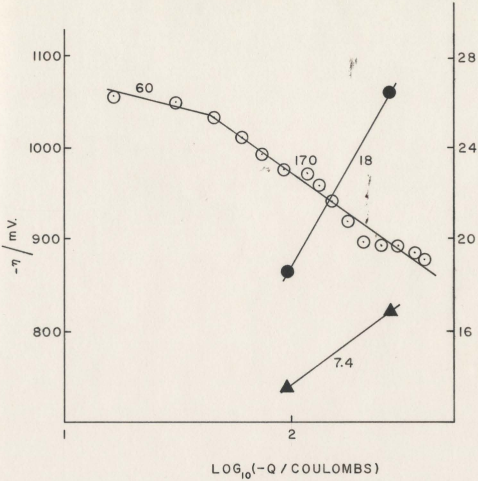

Fig. 53. LINEAR RELATIONSHIP BETWEEN HYDROGEN OVERVOLTAGE AT CONSTANT $-i$ (= 570 μA. cm^{-2}.) AND $LOG_{10}(-Q)$ AND ELECTRODE CAPACITIES AT CONSTANT $-\eta$'s (▲ , 1000 mV; ● , 1100 mV.) AND $LOG_{10}(-Q)$ FOR ELECTRODE R5d. NUMBERS ON EACH CURVE ARE RESPECTIVE SLOPES IN mV. AND μF. cm^{-2}.

e.g. Fig. 48, in which successive b"'s of zero, 1.9, 4.8 and 6.3 μF. cm.$^{-2}$ (decade)$^{-1}$ and 16.5, 20.6, 40.5 and 85 μF. cm.$^{-2}$ (decade)$^{-1}$ are observed at $-\eta$ = 700, 800, 860 and 920 mV., respectively. Fig. 52 illustrates an exception to this, but based on only two points this cannot be taken too seriously.

(iii) The sections of linear <u>increase</u> of $C_{expt.}$ and of <u>decrease</u> of $-\eta$ with $\log_{10}(-Q)$ show a certain parallelism. This can be illustrated by dividing the slope, b', of the $-\eta$ versus $\log_{10}(-Q)$ plot by b", as has been done with the data of Table 31. In the last column, it may be seen that the ratio of $\frac{b'}{b''}$ ranges from 1.9 to 23 mV. μF.$^{-1}$ cm.^{2}, with a concentration around 7.0 mV. μF.$^{-1}$ cm.^{2} (sixteen out of twenty within 7.0 ± 3.2 mV. μF.$^{-1}$ cm.^{2}). Of course, since b" in general increased with $-\eta$, the ratio $\frac{b'}{b''}$ must be expected to decrease with $-\eta$, as is found. Comparison of $\frac{b'}{b''}$ ratios at the same η is not very fruitful because of the general lack of reproducibility, already noted in Ives and Smith's work (26, 27) on the overvoltage-charge relationships.

A perhaps interesting point is that a change of the slope b' almost always was accompanied by changes of the slopes b". This is evident from Fig. 48 but also from Figs. 51 and 52. This seems to establish that, whatever process is causing the change of $-\eta$ with charging of the electrode, the same process is responsible for the change of $C_{expt.}$ This will be discussed later.

TABLE 31. VARIATION OF ELECTRODE CAPACITY (AT CONSTANT η) WITH OVERVOLTAGE (AT CONSTANT i) FOR DIFFERENT Pb ELECTRODES

Experiment number	b' = slope of $-\eta$ (at constant i) versus $\log_{10}(-Q)$		b" = slope of $C_{expt.}$ (at constant η) versus $\log_{10}(-Q)$		Ratio of (b'/b") /mV. μF.$^{-1}$ cm.^{2}
	Constant $-i$ /μA. cm.$^{-2}$	b'/mV.	Constant $-\eta$/mV.	b"/ μF. cm.$^{-2}$	
F10	505	38	800	1.9	20
			860	4.8	7.9
			920	6.3	6.0
		157	700	16.5	9.5
			800	20.6	7.6
			860	40.5	3.9
			920	85	1.9
R4a"	655	62	850	6.6	9.4
R4b	790	43	850	4.2	10.2
			950	5.6	7.7
			1050	7.7	5.6
R5b	650	89	1040	11.6	7.7
			1100	12	7.4
			1160	13.1	6.8

TABLE 31. (Continued)

Experiment number	b' = slope of $-\eta$(at constant i) versus $\log_{10}(-Q)$		b" = slope of $C_{expt.}$ (at constant η) versus $\log_{10}(-Q)$		Ratio of (b'/b") /mV. μF.$^{-1}$cm.^{2}
	Constant $-i$ /μA. cm.$^{-2}$	b'/mV.	Constant $-\eta$/mV.	b"/ μF. cm.$^{-2}$	
R5c	775	278	1000	37	7.5
			1100	28	9.9
		85	1000	4.2	20.2
			1100	20	4.3
R5d	570	170	1000	7.4	23
			1100	18	9.4

In some instances, in Figs. 49 and 51, if b' increased to a very high value (685 and 460 mV. in these two cases) a decrease in $C_{expt.}$ (negative b") was observed, in contrast to the usual increase. This may be due to cathodic disintegration resulting in high concentrations of Pb^{++} and a fall of $C_{expt.}$

Since it is apparent that both η and $C_{expt.}$ are functions of Q they must be functionally related to each other. The observed decrease of $-\eta$ at constant i is equivalent to an increase of $\log_{10}(-i)$ at constant η as $\log_{10}(-Q)$ increases. Plots of $C_{expt.}$ versus $\log_{10}(-i)$, both at the same η value, should therefore be linear. By calculating with the aid of the Tafel equation,

$$-\eta = a - b \log_{10}(-i) \qquad (1.2)$$

the value of $\log_{10}(-i)$ at the overvoltage at which $C_{expt.}$ was measured, such plots were made for several different experiments. These sets of plots, each at a common value of η are shown in Figs. 54, 55 and 56. It should be stressed that the plots are of the co-variation of $C_{expt.}$ and of $-\eta$ with $-Q$.

The coincidence of the straight line relationships, at the same value of η but in different experiments, is moderately good.

The most extreme difference is found in Fig. 54 in the case of electrode F10, a foil electrode, the capacity of which increased more rapidly than did $\log_{10}(-i)$ as $-Q$ increased, compared with rod electrodes

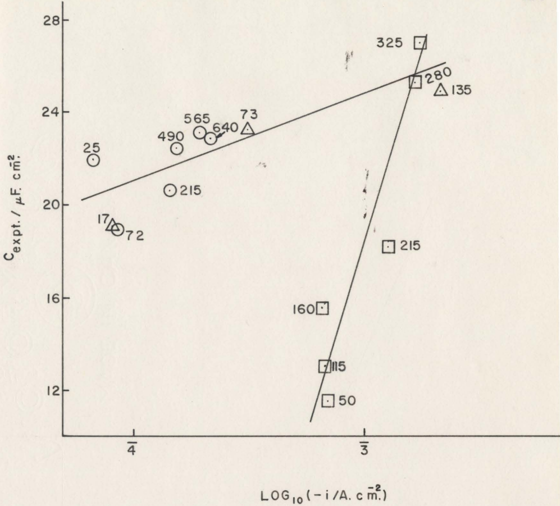

Fig. 54. RELATIONSHIP BETWEEN THE GROWTH OF LOG$_{10}$(-i) AND $C_{expt.}$ WITH -Q (VALUES INDICATED BY NUMERALS ARE -Q IN COULOMBS cm^{-2}) AT $-\eta$ = 850 m
Expt. F10, ⊡ ; Expt. R4a", △ ; Expt. R4b, ⊙.

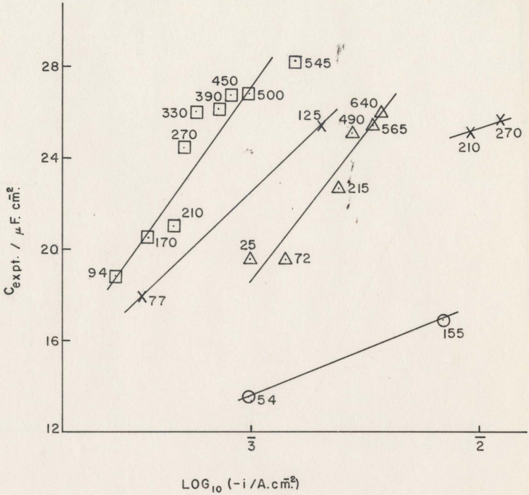

Fig. 55. RELATIONSHIP BETWEEN THE GROWTH OF $LOG_{10}(-i)$ AND $C_{expt.}$ WITH −Q (VALUES INDICATED BY NUMERALS ARE −Q IN COULOMBS cm^{-2}) AT $-\eta$ = 1000 mV. Expt. R4b, △ ; Expt. R5b, ⊡ ; Expt. R5c, X ; Expt. R5d, ⊙.

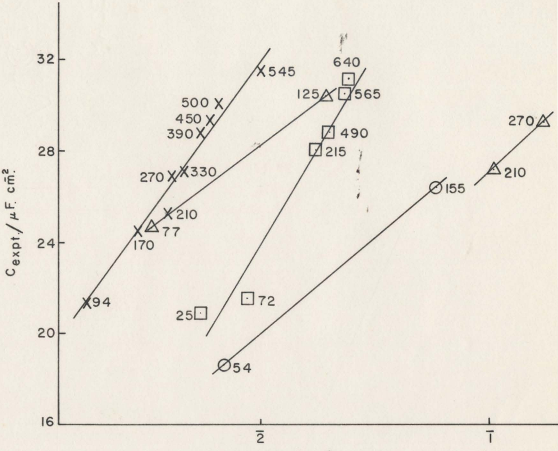

Fig. 56. RELATIONSHIP BETWEEN THE GROWTH OF LOG$_{10}$(-i) AND C$_{expt.}$ WITH $-$Q (VALUES INDICATED BY NUMERALS ARE $-$Q IN COULOMBS cm^{-2}) AT $-\eta$ = 1100 mV. Expt. R4b, ⊡ ; Expt. R5b, X ; Expt. R5c, △ ; Expt. R5d, ⊙.

R4a" and R4b. The best agreement is perhaps that of R4b, R5b and R5c illustrated in Fig. 55. The significance of these results will form a major topic of the Discussion chapter to follow.

There is a suggestion that Tafel slopes decrease as $C_{expt.}$ increases and vice versa. This is illustrated in Table 32 for one particular electrode, where $C_{expt.}$ first increased with -Q and then decreased. Other examples of this type of behaviour were found but it is rather a tentative relationship.

In one experiment, R5b, the Tafel slope decreased from 120 to 108 mV. as $C_{expt.}$ and -Q increased, but later increased to 120 mV. where it remained, while $C_{expt.}$ continued to increase with -Q. Hence, these quantities, b and $C_{expt.}$, are not directly linked.

(c) Calculations of Hydrogen Coverage

The increase in $C_{expt.}$ with -Q is attributed to growth of an adsorption pseudo-capacity component, C_{ps}, arising from a growing surface coverage, θ_H, of the electrode. It was assumed that the early $C_{expt.}$ values at all η's could be considered essentially as double-layer capacities ($C_{ps} = 0$). This is consistent with the variation of double-layer capacity with potential at an initial $\theta_H \simeq 0$. By observing the increase of $C_{expt.}$ at a given potential, from an initial low value of -Q to the value at various higher values of -Q (increase of cathodic charge $-\Delta Q$) and deducting the

TABLE 32. DEPENDENCE OF ELECTRODE CAPACITY AT CONSTANT $-\eta$ (= 850 mV.) ON TAFEL SLOPE AT VARIOUS $-Q$ VALUES FOR AN ELECTRODE R4a" POLARISED AT CONSTANT $-i$ (= 655 μA. cm.$^{-2}$)

Total cathodic charge passed $-Q$/coulombs	$C_{expt.}$/μF. cm.$^{-2}$ at $-\eta$ = 850 mV.	b/mV.
25	19.1	127
105	23.2	107
194	24.9	94
262	24	98
420	18	108
495	18.9	106

former $C_{expt.}$ from the latter, the pseudo-capacities, C_{ps}, have been estimated. This is based on the assumption that $C_{ps} = 0$ initially, i.e. before the electrode has been "charged" by the passage of -Q coulombs.

C_{ps} has been estimated in this way as a function of overvoltage at high values of -Q (towards the end of capacity measurements in a given experiment) and the results presented in Tables 33 to 36. These results have been used to estimate hydrogen coverages, or rather, the increase in hydrogen coverage, $\Delta\theta_H$, from the lowest value of $-\eta$ at which measurements were made. An intermediate step is the calculation of the charge equivalent to the adsorbed hydrogen, or rather, its increase, Δq_H, relative to the value of q_H at the lowest $-\eta$ of the measurements. The equations defining Δq_H and $\Delta\theta_H$ are:

$$\Delta q_H = - \int_{(-\eta)_{min.}}^{-\eta} C_{ps} d\eta \tag{3.1}$$

$$\Delta\theta_H = \int_{\theta_{min.}}^{\theta} d\theta = \frac{N}{nF} \int_{(-\eta)_{min.}}^{-\eta} C_{ps} d\eta$$

$$= \frac{1}{k'} \int_{(-\eta)_{min.}}^{-\eta} C_{ps} d\eta \tag{3.2}$$

{see equation (2.43) in Section 2B (1V)} where N is Avogadro's number, n is the number of adsorption sites $cm.^{-2}$, F is the Faraday, and

TABLE 33. VARIATION OF HYDROGEN COVERAGE WITH OVERVOLTAGE FOR AN ELECTRODE F10 IN 1 M $HClO_4$ AFTER THE PASSAGE OF ADDITIONAL CATHODIC CHARGE $-\Delta Q$ = 416 COULOMBS (AT A CATHODIC CURRENT DENSITY 505 μA. cm.$^{-2}$). TOTAL CATHODIC CHARGE $-Q$ = 491 COULOMBS

$-\eta$/mV.	C_{ps}/μF. cm.$^{-2}$	Δq_H/μcoulombs	$\Delta\theta_H \times 10^2$
603	8.3		
667	6.3	0.47	0.4
724	7.7	0.87	0.7
781	8.3	1.32	1.0
845	14.2	2.04	1.6
916	30.1	3.62	2.8
956	53.7	5.29	4.1
980	87	6.98	5.3

TABLE 34. VARIATION OF HYDROGEN COVERAGE WITH OVERVOLTAGE FOR AN ELECTRODE R4b IN 1 M $HClO_4$ AFTER THE PASSAGE OF ADDITIONAL CATHODIC CHARGE $-\Delta Q$ = 727 COULOMBS (AT A CATHODIC CURRENT DENSITY 790 μA. cm.$^{-2}$). TOTAL CATHODIC CHARGE $-Q$ = 820 COULOMBS

$-\eta$/mV.	C_{ps} /μF. cm.$^{-2}$	Δq_H/μcoulombs	$\Delta\theta_H \times 10^2$
789	3		
856	3.9	0.23	0.2
921	5.7	0.54	0.4
985	5.3	0.90	0.7
1053	7.6	1.34	1.0
1116	10.2	1.90	1.5
1144	12.8	2.22	1.7

TABLE 35. VARIATION OF HYDROGEN COVERAGE WITH OVERVOLTAGE FOR AN ELECTRODE R5b IN 1 M $HClO_4$ AFTER THE PASSAGE OF ADDITIONAL CATHODIC CHARGE $-\Delta Q$ = 693 COULOMBS (AT A CATHODIC CURRENT DENSITY 650 µA. cm.$^{-2}$). TOTAL CATHODIC CHARGE $-Q$ = 838 COULOMBS

$-\eta$/mV.	C_{ps}/µF. cm.$^{-2}$	Δq_H/µcoulombs	$\Delta\theta_H \times 10^2$
951	10.2		
1014	9.2	0.61	0.5
1083	9.8	1.27	1.0
1168	11.7	2.18	1.7
1212	11.5	2.7	2.1

TABLE 36. VARIATION OF HYDROGEN COVERAGE WITH OVERVOLTAGE FOR AN ELECTRODE R5d IN 1 M $HClO_4$ AFTER THE PASSAGE OF ADDITIONAL CATHODIC CHARGE $-\Delta Q$ = 172 COULOMBS (AT A CATHODIC CURRENT DENSITY 570 μA. cm.$^{-2}$). TOTAL CATHODIC CHARGE $-Q$ = 267 COULOMBS

$-\eta$/mV.	C_{ps}/μF. cm.$^{-2}$	Δq_H/μcoulombs	$\Delta\theta_H \times 10^2$
893	1.6		
955	2.7	0.13	0.1
985	2.5	0.21	0.2
1073	6.3	0.6	0.5

$k' = \frac{nF}{N} = 1.31 \times 10^{-4}$ coulombs cm.$^{-2}$, on the assumption of a (100) face-centred-cubic plane* of lead, with one H atom per Pb atom.

Hydrogen coverages up to 5% are indicated by these calculations. This coverage is calculated for a 0.25 mm. thick Pb foil (F10, Table 33) at $-\eta$ of 980 mV. after cathodic charging with 491 coulombs. Problems arise in this calculation and in others because $C_{expt.}$ increased at all overvoltages, suggesting that a pseudo-capacity arises, after sufficiently long cathodic treatment, at all values of $-\eta$ examined.

Because measurements were not extended to such low overvoltages, in the case of the other electrodes (results of Tables 34 to 36), the calculations of θ_H (or, strictly $\Delta\theta_H$) are not comparable with those of F10, the integration being over a narrower range of η in the case of the lead rods. The maximum value of $\Delta\theta_H$ on a lead rod was found to be about 2%. Although this estimate may be low, because of the smaller range of η, it is entirely probable that this is a reasonable estimate

---

* Although polycrystalline Pb samples were used, for the calculation the (100) plane was selected for simplicity. Calculated values of k' for (100), (110) and (111) lead planes are 1.31×10^{-4}, 9.25×10^{-5} and 1.51×10^{-4} coulombs cm.$^{-2}$, respectively. Using the cross sectional area of the lead atom, a value $k' = 1.66 \times 10^{-4}$ coulombs cm.$^{-2}$ results. Pearson's (208) values of Pb-Pb interatomic distance of 3.5003 Å and f.c.c. lattice constant of 4.9502 Å were used in these calculations

in view of the much lower C_{ps} values at different potentials on the lead rods relative to those of the lead foil (compare results of Tables 34 to 36 with those of Table 33).

(1V) Summarising Remarks on Capacity Measurements

1. Capacities measured on lead rods and foils under satisfactory experimental conditions were initially consistent with expectations for double-layer capacities alone. After long periods of cathodisation, capacities increased at most overvoltages studied, the increase in capacity being parallel with the decrease of overvoltage, i.e. both changed proportionally with $\log_{10}(-Q)$. These capacities have been analysed in terms of an increasing pseudo-capacity component caused by an increasing coverage of the electrode with adsorbed hydrogen. Coverages have been computed tentatively on such a basis and range up to 2% for lead rods and up to 5% for a lead foil.

2. The parallel variation of $C_{expt.}$ and η with $\log_{10}(-Q)$ has been tested by comparing the slopes, b" and b', of the two plots. These show strikingly that when b' is large so is b" and when b' changes value so does b".

3. Plots of $C_{expt.}$ and of $\log_{10}(-i)$, computed for a single value of η, each point being for a particular value of Q, are rectilinear and in some cases parallel and nearly coincident for different electrodes.

4. Decrease in Tafel slope and increase in $C_{expt.}$ (at constant η) as -Q increased was observed in all cases, however, increase in Tafel slope and decrease in $C_{expt.}$ was observed only in a few cases.

5. In $HClO_4$ not subjected to pre-electrolysis, $C_{expt.}$ was low at low -i, probably because the presence of impurities, but at current density > 5 mA. cm.$^{-2}$ quite large capacities have been observed.

6. In $HClO_4$, pre-electrolysed at too high a current density, so that Pb^{++} ions were introduced into the solution, capacities were initially large, especially at current density $\gtrsim$ 5 mA. cm.$^{-2}$. However, in the course of cathodisation the capacities fell to more nearly normal (values correspond to the initial measurements in satisfactory experiments) values at high current density and rose to normal values at low current density.

C. Electrolytic Hydrogen and Tritium Radiotracer Permeation Rates and Isotope Separation Factors on Cathode and Diffusion Sides of Lead Membrane

In this section, the experimental techniques and results obtained in electrolytic hydrogen and tritium radiotracer permeation rates and isotope separation factor measurements on the cathode and diffusion sides of Pb membranes cathodised in aqueous $HClO_4$ containing tritium are discussed.

This work was carried out:

(i) To check on Muju and Smith's result (55) that the over-all separation factor (cathodic discharge, diffusion through lead membrane and anodisation on the opposite face) $S_{(H,T)_{DA}}$ is less than unity, i.e. very small in comparison with the $S_{H,T} \simeq 7$ (cathodic gas evolution) of other workers (25, 56).

(ii) To extend the observations to lower current densities if possible.

(1) Materials

Only materials which are not mentioned in Section 3A (1) will be given below.

Tritium: Tritiated water from Tracerlab, and ICN Chemical and Radioisotope Division (100 mCi. ml.$^{-1}$ to 1 Ci. ml.$^{-1}$)* were diluted

---

* The curie (Ci) is a unit of radioactivity (210) defined as the quantity of any radioactive nuclide in which the number of disintegrations per second is 3.7×10^{10}. The millicurie (mCi) and the microcurie (μCi) are practical units in common use.

by volume with 1 M $HClO_4$ to about 2 mCi. ml.$^{-1}$. A tritium standard of 1.89×10^6 D.P.M. ml.$^{-1}$ (disintegrations per minute per ml.) from Tracerlab (counted on 20th December 1966) was used as a reference standard to determine the efficiency of the cocktail (the composition of this cocktail will be mentioned later on).

Potassium hydroxide: BDH reagent grade (maximum impurities - insoluble matter 0.01%; CO_3^{--}, 1%; Cl^-, 0.002%; NO_3^-, 0.001%; PO_4^{---}, 0.0005%; silicate, 0.005%; SO_4^{--}, 0.003%; Al, 0.002%; NH_4^+, 0.0005%; As, 0.0001%; Ca, 0.0025%; Fe, 0.0005%; Pb, 0.0005%; Ni, 0.001%; Zn, 0.0015%;)was used without purification.

Naphthalene: Scintillation grade (Packard Instrument Co. Ltd) naphthalene was used.

2,5 - Diphenyloxazole: Scintillation grade (Packard Instrument Co. Ltd) 2,5 - diphenyloxazole was used.

1,4-Bis-{2-(5-Phenyloxazolyl)}benzene: Scintillation grade (Packard Instrument Co. Ltd) 1,4-bis-{2-(5-Phenyloxazolyl)}benzene was used.

1,4-Dioxane: A.C.S. grade 1,4-dioxane (carbonyl compounds, 0.04%; heavy metals {Pb}, 0.000019%; Fe, 0.000013%; peroxide {as H_2O_2}, 0.003%; water, 0.01%) from Fisher Scientific Co. was used without purification.

Xylene: A.C.S. grade xylene (water, 0.02%; sulphur compounds, 0.003%) from Fisher Scientific Co. was used without purification.

Ethanol: 94% by volume ethanol (remainder distilled water, non-volatile matter, 0.0025%; benzene, 0.0007%) from Consolidated Alcohols Ltd was used without purification.

Polyethylene vials: Polyethylene vials (Packard Instrument Co. Ltd) were used as containers for the scintillation cocktail in tritium analysis.

Gases: Gases were purified as mentioned in Section 3A (1) except that the B.T.S. catalyst was maintained at 140°C in an electric furnace instead of in vapours of boiling n-amyl alcohol.

(ii) Solution and Electrode Preparation

Purification of solutions and electrode cleaning were somewhat restricted during these experiments, as mentioned below, unlike in the overvoltage and capacity measurements {Section 3A (ii) and 3A (iii)} due to the precautions which must be taken into account in handling tritium. However, the experimental conditions were relatively superior to the earlier work of Muju and Smith (55).

Tritium of higher activity (100 mCi. ml.$^{-1}$ to 1 Ci. ml.$^{-1}$) diluted to 1.3 to 2.6 mCi. ml.$^{-1}$ by volume with pre-electrolysed (at $-i \leqslant 2$mA. cm.$^{-2}$ for 15 to 20 days) 1 M $HClO_4$ was used as solution on the cathodic side. Reagent grade 0.2 M KOH, initially free of tritium, was used without further purification as solution on the diffusion side. Both solutions were thoroughly deoxygenated by bubbling purified N_2 prior to the experiment.

Chemically polished Goodfellow Pb foils {Section 3A (iii)} were washed with 3 x distilled water and electrochemically polished in 50% $HClO_4$ at 500 mA. for 5 minutes in a 500 ml. beaker. The electrochemically polished foil was washed with 3 x distilled water and mounted in the cell (Fig. 57) as quickly as possible. Then, the foil was kept under a nitrogen atmosphere before the introduction of the solutions into the respective compartments.

Fig. 57.

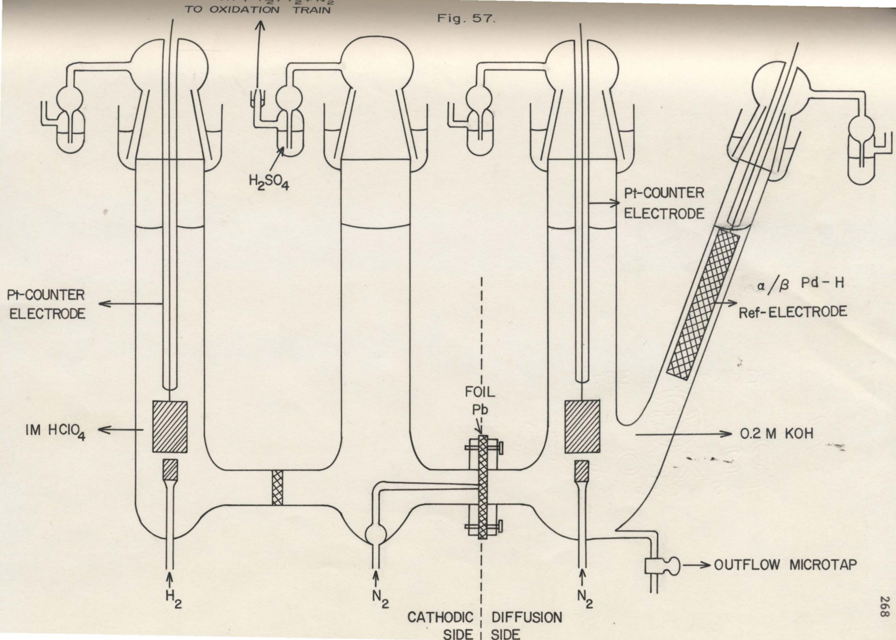
TO OXIDATION TRAIN
H_2SO_4
Pt-COUNTER ELECTRODE
Pt-COUNTER ELECTRODE
α/β Pd-H
Ref-ELECTRODE
IM $HClO_4$
FOIL
Pb
0.2 M KOH
OUTFLOW MICROTAP
H_2
N_2
N_2
CATHODIC SIDE
DIFFUSION SIDE

(111) Cell

The Pyrex cell used in the present work is shown diagrammatically in Fig. 57. It consisted of two units terminating in flat flanges. Each flange carried a Parafilm gasket (1 to 2 thin layers) on the side facing the lead foil. Parafilm gaskets with aluminium clamps secured produced seals which could hold 10^{-5} torr. after heating with hot air (172). The unit on the left hand side (cathodic side) of the lead foil consisted of two compartments (cathode and anode) each fitted with presaturators and all glass-supply lines {Section 3A (1) and 3C (1)}. A large lightly platinised (204) Pt (100 cm.^{2}) counter electrode was supplied with H_2 from an Elhygen generator via the purification train of Fig. 5b in Section 3A (1). The Pb foil, supplied with pre-purified N_2 via the purification train of Fig. 5b in Section 3A (1) but with an ethanol-CO_2 trap, was separated by a frit from the counter electrode. Thus, the flow of hydrogen from the anode compartment to the cathode compartment was restricted. The hydrogen and tritium (H_2, HT and T_2) liberated at the cathodic surface of the Pb foil was swept by the purified N_2 into the oxidation train (which will be explained shortly) as shown in Fig. 57. The unit on the right hand side (diffusion side) of the Pb foil consisted of a similar counter electrode and an α/β Pd-H reference hydrogen electrode (3 mm. diameter x 4 cm. long) fitted with a presaturator and N_2 supply line {Section 3A (1) and 3C (1)}. A solution-wetted outflow microtap

(Springhams, 1 mm. bore) was used to permit the solution from the diffusion side to be run out at the end of each experiment for tritium analysis. Leakage-in of air through the tap was retarded by maintaining a positive pressure of N_2 in the cell, as far as possible.

The oxidation train and the collection system for the cathodically liberated hydrogen and tritium mixture are represented diagrammatically in Fig. 58. It consisted of the following in series: a concentrated sulphuric acid trap, a solid carbon dioxide and ethanol trap, a quartz glass tube containing CuO, enclosed in an electric furnace and maintained at 700 - 800°C, and then finally the tritiated water collection system. The vial collecting the condensed tritiated water was placed within two Pyrex glass tubes, the outermost tube being immersed in liquid nitrogen. The central tube, on the cap of the collection system, ended about half cm. above the bottom of the collecting vial. All joints in the oxidation train were greased (Apiezon T-high temperature grease to ensure a vacuum-tight seal). The oxidation train was attached to the cell by means of flexible glass spiral (not shown in Figs. 57 and 58) and a Quickfit cup-cone and socket joint only when the cathodically generated hydrogen and tritium mixture was ready for collection.

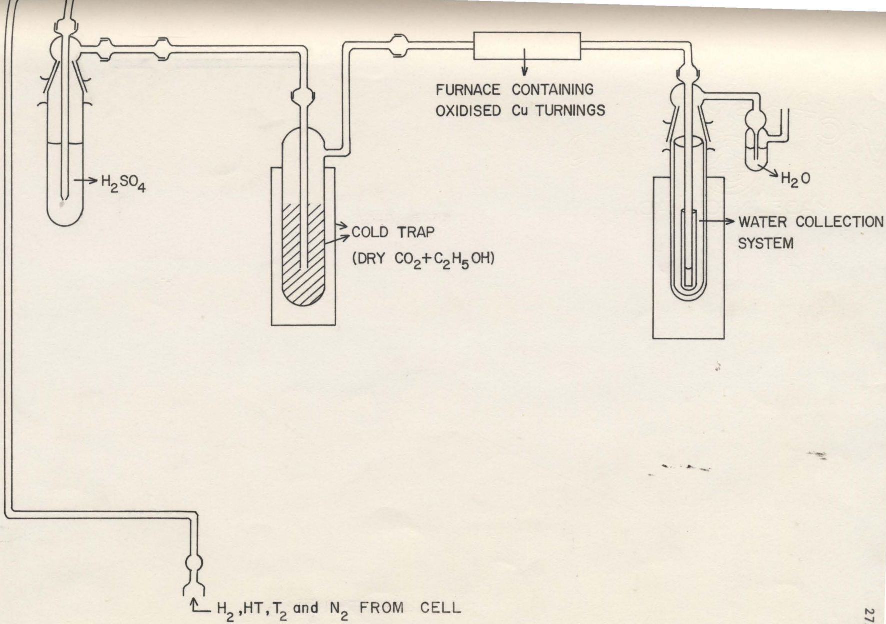
FURNACE CONTAINING
OXIDISED Cu TURNINGS
H_2SO_4
COLD TRAP
(DRY $CO_2+C_2H_5OH$)
H_2O
WATER COLLECTION
SYSTEM
H_2, HT, T_2 and N_2 FROM CELL

(1V) Instrumentation and Procedure

The instrumentation and procedure other than those mentioned in Section 3A (V) and 3B (1) are described below.

A block diagram of the experimental setup is shown in Fig. 59. The cathodic side of the Pb foil was polarised galvanostatically with a Heath EUW 15 Power Supply used at 300 V., a Simpson ammeter and make-before-break switchable resistors (enabling cathodic currents of 30 μA. to 55 mA.). The diffusion side of the foil was potentiostated at +140 mV. versus α/β Pd-H reference electrode with a Memorial University of Newfoundland (M.U.N.)-built circuit of Fig. 60. The electronic potentiostat was built using Analog Devices operational amplifiers 183K(A) and 146K(B). These amplifiers were powered from a ± 15 V. power supply (Analog Devices Model 904). Features are high common mode rejection ratio, low drift and noise, and a 10 mA. output capability at ± 10 V. The operational amplifier B operates as a high impedance (10^{11} Ω.) in the feedback circuit from the reference electrode (R) to control the operational amplifier A. The potentiostat consisted of a set potential (adjustable from 0 to 1 V. with a linear 10- turn potentiometer and 2.7 V. from two mercury batteries in series) which can be applied to the working electrode (W) through an operational amplifier A. Whenever the difference between the set potential and the potential

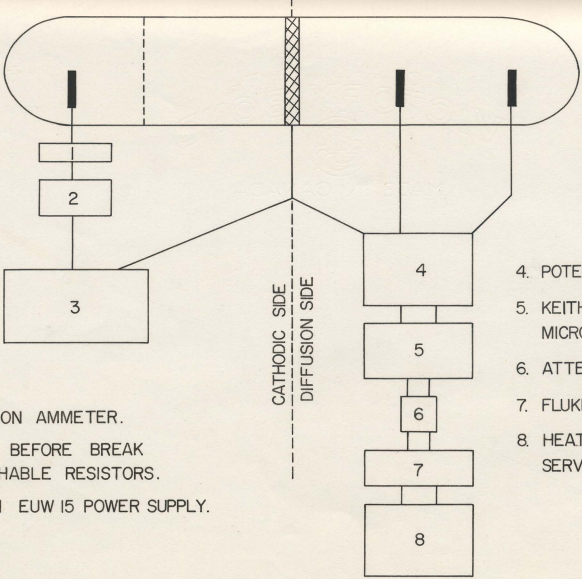

1. SIMPSON AMMETER.
2. MAKE BEFORE BREAK SWITCHABLE RESISTORS.
3. HEATH EUW 15 POWER SUPPLY.
4. POTENTIOSTAT. (M.U.N.)
5. KEITHLEY 155 NULL DETECTOR MICROVOLTMETER.
6. ATTENUATOR.
7. FLUKE A88 AMPLIFIER.
8. HEATH EUW 20A SERVO RECORDER.

Fig. 59.

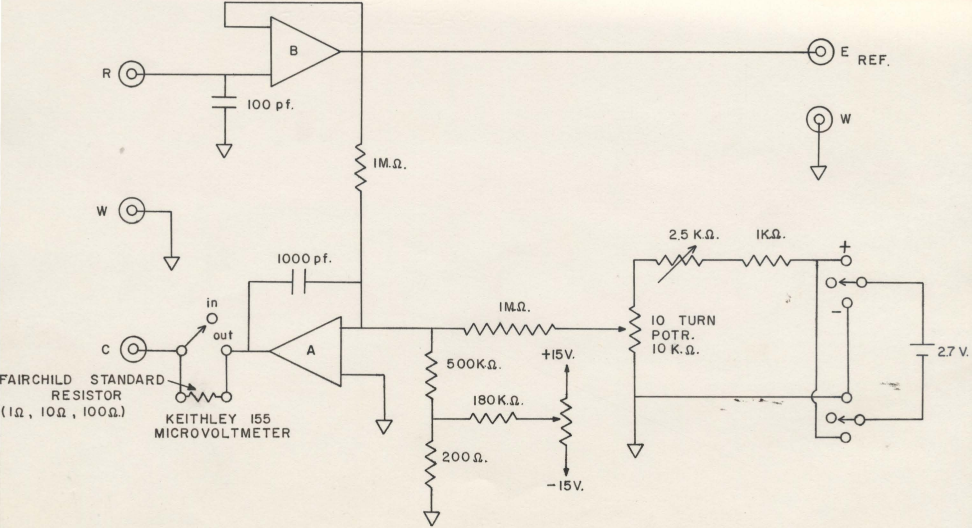

Fig. 60. THE ELECTRONIC POTENTIOSTAT. W = LEAD ANODE INPUT, C = COUNTER ELECTRODE INPUT, R = REFERENCE ELECTRODE INPUT, A AND B···· OPERATIONAL AMPLIFIERS 183K. AND 146K.

difference R-W ($E_{ref.}$ in Fig. 60) differs from zero*, the output is applied to the counter electrode (C), causing a change in current flow between C and W. This changes the working electrode potential back to the set potential, thus maintaining the potential of W constant (i.e. at a set value). **Floating** measurements of the current flow between W and C were made by measuring the potential drop across a Fairchild standard resistor (1 Ω., 10 Ω. or 100 Ω.) on a Keithley 155 Null detector Microvoltmeter, the output of which was attenuated and recorded by a Heath EUW 20A Servo Recorder, which was isolated from the ammeter by a Fluke A88 amplifier.

The Pd rod (3 mm. diameter x 4 cm. long) was anodised in concentrated HCl at 4.0 V. for two minutes, washed with concentrated HNO_3, followed with 3 x distilled water and finally steamed in steam from 3 x distilled water. It was then palladised (211) in 2% aqueous $PdCl_2$ in 1 M HCl at 4.0 V. for 5 minutes. The palladised electrode was washed with 3 x distilled water, steamed in steam from 3 x distilled water and potentiostatically hydrogen-charged during 16 to 20 hours at +50 mV. versus hydrogen reference, both in hydrogen-saturated 0.2 M KOH. Charging with H_2 was carried out in the experimental cell (Fig. 57) in the absence of the Pb foil. Later,

---

* Facilities are available to measure $E_{ref.}$ (within $\pm$ 0.7 mV.).

the electrode was stored under a nitrogen atmosphere (i.e. during the electrode assembly), prior to the experiment. The observed steady-state plateau potential was +50 to +60 mV. versus a reference hydrogen electrode in the same solution. The stability of the reference α/β Pd-H electrode potential was established experimentally to be ± 1 mV. over a period of 40 to 50 hours with continuous N_2 stirring.

To prevent unwanted anodic processes (such as anodic dissolution or passivation of Pb) without affecting the hydrogen oxidation on the diffusion side of the Pd foil, it was attempted unsuccessfully to deposit a thin coating of Pb on this surface. Plating was carried out in a 15 ml. bath (212) consisting of diammino-dinitro-palladium (8 g. liter^{-1}), ammonium nitrate (100 g. liter^{-1}), sodium nitrite (10 g. liter^{-1}) and ammonia (to maintain pH = 9) at 50 to 800 μA. cm.$^{-2}$ for about 3 hours. A clean Pd rod was used as an anode. The solution was stirred with purified nitrogen while plating. High currents gave an even and smooth (in appearance) coating. Upon applying a positive potential (say +140 mV. versus α/β Pd-H reference), however, the Pd-coated surface was found to have cracked. Rapid oxidation of H atoms co-deposited during plating might have cracked the Pd-coated surface. Therefore, it was decided not to plate a thin layer of Pd on the diffusion side of the foil.

The stock solution (about 2 mCi. ml.$^{-1}$ in 1 M $HClO_4$) used in the cathodisation side were prepared by diluting 100 mCi. ml.$^{-1}$ or 1 Ci. ml.$^{-1}$ with 1 M $HClO_4$ as mentioned earlier {Section 3C (1)}. These diluted stock solutions were analysed for tritium activity and listed in Table 37. Since these solutions have a relatively high T activity for analytical purposes, three 100 μl. aliquots of this solution were further diluted to 100 ml. in three 100 ml. standard (A grade) flasks. 15 to 20 samples of 10 μl. each from the three flasks were pipetted out into a polyethylene vial containing 15 ml. scintillation cocktail at -15°C. The scintillation cocktail was composed of (213) naphthalene (80 g. liter^{-1}), 2,5-diphenyloxazole (5 g. liter^{-1}), and 1,4-bis-{2-(5-Phenyloxazolyl)} benzene (50 mg. liter^{-1}) in Xylene (38.5%), 1,4-dioxane (38.5%) and ethanol (23.1%). The tritium activity of these samples were counted in Nuclear Chicago Model 6860 Mark I liquid scintillation computer on channel A, refrigerated to -1 to 1°C. Channel A of the instrument was set to record for a maximum of 40 minutes or 400 k. counts, respectively, by personnel of the School of Medicine, M.U.N., for T analysis. Countings were repeated 3 to 4 times until the last two countings were almost identical. Five blanks containing 15 ml. of scintillation cocktail and 10 μl. of 0.0001 M $HClO_4$ were also counted. The observed backgrounds of 4 to 5 counts per minute (C.P.M.) were negligibly small but were subtracted from the observed activity of T (C.P.M.) in the samples for analysis. The efficiencies of

TABLE 37. ANALYSIS OF TRITIUM-CONTAINING 1 M $HClO_4$ USED ON THE CATHODIC SIDE (ORIGINAL SOLUTION BEFORE DILUTION FOR ANALYSIS)

Experiment number*	Tritium activity in original solution /C.P.M. ml.$^{-1}$	Efficiency of cocktail in %	Tritium activity in original solution /D.P.M. ml.$^{-1}$	Concentration of tritium in original solution /mCi. ml.$^{-1}$
T2,T4	1.29×10^9	22.3	5.77×10^9	2.60
T3,T5,T6,T7	8.16×10^8	22.5	3.63×10^9	1.64
T1,T8,T9	6.28×10^8	21.3	2.96×10^9	1.33

* Electrodes are identified by T and by numerals (indicating the experiments carried out with fresh solutions and new electrodes).

cocktails were calculated by simultaneously counting five 10 μl. tritiated water standards of known activity (1.89×10^6 D.P.M. ml.$^{-1}$) in 15 ml. of cocktail (the background count rate being deducted) and using the equation

$$\text{Efficiency} = \frac{\text{C.P.M.}}{\text{D.P.M.}} \qquad (3.3)$$

The efficiencies* (20.9 ro 22.8%) are expressed in %. Then, knowing the efficiency and C.P.M., T activity in D.P.M. for 1 ml. of stock solution used in the cathodisation side was calculated using equation (3.3). Using 1 mCi = 2.22×10^9 D.P.M., the concentration of T per ml. of stock solution in the cathodisation side was calculated. Mean C.P.M.'s were used throughout the calculation.

About 4 hours before assembling the electrode in the cell, all joints in the oxidation train only (Fig. 58) were greased. Then, oxygen gas was passed into the tube containing Cu enclosed in the electric furnace and maintained at 700 to 800°C until all the Cu was converted into CuO. The oxidation train was flushed with nitrogen for an hour to remove all residual oxygen as well as other gases.

---

* A few standard samples, e.g. 10 μl. of tritium standard (1.89×10^6 D.P.M. ml.$^{-1}$), were analysed with an equal volume (10 μl. in this case) of 1 M $HClO_4$ or 0.2 M KOH or 3 x distilled water present in addition to the standard in 15 ml. of cocktail. The difference in cocktail efficiency with or without acid, alkali or water was negligible, i.e. about 0.1%.

After assembling the electropolished Pb foil in the cell (Fig. 57) as mentioned before, the diffusion side was filled with nitrogen-saturated 0.2 M KOH. Then the α/β Pd-H reference and Pt counter electrodes were introduced into their respective positions. The diffusion side of the Pb foil was potentiostated, initially at 0 V. versus α/β Pd-H reference and then slowly changed to +140 mV.* The corresponding currents between the working Pb and counter electrodes were recorded.

After a constant background current was established in the potentiostatic circuit on the diffusion side, a counter anode was placed in the cathodisation side of the cell. Then, 1M $HClO_4$ with a T concentration of about 2 $mCi. ml.^{-1}$ was introduced and the cathodic side of the Pb foil became galvanostatically polarised at $-i \simeq 30\ \mu A.\ cm.^{-2}$ as soon as the solution contacted the electrode. If the recorded current between working Pb and counter electrodes on the diffusion side of the circuit remained the same or became steady, the oxidation train which was previously assembled and set ready for tritiated water collection was connected to the cell (Fig. 57). The temperature of the furnace containing CuO was checked

---

* Preliminary work by Cadersky et al. (214) established that H atom oxidation occurs on lead with high efficiency at potentials $\geqslant$ 190 mV. versus a hydrogen reference in 0.2 M KOH.

and maintained constant at 700 to 800°C. The vial collecting the tritiated water was placed in the collection system, the system then being ready to collect the gas phase H_2,HT and T_2 generated on the cathodic surface of the Pb foil. Immediately after this, the current on the cathodisation side was increased to the desired value ($-i = 1$ to 46 mA. cm.$^{-2}$) and electrolysis was continued at this constant current for another 9 to 24 hours. The permeation current (i.e. oxidation current in excess of the background current) of H and T was recorded as usual.

At the end of the desired period, a 30 μA. cm.$^{-2}$ cathodic protection current was switched in on the cathodisation side. The diffusion side electrolyte was withdrawn via the 1 mm. bore outflow microtap into a 25 ml. measuring cylinder. The interior of the diffusion side cell was washed with 1 to 2 ml. of 0.2 M KOH and washings were also collected in the same measuring cylinder and its total volume was measured.* However, the passage of nitrogen was continued for another 30 minutes to flush all cathodically generated H_2,HT and T_2 on the cathodisation side of the Pb foil

---

* In experiments T2 and T4, the diffusion side sample was withdrawn (after 12 hours of cathodisation) while cathodisation continued further at the same value instead of at $-i \simeq 30$ μA. cm.$^{-2}$ (see Table 38).

into the oxidation train and finally into the collection system.* The collection system was then disconnected from the oxidation train. The tritiated water collected in the vial was transferred into a standard flask (A grade, 100 or 250 ml. depending on T activity). The vial inner and outer parts of the central tube of the cap were washed with 3 x distilled water several times. All washings were transferred into the flask and solution was made up to the mark. Meantime, the solution in the cathodisation side was withdrawn while the Pb was still cathodic ($-i \approx 30$ μA. cm.$^{-2}$). Finally, Pb foil was removed from the cell, washed thoroughly with 3 x distilled water, dried and its thickness was determined with a micrometer. The collected diffusion side sample and gas phase tritiated water obtained from the cathodically generated H_2,HT and T_2 were analysed as explained earlier. About 15 to 20 samples each of the tritiated water from the diffusion side and gas phase, of volumes varying from 10 μl. to 250 μl. (depending on T activity) were used for analysis in 15 ml. of scintillation cocktail. Then, 5 samples of the standard, of volumes

---

* In experiment T7, after 9 hours of cathodisation at 23.5 mA. cm.$^{-2}$, the oxidation train was disconnected from the cell and the oxidation train only was flushed with purified nitrogen for another 30 minutes.

varying from 10 μl. to 250 μl. in 15 ml. of scintillation cocktail were analysed to estimate the efficiency of the cocktail (fresh cocktail was prepared for each experiment) using equation (3.3) and hence enabling calculation of the T activity in D.P.M. Correspondingly, 5 blanks (0.2 M KOH in the case of diffusion side samples or 3 x distilled water in the case of gas phase samples), of volume from 10 μl. to 250 μl. in 15 ml. scintillation cocktail were analysed to correct for the background counts.

Knowledge of the decay constant $\lambda = 1.79 \times 10^{-9}$ sec.$^{-1}$ for T (215) enabled calculation of the T concentration in the cathodisation side solution, diffusion side solution and in the cathodically generated gas phase tritiated water from respective measured D.P.M.'s using the relation

$$C_T = \frac{-dC_T/dt}{1.79 \times 10^{-9}} \qquad (3.4)$$

where C_T = number of T atoms and dC_T/dt is the rate of disintegrations per second (D.P.S.). The total numbers of H (including T) atoms cathodically generated in the gas phase and of H (including T) atoms ionised at the diffusion side were calculated using respective cathodisation currents and permeation currents (ignoring the difference between the steady-state and transient values) as

$$\frac{\text{Current in A. x time of electrolysis in sec. x } 6.023 \times 10^{23}}{96500} \qquad (3.5)$$

Finally, the total number of H atoms = 6.35×10^{22} atoms ml.$^{-1}$ present in the cathodisation solution was calculated for 1M aqueous $HClO_4$ (diluted from 11 M $HClO_4$, density = 1.67 g. ml.$^{-1}$). Then, $S_{H,T}$ and $S_{(H,T)_{DA}}$ were calculated using equations (2.65) and (2.69),* respectively.

Consideration of errors is appropriate at this point. The electrochemical permeation rates were the measured currents to overall microvoltmeter/recorder system accuracy being about ± 2%, while the measured currents were about ± 3% accurate. The foil thicknesses were precise to ± 5% or better. Since the analysis was carried out using A grade burettes (for measuring 15 ml. of cocktail), A grade standard flasks, Eppendorf microliter pipettes with disposable polyethylene plastic tips (for pipetting small volumes $\leq$ 250 µl., standard deviation < 0.6%), the estimated error was probably < 1%. From the number of sample counts and background counts, assuming a Poisson distribution, the relative standard

---

* But J_∞ and $(J_\infty)_T$ in equation (2.69) were expressed instead in terms of the total numbers of H and T atoms, respectively. And it is assumed that cathodisation currents and permeation currents are mainly contributed by the H_3O^+ discharge on the cathodic side and by the H ionisation on the diffusion side because of the low $\frac{T}{H}$ ratio in the cathodic solution. Also the $\left[\frac{(H)}{(T)}\right]_S$ ratio in equations (2.65) and (2.69) was assumed to remain constant throughout an experiment.

deviation calculated was in no case greater than 1.5%. Relative standard deviations of the sampling (15 to 20 samples) were < 4%.

Experiments were conducted in a fumehood in a thermostated room at 26 ± 3°C. The cell and other electrodes (used for previous experiments or found contaminated with T) were leached several times with plenty of water and the last washings were tested for T. Only after positive evidence was obtained for the absence of traces of T, was the final cleaning procedure and electrode preparation carried out. Thorough cleaning was essential for the success of this work.

(V) Results of Experiments with Electropolished Foils

The results obtained with nine electrochemically polished {Section 3C (ll)} Pb foils (thickness varying from 0.011 to 0.017 cm.), cathodically polarised at different current densities (-i ranging 1 to 46 mA. cm.$^{-2}$) at one side of the foil in tritiated 1 M $HClO_4$ (concentration of T varying 1.33 to 2.6 mCi. ml.$^{-1}$) and held anodically at +140 mV. in 0.2 M KOH versus α/β Pd-H reference electrode on the other side of the foil are listed in Table 38. In most of the experiments, the cathodic electrolysis was carried out for 12 hours. In T1 and T9, the cathodisation was extended to 24 hours and gas phase collection of cathodically generated H_2,HT and T_2 was omitted. On the other hand, in T2, T4 and T7, the cathodic electrolysis for the gas phase collection of H_2,HT and T_2 were 15.17, 55 and 9 hours, respectively, while diffusion side samples were withdrawn after 12 hours of cathodisation.

Anodic background currents of +140 mV. versus α/β Pd-H reference on the diffusion side were often high (tens of μA.). Moreover, shifting of total anodic currents (by say 10 μA.) and fluctuation of the total anodic currents (± 3 μA. or more) were observed. Fig. 61 illustrates one such example in experiment T9. In T8 no H permeation and in T6 no T permeation (Table 38) were observed. These failures are thought to arise from the experimental

TABLE 38. MEASUREMENTS ON CATHODISATION AND DIFFUSION SIDES OF LEAD MEMBRANE AFTER CATHODIC ELECTROLYSIS FOR THE DESIRED PERIODS AT DIFFERENT CURRENT DENSITIES

Experiment number	Area of Pb electrode /cm.^{2}	Thickness of Pb foil /cm.	Efficiency of cocktail in %	Cathodic current density/ mA.cm.$^{-2}$	Cathodisation side measurements			Diffusion side measurements				
					Time of cathodic electrolysis /hours	Total T activity of tritiated water from gas phase /C.P.M. x 10^{-6}	Total T activity of tritiated water from gas phase /D.P.M. x 10^{-7}	Time of cathodic electrolysis /hours	Total volume of diffusion side solution /ml.	Permeation current density /µA. cm.$^{-2}$	Total T activity /C.P.M. x 10^{-5}	Total T activity /D.P.M. x 10^{-5}
T1*	1.13	0.012	22.8	1.00	-	-	-	24	14.3	0	0	0
T2	0.85	0.0165	22.1	5.85	15.17	5.40	2.45	12	15	0	0	0
T3	0.85	0.0115	21.7	5.90	12	2.98	1.38	12	14.6	0	0	0
T4	0.85	0.015	22.3	11.3	55	36.4	16.3	12	15	1	0.394	1.77
T5**	0.85	0.0115	21.9	11.8	11	5.22	2.38	-	-	-	-	-
T6	1.13	0.016	21.8	11.8	12	5.67	2.60	12	14.1	1.8	0	0
T7***	1.13	0.0155	21.8	23.5	9	8.21	3.78	12	14	2.8	1.86	8.57
T8	1.13	0.011	20.9	30.5	12	11.7	5.6	12	14.2	0	2.84	13.6
T9*	1.13	0.017	20.9	46	-	-	-	24	11.2	11	14.5	69.6

* Gas phase collection of cathodically generated H_2, HT and T_2 omitted.

** Diffusion side experiment omitted.

*** Efficiency of the cocktail used in diffusion side T analysis was 21.7%.

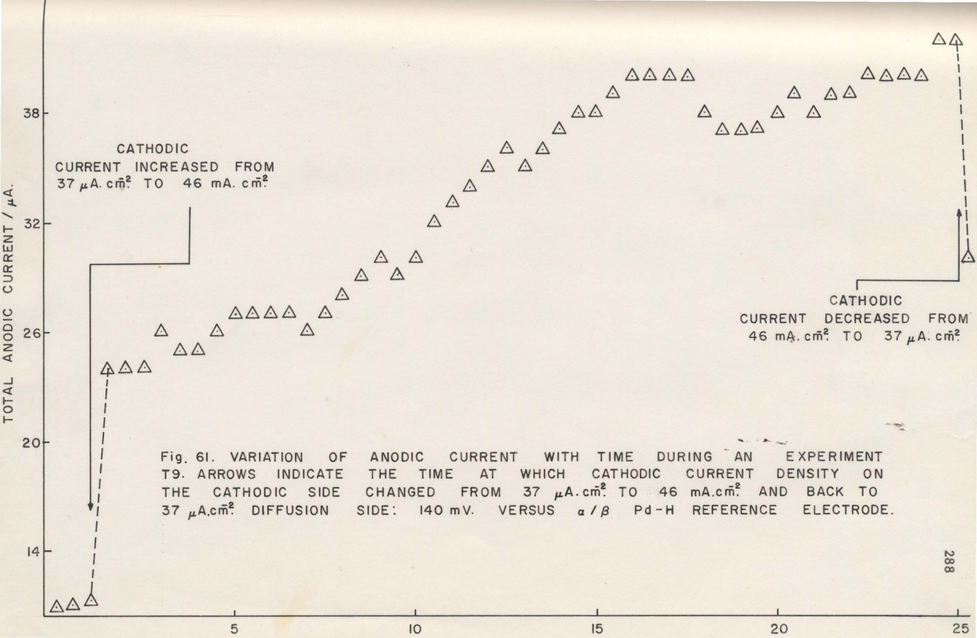

Fig. 61. VARIATION OF ANODIC CURRENT WITH TIME DURING AN EXPERIMENT T9. ARROWS INDICATE THE TIME AT WHICH CATHODIC CURRENT DENSITY ON THE CATHODIC SIDE CHANGED FROM 37 μA.cm^{-2} TO 46 mA.cm^{-2} AND BACK TO 37 μA.cm^{-2} DIFFUSION SIDE: 140 mV. VERSUS α / β Pd-H REFERENCE ELECTRODE.

difficulties associated with the bare metal surface or the complete elimination of oxygen from the system. These reasons may well explain the complete failure of a few other experiments which are not mentioned here.

It is apparent from Table 38 that permeation current increased from 1 to 11 μA. cm.$^{-2}$ as -i increased, but <u>only</u> at $-i \geqslant 11.3$ mA. cm.$^{-2}$. The activities of T, both in the gas-phase-collected tritiated water on the cathodisation side and in the solution in the diffusion side in C.P.M. and D.P.M., respectively, are listed in Table 38.

The calculated $S_{H,T}$ and $S_{(H,T)_{DA}}$ at different -i values are shown in Table 39. The average value of $S_{H,T} = 7.2 \pm 0.7$, independent of cathodic current densities*, are close to the value of Bockris and Srinivasan (25), i.e. $S_{H,T} = 6.7 \pm 0.7$ at $-i = 10$ mA. cm.$^{-2}$. While, $S_{(H,T)_{DA}}$ <], as observed by Muju and Smith (55), but found to decrease with -i. $S_{(H,T)_{DA}}$ decreased from 0.14 to 0.04 as -i increased from 11.3 to 46 mA. cm.$^{-2}$. The presence of an oxide film on the diffusion side might explain the observed low $S_{(H,T)_{DA}}$ values. The decrease of $S_{(H,T)_{DA}}$ with -i likely resulted from either the increase in solubilities of H and T atoms with -i or the low observed H atom

---

* However, if we look only at experiments T4, T7 and T8 (Table 39), there is a sign of $S_{H,T}$ decreasing with -i.

TABLE 39. SEPARATION FACTORS ON THE CATHODIC SURFACE, $S_{H,T}$, AND ON THE DIFFUSION SIDE, $S_{(H,T)_{DA}}$, AT DIFFERENT CATHODIC CURRENT DENSITIES

Experiment number	Cathodic current density/ mA.cm.$^{-2}$	Cathodic side solution			Gas phase H and T on the cathodisation side			$S_{H,T}$	Ionised H and T on the diffusion side			$S_{(H,T)_{DA}}$
		Total number of H atoms ml.$^{-1}$ x 10^{-22}	Total number of T atoms ml.$^{-1}$ x 10^{-16}	Ratio of $\frac{(H)}{(T)}$ x 10^{-6}	Total number of H atoms x 10^{-21}	Total number of T atoms x 10^{-14}	Ratio of $\frac{(H)}{(T)}$ x 10^{-6}		Total number of H atoms x 10^{-17}	Total number of T atoms x 10^{-12}	Ratio of $\frac{(H)}{(T)}$ x 10^{-4}	
T2	5.85	6.35	5.37	1.18	2.0	2.28	8.76	7.4	–	–	–	–
T3	5.90	6.35	3.39	1.87	1.59	1.28	12.4	6.6	–	–	–	–
T4	11.3	6.35	5.37	1.18	14.0	15.2	9.29	7.9	2.70	1.65	16.4	0.14
T5**	11.8	6.35	3.39	1.87	2.91	2.22	13.1	7.0	–	–	–	–
T6	11.8	6.35	3.39	1.87	3.17	2.42	13.1	7.0	–	–	–	–
T7	23.5	6.35	3.39	1.87	4.76	3.52	13.5	7.2	7.55	7.98	9.47	0.05
T8	30.5	6.35	2.75	2.31	8.2	5.22	15.7	6.8	–	–	–	–
T9*	46	6.35	2.75	2.31	–	–	–	–	59.3	64.8	9.15	0.04

* Gas phase collection of cathodically generated H_2, HT and T_2 omitted.

** Diffusion side experiment was omitted.

permeation currents because H atoms might be used up for the reduction of the oxide film present on the diffusion side. Even large anodic currents might thicken the oxide film already present on the diffusion side and hence decrease the $S_{(H,T)_{DA}}$.

Table 40 and Figs. 62 and 63 show the steady-state H permeation currents (μA. cm.$^{-2}$) and mean T atom permeation rate (number of T atoms cm.$^{-2}$ sec.$^{-1}$) computed* for a chosen thickness (0.015 cm.) of foil at different -i values. No H or T permeation was observed below -i = 11.3 mA. cm.$^{-2}$ during a period of 12 to 24 hours of cathodic electrolysis. At -i $\gtrsim$ 11.3 mA. cm.$^{-2}$, both H and T permeation rates increase linearly at low values, but later at a greater rate with -i. This clearly indicates the cathodic permeation effects, i.e. increase of the H concentration just beneath the cathode surface as -i increases.

---

* Using equation (2.49) and assuming J_∞ inversely proportional to the thickness of the Pb foil.

TABLE 40. EFFECT OF CATHODIC CURRENT DENSITY ON HYDROGEN AND TRITIUM PERMEATION RATE ON THE DIFFUSION SIDE

Experiment number	Thickness of Pb foil /cm.	Cathodic current density/mA. cm.$^{-2}$	Computed values for a 0.015 cm. thick foil	
			Hydrogen permeation current/μA. cm.$^{-2}$	Number of tritium atoms /cm.$^{-2}$ sec.$^{-1}$
T1	0.012	1.0	0	0
T2	0.0165	5.85	0	0
T3	0.0115	5.9	0	0
T4	0.015	11.3	1.0	4.49×10^7
T6	0.016	11.8	1.9	0
T7	0.0155	23.5	2.9	1.69×10^8
T8	0.011	30.5	0	1.90×10^8
T9	0.017	46	12.5	7.52×10^8

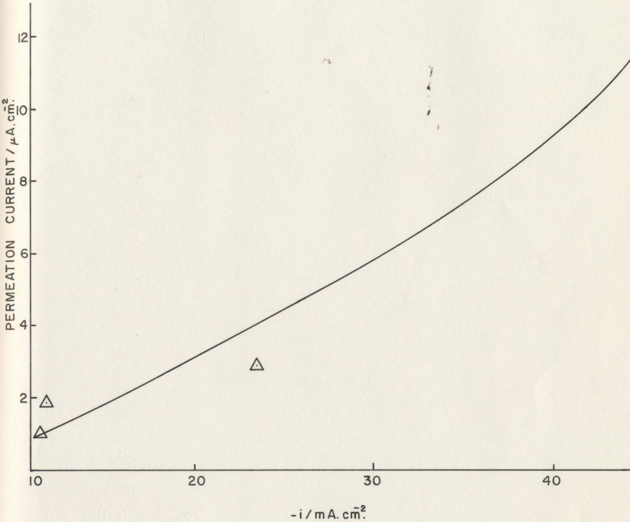

Fig. 62. STEADY – STATE H ATOM PERMEATION CURRENT DENSITY VERSUS CATHODIC CURRENT DENSITY.

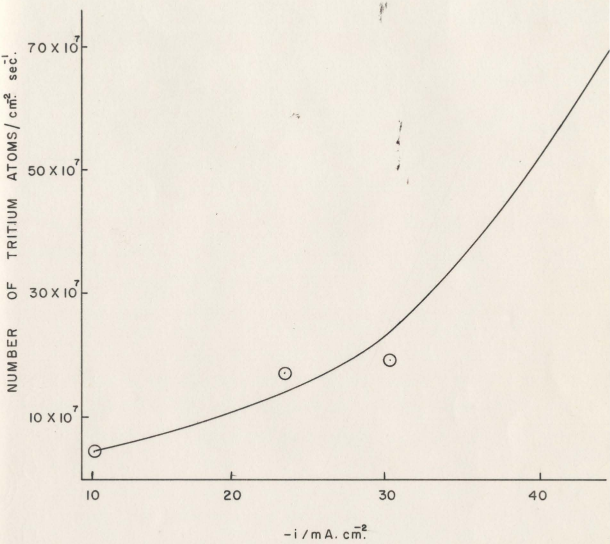

Fig. 63. MEAN TRITIUM ATOM PERMEATION RATE VERSUS CATHODIC CURRENT DENSITY.

(Vl) Summarising Remarks on Separation Factor Measurements

1. The electrolytic H-T separation factor has been measured simultaneously on the cathodic side and the diffusion side of electropolished Pb foils in $HClO_4$ as a function of cathodic current density.

$S_{H,T} = 7.2 \pm 0.7$ for H_2, HT and T_2 atoms generated cathodically on the cathodisation side and has little or no dependence on -i from 5.85 to 30.5 mA. cm.$^{-2}$, but is close to the value of Bockris and Srinivasan (25), of $S_{H,T} = 6.7 \pm 0.7$ at -i = 10 mA. cm.$^{-2}$. $S_{(H,T)_{DA}} < 1$ for H and T originating in the catholyte, entering the metal membrane, diffusing through the membrane and being ionised into the diffusion side electrolyte, as previously observed by Muju and Smith (55), but appears to decrease with -i.

2. Cathodic permeation effects have been observed at $-i \gtrsim 11.3$ mA. cm.$^{-2}$, i.e. both H and T atoms have been found to pass through a lead foil of 0.011 to 0.017 cm. thickness under the present experimental conditions. The permeation rate of each increases as -i increases.

4. DISCUSSION

This discussion is concerned primarily with those results of satisfactory experiments (electropolished lead electrodes in properly pre-electrolysed solutions) described in Sections 3A (V11) and 3B (111). Studies of hydrogen overvoltage and adsorption pseudo-capacity confirmed that hydrogen adsorption by lead cathodes is measureable. This is the first report of measurements of this sort on a weakly adsorbing metal.

A. General

Much early work on hydrogen overvoltage must be regarded with suspicion because no great precautions were taken in electrode preparation, solution purification or gas purification. All these factors reflected on the poor results obtained also in the preliminary experiments of this work {Sections 3A (Vla) and 3B (11a)}.

Kabanov et al. (6) introduced a large volume of 0_2 into the system during an h.e.r. study and corrected the H_30^+ discharge rate (by subtracting oxygen reduction current from the measured current). Moreover, Hickling and Salt (14), Bockris and Azzam (15, 16, 17) claimed that no stringent deoxygenation was necessary at $-i > 1$ mA. cm.$^{-2}$. These arguments contradict some well known facts. It is well known that chemisorption of O_2 by most metals is extremely rapid and in many cases irreversible. Thus, despite very favourable chemisorption equilibria for hydrogen on metals such as W, pre-adsorption of O_2 inhibits the chemisorption of H_2 (216, 217). Perhaps, it may be equally true in the case of Pb because of the rapid interaction of Pb and O_2, as observed by Hackerman and Lee (218) and Nesmeyanov et al. (219). Hackerman and Lee (218) failed to measure the work function of clean Pb using evaporated films in a vacuum of 10^{-6} torr., but obtained a higher value corresponding to an O_2-covered surface. Also, Nesmeyanov et al. (219) were unable to measure the vapour pressure of pure solid Pb, which was greater than extrapolation from liquid Pb suggested because of the presence of a thin oxide film.

Nevertheless, Pb and H_2O interact slowly in the absence of O_2, while the initial tarnish film soon reaches a limiting thickness in dry O_2. This suggests that hydrogen overvoltage studies on smooth Pb will be very sensitive to traces of O_2 in the system. Considering only the work of Bockris and Srinivasan (25), this was obviously affected by the presence of O_2 in the gas stream, because it was necessary to make measurements <u>in the absence of gas passing through the cathode compartment</u>. These workers admitted that they sometimes obtained Tafel slopes $> 4.6RT/F$, which they excluded from further consideration.

The hydrogen overvoltage measurements on lead of Piontelli, Bicelli et al. (20 to 24) and the capacity measurements of Hampson et al. (220, 221) in solutions containing Pb^{++} ions resemble the results obtained in this work for electropolished Pb in solution pre-electrolysed at too high current densities. Stripping analysis, as detailed in Section 3A (11c), confirmed the presence of Pb^{++} ions $\{ (Pb^{++}) \simeq 10^{-6}$ M$\}$ in acid solutions under such conditions. Low overvoltages (Table 5), multilinear Tafel lines with large amounts of hysteresis (Fig. 17) and large capacities, especially at current density $\geqslant 5$ mA. cm.$^{-2}$ (Table 24) were observed. Evidently, this kind of behaviour is associated with a significant concentration of Pb^{++} in solution. Moreover, in the course of cathodisation, $-\eta$ increased continuously, while the capacities fell to more normal values at high current density and rose to normal values at low current density. Gradual decrease of the Pb^{++} ion concentration during cathodisation explains the increase in $-\eta$ and decrease in $C_{expt.}$ during cathodisation. Nevertheless, the failure to observe overshoot hysteresis indicates the unsatisfactory state of the system.

Many early Russian workers (5, 6, 7, 31) studied scraped electrodes in acid solution. The main difference between the present work and that of the Russians is their failure to observe any time dependence of $-\eta$, at least under their experimental conditions. As shown in Fig. 19, disregarding the deviations at low $-Q$, most of the scraped electrodes used in the present work showed a slow initial decrease and then a more rapid decrease of $-\eta$ at higher $-Q$ values. A rapid decrease of overvoltage was generally observed with electropolished electrodes in this work and in Ives and Smith's work (26, 27). Overvoltages were initially (Table 6) similar to those of Russian work (5, 6, 7, 31) in acid solution, but decreased with time, to values of the order of 100 mV. or more less negative. Scraped lead electrodes also followed a linear $-\eta$ versus $\log_{10}(-Q)$ relationship. However, the scraped electrodes behaved similarly to polished ones only after the passage of sufficient cathodic charge (≃ 70 coulombs). A charge of this magnitude may be required to reduce an oxide film* initially present on the Pb surface. Oxides of metals, such as Pb, are said to be reduced by atomic hydrogen (222), so that cathodisation might be expected to reduce the oxide film present on the metal surface. This reduction process appears to proceed slowly under electrolysis conditions.

As cathodisation of scraped electrodes proceeded their Tafel behaviour improved, the plots becoming linear over a wider current range. High Tafel slopes of about 180 mV. were still found, however, which may be explained (4) as being due to the presence of oxide film on the metal.

---

* The metal, with its film (perhaps consolidated by other impurities), then shows high overvoltage behaviour.

Moreover, overshoot hysteresis was less frequently observed on scraped electrodes. This indicates that the scraped Pb surface is not very clean, perhaps being covered with an oxide film for reasons mentioned above.

Thus, the above evidence indicates that the properties of the lead + hydrogen + hydronium ion system are not well suited to critical examination of the h.e.r. unless a high degree of purity and deoxygenation is maintained. Such conditions were approached in our satisfactory experiments, which involved electropolished Pb in $HClO_4$, pre-electrolysed at current densities lower than 2 mA. cm.$^{-2}$. In these satisfactory experiments the initial overvoltages (Tables 9 to 11) were close to or slightly higher than those of Ives and Smith (26, 27). These values are lower by one or more hundred mV. than most of the earlier workers (7, 11, 12, 25, 31, 34 and 35). Moreover, overvoltages fell by 150 to 300 mV. at the end of long periods of cathodisation (Figs. 29 to 31). Initial capacities (Tables 25 to 30) were close to or a little higher than literature values (12, 29, 30, 31, 34, 35, 38, 39a, 39b) but they have been found to increase with -Q when values at constant η were compared (see Figs. 43 to 47).

In satisfactory experiments with electropolished lead electrodes, three features previously observed by Ives and Smith (26, 27) have been confirmed:

(i) The existence of overshoot hysteresis when changing the current density to larger or smaller values.

(ii) The linear fall of overvoltage with $\log_{10}(-Q)$, and

(iii) a simultaneous decrease of Tafel slope as the overvoltage decreased.

New features have been observed. These are:

(i) The increase in electrode capacity over a wide range of constant η values as $-Q$ increased.

(ii) The parallel growth of $C_{expt.}$ and of $\log_{10}(-i)$ at constant η, both linearly with $\log_{10}(-Q)$.

(iii) Parallel variation of the slope, b", of the $C_{expt.}$ versus $\log_{10}(-Q)$ plot with the slope, b', of the $-\eta$ versus $\log_{10}(-Q)$ plot.

There is also the suggestion that the Tafel slope changes with the electrode condition, decreasing as the electrode capacity increases at constant η. Finally, the limited evidence that there is suggests that the enthalpy of activation, $\Delta H^{\ddagger}_{\eta=0}$, decreases as electrolysis proceeds ($-Q$ increases).

Ives and Smith (26, 27) concluded from their results that the hydrogen surface coverage of a lead electrode might increase in the course of cathodisation as a result of hydrogen continuously entering the metal during this process. They presented no evidence to confirm this hypothesis, but Cadersky, Muju and Smith (55, 147) later showed that atomic hydrogen can dissolve in metallic lead when this species is generated by electrolysis. The growth of hydrogen coverage (see Tables 33 to 36), which appears to us to be the only reasonable explanation of the capacity data obtained in the present work, provides additional evidence favourable to Ives and Smith's hypothesis (26, 27). The best evidence comes from the parallel behaviour of the capacity and overvoltage {or $\log_{10}(-i)$}, both changing linearly with $\log_{10}(-Q)$. Much of the discussion will be concerned with possible alternative explanations and with accounting for the capacity and overvoltage behaviour on the basis of the electronic band structure of lead.

Before considering these matters further, it is necessary to consider the topics of atomic hydrogen and lead and the permeation of hydrogen and tritium atoms through lead membranes.

B. Interaction of Atomic Hydrogen with Lead

The general behaviour of hydrogen atoms on the surface and in the interior of metals has already been described in Sections 1C and D and 2B, C and D, with particular reference to lead. Although many different techniques could be applied to study the interaction of H atoms with Pb, the techniques used in this laboratory are mainly overvoltage, capacity and electrolytic permeation measurements, Information obtainable from these types of measurements are H coverage, H solubility in the metal and parameters relating to H diffusion through the bulk metal, and cathodic disintegration of Pb; these topics will be discussed in this section in conjunction with data available from other sources.

Although the thermally unstable gaseous PbH_4 is known, higher plumbanes are unknown. Since gaseous PbH_4 is not stable at room temperature, there is no agreement as to whether it has been synthesised or not. The careful investigations by Paneth et al. (54) in 1920 first indicated the existence of the volatile hydride PbH_4. Mass-spectrometrically detectable amounts of PbH_4 have been found in the decomposition of Mg-Pb alloys in acid (223). Thus, the existence of volatile PbH_4 has been demonstrated only in respect of trace amounts. Atomic hydrogen removes a lead mirror prepared by the pyrolysis of $(CH_3)_4Pb$. The gas so formed redeposits a lead mirror on heating: another indication of the existence of a gaseous lead hydride (224). During reduction of alkali-metal plumbates, $MPb(OH)_3$, with aluminum foil in aqueous solution a grey solid of composition Pb_2H_2, which decomposes into Pb and H_2 is said to be formed (225). Moreover, Roberts and Eachus recently detected PbH^{++} species (226) during their electron paramagnetic resonance study with X-irradiated $Pb(C_2H_3O_2)_2.3H_2O$ single crystals and powders at 77° K.

There is indirect evidence for the formation of lead hydride of formula PbH_2. Salzberg et al. (41, 42) reported that lead electrodes disintegrate into colloidal lead (identified by X-rays) at high current densities in acid and alkaline solution of varying pH and salt concentrations. According to them, cathodic disintegration of lead* was due to the formation of PbH_2 and its subsequent decomposition. Pourbaix et al. (40) have obtained evidence supporting the "hydride" theory of cathodic disintegration of Salzberg et al. In contrast the Russian (43, 44) and Polish (45) Schools argued that cathodic disintegration of lead is caused solely by alkali metal penetration into the cathode and subsequent decomposition of the alkali alloy.

We must emphasize, however, that we do not accept the views of the Russian and Polish Schools. Experiments of Salzberg et al. (41, 42) have provided clear evidence that alkali metal ions are not essential to such a disintegration process.

---

* A brief account of cathodic disintegration has been given in Section 1C.

The evidence is:

(i) Cathodic disintegration occurs in acid solutions at high enough current densities ($-i > 100$ mA. cm.$^{-2}$) in the absence of alkali metal cations.

(ii) At a constant current density and constant ionic strength, the disintegration rate decreased with increase in H_3O^+ ion concentration in the pH range 4.0 to 1.3, presumably because of a strongly inhibitive action of hydronium ions. The disintegration rate also decreased with increase of OH^- ion concentration (0.04 to 4 N NaOH) and with the increase of salt concentration (0.1 to 4 M KCl or 0.1 to 1.4 M Na_2SO_4). A linear relationship was found between the disintegration rate (weight loss of lead sec.$^{-1}$ A.$^{-1}$) and the water activity.

(iii) The observed threshold current density (current density for the commencement of weight loss - measureable disintegration) has little or no dependence on the nature of alkali metal cation, i.e. the threshold current densities for K^+ to Cs^+ are about the same but Li^+ showed a lower threshold current density relative to K^+ to Cs^+.

Both in Ives and Smith's (26, 27) work and in the present study evidence has been obtained for cathodic disintegration in $HClO_4$ at current densities ≤ 10 mA. cm.$^{-2}$ after 'charging' the electrode sufficiently over a long period of cathodisation. Ives and Smith (26, 27) in one instance observed a rise of constant current density from 8 mA. cm.$^{-2}$ to

10 mA. cm.$^{-2}$ (despite the stabilising resistors) with a simultaneous fall of overvoltage from 990 to 870 mV. This event led to a drastic alteration in the state of the system; the overvoltage at 100 μA. cm.$^{-2}$ was only 260 mV. (within a few mV. of the previous open-circuit potential which was -210 mV.), corresponding with about a 100-fold increase in Pb^{++} activity (provided that such calculation is significant). Over a range of current densities, overvoltages were greatly depressed and Tafel slopes much increased. Several days of cathodisation at 100 - 400 μA. cm.$^{-2}$ led to increased overvoltages, linear Tafel slopes and more negative open-circuit potentials, presumably because of the slow decrease of Pb^{++} concentration.

In the present work, some of the features observed which support the hydride mechanism of cathodic disintegration are:

(i) A significant concentration of Pb^{++} ions of about 10^{-6} M was detected in $HClO_4$, after pre-electrolysis at $-i = 4$ to 6 mA. cm.$^{-2}$ for 6 to 30 days {Section 3A (11c)}. Electrodes studied in solutions "purified" in this manner showed low $-\eta$ and high $C_{expt.}$ which reached normal values only upon continued cathodisation at 535 to 665 μA. cm.$^{-2}$ for several days {Sections 3A (V1b) and 3B (11b)}. It is argued that Pb^{++} ions were introduced into the acid solution as a result of the cathodic disintegration occurring at the relatively high current density in pre-electrolysis.

(ii) In one experiment (R3c), increasing the cathodic current density to 3.85 mA. cm.$^{-2}$ and maintaining it at this value for 50 hours (-Q increasing from 520 to 2290 coulombs) led to increases in the Tafel slope from ca. 110 mV. to > 300 mV. at intermediate currents (ca. 30 μA.), an increase in the -η versus $\log_{10}$(-Q) slope from 66 to 580 mV. (see Fig. 29). Resumption of cathodisation at 385 μA. cm.$^{-2}$ caused -η to increase and the Tafel plots again became linear {see Section 3A (V11a) and Fig. 24}. Again, it is argued that cathodisation at the current density of ca. 4 mA. cm.$^{-2}$ led to cathodic disintegration.

(iii) In some instances (see Figs. 49 and 51), after an electrode had been charged to a sufficient extent, the slope b', of -η versus $\log_{10}$(-Q) plots increased to a very high value (62 to 685 mV. in experiment R4a" at -Q = 194 coulombs, and 89 to 460 mV. in experiment R5b at -Q = 838 coulombs, both electrodes being cathodised at 650 μA. cm.$^{-2}$) accompanied by a simultaneous decrease in $C_{expt.}$ {negative b", slope of $C_{expt.}$ versus $\log_{10}$(-Q) plot} in contrast to the usual increase.

The evidence of (i) and (ii) and possibly also of (iii) indicates that Pb^{++} ions, formed during cathodic disintegration were introduced into the solutions. After cathodisation at lower current density, progressive removal of Pb^{++} ions led to better behaviour by such electrodes. However, no hydride of composition PbH_2 as suggested by Salzberg et al. (41, 42) has been identified. More work is needed to clarify this situation.

The dissociative chemisorption of molecular hydrogen by sp metals like Pb is not normally observed. Dissociative adsorption is only possible* for metals with E(M-H) $\geq$ 51 k. cal. mole^{-1}, as mentioned in Section 2B (1). Therefore, for sp metals direct atomic adsorption is necessary to investigate hydrogen adsorption at these metals. The direct interaction of atomic hydrogen with evaporated lead films was studied by Wells, Roberts and Young (51, 118). Roberts and Young (118) suggest that the hydrogen surface coverage, θ_H, at -195°C is close to unity and much greater than at 0°C, so that $(1 - \theta_H)_{-195^oC} < (1 - \theta_H)_{0^oC}$.

As stated earlier, Ives and Smith's proposal (26. 27), that the linear decreases of overvoltage with $\log_{10}(-Q)$, observed by them and in the present investigation, were caused by a continuous increase in the adsorbed hydrogen coverage of the lead cathode during electrolysis, receives support from the present observations of electrode capacities increasing with the period of cathodisation. The fact that both $C_{expt.}$ and η increase linearly with $\log_{10}(-Q)$ points to a connection between the underlying processes. This will be dealt with in Section D of this chapter. For the present, discussion will be confined to consideration of the significance of the capacities quoted in Table 33 for a foil electrode and in Tables 34 to 36 for rod electrodes. Other workers have failed to observe a hydrogen pseudocapacity at Pb, Hg or any

---

* The entropy of dissociative adsorption (ΔS) of H_2 from gas phase or solution will probably be negative.

other high overvoltage, i.e. sp metal. We also failed to observe a pseudocapacity attributable to hydrogen in the early stages of our experiments. However, the measured capacities increased with time of cathodisation by quite large amounts and it is difficult to conceive of any other explanation consistent with all of the facts than that of a growing hydrogen adsorption pseudocapacity. Alternative possibilities will be considered early in Section D of this chapter.

The hydrogen surface coverages deduced range up to about 5% of a monolayer, i.e. $\theta_H \approx 0.05$, for a 0.25 mm. thick foil, produced by an additional 416 coulombs (Table 33). The coverage was smaller, $\theta_H \approx 0.02$, in the case of 2 to 3 mm. diameter rods, charged with ca. 800 coulombs. There are two possible reasons for the difference in behaviour, either the smaller range of current density in the cathodisation of rods or the different volumes of the electrodes, the rods having a larger volume/surface area ratio. It is also possible that differences in the apparatus design had some influence on the behaviour.

Although much of the earlier (46) and recent (47, 48) work indicated a negligible solubility for hydrogen in lead, and consequently no information concerning the diffusion of hydrogen in the metal at room temperature, the early experiments of Deming and Hendricks (227) that molecular hydrogen permeated through Pb at a rate 1 μg. cm.$^{-2}$ hour^{-1} at 265 ± 15°C, is remarkable for the fact that no attention was paid to surface preparation. However, the solubility of H in molten lead has been reported by Opie and Grant (228), their values (solubilities in atomic ratios) ranging from H/Pb = 0.18×10^{-4} at 500°C to H/Pb = 2.3×10^{-4} at 900°C.

Evidence that lead dissolves hydrogen has also come from the gas phase studies with H atoms of Wells, Roberts and Young (51, 118). They had shown that pure coatings of lead evaporated on glass at about 10^{-7} torr. (up to 80 mg., surface area ≈ 200 cm.^{-2}) absorb large amounts of atomic hydrogen at room temperature. Similar behaviour was observed at other temperatures, but the uptake was faster the higher the temperature. Moreover, the amount of H absorbed was a function of the weight of the lead, but <u>not of its surface area</u>. The linear relationship between hydrogen uptake and the weight of lead phase (up to 30 mg.) observed by Roberts and Young (118) suggested a definite stoichiometric ratio between lead and hydrogen. From the slope, they derived a formula $PbH_{0.2}$ at 0°C ($PbH_{0.22}$ at -78°C) for the composition of the hydride, which appears to be remarkably stable either in a hydrogen atmosphere or in vacuo. The hydride only very slowly absorbs atomic hydrogen passed over it. Slow desorption of a small fraction (8%) of the hydrogen as molecules occurred at 0°C and a greater fraction (25%) at 140°C, and so on; which indicates either discrete absorption centres of different energies or possibly rate-limiting diffusion or recombination of H atoms. They concluded from their data that the activation energy of desorption (16 - 20 k. cal. $mole^{-1}$) corresponds with that for H atom mobility and also suggested that at low hydrogen concentrations ($PbH_{<0.1}$) this might approach the Pb-H bond energy (less than 52 k. cal. $mole^{-1}$). At low temperatures (-195°C), i.e. at higher surface coverages, the surface H atoms were removed by the combination of $H_{ads.}$ and H atoms from gas phase. However, at temperatures $\geq 0^{o}C$, i.e. at lower surface coverage, the recombination of H atoms <u>within</u> the lattice leading to molecular desorption via the solid may become significant when the probability of an H atom finding a stable lattice site is comparable to the probability of recombination within the lattice. This occurs when one H atom is present per five lead lattice atoms, i.e. when lead hydride has a composition $PbH_{0.2}$.

Another interesting observation of Roberts and Young (118) is that the reversible adsorption of molecular hydrogen occurs on the hydride surface in the temperature range -195°C to -78°C, contrasting with the absence of any molecular interaction with a clean lead surface. It is likely to arise from the polarisation of the H_2 molecule by the lead hydride, which will have some ionic character and its extent is that expected of a process confined to the surface. The elements of Fourth Group IVA (C, Si, Ge, Sn, Pb) all form covalent hydrides MH_4. But, lead hydrides are distinguished by their polarisation (229):

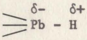

It is interesting, for example, that attempts (229) to hydrogenate $PbCl_4$ with $LiAlH_4$ fail, the product being, not PbH_4, but H_2. This is in contrast to the behaviour of alkyl lead chlorides R_2PbCl_2 which yield R_2PbH_2.

To explain the linear decrease of $-\eta$ versus $\log_{10}(-Q)$, Ives and Smith (26, 27) also proposed that H atoms were continuously absorbed by lead. Evidence in favour of this idea has been recently obtained (209). Ives and Smith estimated the upper and lower limits of diffusivity of H atoms in lead as 10^{-6} and 2.5×10^{-11} cm.^{2} sec.$^{-1}$. Their lower limit, 2.5×10^{-11} cm.^{2} sec.$^{-1}$, is based on the diffusivity of Au in Pb. Au is presumed to diffuse interstitially (230, 231), with an activation energy of about 15 k.cal. g. atom^{-1}. The upper limit, 10^{-6} cm.^{2} sec.$^{-1}$ is, however, based on the general property of metal atoms of diffusing faster in lead than in any other solid metal phase while H atoms diffuse much faster than any other metal atoms because of their smaller radius and low valency* (231).

The first direct evidence for the solubility and diffusivity of H in Pb came from the work of Cadersky, Muju and Smith (147). They have shown that electrolytic permeation of hydrogen through Pb foils of 0.015 cm. thickness does indeed occur. Their diffusion coefficients for H in Pb at 25°C at cathodic current densities of 10, 25 and 50 mA. cm.$^{-2}$ are 1.2×10^{-7}, 2.9×10^{-7} and 7×10^{-7} cm.^{2} sec.$^{-1}$, respectively. This suggests that D for H in Pb

---

* Barr (231) has shown that there is a decreasing diffusivity in lead with increasing valence in the sequence of Ag, Cd and In.

depends on the applied cathodic current density, presumably because of a dependence of D for H on the bulk concentration of hydrogen in the metal.

The virtue of radioactive tracers is that they can be accurately assayed even at very low concentrations. Such a technique was employed using T as radiotracer by Muju and Smith (55) to confirm the earlier findings of Cadersky, Muju and Smith (147), i.e. the permeation of H atoms through lead. The linear relationship found by them between the permeation rates of both H and T atoms (under conditions of cathodisation at 53 mA. cm.$^{-2}$ in 1 M $HClO_4$, containing 2 mCi. ml.$^{-1}$ T activity), and the reciprocal thickness (1/L) of the foils for thicknesses of 0.005 to 0.025 cm., proved that the permeation rate is governed by diffusion in the solid phase.

The extension of electrochemical and radiochemical permeation studies to lower current densities, ca. 1 mA. cm.$^{-2}$, are reported in Section 3C (V). As shown in Table 40 and Figs. 62 and 63, both H and T permeation rates increase linearly with current density at low -i, but at higher current densities at a greater rate. This indicates the existence of cathodic permeation effects, i.e. increase of H concentration just beneath the cathodic surface as -i increases. The greater rate of permeation at higher -i may be due to an increase in the diffusivity of hydrogen with current density as observed by Cadersky, Muju and Smith (147). Then, it is likely that the H concentration in the bulk metal is linearly related to the current density applied on the cathodic side.

The H atom concentration just beneath the cathode surface (C_0) can be calculated using equation (2.49) and using the several D values for H from the work of Cadersky, Muju and Smith (147). In the present work, the C_0 is indicated to be 5 x 10^{-7} to 10^{-5} g. atom cm.$^{-3}$ at cathodic current densities of 11.3 to 46 mA. cm.$^{-2}$; the corresponding value of Muju and Smith (55) being 4 x 10^{-7} g. atom cm.$^{-3}$ at 53 mA. cm.$^{-2}$.

In the absence of a measured diffusivity for T in Pb, the estimate of the tritium concentration just beneath the cathode surface must be somewhat approximate, judging by the isotope effects on the diffusivity of hydrogen in Pd and its alloys {145a, 176, 177a; see Sections 2D (11a) and (11b)}. The calculated T atom concentration just beneath the cathode surface using our equation (2.49)*, is indicated to be 10^{-12} to 10^{-10} g. atom cm.$^{-3}$ at current densities of 11.3 to 46 mA. cm.$^{-2}$; while the corresponding value of Muju and Smith (55) was 10^{-12} g. atom cm.$^{-3}$ at 53 mA. cm.$^{-2}$.** A higher bulk H concentration observed in the present work compared with that in

---

* But with J_∞ replaced by $(J_\infty)_T$.

** The range of T activity being the same in both works.

Muju and Smith's work (55) might be expected because of the relatively superior experimental conditions {Section 3C (11)} of this work.

A most probable hydride composition of $PbH_{0.00002}$, reported earlier by Cadersky, Muju and Smith (147), was calculated from their estimated bulk H concentration in lead of 10^{-6} g. atom cm.$^{-3}$. As mentioned by Muju and Smith (55), it is possible to calculate a more reasonable upper limit for the H atom concentration in the bulk of lead giving rise to a formula $PbH_{0.0002}$ in their case, if the radiochemical observations are taken as correct, the electrochemical ones being assumed to be less accurate,* using also the cathodic separation factor, $S_{H,T} = 7.2$, instead of the observed $S_{(H,T)_{DA}} = 0.9 \pm 0.5$.** This upper limit would have a composition of $PbH_{0.0008}$ to $PbH_{0.03}$ at cathodic current densities of 11.3 to 46 mA. cm.$^{-2}$, the composition being still less hydrogen rich than the $PbH_{0.2}$ of Wells, Roberts and Young (51, 118).

---

* Because of the experimental difficulties associated with obtaining a clean metal surface or with the complete elimination of O_2 from the system {Section 3C (V)}.

** One would expect $S_{(H,T)_{DA}} > S_{H,T} = 7.2 \pm 0.7$ from the existing evidence of additional separation by the diffusion of hydrogen isotopes through metal membranes {see Sections 2D (11a) and (11b)}, at least for Pd and its alloys (145a, 176, 177a).

It is obvious that the water-sealed apparatus used in the overvoltage and capacity work (Figs. 10 and 11), with its plunger tube, flanges and tap cannot be as gas-tight as, for instance, the high vacuum system used by Wells, Roberts and Young (51, 118) in their gas phase adsorption studies with H atoms. The difficulties are equally great with the radiochemical experiments. This highlights one of the main difficulties of electrochemical studies of the adsorption of air-sensitive atoms and also explains our low H coverages and bulk H concentrations compared with those in the work of Wells, Roberts and Young.

Since the H coverage (θ_H) calculated from our capacity measurements and the bulk H concentration (C_0) from our permeation measurements were not measured simultaneously, it is not possible to derive an exact (quantitative) relationship between θ_H and C_0. Moreover, our capacity studies were carried out at low constant cathodic current densities (500 to 800 μA. cm.$^{-2}$) over long periods (several days) of polarisation while the permeation studies were carried out at cathodic current densities of 1 to 46 mA. cm.$^{-2}$ over relatively short periods (12 to 24 hours) of polarisation. In the latter measurements, the permeation of H atoms was detected only above 11.3 mA. cm.$^{-2}$, at least under these conditions. Nevertheless, the experimental conditions for capacity measurements were in general superior to those of the permeation measurements; this is a factor to be borne in mind. It has been mentioned earlier that the bulk

H atom concentration (C_0) is linearly related to the current density applied on the cathodic side. Since each permeation experiment was conducted at constant i for 12 to 24 hours, it may as well be assumed that C_0 increases linearly with -Q. As shown in Figs. 48 to 53, the linear increase of $C_{expt.}$ with $\log_{10}(-Q)$, indicates that the fractional surface coverage with adsorbed H atoms, θ_H, is directly related to $\log_{10}(-Q)$. Then, it is possible to propose an exponential relationship between C_0 and θ_H, namely

$$C_0 \propto \exp.\ (\theta_H) \qquad (4.1)$$

Breger and Gileadi recently proposed such a relationship between C_0 and θ_H for Pd (144) at low $\theta_H \lesssim 0.15$. However, further study, for example <u>simultaneous</u> <u>measurements</u> of θ_H and C_0 on Pb, is required to confirm the tentative relationship suggested in equation (4.1) for the case of lead.

C. Isotopic Separation in Hydrogen Evolution and Membrane Diffusion

The hydrogen-tritium separation factor on the cathodisation side of a metal membrane ($S_{H,T}$) and the over-all separation factors for hydrogen and tritium originating in the catholyte, entering the metal membrane, diffusing through the membrane and being evolved as gas ($S_{(H,T)_D}$) or being ionised into the diffusion side ($S_{(H,T)_{DA}}$) are discussed for several metals, including lead, in Sections 2D (1) and (11). The theoretical predictions and explanations for the experimental separation factors and its variation with overvoltage, time and temperature, discussed in Section 2D are in disagreement because of the different assumptions used by the different workers. Since $S_{H,T}$ may be helpful in distinguishing mechanisms of the h.e.r. and $S_{(H,T)_{DA}}$ could be used to measure the relative rates of diffusion and relative solubilities of hydrogen isotopes, both $S_{H,T}$ and $S_{(H,T)_{DA}}$ for lead will be discussed in this section before coming to the main section dealing with the changes of overvoltage and capacity during prolonged cathodisation.

As mentioned in Section 3C (V), our $S_{H,T} = 7.2 \pm 0.7$ has little or no dependence on $-i$ from 5.85 to 30.5 mA. cm.$^{-2}$, but is close to the value of Bockris and Srinivasan (25), of $S_{H,T} = 6.7 \pm 0.7$ at $-i = 10$ mA. cm.$^{-2}$. This value is consistent with

$S_{H,D} \simeq 3$ to 4 observed on Pb and on Hg (102, 232, 233), metals which are generally held to have a rate-determining discharge step (2.1) followed by rapid ion + atom desorption (2.3) for the h.e.r. (88, 88a).

The separation of hydrogen and tritium during the cathodic gas evolution is believed to involve the following stages:

$$H_2O + H^+_{aq.} = H_3O^+_{aq.} \qquad (4.2)$$

$$HOT + H^+_{aq.} = H_2TO^+_{aq.} \qquad (4.3)$$

$$H_3O^+_{aq.} + e^- + Pb = H_2O + Pb - H_{ads.} \qquad (1.4)$$

$$H_2TO^+_{aq.} + e^- + Pb = H_2O + Pb - T_{ads.} \qquad (4.4)$$

$$H_3O^+_{aq.} + e^- + Pb - H_{ads.} = Pb + H_2 + H_2O \qquad (1.5)$$

$$H_2TO^+_{aq.} + e^- + Pb - H_{ads.} = Pb + HT + H_2O \qquad (4.5)$$

$$H_3O^+_{aq.} + e^- + Pb - T_{ads.} = Pb + HT + H_2O \qquad (4.6)$$

$$H_2TO^+_{aq.} + e^- + Pb - T_{ads.} = Pb + T_2 + H_2O \qquad (4.6a)$$

In acid solution, $S_{H,T}$ on cathodes of Pb (56) and other high overvoltage metals such as Hg (56, 166, 167), Ga (56), Sn (166, 167) and Cd (166, 167), was found to decrease with increase of $-\eta$. This decrease was explained in terms of proton tunnelling (56, 166, 167). However, the proton jump was facilitated by diminishing the activation energy for discharge in one model (the current view of the Bockris School) and by the increased overlap of initial and final state wave functions in the other model (Krishtalik's view), respectively {for fuller account, see Section 2D (1)}.

The idea of proton tunnelling for lead in acid solution on the basis of decrease of $S_{H,T}$ with increase of $-\eta$ is not yet clearly supported. Our $S_{H,T}$ was apparently independent of $-\eta$, for the applied cathodic currents from 5.85 to 30.5 mA. cm.$^{-2}$. Nevertheless, except the first two values of $S_{H,T} = 8.4$ and 8.8 at $-\eta = 1050$ mV., Krishtalik's $S_{H,T} = 6.6 \pm 1$ at various overvoltages between 1100 and 1260 mV. for lead in 0.5 M H_2SO_4 (56) is close to our value in 1 M $HClO_4$.

Until recently, a <u>continuous</u> variation of cathodic separation factors with $-\eta$ had not been observed by Bockris et al. (166) for low and medium overvoltage metals. Now, it is known that $S_{H,D}$ depends on η for transition metals. Thus, Hammerli et al. (170, 234) observed a continuous increase in $S_{H,D}$ from ca. 3.8 at $-\eta = 50$ mV. to a plateau value of ca. 6.2 at $-\eta \gtrsim 300$ mV. on Pt in HCl. Hammerli et al. (172) also observed a continuous decrease, i.e. $S_{H,D}$ decreased from 8.8 ± 0.2 at $-\eta = 300$ mV. to 7.1 ± 0.3 at $-\eta = 610$ mV., on Fe in H_2SO_4. In this latter work, they (172) observed both an increase of $-\eta$ and decrease of $S_{H,D}$ at Fe with the period of electrolysis.

A dependence of $S_{H,D}$ on $\log_{10}(-Q)$ was found in the case of Fe. A time-dependent $S_{H,D}$ was earlier observed on 25% Ag-Pd alloy (173) and on Pt (235). A charge-dependent $S_{H,D}$ was also known for Pd (235). These effects were interpreted in terms of progressive changes in the M-H and M-D bond strength due to changes in the absorbed H and D content in the metal electrode. Since our separation factor experiments on Pb were carried out at constant current densities and it is known from our overvoltage measurements that $-\eta$ decreased with increase of $-Q$, time dependence of $S_{H,T}$ at constant i ($S_{H,T}$ may increase with the period of electrolysis ?) is quite likely from the above evidence.

More work on Pb under ultra-pure conditions is needed to clarify the various dependences of $S_{H,T}$ on η and Q.

On the other hand, the over-all H-T separation factor, $S_{(H,T)_{DA}}$, measured in the present work is more controversial. The value $S_{(H,T)_{DA}} = 0.9 \pm 0.5$ of this work is the same, within experimental error, as previously observed by Muju and Smith (55). In discussing our abnormally low $S_{(H,T)_{DA}}$, the first stages that must be considered are steps (4.2), (4.3), (1.4) and (4.4)* which occur in the catholyte and on the cathodisation surface of the lead foil, respectively. The stages that succeed the steps (1.4) and (4.4) are as follows:

Diffusion of H atoms from cathode to diffusion side of lead (4.7)

---

* see p. 319

Diffusion of T atoms from cathode to diffusion side of lead (4.8)

$$Pb - H_{ads.} + OH^{-}_{aq.} \rightleftharpoons H_2O + e^{-} + Pb \qquad (4.9)$$

$$Pb - T_{ads.} + OH^{-}_{aq.} \rightleftharpoons HOT + e^{-} + Pb \qquad (4.10)$$

Steps (4.7) and (4.8) occur within the metal membrane, while steps (4.9) and (4.10) occur on the diffusion side. A pictorial representation of all such steps except (4.2) and (4.3), has been given in Fig. 4a.*

The fact that $S_{(H,D)_D} > S_{H,D}$ for 25% Ag-Pd (173) and for Fe (172) suggests that the additional separation of H and T for steps (4.7) to (4.10) considered for $S_{(H,T)_{DA}}$ must result in an increased separation factor, i.e. on this basis $S_{(H,T)_{DA}}$ is likely to be larger than $S_{(H,T)}$. Under the chosen potentiostatic conditions (in the present work), the additional separation of H and T for steps (4.7) to (4.10) is determined solely by diffusion steps (4.7) and (4.8), since the separation factor for anodic processes ought to be unity, because atoms of H and T are ionised immediately they reach the surface. Moreover, the H-D separation factor for diffusion processes like steps (4.7) and (4.8), for H and D was found to be 1.6 ± 0.1 for Pd (175, 177) which was interpreted in terms of an equilibrium (solubility) ratio of 2.4 and a diffusivity ratio of 0.7, the product of these quantities being 1.7.

---

* see p. 70

From the facts mentioned above, the result $S_{(H,T)_{DA}} > S_{H,T}$ might be expected also for lead. Experimentally, however, we observe $S_{H,T} >> S_{(H,T)_{DA}}$. The decrease of $S_{(H,T)_{DA}}$ from 0.14 to 0.04 as -i increased from 11.3 to 46 mA. cm.$^{-2}$ observed for lead in this work (if significant) suggests that the solubilities of both H and T increase with -i. Since the diffusivity depends on the bulk concentration (147), the change in separation factor must be due to changes in diffusivity of H and T atoms in the lead membrane. Then, $S_{(H,T)_{DA}} = 0.9 \pm 0.5$ can be explained only if the T atom diffuses 50 to 100 times faster than H atom in lead. This seems unlikely, because H diffuses faster than T in Pd (177a) although D diffuses most rapidly (145a, 176).

We are therefore forced to the conclusion that our low $S_{(H,T)_{DA}}$ arises from experimental difficulties associated {see Section 3C (V)} with the metal surface <u>or</u> with the incomplete elimination of oxygen from the system. A possible explanation (55) is that H and T atoms diffusing through the foil {steps (4.7) and (4.8)} to the diffusion side, may interact with O_2, and enter the solution without undergoing steps (4.9) and (4.10). No error would result from this in the radiochemical counting method, but the electrochemically measured permeation current would be diminished since only those H atoms undergoing ionisation {step (4.9)} would be counted in this manner.

The high background currents observed in this work {tens of μA., see Section 3C (V)} indicate the presence of oxide film on the diffusion side of the lead and hence this suggests an alternative interpretation for our low $S_{(H,T)_{DA}}$ value. Such a conclusion can also be drawn from the recent cathodic H-D separation factor work on oxidised Ni, Pt, Pd and Ag surfaces of Bucur and Stoicovici (236), according to which oxide-covered surfaces of Ni, Pt, Pd and Ag gave lower $S_{H,D}$ than the clean metal surface. The decrease in $S_{H,D}$ on Ni, among other metals, was appreciable. Their $S_{H,D}$ values for chemically passivated, polished and freshly reduced oxide surfaces were 2.2, 6.5 and 7.9, respectively.

Many unwanted processes such as dissolution of Pb, oxide formation, aerial oxidation of H atoms, etc. which proceed simultaneously with the oxidation of H and T atoms on the diffusion side complicate the situation. Further H-T separation factor work on Pb, with both the cathode and diffusion sides properly protected, is required to measure accurate and reliable $S_{(H,T)_{DA}}$ values.

D. Catalysis of Electrolytic Hydrogen Evolution at Lead by Absorbed Atomic Hydrogen

The most important phenomena observed in the present work are the simultaneous linear fall of overvoltage and rise of capacity with the logarithm of the total charge passed in prolonged cathodisation. These phenomena and overshoot hysteresis are discussed and interpreted in this section. Moreover, the relations between b' and b", the decrease of $\Delta H^{\ddagger}_{\eta=0}$ with increase of -Q, and the dependence of b on the capacity are also considered.

Both a linear increase in $C_{expt.}$ and a linear decrease in $-\eta$ with $\log_{10}(-Q)$ and the overshoot hysteresis phenomena were regularly and systematically obtained only on electropolished lead electrodes in properly pre-electrolysed solutions. The possibility that these phenomena are due to anion adsorption, impurities, oxygen evolution at the anode or Pt dissolution from the anode and plating out on the cathode, area increase or cathodic disintegration can, we believe, be discounted for the following reasons:

(i) Kolotyrkin observed a decrease in $-\eta$, an increase in $C_{expt.}$ and overshoot hysteresis in the lower region of overvoltage, the "sulphate-adsorption" region, at porous lead electrodes in aqueous sulphuric acid (9, 10, 12). His explanation was that the effects were due to anion adsorption at low $-\eta$ values, desorption of SO_4^{--} being demonstrated at higher overvoltages. The present phenomena, however, are not caused by anion adsorption because the measurements were all carried out in $HClO_4$ at relatively high current densities. Moreover, the effects observed in the present work are more marked the higher the cathodic current density, i.e. the more negative the electrode potential. The observed dependence of overshoot hysteresis on -Q and the linear variation of both overvoltage and capacity with $\log_{10}(-Q)$ cannot be explained in terms of anion adsorption, which is a reversible phenomenon, whereas the present observations seem irreversible.

(ii) The presence of impurities such as O_2, Pb^{++} ions or other metal ions, in solution either caused irregular behaviour or complete reversal of the above-mentioned effects. No overshoot hysteresis was observed under such experimental conditions. Moreover, initial overvoltages were low and initial capacities were usually high (at least at high current densities) and very high in solutions containing Pb^{++} ions. Overvoltages increased in all such cases, but $C_{expt.}$ decreased to "normal" values in solutions containing Pb^{++} ions while $C_{expt.}$ increased slightly or remained constant in unpre-electrolysed solution.

In Section 3A (VIc), it has been suggested that the presence of an oxide film on a scraped electrode caused this to show a very slow decrease of $-\eta$ and less frequent overshoot hysteresis during the period of cathodisation up to -Q = 70 coulombs (Fig. 19).

Also, the negligible difference between experiments with electropolished electrodes in properly pre-electrolysed $HClO_4$, <u>with</u> or <u>without</u> charcoal cleaning disproves that the formation of a Pb-C matrix (206a), if it occurred, is a relevant factor leading to the decrease in $-\eta$, increase in $C_{expt.}$ and overshoot hysteresis {see Section 3A (Vllc)}.

The above arguments indicate that both the linear decrease in $-\eta$ and the linear increase in $C_{expt.}$ with $\log_{10}(-Q)$ and overshoot hysteresis are not associated with the presence of an oxide film or impurities such as O_2, Pb^{++}, other metal ions or carbon.

(iii) Other possibilities such as oxygen evolution at the anode and Pt dissolution from the anode and plating out on the cathode were less likely to interfere because anode and cathode compartments were separated by one or two sintered Pyrex discs. Moreover, oxygen evolved in the anode compartment should have been largely swept out by the stream of purified hydrogen passing through that compartment. The large anode (of area 110 $cm.^2$, which is 60 to 100 times the area of the working lead cathode) used in this work minimises such anodic processes by increasing the surface available for the anodic oxidation of H_2.

(iv) An increase in surface area was also considered as a possible explanation for the fall of $-\eta$ and increase in $C_{expt.}$ with -Q. If this explanation were to be accepted, then at constant η, the apparent cathodic current density must increase linearly with the electrode capacity. However, we have observed that $C_{expt.}$ increased linearly with $\log_{10}(-i)$ {i.e. the same as a decrease in $-\eta$ at constant i}, both at constant η. Moreover, Palm and Past (35) have observed an insignificant increase in capacity of the electrode (about 1 to 2 μF. cm.$^{-2}$) for the break-up (roughening) of a lead surface in acid solutions.

Results of electrodes studied in solutions, pre-electrolysed at too high current densities, do not support this explanation, i.e. the fall of $-\eta$ and increase in $C_{expt.}$ with $-Q$ in terms of increase in surface area. In such solutions, the Pb^{++} ion concentration was ca. 10^{-6} M {see Section 3A (11c)}. Initially low overvoltages increased with extended cathodisation. Simultaneously, $C_{expt.}$ increased with $-Q$ at current densities < 4.8 mA. cm.$^{-2}$ and decreased at 4.8 mA. cm.$^{-2}$ and higher current densities. Initial capacities at higher current densities are very high (up to 200 μF. cm.$^{-2}$) and could be accounted for by the presence of adsorbed Pb atoms* on the

---

* The observed high capacities may be accounted for by specific adsorption of Pb^{++} ions at the Pb surface. The increase in capacity and higher α (=0.8) at low overvoltages observed as the Pb^{++} concentration increased (from 0.0027 to 0.5 M) by Hampson and Larkin (221) supports this view.

metal surface if the initial adsorbed H atom concentration is assumed to be small. The corresponding decrease in $C_{expt.}$ to normal values (in a relatively short period and requiring the passage of only ca. 200 coulombs, in comparison with the continuous increase in $C_{expt.}$ over long periods of cathodisation up to $\geqslant 800$ coulombs in experiments thought to be satisfactory), may be explained in terms of a decrease in concentration of Pb^{++} ions in solution and in terms of the characteristic process, i.e. the equilibration process* at solid electrodes taking place on the lead surface in the presence of common ions in the electrolyte, as suggested by Hampson and Larkin (237) for Pb and other solid metals (Ag, Sn, Cd and Zn). As the equilibration process proceeds, the adsorbed Pb atoms formed from the reduction of Pb^{++} ions move to low or lower energy sites (i.e. stable sites), thereby decreasing the concentration of adsorbed Pb atoms until the surface Pb atom population is in equilibrium with the Pb^{++} ions in the solution. That the equilibration process occurs rapidly at room temperature is evidence for the faster surface diffusion of Pb atoms at 25°C (237), thereby reducing surface roughness. The small increase in $C_{expt.}$ with $-Q$ to normal values at $-i < 4.8$ mA. cm.$^{-2}$ could be due to an increase in surface area of the electrode. However, the magnitude of such an increase due to increase in surface area is unlikely to be

---

* The equilibration process is the removal of high energy sites on the electrode surface as the electrode surface energy is reduced to a minimum.

very great (237).

Therefore, it is unlikely especially for metals like lead (for which the surface diffusion of lead atoms is extremely fast at $25^{o}C$) that such a large increase in $C_{expt.}$ and decrease in $-\eta$, e.g. in F10 at $-i = 22$ mA. cm.$^{-2}$, $C_{expt.}$ rose from 31.6 to 106 μF. cm.$^{-2}$ while $-\eta$ decreased from 1051 to 980 mV., during the passage of an additional 416 coulombs at 505 μA. cm.$^{-2}$ (Table 25) could be due to increase in surface area.

(v) The steep fall of overvoltage (b' = 460 to 685 mV.) and simultaneous decrease in $C_{expt.}$, in contrast to the usual increase of $C_{expt.}$ with $-Q$ (Figs. 49 and 51) are thought to be associated with cathodic disintegration of lead. Therefore, cathodic disintegration cannot provide an explanation for both a linear decrease in $-\eta$ (b' = 40 to 160 mV.) and a linear increase in $C_{expt.}$ with $\log_{10}(-Q)$.

Thus, our important findings, i.e. both decrease in $-\eta$ and increase in $C_{expt.}$ with $\log_{10}(-Q)$ and overshoot hysteresis, are regarded as the true behaviour of lead + hydrogen + hydronium ion system, because of the use in the work of proven methods of attaining high surface cleanliness, namely electropolishing, cathodic pre-electrolysis at low current densities and continuous adsorptive cleaning with activated carbon. All of these findings can be interpreted with the existing knowledge of H surface coverage, bulk H atom concentration and diffusivity of H atoms within the metal (see Section 4B for a complete account). They must be due to the same phenomenon, i.e. the accumulation of H atoms in the bulk of the metal during cathodic electrolysis and its redistribution when the current was changed.

Firstly, let us consider overshoot hysteresis.* As mentioned in Section 3A (V11d), the extent of overshoot hysteresis increases with the magnitude of current step and decreases as -Q increases. Moreover, the extent of overshoot hysteresis in a given step-change of current decreases as the temperature rises.

Overshoot hysteresis seems to require the operation of two distinguishable but related processes which control the electrode state--one rapidly self-adjusting in response to an imposed change of current density, the other sluggishly following, causing a partial reversal of the initial adjustment. It therefore seems possible to describe the behaviour of lead in the following way.

The bulk of the metal acts as a "sink-reservoir" for H atoms, with a rate-restricted access to and from the surface. The increase in surface coverage, caused by a step-rise of current or decrease in temperature, creates or enhances a step of chemical potential of H atoms, downward to the metal phase. Atoms move across the interface to annul this step, and establish or increase a concentration gradient of H atoms just beneath the metal surface, this initiates or hastens inward diffusion. Recently, Roberts and Young (118) have

---

* P.D. Marsden and J.B. Senior have observed similar overshoot hysteresis on mercurised Pt and pure Au, respectively {see p.447 in ref.(27)}.

shown that this type of uptake is, indeed, very fast at room temperature. H atoms beneath the metal surface diffuse with a diffusivity of 10^{-7} cm.^{2} sec.$^{-1}$ (147) into the centre of the metal until H atoms are uniformly distributed in the bulk metal. This occurs when lead hydride has a composition $PbH'_{0.2}$ at room temperature, if Roberts and Young's gas phase measurements (118) are reliable. All these above-mentioned linked processes, at first rapidly and then more slowly, reduce the inequalities and gradients which called them into play, the surface hydrogen coverage (perhaps asymptotically) and bulk H concentration (perhaps linearly) changing to new steady-state values. Similar events, in reverse, follow a step-fall of current. As long as cathodisation is continued, the comparatively large sink-reservoir gradually fills up with hydrogen, and the steady-state θ_H and C_0 values slowly increase.

The linear relationships of $-\eta$ versus $\log_{10} t$ during overshoot hysteresis may also be used to follow the rate of penetration of H atoms into lead and diffusion of H atom into the centre of the metal phase and vice versa. The higher is the value of slope, the greater is the rate of diffusion. The features of these slopes are rather interesting. For <u>increasing currents</u> at constant temperature:

(i) the slopes tend to decrease as $-Q$ increases,

(ii) the larger the current ratio (at the same -Q), the larger is the slope,

(iii) the slope appears to be higher, the higher the final current density.

The first two features, i.e. (i) and (ii), can be explained in terms of change in the concentration gradient of H atoms between the surface and the centre of the bulk metal. The larger the current ratio, the greater is the concentration gradient of H atoms and hence the larger is the magnitude of the $-\eta$ versus $\log_{10} t$ slope. The gradual reduction of the concentration gradient of atoms with the increase of -Q, as the bulk fills up, must decrease the magnitude of the $-\eta$ versus $\log_{10} t$ slope. The feature (iii) is somewhat complicated and may be explained as follows. The rate of diffusion depends on the diffusion constant for H as well as on the concentration gradient. Since D for H atoms in lead increases (147) with the applied current density (presumably because of a dependence on the bulk hydrogen content of the metal) this is likely to cause the rate of diffusion of H atoms to be greater at higher mean surface H concentrations, i.e. increases the magnitude of the $-\eta$ versus $\log_{10} t$ slope, as in (iii).

Slopes for decreasing currents in a step-change at constant temperature may be similarly explained. However, further explanation is necessary to account for slopes that are independent of -Q and of the magnitude of the initial and final currents in a step-change of the same current ratio. The decrease in surface coverage of H atoms assumed to be caused by a step-fall of current, enhances the <u>out-diffusion</u> of H atoms (which may be fast) from bulk to surface. The concentration of H atoms just beneath the surface is lowered initially and thus creates a condition for H atoms to move away from the centre to the surface. There may be a time-lag for the redistribution of H atoms from the previously existing concentration gradient (corresponding to the steady-state before the current change), in which the bulk H atom concentration decreases continuously from the surface region to the centre of the metal. The actual situation is very complicated.

Finally, the effect of temperature on these slopes, i.e. decreasing the magnitude of the slope at higher temperatures for the same current ratio at approximately the same Q, could be accounted for by the likely decrease in coverage θ_H with increase of temperature. The hydrogen coverage decreases with increase of temperature in gas phase studies because of the faster desorption rate of adsorbed H atoms at higher temperatures (118). The decrease in stability of lead hydride ($PbH_{0.2}$ at $0^{o}C \rightarrow PbH_{0.09}$ at $190^{o}C$) at higher temperatures may also help to explain this. Therefore, it is likely that the concentration gradient of H atoms from the surface to the centre of the metal may decrease as the temperature increases, resulting in a decline in the H atom diffusion rate and hence a decrease in slope as the temperature increases. However, it must be stressed that the dependence of the rate of diffusion on the temperature is presumably because of a dependence on θ_H, rather than a decrease of D itself with rising temperature.

Overshoot hysteresis during increasing currents is most interesting because this closely resembles the continuous fall of overvoltage when the electrode is changed from zero to a finite current. However, one important difference exists between the two phenomena: overshoot hysteresis and fall of overvoltage may be considered as the short-term "reversible" and long-term "irreversible" parts, respectively. Therefore, the above interpretation of overshoot hysteresis can be extended to include the over-all decrease of overvoltage as -Q increases. This must involve the gradual saturation of the bulk of the electrode with atomic hydrogen and a corresponding increase in the surface coverage, commencing at $\theta_H = 0$. As mentioned in Section 2C (1V), the variation of $-\eta$ with time of electrolysis during the h.e.r. has been observed for many metals: Pb (26, 27), Pt (148, 148a), Fe (172) and Pd (148b). Both increase in $-\eta$ (on Pd, Pt, Fe) and decrease in $-\eta$ (on Pb) with time have been interpreted in terms of a change in the properties of the electrode due to hydrogen absorption.

The facts that $-\eta$ decreases and $C_{expt.}$ increases linearly with $\log_{10}(-Q)$ in all satisfactory experiments suggests that both variations are caused by the same phenomenon, which we take to be a gradual increase in both the H surface coverage and the bulk H concentration. In order to understand this on a more fundamental basis, we must obtain relations between the increase of cathodic current density and capacity both at constant potential.

Ives and Smith (26, 27) deduced a relationship between the steady-state overvoltages at different times and the total cathodic charge passed, from the observed linear decrease in $-\eta$ with $\log_{10}(-Q)$. For a constant current density, their relationship between $-\eta$ and $-Q$ is:

$$\eta = \eta_1 + b' \log_{10}(-Q) \qquad (4.11)$$

where b' (slope) and η_1 (initial overvoltage) are constants which depend on the current density. The dependence of b' on the cathodic current density was reported by Smith (27) in one case: after 15 days of cathodisation ($-Q \simeq 800$ coulombs) of electrode XIIb the overvoltage at 25 μA. fell by 160 mV. whereas at 1500 μA. it fell by 300 mV. His b' values at 1500 μA. were 50, 101 and 340 mV. for $-Q < 8$, $8 < -Q < 700$ and $-Q > 700$ coulombs, respectively. On the basis of the most probable value of b' = 101 mV. (middle region of Q) at 1500 μA., the calculated value of b' is ca. 55 mV. at 25 μA. for $8 < -Q < 700$ coulombs. A linear relationship between $-\eta$ and $\log_{10}(-Q)$, following equation (4.11) has been broadly confirmed in this work (Figs. 29, 30 and 31) with values of b' ranging from 40 to 90 mV. for $-Q \lesssim 100$ coulombs and 150 to 685 mV. for $-Q \gtrsim 100$ coulombs, respectively.

Nothing can be said about the dependence of b' on current density in the present work (Figs. 29, 30 and 31), because most of the experiments were carried out essentially at a single current density (500 to 800 μA. cm.$^{-2}$). Also this is likely to be of doubtful value until really reproducible overvoltage-charge relations are obtained on different electrodes. However, Tafel runs at different periods of cathodisation (i.e. at different -Q values) show that the fall of $-\eta$ is greater at higher current density, e.g. see Figs. 24 and 25, as Smith also found to be the case.

Recently, a linear relationship similar to equation (4.11) was observed with Fe foils cathodised in 1 M H_2SO_4 - 10% D_2O (172), however, $-\eta$ increased with $\log_{10}(-Q)$, an increase that was attributed to an increase in surface coverage θ_H and bulk hydrogen content of the Fe electrode.

It was shown earlier in Figs. 48 to 53 that $C_{expt.}$ at a given η increased linearly with $\log_{10}(-Q)$ in a similar manner to the relation {equation (4.11)} between $-\eta$ and $\log_{10}(-Q)$. Then, at a given η, $C_{expt.}$ and -Q are related as

$$C_{expt.} = C_1 + b'' \log_{10}(-Q) \qquad (4.12)$$

where b" (slope) and C_1 (initial capacity) are constants which may depend on η. The slopes, b", ranging from 1.9 to 85 μF. cm.$^{-2}$ per decade of -Q, are either indistinguishable within experimental error as η is changed (Fig. 51), or there is a trend to higher values as $-\eta$ is increased, e.g. Fig. 48.

Some sort of parallel variation of both the slopes b' and b" has been observed in this work. These show strikingly that when b' is large so is b" and when b' changes value so does b". If b' and b" are indicative of the rate of interaction of H atoms with lead, a greater rate of penetration of H atoms must be occurring at higher values of these slopes. The greatest rates of penetration of H atoms were observed only after electrodes were sufficiently charged, e.g. at $-Q = 200$ coulombs for experiment F10 (Fig. 48), b' changed from 38 to 157 mV. $(\text{decade})^{-1}$, while b" at $-\eta = 920$ mV. changed from 6.3 to 85 μF. $\text{cm.}^{-2}(\text{decade})^{-1}$. The increase of b" from 16.5 μF. $\text{cm.}^{-2}(\text{decade})^{-1}$ at $-\eta = 700$ mV. to 85 μF. $\text{cm.}^{-2}(\text{decade})^{-1}$ at $-\eta = 920$ mV., both at $-Q \simeq 200$ coulombs (Fig. 48) may be interpreted in terms of increase in the rate of growth of surface coverage θ_H at more negative potentials. If the slope b' changed to very large values, e.g. in the range 460 to 685 mV., a negative b" (i.e. $C_{\text{expt.}}$ decreased, in contrast to the usual increase) was observed (Figs. 49 and 51). At this stage, the approach of θ_H to very high values (PbH or PbH_2 ?) seems to be a condition favourable to the onset of "avalanche penetration" and cathodic disintegration.

At constant η it follows intuitively from equation (4.11) that

$$\log_{10}(-i) = \log_{10}(-i_1) + s' \log_{10}(-Q) \qquad (4.13)$$

where the cathodic current density initially is $-i_1$ and at time t is $-i$. s' is a constant which probably depends on η and should be relatable to the constant b' of equation (4.11). Combining equations (4.12) and (4.13) for the same value of Q, i.e. substituting

$$\log_{10}(-Q) = \frac{C_{\text{expt.}} - C_1}{b''}$$

from equation (4.12) in equation (4.13)

$$\log_{10}(-i) = \log_{10}(-i_1) + \frac{s'}{b''}(C_{\text{expt.}} - C_1)$$

$$\log_{10}(-i) = \frac{s'}{b''} C_{\text{expt.}} + \log_{10}(-i_1) - \frac{s'}{b''} C_1$$

i.e. $$\log_{10}(-i) = \frac{s'}{b''} C_{\text{expt.}} + s'' \qquad (4.14)$$

where $s'' = \log_{10}(-i_1) - (s'C_1/b'')$ is a new constant. A plot of $\log_{10}(-i)$ versus $C_{\text{expt.}}$ at the same constant η, but at different periods of cathodisation should be linear with positive slope (s'/b''). Such plots have already been made in Figs. 54, 55 and 56.

The relationship between s' and b' is complicated, but some approach to it must be attempted. Tafel equations, initially and at time t can be written as

$$\log_{10}(-i_1) = \log_{10}(i_{10}) + \frac{\eta_1}{b_1} \qquad (4.15)$$

$$\log_{10}(-i) = \log_{10}(i_0) + \frac{\eta}{b} \qquad (4.16)$$

where i_{10} and i_0 are exchange current densities, initially and at time t, respectively. b_1 and b are Tafel slopes initially and at time t, respectively. On substituting equations (4.15) and (4.16) for $\log_{10}(-i_1)$ and $\log_{10}(-i)$ in equation (4.13) we get

$$\log_{10}(i_0) + \frac{\eta}{b} = \log_{10}(i_{10}) + \frac{\eta_1}{b_1} + s' \log_{10}(-Q)$$

$$\frac{\eta}{b} = \frac{\eta_1}{b_1} + \log_{10}\left[\frac{(i_{10})}{(i_0)}\right] + s' \log_{10}(-Q) \qquad (4.17)$$

Assuming $b_1 = b$ (the most commonly observed slope was 110 mV.) and multiplying equation (4.17) throughout by b, we can write

$$\eta = \eta_1 + b \log_{10}\left[\frac{(i_{10})}{(i_0)}\right] + s'b \log_{10}(-Q) \qquad (4.18)$$

Equations (4.11) and (4.18) are identical if $i_{10} = i_0$ and $s'b = b'$. These relations can be checked by obtaining s' from experimental slopes (b''/s'), of $C_{expt.}$ versus $\log_{10}(-i)$ {Figs. 54, 55 and 56} and b" from the slope of $C_{expt.}$ versus $\log_{10}(-Q)$ {Figs. 48 to 53 and Table 31}. Then, b' calculated using the relation $b' = s'b$ {with b = 110 mV. assumed} may be compared with the experimental slopes b', of $-\eta$ versus $\log_{10}(-Q)$ {equation (4.11) and Figs. 30 and 31}, as shown in Table 41.

TABLE 41. COMPARISON OF COEFFICIENT b' OF EQUATION (4.11) OBTAINED FROM FIGS. 30 AND 31 WITH THAT CALCULATED FROM RELATION b' = s'b USING s' FROM FIGS. 54, 55 AND 56.

$-\eta$/mV.	Experiment number	b"=slope of $C_{expt.}$ versus $\log_{10}(-Q)/\mu F.cm.^{-2}$	(b"/s')=slope of $C_{expt.}$ versus $\log_{10}(-i)/\mu F.cm.^{-2}$	s' (from columns 3 and 4)	b'=s'b, calculated (b=110 mV. assumed) from s'/mV.	b'=slope of $-\eta$ versus $\log_{10}(-Q)$/mV.
850	F10	4.8	34	0.14	15.4	38
	F10	40.5	34	1.19	131	157
	R4a"	6.6	3.8	1.73	190	62
	R4b	4.2	3.8	1.1	122	43
1000	R4b	6.7	12.8	0.52	57	43
	R5b	11.6	14.2	0.85	93	89
	R5c	37	9.4	3.94	432	278
	R5c	4.2	3.2	1.31	144	85
	R5d	7.4	4	1.85	204	170
1100	R4b	8	17	0.47	52	43
	R5b	12	13.8	0.87	96	89
	R5c	28	7.6	3.68	405	278
	R5c	20	9.4	2.13	234	85
	R5d	18	8.4	2.14	236	170

The values of b' in columns 6 and 7 of Table 41 differ slightly in some cases (with values 131 and 157 for F10 at $-\eta = 850$ mV., 57 and 43 for R4b at $-\eta = 1000$ mV., 93 and 89 for R5b at $-\eta = 1000$ mV., 204 and 170 for R5d at $-\eta = 1000$ mV., 52 and 43 for R4b at $-\eta = 1100$ mV., 96 and 89 for R5b at $-\eta = 1100$ mV.). However, in other cases, b' values in column 6 (s'b) are generally greater than in column 7. This may suggest that $i_0 \neq i_{10}$ in equation (4.18), i.e. the exchange current density may increase with the cathodic charging. The increase in catalytic activity for h.e.r. on lead with continued cathodisation may either be due to an increase of i_0 or a decrease of b or both. The present evidence, from Table 41, is that increases of i_0 are responsible for the increase in catalytic activity, rather than decreases of b. Unfortunately, the exchange current density cannot be determined accurately because of the long extrapolation on metals like lead. Therefore, it is difficult to obtain an exact relationship between s' and b'.

We interpret the linear relation between $\log_{10}(-i)$ and $C_{expt.}$ to mean that an increase of cathodic current occurs because of changes in the electrode, which we deduce to be bulk rather than surface changes. Let us consider the alternative explanations available.

If the reaction

$$H_3O^+_{aq.} + e^- + Pb\text{-}H_{ads.} = Pb + H_2 + H_2O \qquad (1.5)$$

were rate limiting on Pb, then, at constant η we should have

$$-i \text{ (h.e.r. rate)} \propto \theta_H \tag{4.19}$$

But our results do not imply such a relation. On substituting $C_{ps} = C_{expt.} - C$ in equation (4.14) and rewriting it with the assumption that C is a constant as

$$\log_{10}(-i) \propto C_{ps} \tag{4.20}$$

and also

$$\log_{10}(-i) \propto \theta_H \tag{4.21}$$

since $C_{ps} \propto \theta_H$.

Equation (4.21) implies that

$$-i \propto \exp.(\theta_H) \tag{4.22}$$

but not $-i \propto \theta_H$, as required in equation (4.19) if desorption were rate limiting.

It is the usually held view that the step

$$H_3O^+_{aq.} + e^- + Pb \rightleftharpoons H_2O + Pb\text{-}H_{ads.} \tag{1.4}$$

is rate determining on Pb (86, 88a), since Pb belongs to the group of high overvoltage metals such as Hg, Cd, Sn, Tl, Zn, Ga, In, etc.

Moreover, the Tafel slope, b = 110 ± 10 mV., and H-T separation factor, $S_{(H,T)} = 7.2 \pm 0.7$,* obtained in this work suggests that the discharge step (1.4) may be slow.

Since the H_3O^+ discharge step (1.4) is thought to be rate-limiting at lead, the observed decrease of $-\eta$ {equivalent increase in $\log_{10}(-i)$} must be due to catalysis of this reaction.

The calculated values of $\Delta H^{\ddagger}_{\eta=0} = 9.3 \pm 1.3$ k.cal.g.ion^{-1} at $-Q \gtrsim 2600$ coulombs (in this work) and $\Delta H^{\ddagger}_{\eta=0} = 15.6 \pm 2$ k.cal.g.ion^{-1} at $-Q \approx 600 - 700$ coulombs {from Smith's data (27)} for Pb in $HClO_4$ reported in Section 3A (V11b) are lower than the 20 k.cal.g.ion^{-1} for Pb in $HClO_4$ observed by Piontelli and Bicelli (22). The last value is close to that of Hg in HCl {21.7 k.cal.g.ion^{-1} (112a)} for which the discharge step (1.4) is also considered to be the r.d.s. Therefore, the decrease in the enthalpy of activation with -Q may be evidence for the enhancement of H_3O^+ discharge during the h.e.r. on Pb as -Q increases. More work is needed to establish this as a fact.

Hitherto, following Dolin and Ershler (238) it has been assumed that the rate of H_3O^+ ion discharge increases with $(1 - \theta_H)$, the fraction of unoccupied sites. This means that an increase of θ_H at constant η might be expected to diminish the rate of H_3O^+ ion discharge,

---

* According to Srinivasan, Bockris and Reddy (25, 86), this value corresponds to rate-limiting discharge followed by fast atom + ion desorption.

step (1.4), which would therefore be expected to fall as the density of unoccupied adsorption sites is decreased, <u>if this were the only factor at work</u>. Therefore, it is proposed (26, 27) that acceleration of the r.d.s. (1.4) is caused by H atoms in the bulk. Until recently, the solubility of H in Pb at 25°C was thought to be negligible but now appears to be 10^{-2} g. atom cm.$^{-3}$ from gas phase adsorption studies (118) and 10^{-5} g. atom cm.$^{-3}$ from our own permeation measurements (see Section 4B). If the exponential relationship between θ_H and C_0 as proposed in Section 4B:

$$C_0 \propto \exp.(\theta_H) \qquad (4.1)$$

is accepted, then the equation (4.22) becomes

$$-i \propto C_0 \qquad (4.23)$$

and

$$\log_{10}(-i) \propto \log_{10}(C_0) \qquad (4.24)$$

i.e.

$$\log_{10}(-i) \propto \log_{10}(-Q) \qquad (4.25)$$

at constant η. This simple relationship is intelligible if the catalysis of H_3O^+ discharge is directly proportional to the bulk H atom concentration, C_0, which it is argued above, will itself be directly proportional to -Q.

This catalytic effect appears to operate through donation of electrons to the metallic bond by the dissolved H atoms, as earlier postulated by Ives and Smith (26, 27). As mentioned in Section 2C (1V), the dissolved hydrogen in metals is probably ionised to interstitial $H^+ + e^-$, the latter entering the electron gas of the metal. This "screened proton" model (177b) has been used to discuss the behaviour of H in metals such as Ni (239), Pt (240) and Fe (172); additional electrons participating in metallic bonding, could contribute to the free electron density. This is mostly applicable to transition metals with high electron state densities near the Fermi energy. Whether such a possibility exists in the case of Pb depends on its detailed band structure.

The argument that H atoms entering the lead lattice and contributing electrons to the metallic conduction band, causing an enhancement of catalytic properties of the metal with respect to the electrochemical h.e.r., could be supported by evidence of the electronic band structure, worked out by Anderson and Gold (241) in 1965. This band structure predicts a completely filled first Brillouin zone (2 electrons per atom), with holes in the second Brillouin zone (0.375 holes per atom), electrons in the third Brillouin zone (0.393 electrons per atom) and a completely empty fourth Brillouin zone. The total occupied volume in the first, second and third Brillouin zones thus corresponds to

$2 + (2 - 0.375) + 0.393 = 4.02 \pm 0.02$ conduction electrons per atom, in agreement with the expectation of four per atom for a Group IV metal.

Fig. 64 represents the contributions from the various Brillouin zones to the total density of states curve for energies near Fermi level (E_f) and also the individual contributions from the second, third and fourth Brillouin zones, respectively. The density of states here is lower than in transition metals, but still high enough to account for an increase in electrode activity of 10^2 to 10^3 fold as observed in our work. It can be seen in Fig. 64 that the density of states of the third Brillouin zone is twice that of the second Brillouin zone at the Fermi level. Therefore, it is possible for us to discuss the behaviour of a dilute alloy of hydrogen in lead in terms of the density of donated electrons in the third Brillouin zone, which should increase at about double the rate that the density of holes in the second Brillouin zone decreases. This should enhance the electron availability for the H_3O^+ ion discharge step (1.4) of h.e.r. on lead.

Alternatively, specific adsorption of H_3O^+ ions might explain the increase in rate of H_3O^+ ion discharge (1.4), in accordance with equation (4.14). According to Krishtalik (112), as mentioned in Section 2A (lV), only H_3O^+ ions which are in direct contact with the electrode can discharge and this is only a small fraction of the total

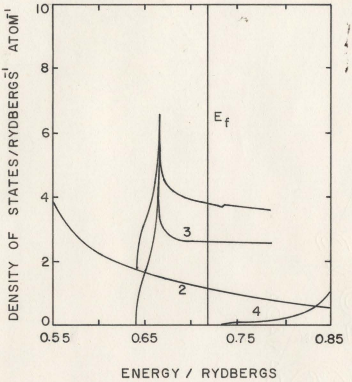

Fig. 64. CURVE OF TOTAL DENSITY OF STATES AGAINST ENERGY, NEAR THE FERMI LEVEL (E_f) GIVEN BY ANDERSON AND GOLD (241). THE INDIVIDUAL CONTRIBUTIONS FROM THE SECOND, THIRD AND FOURTH BRILLOUIN ZONES ARE ALSO SHOWN NUMBERED.

number in the double layer. Therefore an increase in concentration of specifically adsorbed H_3O^+ ions must increase the rate of the H_3O^+ ion discharge step (1.4). Specific adsorption of H_3O^+ ions may be indicated by the decreases in Tafel slope ($\alpha > 0.5$) observed to occur as $-\eta$ fell and $C_{expt.}$ increased. High values of the transfer coefficient ($\alpha > 0.5$) are generally held to be due to specific adsorption of reactant species (26, 27) .

The suggestion that the specifically adsorbed H_3O^+ ions on lead increase its catalytic activity for the H_3O^+ ion discharge step (1.4) cannot be regarded as proven because:

(i) The continuous decrease of Tafel slope in this work was only to ca. 90 mV., in contrast to the decrease to 70 mV. in previous work by Ives and Smith (26, 27).

(ii) The $S_{H,T} = 7.2 \pm 0.7$ independent of $-i$ from 5.85 to 30.5 mA. cm.$^{-2}$ (admittedly, a rather small range of i) does not agree with the report of Krishtalik (56) which he supposed to indicate the closer approach of H_3O^+ ions to the electrode (i.e. concentration of H_3O^+ ions in direct contact with the electrode increasing) with increase of negative potential (112).

E. Concluding Remarks

The surface hydrogen coverage, θ_H, and bulk H concentration, C_0, are not negligible, but can be measured. Summing up the evidence about the mechanism of hydrogen evolution at lead in acid solution, it may be concluded that discharge is probably rate-determining, followed by atom + ion desorption. The rate of discharge increases with the charge passed in cathodic electrolysis, interpreted here as proportional to the hydrogen content of the metal.

As the h.e.r. proceeds at constant -i, a constant fraction of H atoms enter the lattice, resulting in an increased electron availability and enhancement of electron transfer reactions. This hypothesis could perhaps be tested by resistivity measurements during electrolysis in a solution containing H_3O^+ ions. Such a test is not likely to be conclusive, however (242). We certainly cannot explain the enhancement of h.e.r. in terms of the Heyrovsky reaction or simply as an effect of increasing θ_H on the Volmer reaction.

However, if θ_H grows to very high values (PbH or PbH_2 ?), after cathodisation at very high current densities or over a long period at low current densities, the interaction of H atoms with lead becomes maximal. This leads to the onset of avalanche penetration and cathodic disintegration.

Further work must involve determination of θ_H and C_0, simultaneously as a function of -Q by combined capacity and permeation measurements if these are feasible. These measurements should be carried out over a wide range of cathodic currents (or potentials) under ultrapure conditions with both the cathodic and diffusion sides of the foil properly protected against oxidation. $S_{H,T}$ and $S_{(H,T)_{DA}}$ also deserve re-investigation under similarly rigorous experimental conditions. Moreover, the study of the time- and potential-dependence of $S_{H,T}$ and $S_{(H,T)_{DA}}$ might prove very interesting. Determination of the Pb^{++} ion concentrations in solution before and during the very rapid fall of $-\eta$ and decrease in capacity (in contrast to the normal increase of capacity) might provide further proof of cathodic disintegration. Finally, determination of exchange current density, transfer coefficient and enthalpy of activation as a function of $-Q$ is essential to support the hypothesis of the increase in catalytic activity of lead after prolonged cathodisation.

REFERENCES

1. J. Tafel, *Z. Phys. Chem.*, 1905, *50*, 641.
2. S. Glasstone, *J. Chem. Soc.*, 1923, *123*, 1745, 2926; 1924, *125*, 250, 2414.
3. E. Baars, *Handb. Phys.*, 1928, *13*, 564.
4. T. Erdey-Gruz and H. Wick, *Z. Phys. Chem.*, 1932, *A162*, 53.
5. B.N. Kabanov and Z.A. Jofa, *Acta Physicochim. U.R.S.S.*, 1939, *10*, 617.
6. B.N. Kabanov, Z.A. Jofa, S. Filippov, L. Vanyukova and A. Prokofeva, *Zhur. Fiz. Khim.*, 1939, *13*, 341.
7. Z.A. Jofa, *Zhur. Fiz. Khim.*, 1945, *19*, 117.
8. L. Vanyukova and B.N. Kabanov, *Zhur. Fiz. Khim.*, 1940, *14*, 1620.
9. Ya. M. Kolotyrkin and A.N. Frumkin, *Zhur. Fiz. Khim.*, 1941, *15*, 346.
10. Ya. M. Kolotyrkin, *Zhur. Fiz. Khim.*, 1946, *20*, 667.
11. Ya. M. Kolotyrkin and N. Bune, *Zhur. Fiz. Khim.*, 1947, *21*, 581.
12. Ya. M. Kolotyrkin, *C.I.T.C.E. Rept.*, Nineth Mtg. (1957), Butterworths, London, 1959, 406.
13. Ya. M. Kolotyrkin and L. Medvedeva, *Zhur. Fiz. Khim.*, 1951, *25*, 1355.
14. A. Hickling and F.W. Salt, *Trans. Faraday Soc.*, 1940, *36*, 1226; 1941, *37*, 451.

15. J.O'M. Bockris, Trans. Faraday Soc., 1947, 43, 417.

16. A.M. Azzam, Ph.D. Thesis, London, 1949.

17. J.O'M. Bockris and A.M. Azzam, Trans. Faraday Soc., 1952, 48, 145.

18. P. Ruetschi and B.D. Cahan, J. Electrochem. Soc., 1957, 104, 406.

19. M.I. Gillibrand and G.R. Lomax, Trans. Faraday Soc., 1959, 55, 643.

20. I.M. Tordesillas and L.P. Bicelli, Z. Elektrochem., 1959, 63, 1049.

21. L.P. Bicelli and B. Rivolta, U.S. Dept. Com., Office Tech. Serv., P.B. Rept., 1960, 161, 801.

22. R. Piontelli and L.P. Bicelli, Bull. Nat. Inst. Sci. India, 1965, No. 29, 80.

23. L.P. Bicelli and C. Romagnani, Ric. Soc., Rend., 1965, A8(6), 1345.

24. R. Piontelli, B. Rivolta and M. Rossi, Atti. Accad. Sci. Torino, Cl. Sci. Fis., 1965, Mat. Nat. 99, 199.

25. J. O'M. Bockris and S. Srinivasan, Electrochim. Acta, 1964, 9, 31.

26. D.J.G. Ives and F.R. Smith, Trans. Faraday Soc., 1967, 63, 217.

27. F.R. Smith, Ph.D. Thesis, London, 1964.

28. I.A. Bagotskaya and A.I. Oshe, "Soviet Electrochemistry", Consultants Bureau, New York, Vol. 1, 1961, 117, 134.

29. T. Borisova and B. Ershler, Zhur. Fiz. Khim., 1950, 24, 337.

30. T. Borisova, B. Ershler and A.N. Frumkin, Zhur. Fiz. Khim., 1948, 22, 925.

31. Ya. M. Kolotyrkin and N. Bune, Zhur. Fiz. Khim., 1955, 29, 435.

32. P. Ruetschi, J.B. Ockerman and R. Amlie, J. Electrochem. Soc., 1960, 107, 325.

33. R.J. Brodd and N. Hackerman, J. Electrochem. Soc., 1957, 104, 704.

33a. C. Wagner, J. Electrochem. Soc., 1950, 97, 72.

34. U.V. Palm and V.E. Past, Dokl. Akad. Nauk. S.S.S.R., 1962, 146, 1374.

35. U.V. Palm and V.E. Past, Soviet Electrochem., 1965, 1, 527.

36. U.V. Palm and V.E. Past, Izv. Vysshikh. Uchebn. Zavendenii Khim. i. Khim. Teknol., 1964, 7, 583.

37. U.V. Palm and V.E. Past, Uch. Zap. Tartusk. Gos. Univ., 1966, No. 193, 89.

38. K.V. Rybalka and D.I. Leikis, Soviet Electrochem., 1967, 3, 332, 1013.

39. K.V. Rybalka, Soviet Electrochem., 1968, 4, 1223.

39a. J.P. Carr, N.A. Hampson, S.N. Holley and R. Taylor, J. Electroanal. Chem., 1971, 32, 345.

39b. J.P. Carr and N.A. Hampson, J. Electrochem. Soc., 1971, 118, 1262.

40. J. van Muylder and M. Pourbaix, C.I.T.C.E. Rept., Sixth Mtg. (1954), Butterworths, London, 1955, 342.

41. H.W. Salzberg, *J. Electrochem. Soc.*, 1953, *100*, 146.

42. H.W. Salzberg and L.W. Gastwirt, *J. Electrochem Soc.*, 1957, *104*, 701.

43. B.N. Kabanov, I.G. Kiseleva, I.I. Astakhov and N.N. Tomashova, *Soviet Electrochem.*, 1965, *1*, 911.

44. B.N. Kabanov, *Electrochim. Acta*, 1968, *13*, 19.

45. H. Angerstein, *Bull. Acad. Pol. Sci.*, 1955, *3*, 447.

46. D.P. Smith, "Hydrogen in Metals", Univ. of Chicago Press, Chicago, 1948.

47. H.R. Heath, *Brit. J. Appl. Phys.*, 1952, *3*, 13.

48. H.B. Wahlin and V.O. Naumann, *J. Appl. Phys.*, 1953, *24*, 42.

49. R.M. Barrer, "Diffusion in and through Solids", Cambridge Univ. Press, Cambridge, 1951.

50. J.M. Saleh, B.R. Wells and M.W. Roberts, *Trans. Faraday Soc.*, 1964, *60*, 1865.

51. B.R. Wells and M.W. Roberts, *Proc. Chem. Soc.*, 1964, 173.

52. F. Streintz, *Ann. Phys.*, 1889, *38*, 344.

53. G.D. Parkes, "Mellor's Modern Inorganic Chemistry", Longmans, Green, London, 1961.

54. F. Paneth and O. Norring, *Ber.*, 1920, *53B*, 1693; see, however, F.G.A. Stone, "Hydrogen compounds of Group IV Elements", Prentice-Hall, Englewood Cliffs, New Jersey, 1962.

55. B.L. Muju and F.R. Smith, *Can. J. Chem.*, 1971, *49*, 2406.

56. L.I. Krishtalik and V.M. Tsionsky, *J. Electroanal. Chem.*, 1971, *31*, 363.

57. K.J. Vetter, "Electrochemical Kinetics", Academic Press, New York, 1967.

58. J.O'M. Bockris and E.C. Potter, *J. Electrochem. Soc.*, 1952, *99*, 169.

59. R. Parsons, *J. Chim. Phys.*, 1952, *49*, C82.

60. S. Schuldiner and J.P. Hoare, *J. Phys. Chem.*, 1957, *61*, 705.

61. D.J.G. Ives, *Can. J. Chem.*, 1959, *37*, 213.

62. F.A. Lewis, "Recent Progress in Surface Science", eds. J.F. Danielli, A.C. Riddiford and M.D. Rosenberg, Academic Press, New York, Vol. 3, 1970, 71.

63. L. Kandler, C.A. Knorr and C. Schwitzer, *Z. Phys. Chem.*, 1937, *180A*, 281.

64. L.P. Hammett, *J. Amer. Chem. Soc.*, 1924, *46*, 7.

65. C.A. Knorr and E. Schwartz, *Z. Elektrochem.*, 1934, *40*, 38.

65a. C.A. Knorr, *Z. Elektrochem.*, 1955, *59*, 647.

66. C.V. King, *J. Electrochem. Soc.*, 1955, *102*, 193.

67. H.L.F. von Helmholtz, *Wiss. Abhandl. Phys.-tech. Reichsanstalt*, 1879, *1*, 925.

68. G. Gouy, *J. Phys. Radium*, 1910, *9*, 457.

69. D.L. Chapman, *Phil. Mag.*, 1913, *25*, 475.

70. O. Stern, *Z. Elektrochem.*, 1924, *30*, 508.

71. D.C. Grahame, *J. Chem. Phys.*, 1950, *18*, 903.

72. L. Levine, G.M. Bell and D. Calvert, Can. J. Chem., 1962, 40, 518.

73. J.O'M. Bockris, M.A.V. Devanathan and K. Muller, Proc. Roy. Soc. (London), 1963, A274, 55.

74. T. N. Andersen and J.O'M. Bockris, Electrochim. Acta, 1964, 9, 347.

75. B.B. Damaskin and A.N. Frumkin, J. Electroanal. Chem., 1972, 34, 191.

76. J.A.V. Butler, Trans. Faraday Soc., 1923, 19, 729; 1932, 28, 379.

77. R.W. Gurney, Proc. Roy. Soc. (London), 1931, A134, 137.

78. A.N. Frumkin, Z. Phys. Chem., 1932, A160, 116; 1933, A164, 121.

79. M. Volmer and T. Erdey-Gruz, Z. Phys. Chem., 1930, A150, 203.

80. J. Horiuti and M. Polanyi, Acta Physicochim. U.R.S.S., 1935, 2, 505.

81. J.O'M. Bockris and D.B. Matthews, Proc. Roy. Soc. (London), 1966, A292, 479.

82. R.R. Dogonadze, A.M. Kuznetsov and V.G. Levich, Soviet Electrochem., 1967, 3, 648.

82a. R.R. Dogonadze, "Reactions of Molecules at Electrodes", ed. N.S. Hush, Interscience-Wiley, London, 1971, 135.

83. R.R. Dogonadze, A.M. Kuznetsov and V.G. Levich, Electrochim. Acta, 1968, 13, 1025.

84. V.G. Levich, "Physical Chemistry, An Advanced Treatise", ed. H. Eyring, Academic Press, New York, Vol. IXB, 1970, 985.

85. D.B. Matthews, Austral. J. Chem., 1959, 22, 1349.

86. J.O'M. Bockris and A.K.N. Reddy, "Modern Electrochemistry", Plenum Press, New York, Vols. 1 and 2, 1970.

87. B.E. Conway, "Theory and Principles of Electrode Processes", Ronald Press, New York, 1965.

88. A.N. Frumkin, "Adv. Electrochem. and Electrochem. Eng.", ed. P. Delahay, Interscience-Wiley, New York, Vol. 1, 1961, 65.

88a. A.N. Frumkin, "Adv. Electrochem. and Electrochem. Eng.", ed. P. Delahay, Interscience-Wiley, New York, Vol. 3, 1963, 287.

89. S. Glasstone, K.J. Laidler and H. Eyring, "The Theory of Rate Processes", McGraw-Hill, New York, 1941.

90. T.N. Andersen and H. Eyring, "Physical Chemistry, An Advanced Treatise", ed. H. Eyring, Academic Press, New York, Vol. IXA, 1970, 247.

91. R. Parsons, Trans. Faraday Soc., 1958, 54, 1053.

92. B.E. Conway and J.O'M. Bockris, J. Chem. Phys., 1957, 26, 532.

93. H. Kita, J. Electrochem. Soc., 1966, 113, 1095.

94. A.T. Kuhn, C.J. Mortimer, G.C. Bond and J. Lindley, J. Electroanal. Chem., 1972, 34, 1.

95. J. Horiuti, J. Res. Inst. Catalysis, Hokkaido Univ., 1948, 1, 8.

96. J. O'M. Bockris, "Modern Aspects of Electrochemistry", eds. J.O'M. Bockris and B.E. Conway, Butterworths, London, Vol. 1, 1954, 180.

97. K.J. Vetter, "Trans. Symp. on Electrode Processes" (1959), ed. E. Yeager, The Electrochemical Society, John Wiley and Sons, New York, 1961, 47.

98. B.E. Conway and M. Salomon, Electrochim. Acta, 1964, 9, 1599.

99. M. Enyo and T. Yokoyama, Electrochim. Acta, 1971, 16, 223.

100. J. Horiuti and T. Nakamura, J. Chem. Phys., 1950, 18, 395.

101. J. Horiuti, "Trans. Symp. on Electrode Processes" (1959), ed. E. Yeager, The Electrochemical Society, John Wiley and Sons, New York, 1961, 17.

102. M. Rome and C.F. Hiskey, J. Amer. Chem. Soc., 1954, 76, 5207.

103. B.E. Conway, Proc. Roy. Soc. (London), 1958, A247, 400; 1960, A256, 128.

104. B.E. Conway, "Trans. Symp. on Electrode Processes" (1959), ed. E. Yeager, The Electrochemical Society, John Wiley and Sons, New York, 1961, 267.

105. R. Parsons, "Adv. Electrochem. and Electrochem. Eng.", ed. P. Delahay, Interscience-Wiley, New York, Vol. 1, 1961, 1.

106. P. Delahay, "Double Layer and Electrode Kinetics", Interscience-Wiley, New York, 1965.

107. V. Bagozky, Dokl. Akad. Nauk S.S.S.R., 1947, 58, 1387.

108. E.A. Maznichenko, B.B. Damaskin and Z.A. Jofa, Dokl. Akad. Nauk S.S.S.R., 1961, 138, 1377.

109. Z.A. Jofa, B.N. Kabanov, E. Kuchinsky and F. Chistyakov, Zhur. Fiz. Khim., 1939, 13, 1105.

110. Z.A. Jofa and Tsa Chuang-Hsin, *Dokl. Akad. Nauk S.S.S.R.*, 1959, *126*, 1308.

111. R. Parsons, *J. Electroanal. Chem.*, 1969, *21*, 35.

112. L.I. Krishtalik, *J. Electroanal. Chem.*, 1972, *35*, 157.

112a. B. Post and C.F. Hiskey, *J. Amer. Chem. Soc.*, 1950, *72*, 4203.

112b. B. Post and C.F. Hiskey, *J. Amer. Chem. Soc.*, 1951, *73*, 161.

112c. M.W. Breiter, *J. Phys. Chem.*, 1964, *68*, 2254.

112d. K.M. Joshi, W. Mehl and R. Parsons, "Trans. Symp. on Electrode Processes" (1959), ed. E. Yeager, The Electrochemical Society, John Wiley and Sons, New York, 1961, 249.

113. J.O'M. Bockris and P.K. Subramanyan, *Electrochim. Acta*, 1971, *16*, 2169.

113a. M.W. Breiter, *Ann. New York Acad. Sci.*, 1963, *101*, 709.

114. D.D. Eley, *Disc. Faraday Soc.*, 1950, *8*, 34.

115. S. Trasatti, *J. Chem. Soc.: Faraday Trans. I*, 1972, *68*, 229.

116. F.R. Smith, in preparation for *Chemical Society Reviews, London*, 1973.

117. L.I. Krishtalik, "Adv. Electrochem. and Electrochem. Eng.", ed. P. Delahay, Interscience-Wiley, New York, Vol. 7, 1970, 283.

118. M.W. Roberts and N.J. Young, *Trans. Faraday Soc.*, 1970, *66*, 2636.

119. A.K. Vijh, *J. Electrochem. Soc.*, 1971, *118*, 263.

120. G. Armstrong and J.A.V. Butler, *Trans. Faraday Soc.*, 1933, *29*, 1261.

120a. A.N. Frumkin, V.S. Bagotsky, Z.A. Jofa and B.N. Kabanov, "Kinetics of Electrode Processes", Moscow Univ. Press, Moscow, 1952.

121. A. Hickling and F.W. Salt, Trans. Faraday Soc., 1942, 38, 474.

122. A. Eucken and B. Weblus, Z. Elektrochem., 1951, 55, 114.

123. D.C. Grahame, J. Electrochem. Soc., 1952, 99, 370C.

124. J.O'M. Bockris and H. Kita, J. Electrochem. Soc., 1961, 108, 676.

125. B.E. Conway and E. Gileadi, Trans. Faraday Soc., 1962, 58, 2493.

126. E. Gileadi and B.E. Conway, "Modern Aspects of Electrochemistry", eds. J.O'M. Bockris and B.E. Conway, Butterworths, London, Vol. 3, 1964, 347.

127. M.A.V. Devanathan, J.O'M. Bockris and W. Mehl, J. Electroanal. Chem., 1959/60, 1, 143.

128. B.E. Conway and E. Gileadi, Can. J. Chem., 1964, 42, 90.

129. E. Gileadi and B.E. Conway, J. Chem. Phys., 1963, 39, 3420.

129a. B.E. Conway, E. Gileadi and M. Dzieciuch, Electrochim. Acta, 1963, 8, 143.

130. M. Breiter, "Trans. Symp. on Electrode Processes" (1959), ed. E. Yeager, The Electrochemical Society, John Wiley and Sons, New York, 1961, 307.

131. H. Angerstein-Kozlowska and B.E. Conway, J. Electroanal. Chem., 1964, 7, 109.

132. B.E. Conway, E. Gileadi and H. Angerstein-Kozlowska, J. Electrochem. Soc., 1965, 112, 341.

133. V.E. Past and Z.A. Jofa, Zhur. Fiz. Khim., 1959, 33, 913.

134. H.B. Morley and F.E.W. Wetmore, Can. J. Chem., 1956, 34, 359.

135. B.E. Conway and P.L. Bourgault, Can. J. Chem., 1959, 37, 292; 1960, 38, 1557; 1962, 40, 1690.

136. M. Breiter, C.A. Knorr and W. Volkl, *Z. Elektrochem.*, 1955, *59*, 881.

137. F.G. Will and C.A. Knorr, *Z. Elektrochem.*, 1960, *64*, 258.

138. C.D. Kim and B.E. Wilde, *J. Electrochem. Soc.*, 1971, *118*, 202.

139. R. Parsons, "Adv. Electrochem. and Electrochem. Eng.", ed. P. Delahay, Interscience-Wiley, New York, Vol. 7, 1970, 177.

140. See Ref. 125.

141. J.J. MacDonald and B.E. Conway, *Proc. Roy. Soc. (London)*, 1962, *A269*, 419.

142. B.E. Conway and P.L. Bourgault, *Trans. Faraday Soc.*, 1962, *58*, 593.

143. M.I. Temkin, *Zhur. Fiz. Khim.*, 1941, *15*, 296.

144. V. Breger and E. Gileadi, *Electrochim. Acta*, 1971, *16*, 177.

144a. N. Pangarov and I. Christova, *Bulg. Acad. Sci.*, 1969, *II*, 813.

144b. I.I. Phillips, P. Poole and L.L. Shreir, *Corros. Sci.*, 1972, *12*, 855.

144c. T.P. Radhakrishnan and L.L. Shrier, *Electrochim. Acta*, 1966, *11*, 1007.

145. M.A.V. Devanathan and Z. Stachurski, *Proc. Roy. Soc. (London)*, 1962, *A270*, 90.

145a. H. Zuchner and N. Boes, *Ber. Bunsenges Phys. Chem.*, 1972, *76*, 783.

146. J. McBreen, L. Nanis and W. Beck, *J. Electrochem. Soc.*, 1966, *113*, 1218.

147. I. Cadersky, B.L. Muju and F.R. Smith, Can. J. Chem., 1970, 48, 1789.

148. E. Gileadi, M.A. Fullenwider and J.O'M. Bockris, J. Electrochem. Soc., 1966, 113, 926.

148a. J.O'M. Bockris, I.A. Ammar, and A.K.M.S. Huq, J. Phys. Chem., 1957, 61, 879.

148b. A.N. Frumkin and N.A. Aladjalova, Acta Physicochim. U.R.S.S., 1944, 19, 1.

149. J.O'M. Bockris, M.A. Genshaw and M.A. Fullenwider, Electrochim. Acta, 1970, 15, 47.

150. W. Beck, J.O'M. Bockris, J. McBreen and L. Nanis, Proc. Roy. Soc. (London), 1966, A290, 220.

151. L. Nanis and T.K.G. Namboodhiri, J. Electrochem. Soc., 1972, 119, 691.

152. L.S. Darken and R.P. Smith, Corrosion, 1949, 5, 1.

153. A. McNabb and P.K. Foster, Trans. A.I.M.E., 1963, 227, 618.

154. R.A. Oriani, Acta Met., 1970, 18, 147.

155. J.O'M.Bockris and P.K. Subramanyan, J. Electrochem. Soc., 1971, 118, 1114.

156. J.O'M. Bockris and P.K. Subramanyan, Corros. Sci., 1970, 10, 435.

157. J.O'M. Bockris, J. McBreen and L. Nanis, J. Electrochem. Soc., 1965, 112, 1025.

157a. J.O'M. Bockris and R. Thacker, Tech. Rept. No. 3 to Office of Naval Research (U.S. Govt.), Nonr. 551(22), NR 036-028, 1959.

158. F.A. Lewis, "The Hydrogen-Palladium System", Academic Press, London, 1967.

159. L.I. Krishtalik, Soviet Electrochem., 1966, 2, 575.

160. T.C. Franklin and P.E. Hudson, J. Electrochem. Soc., 1967, 114, 568.

161. J.O'M. Bockris and S. Srinivasan, J. Electrochem. Soc., 1964, 111, 844, 853, 858.

162. L.I. Krishtalik, Soviet Electrochem., 1970, 6, 1406.

163. J. Bigeleisen, "Tritium Phys. Biol. Sci., Proc. Symp.", Vienna, Austria (1961), Vol. 1, 1962, 161.

164. M. Salomon and B.E. Conway, Disc. Faraday Soc., 1965, 39, 223.

164a. J. Horiuti, A. Matsuda, M. Enyo and H. Kita, "Proc. of the First Australian Conference on Electrochemistry" (1963), eds. J.A. Friend and F. Gutmann, Pergamon Press, London, 1965, 750.

164b. B.E. Conway, "Progress in Reaction Kinetics", ed. G. Porter, Pergamon Press, London, Vol. 4, 1967, 399.

165. J.O'M. Bockris, S. Srinivasan and D.B. Matthews, Disc. Faraday Soc., 1965, 39, 239.

166. J.O'M. Bockris, E. Gileadi and R. Haynes, J. Electroanal. Chem., 1968, 19, 446.

167. R. Haynes, Electrochim. Acta, 1971, 16, 1129.

168. B.E. Conway and M. Salomon, J. Chem. Phys., 1964, 41, 3169.

169. J.O'M. Bockris and D.B. Matthews, J. Chem. Phys., 1966, 44, 298.

170. M. Hammerli, J.P. Mislan and W.J. Olmstead, J. Electrochem. Soc., 1970, 117, 751.

171. L.P. Roy, Can. J. Chem., 1962, 40, 1452.

172. M. Hammerli, W.J. Olmstead, B.L. Muju and F.R. Smith, J. Electroanal. Chem., 1973, 43, 45.

173. F.R. Smith and M. Hammerli, Z. Phys. Chem. (N.F.), 1971, 74, 75.

174. R. Bucur and F.A. Lewis, Z. Phys. Chem. (N.F.), 1971, 75, 207.

175. H. Brodowsky, H. Gibmeier and E. Wicke, Z. Phys. Chem. (N.F.), 1966, 49, 222.

176. G. Bohmholdt and E. Wicke, Z. Phys. Chem. (N.F.), 1967, 56, 133.

177. E. Wicke and H. Gibmeier, Z. Phys. Chem. (N.F.), 1964, 42, 112.

177a. G. Sicking, Ber. Bunsenges Phys. Chem., 1972, 76, 790.

177b. Y. Ebisuzaki and M. O'Keeffe, "Progress in Solid State Chemistry", ed. H. Reiss, Pergamon Press, New York, Vol. 4, 1967, 187.

178. M. Schutze, Angew. Chem., 1958, 70, 697.

179. D.J.C. Yates, J. Chem. Ed., 1967, 44, 699.

179a. H.P. Dibbs, D.J.G. Ives and R.W. Pittman, J. Chem. Soc., 1957, 3370.

179b. See 449 in Ref. 27.

180. G.C. Barker, "Trans. Symp. on Electrode Processes" (1959), ed. E. Yeager, The Electrochemical Society, John Wiley and Sons, New York, 1961, 366.

180a. N.A. Hampson and D. Larkin, J. Electroanal. Chem., 1968, 18, 401.

181. D.C. Cornish, H.P. Dibbs, F.S. Feates, D.J.G. Ives and R.W. Pittman, J. Chem. Soc., 1962, 4104.

182. J.J. Bikerman, "Surface Chemistry", Academic Press, New York, 1958.

183. W. Kemula, Pure Appl. Chem., 1967, 15, 283.

184. W. Kemula, Z. Kublik and S. Glodowski, J. Electroanal. Chem., 1959/60, 1, 91.

185. G. van Dijck and F. Verbeek, Anal. Chim. Acta, 1971, 54, 475.

186. F.R. Smith and P. Delahay, J. Electroanal. Chem., 1965, 10, 435.

187. L.E. Samuels, J. Inst. Metals, 1957, 85, 177.

188. A.L. Norbury, Trans. Faraday Soc., 1923, 19, 140.

189. J.O'M. Bockris and B.E. Conway, J. Sci. Instr., 1948, 25, 283.

190. P.A. Jacquet, Nature, 1935, 135, 1076.

191. J. Edwards, J. Electrochem. Soc., 1953, 100, 189C, 223C.

192. T.P. Hoar and J.A.S. Mowat, Nature, 1950, 165, 64.

193. T.P. Hoar and T.W. Farthing, Nature, 1952, 169, 324.

194. M. Cole and T.P. Hoar, C.I.T.C.E. Rept., Eighth Mtg. (1956), Butterworths, London, 1958, 158.

195. I.A. Menzies, G.W. Marshall and G.B. Griffin, Corros. Sci., 1969, 9, 287.

196. M. Novak, A.K.N. Reddy and H. Wroblowa, J. Electrochem. Soc., 1970, 117, 733.

197. T.P. Hoar, "Modern Aspects of Electrochemistry", ed. J.O'M. Bockris, Butterworths, London, Vol. 2, 1959, 262.

198. E. Darmois and I. Epelboin, *Compt. Rend. Acad. Sci. (Paris)*, 1953, *237*, 501.

199. I. Epelboin, *Z. Elektrochem.*, 1955, *59*, 689.

200. C. Wagner, *J. Electrochem. Soc.*, 1954, *101*, 225.

201. E.J. Casey and R.E. Bergeron, *Can. J. Chem.*, 1953, *31*, 422.

202. I. Epelboin, P. Brouillet and M. Froment, *Compt. Rend. Acad. Sci. (Paris)*, 1954, *239*, 1795.

203. M.M. Nikiforova and Z.A. Jofa, *Proc. Acad. Sci. U.S.S.R.: Sect. Phys. Chem.*, 1957, *115*, 575.

204. G.J. Hills and D.J.G. Ives, "Reference Electrodes", eds. D.J.G. Ives and G.J. Janz, Academic Press, New York, 1961, 71.

205. W.P. Senett and C.F. Hiskey, *J. Amer. Chem. Soc.*, 1952, *74*, 3754.

206. T.S. Lee, *J. Electrochem. Soc.*, 1971, *118*, 1278.

206a. D.A. Jenkins and C.J. Weedon, *J. Electroanal. Chem.*, 1971, *31*, App. 13.

207. I. Cadersky, G.M. Rao and F.R. Smith, in preparation.

208. W.B. Pearson, "Handbook of Lattice Spacings and Structures of Metals", Pergamon Press, London, Vol. 2, 1967.

209. G.M. Rao and F.R. Smith, *J. Chem. Soc.: Chem. Comm.*, 1972, 266.

210. G. Friedlander and J.W. Kennedy, "Nuclear and Radiochemistry", John Wiley and Sons, New York, 1960.

211. T.B. Flanagan and F.A. Lewis, *Trans. Faraday Soc.*, 1959, *55*, 1409.

212. F.H. Reid, Metal Rev., 1963, 8, 167.

213. F.E. Kinard, Rev. Sci. Instr., 1957, 28, 293.

214. I. Cadersky, B.L. Muju and F.R. Smith, unpublished work.

215. See Ref. 210.

216. I. Langmuir, Trans. Amer. Electrochem. Soc., 1916, 29, 260.

217. I. Langmuir, J. Chem. Soc., 1940, 511.

218. N. Hackerman and E.H. Lee, J. Phys. Chem., 1955, 59, 900.

219. A.N. Nesmeyanov, N.A. Khandomirova, V.D. Vilenskii, E.A. Birin and E.A. Borisov, Russ. J. Phys. Chem., 1960, 34, 681.

220. J.P.G. Farr and N.A. Hampson, Trans. Faraday Soc., 1966, 62, 3502.

221. N.A. Hampson and D. Larkin, Trans. Faraday Soc., 1969, 65, 1660.

222. T. Moeller, "Inorganic Chemistry, An Advanced Textbook", John Wiley and Sons, New York, 1952.

223. F.E. Saalfeld and H.J. Svec, Inorg. Chem., 1963, 2, 46.

224. T.G. Pearson, P.L. Robinson and E.M. Stoddart, Proc. Roy. Soc. (London), 1933, A152, 275.

225. E.J. Weeks, J. Chem. Soc., 1925, 127, 2845.

226. H.C. Roberts and R.S. Eachus, J. Chem. Phys., 1972, 57, 3022.

227. H.G. Deming and B.C. Hendricks, J. Amer. Chem. Soc., 1923, 45, 2857.

228. W.R. Opie and N.J. Grant, Trans. Met. Soc. A.I.M.E., 1951, 191, 244.

229. E. Wiberg and E. Amberger, "Hydrides of the Elements of Main Groups I-IV", Elsevier, Amsterdam, 1971.

230. W. Jost, "Diffusion in Solids, Liquids and Gases", Academic Press, New York, 1965.

231. L.W. Barr, "Diffusion Processes", eds. J.N. Sherwood, A.V. Chadwick, W.M. Muir and F.L. Swinton, Gordon and Breach Science, London, Vol. 1, 1971, 173.

232. J. Horiuti and G. Okamoto, Sci. Pap. Inst. Phys. Chem. Res. Tokyo, 1936, 28, 231.

233. H.F. Walton and J.H. Wolfenden, Trans. Faraday Soc., 1938, 34, 436.

234. M. Hammerli, J.P. Mislan and W.J.Olmstead, J. Electrochem. Soc., 1969, 116, 779.

235. B. Dandapani and M. Fleischmann, J. Electroanal. Chem., 1972, 39, 315, 323.

236. R.V. Bucur and L. Stoicovici, J. Electroanal. Chem., 1972, 36, 243.

237. N.A. Hampson and D. Larkin, Electrochim. Acta, 1970, 15, 581.

238. P. Dolin and B. Ershler, Acta Physicochim. U.R.S.S., 1940, 13, 747.

239. R.P. Eischens, "Surface Chemistry of Metals and Semiconductors", ed. H.C. Gatos, John Wiley and Sons, 1960, 421.

240. T. Toya, J. Res. Inst. Catalysis, Hokkaido Univ., 1962, 10, 236.

241. J.R. Anderson and A.V. Gold, Phys. Rev., 1965, 139, A1459.

242. A.V. Gold, private communication to F.R. Smith.